Polymeric Materials for Controlled Ophthalmic Drug Delivery

Thesis submitted in accordance with the requirements of the
University of Liverpool for the degree of Doctor in Philosophy

Helen Cauldbeck

September 2015

ACKNOWLEDGEMENTS

Firstly, I would like to say thank you to my family, particularly Mum, Dad and Mary for all their encouragement during my academic journey and for their patience throughout. Without them this wouldn't have been possible!

Secondly, I would like to thank Steve Rannard and Victoria Kearns for giving me the opportunity to undertake my PhD studies under their supervision. I'm truly grateful for all their guidance and continual support over the last four years and their enthusiasm which made the good times better and the bad times bearable.

I would like to give a special thanks to Maude Le Hellaye for being a brilliant post-doc throughout the project, not only in terms of teaching me, but also for her endless support and the day-to-day help she has provided both inside and out of the lab. Maude has been a pleasure to work with and as well as appreciating her scientific input in this project, I truly appreciate her friendship over the past four years.

I would like to thank each member of the Rannard group, both past and present, for making my time studying in the group such an enjoyable experience and providing such a friendly working environment. I would also like to thank everyone in EVS for helping me gain an understanding for what was a new field to me four years ago. The friends I have made within these groups have truly made my time studying fantastic; it would not have been as fun without you all. I will miss each and every one of you.

Finally, I would like to thank all my other friends at the university who I have made throughout my time at Liverpool; in particular Sam for all the fun and laughter as well as keeping me going through the tough times. A special thanks goes to my boyfriend, Sean, for all his support and helping me stay sane through the last few months!

ABSTRACT

Polymeric Materials for Controlled Ophthalmic Drug Delivery.

Proliferative vitreoretinopathy, a potentially blinding condition, involves excessive proliferation of retinal pigment epithelium (RPE) cells and is the main complication following retinal detachment (RD). Complicated cases of RD are treated with silicone oil (SiO) tamponades which can potentially be used as drug reservoirs. The aim of this study was to investigate different methodologies to develop a sustained and controlled drug release of anti-proliferative and anti-inflammatory drugs from SiO tamponades using all-trans retinoic acid (atRA) and ibuprofen (Ibu).

In detailed studies of atRA and Ibu, including atRA degradation behaviour, the drugs were found to be non-toxic to an adult RPE cell line (ARPE-19) below 10^{-5} M. The solubility of both drugs in SiO was assessed using radioisotope techniques. Prodrugs of atRA and Ibu were synthesised *via* conjugation to polyethylene oxide (PEO), and cleavage of the resulting ester bond, toxicity towards RPE cells, solubility in SiO and release into media were assessed. Prodrug cleavage was successful *in vitro* for Ibu but not achieved in the case of atRA due to its highly conjugated nature. Cytotoxicity assays showed PEO attachment had no effect on cytotoxicity and PEO-prodrug solubility in SiO followed the expected trend of decreasing solubility with increased PEO chain length. Overall the saturation concentration of drug in SiO achieved through the use of PEO-prodrugs was too low for an effective therapy.

Lipophilic prodrugs with a poly(dimethylsiloxane) (PDMS) pro-moiety were synthesised and investigated. Their cleavage was problematic due to PDMS being highly hydrophobic and cleavage could only be achieved *in vitro* when a small hydrophilic spacer was added between PDMS and the drug. The effects of PDMS prodrugs as additives in SiO were investigated and the presence of PDMS-atRA in SiO was shown to have a positive effect on both atRA solubility and longevity of release. The clinically-relevant release period (6-8 weeks) was independent of atRA starting concentration but dependant on the PDMS-atRA concentration within the blend. This has potential for further development into tamponade drug reservoirs for future patient benefits.

A series of linear and branched amphiphilic copolymer architectures were also evaluated as additives for SiO. Monomer selection included oligoethylene oxide methacrylate (OEGMA), 2-hydroxyethyl methacrylate, PDMS-methacrylate (PDMSMA) and the brancher PDMS-dimethacrylate (PDMSDMA). SiO solubility of p(OEGMA-*co*-PDMSDMA) was investigated and copolymers which contained the smallest hydrophilic and largest lipophilic components only achieved small solubility (0.1 % v/v). To overcome these solubility issues, hydrophobic PDMSMA monomer was utilised. Both linear p(PDMSMA-*co*-OEGMA) and branched p(PDMSMA-*co*-OEGMA-*co*-PDMSDMA) were successfully synthesised and displayed high solubility within SiO, up to 40-50 % v/v.

The potential for SiO tamponades as long-acting drug reservoirs has been demonstrated after inclusion of a novel end-modified PDMS additive leading to long term release of atRA. The formation of novel polymer architectures that show considerable miscibility with SiO also shows the scope of the opportunity for further additive development to tailor release profiles.

CONTENTS

CHAPTER 1

CHAPTER 2

CHAPTER 3

CHAPTER 4

APPENDIX

LIST OF ABBREVIATIONS

AMD	Age-Related Macular Degeneration
ANOVA	Analysis of Variance
AOFV	Adult Onset Foveomacular Vitelliform
ARPE-19	Adult Retinal Pigment Epithelium
ATRP	Atom Transfer Radical Polymerisation
BRB	Blood Retinal Barrier
CI	Chemical Ionisation
CRP	Controlled Radical Polymerisation
CTA	Chain Transfer Agent
DDD	Drug Delivery Device
DDS	Drug Delivery System
DP_n	Degree of Polymerisation
ECM	Extracellular Matrix
ERD	Exudative Retinal Detachment
ES	Electrospray
GPC	Gel Permeation Chromatography
HPLC	High-Performance Liquid Chromatography
ILM	Inner Limiting Membrane
IOP	Intraocular Pressure
M_n	Number Average Molecular Weight
MS	Mass Spectroscopy
M_w	Weight Average Molecular Weight
MW	Molecular Weight
NMP	Nitroxide Mediated Polymerisation
NMR	Nuclear Magnetic Resonance
NSAID	Non-Steroidal Anti-Inflammatory Drug
PD	Pattern Dystrophy
PVR	Proliferative Vitreoretinopathy
RAFT	Reversible Addition-Fragmentation Chain Transfer
RALS	Right Angle Light Scattering
RAR-ß2	Retinoic Acid Receptor Beta-2
RD	Retinal Detachment
RI	Refractive Index
RPE	Retinal Pigment Epithelium
RRD	Rhegmatogenous Retinal Detachment
TRD	Tractional Retinal Detachment
UV-Vis	Ultraviolet-Visible Spectroscopy

LIST OF CHEMICAL ABBREVIATIONS

5-FU	5-Fluorouracil
ACN	Acetonitrile
AIBN	2,2'-Azobis(2-Methylpropionitrile)
Ar	Argon
atRA	All-trans Retinoic Acid
BA	Benzoic Acid
bFGF	Basic Fibroblast Growth Factor
Bpy	Bipyridyl
BrdU	Bromodeoxyrubicin
CDCl$_3$	Deuterated Chloroform
CDI	1,1'-Carbonyldiimidazole
CPBD	2-Cyano-2-Propyl Benzodithioate
D$_2$O	Deuterium Oxide
DAPI	Dianidine-2-Phenylindole
DCC	Dicyclohexylcarbodiimide
DCl	Deuterium Chloride
DCM	Dicholoromethane
DCU	Dicyclohexylurea
DMAP	4-(Dimethylamino)pyridine
DMF	Dimethylformamide
DMSO	Dimethyl Sulfoxide
EtBrB	Ethyl α-bromoisobutyrate
EPGF	Epidermal Growth Factor
FGF	Fibroblast Growth Factor
FSiO	Fluorinated Silicone Oil
HCl	Hydrochloric Acid
Ibu	Ibuprofen
IF-ɣ	Interferon-Gamma
IL-	Interlukin
IPA	Isopropanol
MeOH	Methanol
Me-PEO	Methyl Terminated Poly(ethyleneoxide)
MTT	3-(4,5-Dimethylthiazol-2-yl)-2,5-Diphenyltetrazolium Bromide
NaOD	Sodium Deuteroxide
OEGMA	Oligoethylene Glycol Methacrylate
PDMS	Poly(dimethylsiloxane)
PDMS-diOH	Bis(hydroxyalkyl) Terminated Poly(dimethylsiloxane)
PDMSDMA	Methacryloxypropyl Terminated Poly(dimethylsiloxane)
PDMSMA	Mono-Methacryloxypropyl Terminated Poly(dimethylsiloxane)
PEO	Poly(ethyleneoxide)
PDGF	Platelet-Derived Growth Factor
PGA	Polyglycolic Acid

p(HEMA)	Poly(2-Hydroxyethyl Methacylate)
PLA	Polylactic Acid
PLGA	Polylactic-*co*-glycolic Acid
PVA	Polyvinyl Acetate
RA	Retinoic Acid
SFA	Semi-Fluorinated Alkane
SiO	Silicone Oil
TAA	Triamcinolone Acetonide
^{t}BuOH	Tertiary Butanol
TGF-ß	Tumour Growth Factor-Beta
THF	Tetrahydrofuran
VEGF	Vascular Endothelial Growth Factor

CHAPTER 1

General Introduction

1.1 THE EYE

The eye is the structure in the body which receives light signals and converts them into neural signals, which the brain then transforms into visual images.[1]

1.1.1 Structure

The eye (Figure 1.1) consists of two partial spheres, the anterior chamber which is the region between the cornea and the lens containing aqueous humour, and the larger posterior region between the lens and the retina containing the vitreous humour. The sclera is the tough white outer layer which protects the eye, fuses with the cornea anteriorly and is attached to the optic nerve posteriorly, whilst being nourished by a blood supply from the choroid.
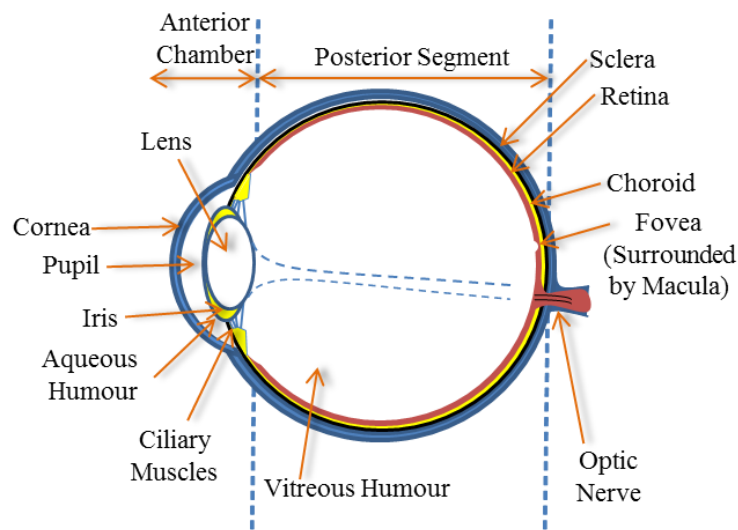
Figure 1.1 An illustration of the human eye, and its structure.

1.1.2 Light Pathway

Light enters the eye through the cornea, which is clear and convex in shape, causing the light to refract. The light then passes through the aqueous humour (which provides nutrients and oxygen to the eye, as well as removing waste products), to the pupil.[2] The amount of light which enters the pupil (a gap in the iris) is controlled by the contraction and expansion of the muscular iris. Light is further refracted by the lens which is an important structure in focussing light; the lens adjusts its thickness *via* the ciliary muscles attached to it. If an object is nearby the lens bulges but if the

object is far away the lens flattens. Then, the light passes through the vitreous humour which not only helps maintain the shape of the eye but also helps to focus. It finally reaches the macula area of the retina surrounding the fovea. The fovea is the thinnest area of the retina which contains the most photoreceptors and no capillaries. Once the retina processes the inverted and reversed image of the object being viewed, it is sent through the optic nerve to the visual cortex where the image is rearranged, enabling us to view the object as it is in reality.

1.1.3 The Retina

The retina is a light sensitive layer which is approximately 30-40 mm in diameter and lines the back of the interior of the eye. The main function of the retina is to detect an inverted image *via* a light signal which is then converted into a communicable chemical signal by photo-transduction. The ordered pattern is then sent to the brain through the optic nerve.

The structure of the retina can be divided into two layers, the inner neuroretina and the outer epithelial monolayer consisting of retinal pigment epithelium (RPE), as depicted in Figure 1.2. The neuroretina is made up of 9 layers including the inner limiting membrane (ILM) which is the structure of the retina closest to the lens and front of the eye.
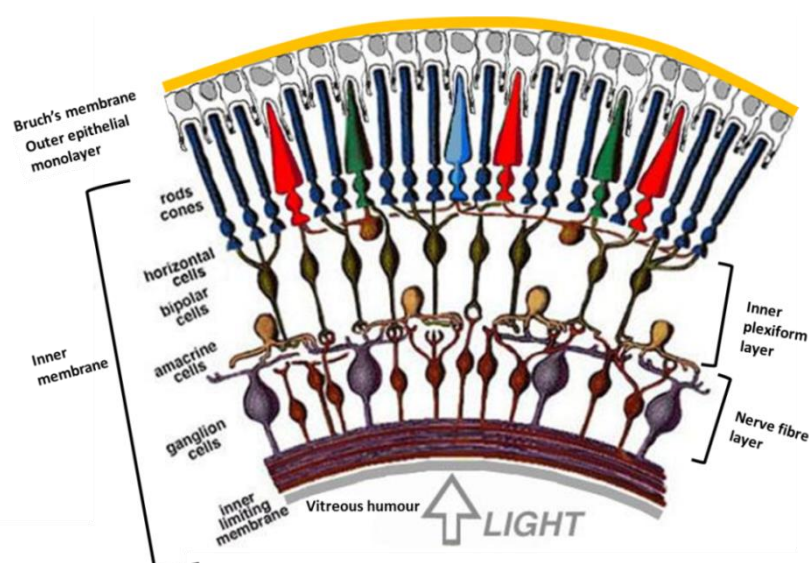
Figure 1.2 An illustration of the organisation of the retina. Adapted from ref: [3]

Light travels through the majority of the retina before photons of light are absorbed by visual pigment within the photoreceptors (rods and cones). The light activates the photoreceptors to produce a biochemical message which is sent synaptically to bipolar cells as an image by patterned excitation. The photoreceptors are surrounded by horizontal and amacrine cells which modify the electrical signal before relaying it to the ganglion cells. These spiking discharge patterns produced by both rods and cones are intermixed and combined when they are transmitted to the brain by the ganglion cells to produce a representation of the external environment.

The outer epithelial layer consists of hexagonally packed cuboidal RPE which supply nutrients to the inner retinal visual cells and transports metabolic waste to the choroid. The innermost layer of the choroid is the Bruch's membrane which thickens with age, therefore, slowing down the transport of metabolites.

1.1.4 Retinal Pigment Epithelium

In humans the monolayer of RPE cells is situated at the back of the eye with its apical membrane facing the subretina, whilst the basolateral membrane is in contact with the Bruch's membrane attached to the choroid. There are approximately 3.5-6.1 million RPE cells per eye.[4] They are hexagonally close packed with simple cuboidal and columnar morphology, and vary in size depending on which area of the retina they are located. Near the macular region they are narrower but taller (10-12 μm wide, 14 μm tall), however, near the periphery they are flatter and broader (60 μm wide and 10-14 μm tall).[5] The RPE and neural retina are very closely linked; from embryonic development RPE cells and photoreceptor cells co-differentiate during the evolution of the eye. Vitamin A (retinol) acts as a differentiation signal for both cells. The RPE cells express receptors such as the retinoic acid receptor beta-2 (RAR-ß2) for retinoic acid (RA), a vitamin A derivative which is secreted by the developing retina. The exchange of RA between primitive RPE and the neuroretina promotes the differentiation.[4, 6]

Initially it was thought that the sole purpose of the RPE was to absorb scattered light. In fact, RPE cells have multiple functions including light absorption, epithelial

transport, spatial buffering of ions, visual cycle, phagocytosis, secretion and immune modulation, all of which are illustrated in Figure 1.3.
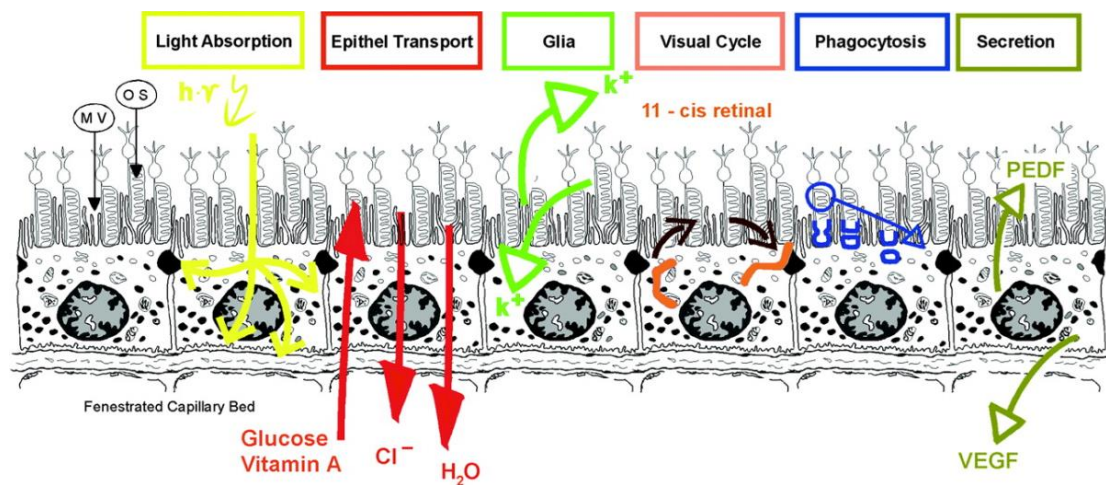
Figure 1.3 Diagram of the major functions of RPE.[6]

The retina is at high risk of photo-oxidative stress due to the high concentration of photo-oxidative energy within its environment. This energy is created by the lens concentrating light radiation onto the macula, as well as the choroid supplying a high oxygen flow.[7, 8] Photo-oxidation leads to damage of the photoreceptor outer segment tips which then require constant renewal. This renewal process involves phagocytosis, which is the ingestion of solid particles into a phagosome within the cell; this is then removed by lysosomes. The damaged photoreceptor outer segments near the RPE undergo phagocytosis which in turn leads to the release of free radicals to the high photo-oxidative environment.[9] Therefore, the RPE has to be able to maintain the structural integrity of the retina by combating free radicals, photo-oxidative exposure and light energy. The melanin present in the RPE contributes to removing the risk of photo-oxidative stress on other cells.

RPE cells are also responsible for epithelial transport (Figure 1.3). Metabolites and water accumulate in the subretinal space due to the retina having the highest cell density of any tissue in the body, as well as the intraocular pressure moving water from the anterior of the eye towards the retina.[10] RPE cells, which form tight junctions that lead to the formation of the outer blood retinal barrier (BRB), are responsible for supplying nutrients and removing metabolites and water *via* active transport from the subretinal space.[11]

RPE cells regulate the spatial buffering of ions which is necessary due to the fast changes in ion concentration, and at this rate cannot be compensated for by normal transepithelial transport. Mechanisms such as transduction of light by cells require the RPE to capacitatively compensate for the change in ion concentration.[12] Without this, the cells would no longer be excitable, therefore, the electrical signals produced would be halted and the pattern sent to the brain disjointed, resulting in incorrect image perception.

RPE cells play a key role in the visual cycle *via* retinoid metabolism. When a photon of light is absorbed by chromophores in a photoreceptor, chemical reactions such as the isomerisation of rhodopsin to meta-rhodopsin as well as 11-cis retinal to all-trans retinal are initiated.[13] Phosphorylation determines the rate at which rhodopsin reforms; rhodopsin then requires the exchange of all-trans retinal to 11-cis retinal in order to be reactivated by another photon. Photoreceptors do not express re-isomerase for all-trans retinal, so this takes place in RPE cells for rods and RPE and Muller glia cells for cones.[14]

RPE cells must interact with both subretinal cells[15] and cells on their basolateral side.[16] RPE cells secrete numerous growth factors such as transforming growth factors beta (TGF-ß) and fibroblast growth factor (FGF) as well as transcription factors and signalling molecules.[6] These are then directed to cells which have important physiopathogenic roles such as maintaining the integrity of surrounding tissues.

The eye is an immune privileged space which, due to the BRB, is disconnected from the blood stream and therefore, the body's immune system.[17] As the eye is separated from the immune system, the RPE cells must communicate with each other and other cells *via* a variety of chemical and mechanical signals to provoke an immune response such as inflammation, if the eye becomes diseased, but ensure silence in a healthy eye.[18]

1.2 RETINAL DETACHMENT

Retinal detachment (RD) is a potentially blinding condition when the inner neuroretina becomes detached from the supporting RPE. RD has become one of the

most common ophthalmic emergencies in the UK.[19] Population-based studies from around the world have found annual incidence rates ranging from 6.8 to 17.9 per 100,000 population,[20-23] whereas within the UK the figures range from 6.3 to 13.6 per 100,000 people.[19, 24, 25]

1.2.1 Types of Retinal Detachment

There are 3 different types of RD (Figure 1.4): rhegmatogenous RD (RRD, Figure 1.4 B), exudative RD (ERD, Figure 1.4 C) and traction RD (TRD, Figure 1.4 C). The most common is RRD, which occurs when there is a tear in the retina.[26]
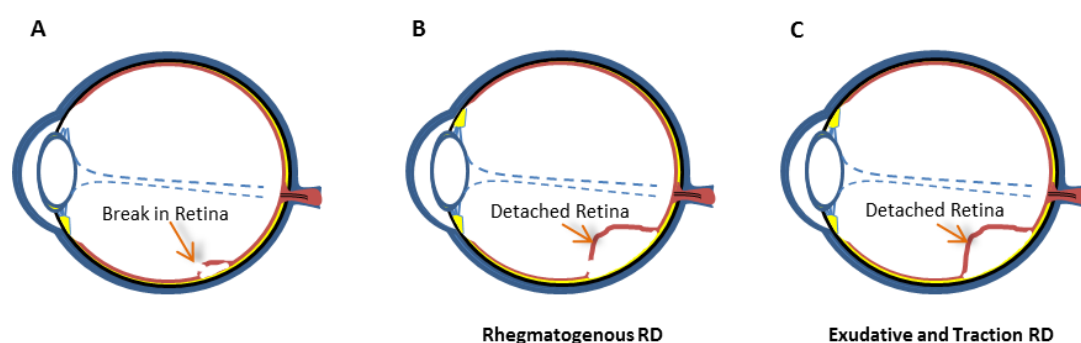
Figure 1.4 Diagram of A: Tear in the retina, B: rhegmatogenous retinal detachment and C: exudative and tractional retinal detachment.

Retinal tears (Figure 1.4 A) can be triggered by numerous causes including trauma, such as those experienced during boxing and bungee jumping, advanced diabetes, myopia, inflammatory eye diseases, retinal disorders or complications following cataract surgery.[27-29] Myopia is the most common cause of non-traumatic RRD and accounts for 55 % of cases.[27] Ageing also increases the risk of RRD to 20 in 100,000 for middle aged/elderly people with the greatest risk in the age range 55-70 years[30] due to the retina becoming thinner as well as a change in vitreous. The vitreous humour is a gel (97 % by weight of water) made up of a network of long collagen fibres with glycoprotein such as hyaluronic acid which non-covalently binds the water. The vitreous moves as a single entity and is normally loosely attached to the back of the lens, the retina and the optic nerve; with age the consistency of the vitreous can shrink or become more fluid-like as the collagen network collapses. The vitreous then becomes detached from the optic nerve and the posterior retina whilst remaining attached to the anterior. With eye movement the vitreous and the

retina move relative to each other and can result in forces that cause the retina to tear and detach. All of these factors can lead to the vitreous separating from the retina with enough force to cause a tear. Vitreous humour then may leak through the tear and accumulate underneath the retina separating it further from the RPE.[31]

Both TRD and ERD result in RD without a tear in the retina (Figure 1.4 C). TRD is the second most common form of RD, and usually occurs as a complication of other diseases or conditions such as diabetic proliferative retinopathy and proliferative vitreoretinopathy (PVR), discussed in more detail in Section 1.4. Scar tissue forms on the rods and cones and contracts, pulling the neurosensory retina away from the supporting RPE.[32]

ERD occurs following the build-up of fluid from blood vessels into the space between the retina and the RPE. ERD is triggered by other retinal diseases and conditions which cause abnormal development in blood vessels behind the retina, such as severe macular degeneration, very high blood pressure, certain cancers such as choroidal melanoma and rare blood vessel disorders.[31]

1.2.2 Symptoms

Patients with RD usually experience symptoms, however, some RDs are found following routine eye checks where the patient's vision is perceived as normal. Common symptoms include the appearance of floaters or the increase number of floaters in the field of vision; these are caused by debris within the vitreous humour blocking the retina from receiving light signals. 6 out of 10 people with RD experience photopsia, i.e. flashing lights in vision even when eyes are closed or in a darkened room. Patients also experience vision loss either centrally or from shadows in the peripheral, which can be described as a "curtain effect" where a portion of their visual field slowly progresses in being blocked out.

1.2.3 Treatments

There are numerous treatments available for RD, all with the aim of reattaching the retina to the RPE and fixing any tears present (Figure 1.5). It is crucial for RD to be treated urgently for a successful outcome. The longer RD is left untreated, the more

widespread the detachment may become and more severe, especially if the macula region is reached. Ideally RD is treated within 24 to 72 hours. The procedure carried out is determined by a number of factors including size, location, severity and type of RD. However, a combination of treatments can be used at the same time.[30]
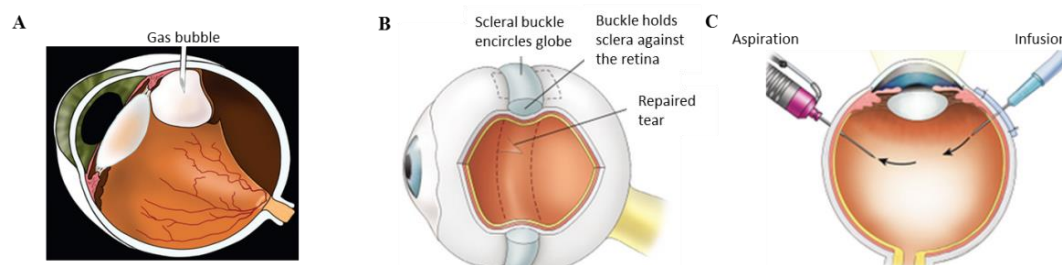
Figure 1.5 Images of different treatments for RD. A: pneumatic retinopexy, B: scleral buckle surgery and C: vitrectomy with tamponade replacement. Adapted from refs:[33, 34]

1.2.3.1 Pneumatic Retinopexy

To treat a retinal tear where no fluid has seeped through between the retina and RPE, laser or cryotherapy may be used. This creates a small amount of scar tissue to seal the break and prevent RD progressing. Laser or cryotherapy can be used in conjunction with other treatments such as pneumatic retinopexy. Pneumatic retinopexy involves the injection of a gas bubble into the vitreous cavity forcing the retina back against the RPE (Figure 1.5 A), the RPE will then remove any build-up of subretinal fluid.[35] The gas used is either air or perfluorocarbon gases such as sulphur hexafluoride (SF_6), perfluoropropane (C_3F_8) or perfluoroethane (C_2F_6). Air has a short residency time (days) within the vitreous cavity due to diffusion into the surrounding tissues, therefore, cannot be used for a long period of time to support the retina reattaching. Perfluorocarbon gases are utilised because they have a longer residency time than air (a few weeks), they are inert within the vitreous cavity due to steric hindrance, their volume increases after insertion and they are poorly water soluble.[36-38] This treatment is usually used for people with RD in the top segment of the retina as the head must be kept in a set position for the majority of time over a 2 week period, the most common position being head down and forward. However, this positioning means it is not suitable for all, as some people find it too uncomfortable to maintain the correct position leading to the failure of retinal reattachment. Incorrect positioning results in pneumatic retinopexy having the lowest success rate of the treatments available.

1.2.3.2 Scleral Buckle Surgery

Scleral buckle surgery is performed by stitching a small piece of silicone or hard plastic onto the sclera which pushes the sclera inwards against the detached segment (Figure 1.5 B). Sometimes a circumferential band is used when multiple, wide or anterior breaks are present, and encircling buckles are used either when breaks cover a large area or are undetectable.[39, 40] These are usually permanent but cannot be seen. Fluid build-up may either be surgically removed or left to be absorbed by the RPE. Pneumatic retinopexy and laser or cryotherapy may be used in conjunction with this technique depending on the severity of detachment.

1.2.3.3 Vitrectomy/ Tamponade Replacement

The final type of treatment is a vitrectomy followed by the insertion of a tamponade which fills the vitreous space. This is the most common treatment in complicated cases or severe RD. The surgical procedure involves the removal of the vitreous which is then replaced with saline followed by the replacement with a gas or silicone oil (SiO) tamponade. The tamponade causes the closure of the retinal tear, forces the retina back into the correct position against the RPE and prevents access of any remaining aqueous to the tear, therefore, inhibiting migration of the aqueous into the subretinal space, excluding any inflammatory factors and initiating retinal reattachment.

1.2.3.3.1 The Tamponade Effect

The ideal tamponade agent would have an "efficient" tamponade effect. The efficiency is dictated by the amount of tamponade contact with the retina and aqueous in the eye. Figure 1.6 shows that both SiO and air float above the aqueous whilst perflurorohexyloctane and Densiron® fill the inferior space but not the superior. Air and perflurorohexyloctane have a flattened top surface and fit into the recess whereas SiO and Densiron® have a rounded top surface and do not fit into the recess space. The interfacial energy of the tamponade determines how the tamponade acts in the vitreous cavity. The hydrophobic nature of the tamponade means it forms a bubble in the aqueous to minimise the surface contact it has with

the aqueous; this also prevents the tamponade agent from migrating through the tear in the retina and acts as a plug instead.
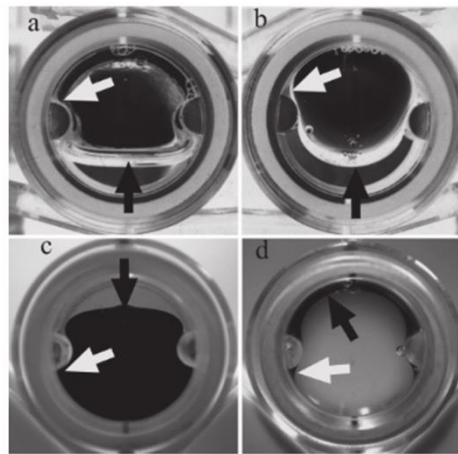
Figure 1.6 Model eye chamber with indents at either side, filled with various tamponade agents (a: air, b: SiO, c: perflurorohexyloctane and d: Densiron®). The white arrows point to filling efficiency of the tamponade agent by the indent and the black arrows point to the top of the bubble.

A total tamponade effect is desirable as this would ensure support of the retina to the RPE for reattachment to occur, however, this is difficult if not impossible to achieve. This is not because of the tamponade itself but because of under filling during surgery, if the eye is considerably under filled this could result in failure of retinal reattachment.[41]

1.2.3.3.2 Gas Tamponade

Currently a number of substances are used as tamponade agents including air, or perfluorocarbon gases. The tamponade effect from gas is reduced quickly due to the short residency time as discussed in Section 1.2.3.1.[42] Perfluorocarbon gases have an advantage over air in that they expand once injected due to diffusion of other gases from the bloodstream, however, if they expand too much this can cause damage to the optic nerve.[43] Perfluorocarbon gases have a longer residency time than air, however, it is still approximately only 2-3 weeks.[42] As with pneumatic retinopexy, gases used as tamponades require patient positioning for a 2 week period during recovery. However, this positioning can be too uncomfortable for patients and can lead to failure of the retinal reattachment.

1.2.3.3.3   Silicone Oil Tamponade

SiO has been used clinically since 1958 as a tamponade agent due to its transparency, low toxicity and chemical inertness within the vitreous cavity, as well as high interfacial surface energy.[43, 44]   SiO is highly hydrophobic, therefore, forms an interface with the aqueous and the hydrophilic retina resulting in exclusion of aqueous from the tear.   SiO has a 75 % anatomical success rate which increases to 85 % for posterior RD; this is relatively high as it is the tamponade agent most often used when long-term retinal support is required, particularly when RD/tears are quite complicated, severe or where PVR (see Section 1.4) is present.[45-47]   The treatment of inferior RD with SiO has been questioned in relation to the coverage of the tear and some surgeons prefer to perform scleral buckle surgery in parallel.   However, studies have found that solely performing a vitrectomy with SiO tamponade replacement is sufficient in treating inferior RD.[48, 49]   Development of a heavier-than-water SiO tamponade (Densiron®) has provided a much more successful treatment option.[50] The chemistry of Densiron® is discussed in Section 1.2.3.3.4.

SiO is the only long term tamponade agent available as its tamponade effects do not dissipate over time, this does mean removal of the SiO is required 2-8 months after the initial surgery.   Disadvantages of SiO include the possibility of oil migrating into the anterior chamber which can lead to damage of the corneal endothelium[51] or cause glaucoma.[52]   Oil can induce cataract formation[53] which is why the lens is replaced in the majority of vitrectomies with SiO tamponade replacements.

Forces at the interface of the SiO with the aqueous or the movement of the retina can cause dispersion, i.e. the breakup of SiO into droplets.   Emulsions can then form if surfactants or cellular debris are present as these will stabilise the SiO droplets.   This can lead to two problems: the tamponade no longer being effective and, if the droplets are small enough, macrophages will be activated and the oil will be engulfed by cells inducing an inflammatory response.[54]

Work is being carried out to reduce the tendency of SiO to emulsify, through tailoring rheological (the higher the shear viscosity, the greater the shearing force required to disperse a tamponade agent into small droplets) and interfacial properties. The viscosity of different types of SiO is expressed in centistokes (1 cSt = $10^{-6}\,\mathrm{m^2/s}$),

and arises from both the molecular weight (MW) and the length of the polymer; increasing SiO molecular weight results in an increased polymer chain length and consequently an increased viscosity. SiOs currently used clinically have a viscosity ranging from 1000 (SiO_{1000}, MW = 37,000 $gmol^{-1}$) to 5000 cSt (SiO_{5000}, MW = 65,000 $gmol^{-1}$) with the majority of clinicians preferentially using a SiO with kinematic viscosity of 1000 cSt. A retrospective study of 24 patients, where a SiO_{1000} tamponade was used, was carried out to determine emulsification rates.[55] It was determined 6 patients had emulsification after 3 months, which increased to 9 patients after 6 months. Another study that investigated emulsification of higher viscosity SiO, found SiO_{5000} to be the most stable with no difference in emulsification when using SiO up to $SiO_{10,000}$. However, SiO_{1000} is usually used as it offers ease of manual injection.[56] The injectability of various SiO, e.g. 1000, 2000 and 5000, as well as blends 56/44 w/w SiO_{1000}/SiO_{5000} and 90/10 w/w SiO_{1000}/SiO 423 000 $gmol^{-1}$, has been studied and it was found that even a small percentage of high MW additive makes it easier to inject than single grade oils with equivalent shear viscosity.[57] This could lead to the development of different varieties of SiO blends for clinical use (fluorinated SiO and semi-fluorinated alkane blends are discussed in Section 1.2.3.3.4). Scott *et al.* investigated the difference between SiO_{1000} and SiO_{5000} in terms of anatomical success and visual acuity.[58] No significant difference was seen between the oils at 6 months, apart from a slight increase in retinal re-detachment when SiO_{1000} had been used to treat RD following trauma.

The advantages of using SiO far outweigh the disadvantages, due to it being the only available long-term tamponade and the normality of day-to-day life during recovery compared with gas tamponades, where patients are required to remain in a set position for up to 2 weeks. No positioning is required due to the specific gravity of SiO being slightly lower than water (0.98 g cm^{-3}) resulting in the SiO floating on top of the remaining aqueous; the buoyancy forces are minimal so it is still an effective treatment for retinal tears in the inferior section of the vitreous cavity.

1.2.3.3.4 *Modified SiO*

Alternatives to SiO have been investigated to find a material which has a better tamponade effect such as copolymers of SiO with fluorinated SiO (SiO-FSiO). The

specific gravity of SiO-FSiO can be tailored depending on the ratio of FSiO/SiO; materials ranging from 1.16 – 2.03 g cm^{-3} were studied.[41] Histological changes to the outer plexiform layer (thinning/loss) and migration of photoreceptor nuclei towards RPE were observed. It was argued that an increase in pressure caused these changes, however, another study investigating intraocular pressure (IOP) with a range of materials found no significant difference compared to normal IOP.[59] Therefore, it is possible that the histological changes observed are due to the exclusion of water. Also, SiO-FSiO with low viscosity (<200 cSt) cause a macrophagic response; however, it is not automatically safe to use highly viscous SiO-FSiO as white deposits on the retina were observed with materials of 1750 mPa.s.[60]

Semifluorinated alkanes (SFA) are being investigated as an additive to SiO; they are transparent and immiscible with water. SFAs act as an amphiphilic surfactant as the hydrocarbon end is highly hydrophobic whereas the fluorocarbon end is less so. The specific gravity of SFAs can be determined by the length of the alkane. Histological studies have been carried out using a rabbit model and no abnormalities were observed with regards to the retina over 3 months.[61] However, the clinical use of SFAs as the sole tamponade agent is restricted because dispersion, which can induce a macrophagic response, occurred within the first 15 days. Therefore, mixtures of SFA with SiO were studied. The solubility of SFA is determined by the viscosity of the SiO and the MW of the SFA and increasing either will reduce SFA solubility. A mixture of SiO$_{5000}$ and perfluorohexyloctane (Densiron®) causes an egg-shaped tamponade to form with the SiO on top and SFA underneath, resulting in good contact only with the inferior retina (Figure 1.6 d).[62] It is hoped that the SiO cap may reduce the tendency of SFA to disperse. Densiron® underwent a successful multicentre clinical trial in Liverpool and Rotterdam with positive outcomes. Kocak and Koc compared Densiron® with SiO$_{1000}$ and observed 84 % and 74 % success rates respectively in terms of retinal reattachment.[50] As this is a heavy SiO (density = 1.06 g cm^{-3}) it can be used to treat inferior RD much more successfully than unmodified SiO.

1.3 RETINAL PIGMENT EPITHELIUM IN PROLIFERATIVE DISEASES

RPE cells make up a critical tissue in the eye and play multiple roles in retinal homeostasis as outlined in Section 1.1.3. Dysfunctional RPE is a key cause of a number of retinal diseases which ultimately lead to visual disruption and/or irreversible vision loss. Diseases involving the RPE may be classified into 3 categories: degenerative, dystrophic and proliferative; however, proliferation of the RPE cells can occur in all categories.[63] A number of different diseases resulting from abnormality in RPE function are described below.

1.3.1 Degenerative Proliferative Disease

Degenerative diseases result from ageing of the eye and include a decline in tissue cellularity and blood flow. In the retina, degenerative effects can result in neurosensory retinal deterioration and RPE cell dysfunction. The most common sight-threatening degenerative disease in developed countries is age-related macular degeneration (AMD), of which there are two different types: dry and wet.[64] Dry AMD occurs as a consequence of the accumulation of cellular debris and metabolic by-products, which then interfere with the photoreceptors in the macular. Wet AMD develops *via* the formation of abnormal blood vessels underneath the macular, leading to cellular dysfunction.[65, 66]

1.3.2 Retinal Dystrophy

Retinal dystrophy is a term which describes a broad (and growing) group of hereditary disorders affecting the retina. It is a term which can be used to describe a number of diseases including pattern dystrophy (PD) and adult-onset foveomacular vitelliform dystrophy (AOFV). PD of the RPE involves the development of a variety of patterns of deposits of yellow, orange, or grey pigment in the macular area.[67] AOFV is a condition that presents completely differently to PD with bilateral, symmetrical, lesions within the macular area in the RPE or between the RPE and photoreceptor layer.[68]

1.3.3 Proliferation of RPE Cells

Proliferation of RPE cells only occurs during foetal development in a healthy eye, however, proliferation can be reinitiated in response to trauma, inflammation or ageing. Proliferation, dedifferentiation and migration of the RPE cells depend on a number of factors: the size of the initial injury, the condition of the RPE-choroid complex, the state of the neuroretina and the interaction with different growth factors, cytokines and proteins.[69-71] Following minor injury to the RPE and photoreceptors, macrophages remove cellular debris. The RPE cells at the edge of the wound proliferate and if they re-establish a continuous monolayer over the Bruch's membrane, proliferation stops. If the injury involves other layers of the neuroretina and RPE, such as RD, the RPE cells in the vicinity of the wound dedifferentiate to mobile proliferative cells of a fibroblastic-like or macrophage-like phenotype and function.[72]

1.4 PROLIFERATIVE VITREORETINOPATHY

Proliferative vitreoretinopathy (PVR) is a condition that can follow a break in the retina where scar-like membrane formation occurs, analogous to dynamic wound healing with respect to inflammation, proliferation and modulation of scar tissue (see Figure 1.7).[73] Formation of epiretinal and subretinal membranes and traction of this scar tissue leads to TRD.
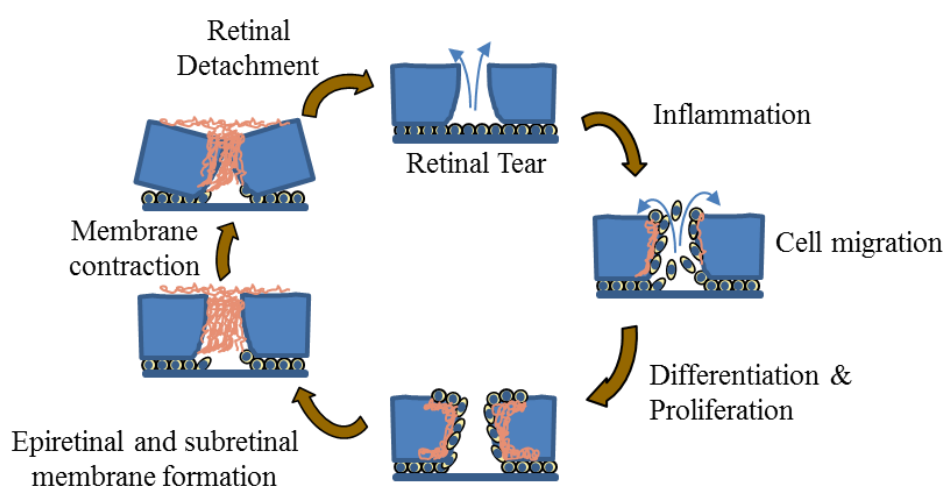
Figure 1.7 Overview of proliferative vitreoretinopathy (PVR) cycle following a tear in the retina: inflammation, proliferation, cell migration and contraction leading to retinal detachment. Adapted from ref:[74]

Traumatic PVR is a consequence at the vitreoretinal interface of a perforating trauma to the posterior segment of the eye, or can happen following surgical intervention.[75] Idiopathic PVR is a complication that follows RRD, especially if there has been a severe retinal tear. PVR occurs in approximately 5-10% of all RRD and re-detachment after surgery occurs in 75 % of these cases making it the most common cause of failure of RRD surgery.[76, 77]

1.4.1 Pathology of PVR

During trauma or RRD, the RPE loses contact with adjacent cells, and consequently loses cellular signalling. RPE then comes into contact with different growth factors and cytokines, triggering the cells to proliferate, de-differentiate and migrate to repair the defect. Dedifferentiation is triggered by the separation of the RPE from the neuroretina and the absence of adjacent RPE. The RPE cells undergo epithelial-mesenchymal transition where the microvilli retract causing a loss of adhesion to the neuroretina and their extracellular matrix (ECM). The cells then round up and detach from their basement membrane.[12, 77, 78] RPE cells then dedifferentiate into a wound repair phenotype, similar to fibroblasts and macrophages which construct a membrane, as they migrate towards the vitreous.[69] This differentiation is regulated by various growth factors (platelet-derived growth factor [PDGF], TGF-ß, epidermal growth factor [EPGF], tumour necrosis factor alpha, FGF and others) as well as cytokines (interleukin-1, 6, 8, 10 [IL-1, IL-6, IL-8, IL-10] and interferon-gamma [IF-γ]).[69, 72, 78-80] RPE cells are the main component of the membranes, however, other cells involved include fibroblasts, which are responsible for tissue repair, in particular scar formation, myofibroblasts and macrophages, as well as minor amounts of glial cells.[79, 81] The resulting membranes contract and distort/pull on the retina leading to TRD.[73, 78]

1.4.2 Current Treatments for PVR

To combat the inflammatory response caused by a break in the retina, corticosteroids are usually administered intravitreously, however, there are no prophylactic measures for the proliferation and migration phase.[82, 83] Surgery called membrane peeling can be performed to remove scar tissue formed during PVR and relieve tractional forces

as well as closing the retina. A vitrectomy is usually performed at the same time as membrane peeling. This type of surgery has a 60-80% anatomic success rate and, of this, 40-80% have functional success.[73, 84, 85] Sigler *et al.*[86] investigated the use of SiO_{1000} in 33 patients where recurrent RD (on average 2.4 previous RD surgeries per patient) had occurred due to PVR. Reoperation under SiO during the initial 6 months, to remove the membranes, resulted in complete success in 29 patients at the 24 month follow up, with visual acuity improved in 25 of these patients.

The reason why there are currently no effective preventative treatments for PVR is partially due to the difficulty of achieving therapeutic drug levels in the vitreous cavity and retina through conventional and systemic routes; this will be discussed later in Section 1.5. It is possible to administer drugs intravitreally or subconjuctivally, however, PVR is a long term complication which requires a treatment period of 4-6 weeks and the half-life of most drugs in the vitreous cavity and subconjuctival is short.[87] Repeated injections could be performed but this can cause complications such as infections, inflammation an elevated intraocular pressure and/or a build-up of drug to toxic levels.

1.4.3 Prospective PVR Treatments

Various pharmacological agents have been investigated to reduce and/or prevent PVR. The two main categories are anti-inflammatory and anti-proliferative drugs, however, antioxidants, antineoplastic and antigrowth factors have also been studied, as well as combination therapies of two or more drugs.

1.4.3.1 Anti-inflammatories

Corticosteroids were among the first anti-inflammatories investigated for PVR. They exert most of their anti-inflammatory response in early stages of inflammation, therefore, before the disease has fully developed.[83, 84] Triamcinolone acetonide (TAA) has been administered intravitreously in a number of *in vivo* studies. [88, 89] Liang *et al.* induced PVR by the injection of macrophages in a rabbit model, and treatment with 1 mg TAA, showed a reduction in PVR by up to 64%.[90] TAA has also been used in collaboration with 5-fluorouracil (5-FU) as both a co-drug powder injected intravitraeously and a co-drug pellet implanted intravitreally. Yang *et al.*

used a rabbit model and observed both therapies (a 10 mg co-drug injected and a 3.3 mg pellet) had no cytotoxic effects and decreased PVR incidence.[91] In human clinical conditions, 100 mg TAA was administered systemically for 5 days, followed by 50 mg for 10 days and 50 mg every other day for 40 days, resulting in weaker effects than experimental conditions where 1 mg intravitreal injections were used.[92]

Other corticosteroids investigated for the treatment of PVR using a rabbit model include: Adriamycin, methotrexate and trifluorothymidine. Adriamycin (1 mg) inhibited proliferation and prevented the formation of membranes, whereas 1 mg of both methotrexate and trifluorothymidine had no beneficial effect.[93] Dexamethasone is another anti-inflammatory which is useful in reducing the BRB breakdown, therefore, allowing an increased amount of drug to pass through to the targeted area.[94] An *in vitro* study with human RPE showed a biphasic effect with respect to stimulating growth at low concentrations (10^{-7}-10^{-6} M) but inhibiting growth at high concentrations (10^{-4} M).[95]

Ibuprofen

Ibuprofen (Ibu, Figure 1.8), chemically known as (±)-(*R*, *S*)-2-(4-isobutylphenyl)-propionic acid, is a non-steroidal anti-inflammatory drug (NSAID).
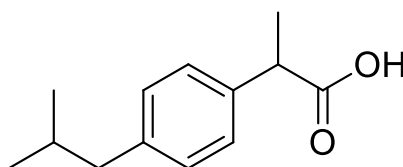
Figure 1.8 Chemical structure of Ibuprofen.

Ibu has been found to be more effective than other NSAIDs, such as aspirin, in pain relief and has a very mild blood-thinning effect in comparison. Ibuprofen has yet to be studied in the context of PVR but its characteristic anti-inflammatory response makes it a candidate of choice to be studied throughout the project.

A double-blind trial of Ibu and aspirin was carried out in 60 soft-tissue injuries in professional footballers. Ibu significantly reduced the severity of pain and allowed training, on average, two days earlier, allowing players to reach match fitness earlier than the controls taking aspirin.[96] Although the exact pathway of how Ibu works as

an anti-inflammatory is unknown, it involves the non-selective inhibition of cyclooxygenase.[97] Rabbit models were used to determine the efficacy of topical administration of Ibu onto the eye. In one study, inflammation was induced by IL-1 and it was found that Ibu inhibited vascular permeability, however, it did not inhibit infiltration of IL-1 into the cells.[98] In another, model paracentesis was induced and it was found that treatment with Ibu reduced inflammation.[99] Ibu is also a nonselective prostaglandin synthetase inhibitor and has been shown to decrease vascular endothelial growth factor (VEGF) signalling when dosed to early postnatal rats at 50 mg/kg. This indicates it could be used as a possible therapy for PVR.

1.4.3.2 Anti-growth Factors and Growth Factor Inhibitors

As discussed in Section 1.4.1, the differentiation of RPE is regulated by growth factors as well as cytokines.[69, 72, 78-80] It is possible to block these growth factors, therefore, altering the pathogenesis and stopping the progression of PVR.[73]

TGF-ß levels in the eye can be correlated with the severity of PVR and is known to be released by RPE cells. TGF-ß has a complex and multifunctional role, and is involved in the regulation of ECM production, membrane contraction and inflammation of RPE. Vitreous aspirates from eyes, with intraocular fibrosis associated with PVR, were studied and more than three times the amount of TGF-ß was measured than in eyes with uncomplicated retinal detachments without intraocular fibrosis.[100] There are three different TGF-ß isoforms TGF-ß1, TGF-ß2 and TGF-ß3. Anderson *et al.* studied the location of the different isoforms within mammalian retinas and found it was the distribution of TGF-ß2 which determined fibroblast formation.[101] TGF-ß inhibitor therapies have shown inhibition of proliferation of RPE cells in numerous animal models as well as humans.[102] Porcine RPE cells were grown on top of bovine corneal ECM to form confluent monolayers. These monolayers were then co-cultured with first passage porcine RPE cells in the presence of various volumes of the confluent cell media as well as different amounts of TGF-ß neutralising antibody (0.1-100 μg/mL). Growth rates of the RPE cells were calculated 72 hours after plating and found it decreased when RPE cells were bathed with the fractions of medium from an adjacent confluent RPE monolayer, and was abolished by adding TGF-ß neutralising antibody (0.1-5 μg/mL). Blocking greater amounts of TGF-ß in the medium with higher doses of antibody (>10 μg/mL) also

inhibited the growth of the newly plated RPE cells, irrespective of media from a confluent cell layer being present or not.[103]

Other inhibitors such as FGF and collagen inhibitors have been explored and found to have dose dependant and time dependant effects on RPE cells. Wang *et al*.[104] investigated the relationship of cell proliferation with basic FGF (bFGF) and EPGF on human RPE (hRPE) cells cultured *in vitro*. They found both regulate cell proliferation but the proliferation effect of EGF was stronger than bFGF when the concentration was above 4 ng/mL. Yasukawa *et al*.[105] investigated the effects of a collagen inhibitor, cis-4-hydroxyproline (CHP), on PVR in a rabbit model. The rate of RD decreased from 89 % to 57 % at 28 days in the presence of 1.7 mg CHP.

1.4.3.3 Antiproliferative Drugs

Antiproliferative drugs are being investigated to inhibit the cell cycle and cellular proliferation which follow retinal damage. Cytotoxic levels have been established as well as antiproliferative effects for a number of drugs such as 5-FU, α-tocopherol, dasatnib, daunorubicin, daunomycin, doxorubicin, mitomycin and RA.

5-FU is one of the most commonly researched compounds as it was one of the first to be tested to stop PVR. It was originally developed as an anticancer drug as it works by altering DNA synthesis through inhibition of thymidine formation.[106] 5-FU has been shown to reduce fibroblastic proliferation, and has a toxic level of $7.7 \ 10^{-6}$ M. However, 5-FU is rapidly eliminated from the vitreous cavity ($t_{1/2} < 3.5$ hours for 1 mg)[107], and its effect slows down after 2 to 4 days of exposure.[95] Therefore, multiple doses are required leading to potential risks as well as dangers of reaching a toxic level. An alternative administration route is the use of a medical device. Borhani *et al*. evaluated a sustained-release using a biodegradable device in a rabbit model of PVR.[108] Devices containing 0.5 mg and 1 mg 5-FU showed significant efficacy in preventing PVR, with the higher-concentration implant being 100% effective in preventing TRD.[108] The use of 5-FU as co-drugs with low molecular weight heparin (an anticoagulant which binds to fibronectin and growth factors) has also been explored and conflicting results reported.[109] Asaria *et al*. carried out a randomised, double-blind, controlled clinical trial and found adjuvant 5-FU and heparin prevented

PVR,[110] whereas Wickman *et al.* carried out a randomised control trial and found no difference between control and treated groups.[111]

Mitomycin is a drug that has been used as a chemotherapeutic and is a DNA cross-linker which arrests the cell cycle without killing cells. Cytotoxic effects have been investigated on RPE cells and it has been found that even 10^{-9} M has significant effects on RPE cell proliferation after 4 days and 10^{-8} M has very significant effects without any toxicity.[95]

Daunorubicin is a topoisomerase inhibitor which prevents DNA and RNA synthesis and inhibits mitotic activity.[112] The toxicity and efficacy of daunorubicin for the prevention of PVR has been investigated by a randomised, controlled clinical trial. It was found that although anatomical success was higher, no significant difference in visual acuity was observed.[113] However, other research has found there to be both anatomical and visual improvements.[114-117] An alternative topoisomerase inhibitor to daunorubicin, which is more appealing due to its decreased toxicity, is aclcainomycin (ALM). Additionally, ALM has no carcinogenic effect compared to 5-FU and daunorubicin making it a good alternative. Morphologic studies of eyes treated with 30 and 60 nmol for 3 days revealed no damage to the retina.[118] Glucosamine has been reported to inhibit growth of many different cell types and have anti-inflammatory effects in ocular disorders making it an ideal candidate for the prevention of PVR.[119-121] Glucosamine has been shown to block TGF-ß signalling, therefore, preventing PVR as discussed in Section 1.4.3.2.[122-124]

Retinoic Acid

The second drug of choice used within this project is all-trans retinoic acid (atRA) (Figure 1.9) due to promising results reported by others in the reduction of PVR and RPE cell proliferation.[125-127]
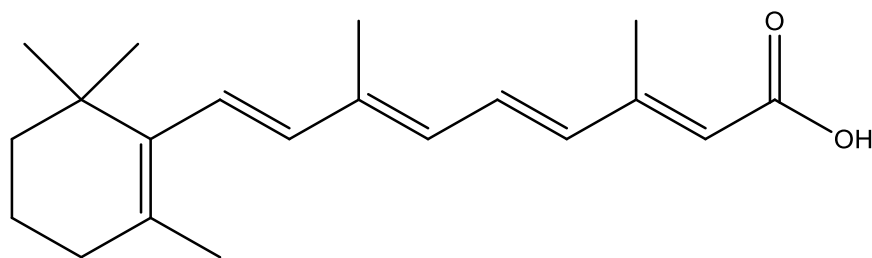
Figure 1.9 Chemical structure of all-trans retinoic acid (atRA).

RA belongs to a family of retinoids including active metabolites of vitamin A as well as a diverse spectrum of synthetic derivatives, which are not closely related to retinol but elicit biological vitamin A or retinoid activity. Vitamin A has many important functions such as: role in vision, immune competence, reproduction, embryonic growth and development and maintenance of epithelial surfaces.[128] Vitamin A plays a crucial role in 2 fundamental processes in vision: phototransduction and the visual (retinoid) cycle of RPE cells (see Figure 1.10). These processes involve photon signals being transformed into electrical signals within the photoreceptor cells (rods, cones and ganglion cells) in the retina as was briefly discussed in Section 1.1.4.
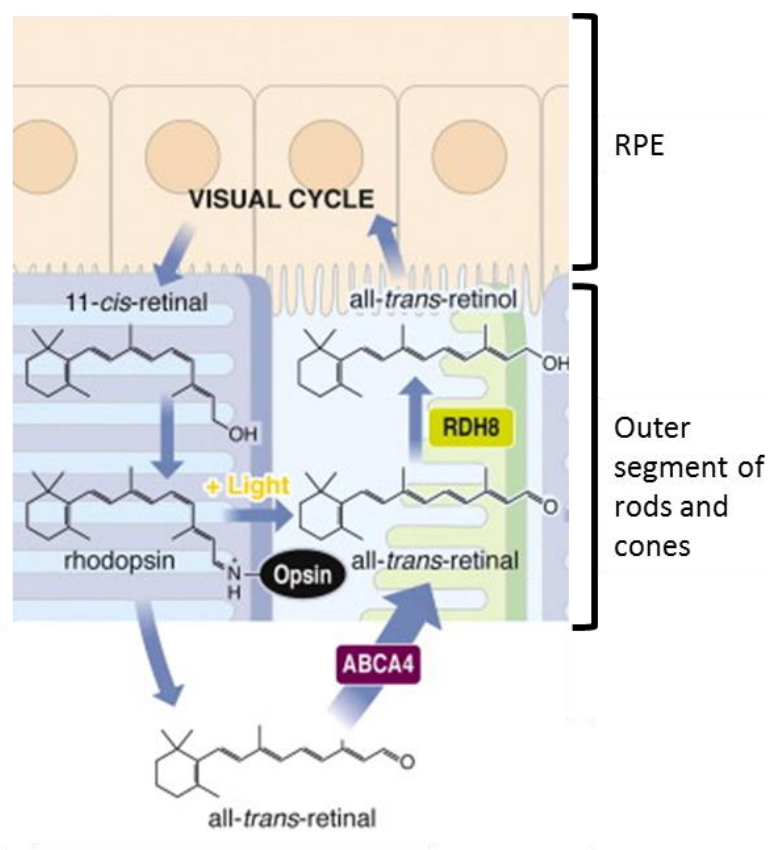
Figure 1.10 Retinoid flow in the visual cycle. Adapted from ref:[129]

Phototransduction involves the photosensitive derivative of vitamin A: 11-cis retinal, which covalently links to opsins to form an inactive, but photosensitive conformation of the retinyldene protein rhodopsin (visual pigment).[129] In humans there are 3 different types of cone photoreceptors that are sensitive to red, green and blue light, these contain slightly different opsins which have a unique interaction with 11-cis retinal, and are sensitive to a specific wavelength (colour) of light.[130] The chromophore in 11-cis retinal leads to the photosensitivity of the opsin which absorbs a photon and photoisomerises to all-trans retinal which no longer fits in the binding site and changes the configuration of the opsin. This leads to a cascade of signal transduction and hyperpolarisation of the photoreceptor cells. Following dissociation of all-trans retinal from opsin it travels into the outer segment and is transferred to the rods and cones *via* a retina-specific ATP-binding cassette transporter called ABCA4 (see Figure 1.10) where it is reduced to all-trans retinol; a process catalysed by NADPH-dependant all-trans retinal dehydrogenase enzyme (RDH8).[131] All-trans retinol is rapidly released by photoreceptor cells to the extracellular space and transferred to the RPE by interphotoreceptor retinoid-binding proteins which contain binding sites for both 11-*cis*- and all-*trans*-retinoids and protect the retinoids from both oxidation and isomerization. All-trans retinol is also taken up from the bloodstream through the basal membranes of RPE cells.

All-trans retinol regenerates 11-cis retinal by a process catalysed by at least 3 enzymes associated with smooth endoplasmic reticulum. All-trans retinol esterified by lecithin retinol acyltransferase is then transformed to 11-cis retinol by retinoid isomerhydrolase (RPE 65) or esterified to form an 11-cis-retinyl ester which stores the pre-isomerized chromophore precursor. The 11-cis retinal travels back to the outer segment of rods and cones where it conjugates with opsin to form rhodopsin, and the cycle can start again.[131-133]

Vitamin A and 11-cis retinal deficiency can lead to short- or long-term visual impairment. A short-term shortage is an uncomfortable but common event, for example, the inability to see at night after passing an oncoming car's bright lights is partially due to the depletion of 11-*cis* retinal in rods. Long-term deficiency, however, can lead to permanent visual impairment.

Vitamin A also has many other important functions such as: immune competence, reproduction, embryonic growth and development and maintenance of epithelial surfaces.[128] The identification of RA receptors within the RPE, such as RPE65 and RAR-ß2, makes it feasible to develop useful drugs to treat retinal and macular degeneration whilst avoiding substantial side effects. Giguere *et al.*[134] and Petkovich *et al.*[135] individually discovered nuclear receptor sites that are specific to RA whilst most had a high affinity for atRA and 9-cis RA, but not 13-cis RA. There are also some receptors that are site specific for atRA which regulate gene expression by binding to short DNA sequences in the vicinity of the target area.

Many studies have shown RA to act as an antiproliferative agent to RPE cells. The cytotoxic effects of RA on RPE cells *in vitro* was investigated and found to be in the range of 10^{-5} M but there are contradicting and imprecise values reported with dependence of the isomer; less than 1×10^{-5} M – 3.33×10^{-5} M (3 μg/mL) and as low as 6.66×10^{-7} M (2 μg/mL) for atRA. [102, 136-138]

Oral doses of RA have been investigated *in vivo*. Chang *et al.* administered 10 mg RA to human subjects twice daily for 8 weeks and found the treated group had significantly lower rates of membrane formation and significantly better rates of ambulatory vision (able to see large objects at close range).[139] Whilst in another study administering 13-cis RA at 40 mg twice daily for 4 weeks, the rate of retinal reattachment was much greater.[140] However, the oral administration of 13-cis RA used for the treatment of acne is linked to mental health issues including increased risk of depression and suicidal tendencies.[141] Oral administration of drugs for treatment of conditions in the eye also have the characteristic disadvantages of any systemic treatment, as well as the added complication of passing through the BRB (see Section 1.1.3 for details).

RA delivered directly to the eye intravitreously or within a SiO tamponade has been investigated in many different animal cell lines such as porcine, bovine, chick, rabbit and cultured primary human RPE cells.[125-127, 136, 137, 142, 143] All studies showed a reduction in PVR when RA is administered. In chick RPE cells it was found that concentrations of 10^{-6}-10^{-7} M for 10 days had an anti-proliferative effect and that there was no difference in viability of the treated and control groups. RA (10^{-5} M)

significantly inhibited PVR membrane formation and TRD (80 %), and significantly inhibited the migration (80 %) and invasion (65 %) behaviours of wound healing human RPE cells.[136] Studies have demonstrated that RA can inhibit proliferation of RPE cells by disrupting some integrin functions such as blocking TGF-ß expression by up to 41 %.[144] Studies by Wu *et al.* involved an *in vitro* model using RPE from excised membranes of PVR and treatment with 10^{-6} M atRA or 13-cis RA; after 12 days only 6.7 % and 9.3 % RPE cells proliferated within a 5 hour time period, respectively,[126] indicating atRA was more effective than 13-cis RA. However, Ariaz *et al.* found that when atRA was administered to cells *in vitro* at 37 °C in light, 60 % had isomerised to 13-cis RA within 1 week.[137]

Many studies have also been performed *in vivo* using rabbit models. Groups that were dosed with 5 or 10 μg (10^{-5} M) RA had significantly less progressed PVR.[137] Nakagawa *et al.*[125] found that 6 μg/mL (2 x 10^{-5} M) atRA and 9 μg/mL (3 x 10^{-5} M) 13-cis RA inhibited PVR to the same extent, therefore concurred with the *in vitro* study performed by Wu *et al.*[126] showed that atRA to be more effective.

1.5 ADMINISTRATION OF DRUGS

In this next section common pathways of drug administration for eye diseases will be discussed, including common topical and systemic administration as well as the more unfamiliar iontophoresis.

1.5.1 Systemic

Systemic administration is a route where the whole body is exposed to the drug, as it is delivered orally or intravenously. Due to the tight junctions within the BRB, most of the administered drug does not pass through into the eye, therefore, high doses are usually required which may have serious side effects on non-target tissue.[43]

1.5.2 Topical

Topical administration involves drug being delivered to surfaces of the body, and eye-drops are a prime example of topical administration to the eye. Advantages of topical drug delivery to the eye are the ease of application and the lack of

invasiveness. Topical application has the disadvantage of poor ocular bioavailability with only 5 % lipophilic drugs and 0.5 % hydrophilic drugs reaching the aqueous humour and even less reaching the retina, but the ease of administration means repetitive dosing is not a problem.[145] Topical administration is primarily used to treat diseases in the anterior or on the surface of the eye as it is an ineffective route for treating diseases in the posterior of the eye, as one of two pathways would need to be taken, i.e. cornea⇨aqueous humour⇨intraocular tissue or conjunctiva⇨sclera⇨choroid/RPE.[146] Eye drops are widely used and repetitive dosing is required as there is rapid clearance by tear drainage which is induced upon administration.[147] Corneal permeability reduces efficacy of eye-drops, however, if the cornea is damaged this could lead to toxic amounts entering the posterior chamber, especially with the variability in dispensing of eye drops.[148] The alternative route to the cornea is *via* the sclera which also has issues of permeability especially with high MW molecules.[146] Eye drops are still widely prescribed despite problems of patient adherence, due to the lack of invasiveness of this route of administration.

1.5.3 Intravitreal Injections

Intravitreal injection is the most common method of drug delivery to treat diseases in the posterior of the eye. An intravitreal injection involves an injection of medicine into the vitreous of the eye. Despite a short drug half-life (only several hours for most low MW drugs) in the vitreous, intravitreal injections are much more efficient than topical or systemic delivery. However, due to the nature of this technique, there are some (low) risks of injuries to the lens, retinal detachment or endophthalmitis (inflammation in the eye).[149] Although it is an invasive technique, current methods of pre-injection of anaesthetics reduce pain for the patient, therefore, it is a much more pain-free and efficient route of drug administration than alternate methods.

1.5.4 Iontophoresis

Iontophoresis provides a local, non-invasive technique to deliver precise amounts of drug to a target area.[150] A specially designed probe generates an electric field which aids penetration of ionised topical drugs across the sclera and cornea.[151] This method

is applicable to a broad range of drugs, however, it is most effective for hydrophilic, negatively charged, low MW drugs.[152]   As for the other delivery methods multiple administrations may be required, which usually leads to low patient adherence, while mild pain is caused in some cases.[153]

1.6 DRUG DELIVERY DEVICES

There are many different drug delivery devices (DDD) currently available for treatments in the eye.   However, there is still a need to develop DDD that target diseases in the posterior segment of the eye such as PVR.   There is also a need for a controlled therapeutic release for a sustained time period to overcome the need of multiple administrations.   Consequently, both implantable and non-implantable devices are currently the object of extensive research.   An ideal DDD would improve drug efficacy, attenuate adverse effects, be biocompatible, be easy to sterilise and would not distort visual acuity.[154]   In this next section a few of the current DDDs available will be discussed as well as those being developed.

1.6.1 Contact lenses

Contact lenses could potentially provide a long term DDD without any modification. It has been shown that soft hydrogel lenses can incorporate drugs upon hydration in an aqueous drug solution.   Drug release from the lenses is dependent on the affinity of the drug to the lens; if it is too high the drug will remain on the lens, if it is too low the drug will be released very quickly.   Collagen corneal shields are similar to contact lenses in the way they are administered, however, the drug is trapped within the collagen matrix when hydrated in an aqueous drug solution.   The drug is only released upon degradation of the collagen, leading to much longer drug exposure time than topical administration or when hydrogel lenses are used.[155, 156]   Contact lenses and corneal shields administer drugs topically, therefore, have all the characteristic disadvantages of topical administration to the eye and those previously discussed for eye drops (see Section 1.5.2).

1.6.2 Inserts

Inserts usually lie in the conjunctival cul-de-sac of the eye between the lower eyelid and the eye so that they are exposed to tears. Inserts have the advantage of increased contact time, therefore improved bioavailability, and possible increased release period with the potential of delivering accurate amounts.

There are three different types of inserts: erodible, soluble and insoluble. Erodible inserts consist of a biodegradable, hydrophobic polymer surface; erosion of this surface determines the release. Soluble inserts consist of a hydrophilic water soluble polymer; if the drug is also hydrophilic the release is controlled by diffusion, but if the drug is hydrophobic, release is restricted by dissolution. Insoluble inserts are made from hydrophobic, water insoluble polymers that will need to be removed once the drug has been released. Two more release systems based on inserts have been described: an osmotic system where drug molecules are dispersed within a polymer matrix and as tears enter the matrix the drug is dissolved and released, and a membrane controlled release system where a drug core is surrounded by a hydrophobic membrane which controls diffusion.[157]

Inserts usually treat conditions in the anterior of the eye. Infection and inflammation would require a high dose for a short period of time whereas glaucoma would require a low dose over a sustained period of time. The first controlled release ocular insert that entered the market was Ocusert® in 1975.[158] Ocusert® is a reservoir model (drug coated with an ethylene vinyl acetate membrane) used to treat glaucoma by releasing pilocarpine hydrochloride over 7 days. However, clinical use is not widespread due to complications with insertion and removal as well as side effects arising from continuous drug exposure. In Russia, a soluble ophthalmic drug insert SODI® is used to treat a variety of diseases with antibiotics or anti-inflammatories. It consists of a thin film of acrylamide, N-vinylpyrrolidone and ethyl acetate copolymer which degrades and releases drugs over several hours; due to this short release time scale SODI® is restricted to Russia and the East.[159] As well as delivering drugs to the eye, inserts can provide platforms for the release of materials to combat keratitis (dry eye). In 1981 Lacrisert® became commercially available.[160]

It consists of hydroxypropyl cellulose which dissolves into the tear film, thickening it and providing lubrication and protection for the eye.

1.6.3 Colloidal Drug Carriers

Colloidal drug carriers discussed here include liposomes and micro/nano-particles. The benefits of using a colloidal drug carrier are: stabilisation of drug, increased drug half-life, localised delivery, and decreased toxicity by minimising the burst release profile seen for many drugs. In recent years there has been an exponential growth in the number of patents filed for the application of nanotechnology in ophthalmic drug delivery.[161]

1.6.4 Implants

Intraocular implants require either surgery or an injection to place the DDD intravitreally. The benefits of implants include avoiding the BRB to deliver drug directly to the area required, and avoiding side effects related to systemic treatments or repeated administration. Implants aim to provide a prolonged controlled drug release from a polymeric material. There are 3 different categories of implants: monolithic, binding polymer hydrogel and reservoir structure (Figure 1.11).
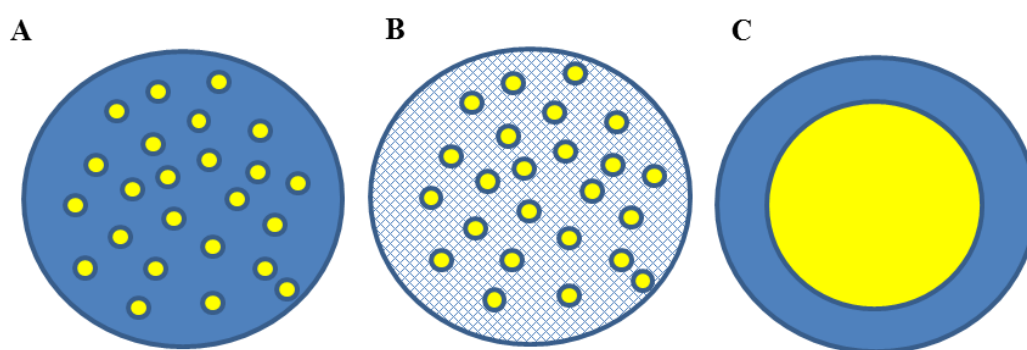
Figure 1.11 Schematic of implants. From left to right: A:monolithic, B: binding polymer hydrogel and C: reservoir structure.

The monolithic type contains a homogenous mix of polymer and drug. A binding polymer hydrogel (three dimensional network of cross-linked hydrophilic polymer) chemically or ionically binds to drugs which are then released by enzymatic hydrolysis of inter- and intramolecular bonds of the polymer.[157] Finally the reservoir

structure consists of an outer shell of polymer coating an inner drug core. Implants can be in an injectable form of colloidal or gelling solutions or an implantable plug, disc, pellet, rod or sheet.

The ocular implants can either be synthesised from non-biodegradable or biodegradable polymers. Non-biodegradable implants can provide a more constant prolonged drug release period than biodegradable equivalents, however, they require surgical removal. Non-biodegradable polymers often used include poly(hydroxyl ethyl methacrylate) (pHEMA), polyvinyl acetate (PVA), ethylene vinyl acetate, methylcellulose and polyacrylamide, due to their biocompatibility.[162-166] Biodegradable polymers frequently used in implants include polylactic acid (PLA), polylactic-*co*-gycolic acid (PLGA), polyanyhdrides, or polyorthoesters, and hydrogels that mainly consist of collagen, gelatin, albumin, chitosan, starch or dextran.[165] The hydrolysis of these polymers produce carbon dioxide (CO_2) and water, *via* the Kreb's cycle, which are then adsorbed by the surrounding tissue.[167] Intravitreal implants currently available on the market include non-biodegradable Vitrasert® which delivers ganciclovir for 8 months, Retisert® which delivers fluocinolone for up to 2.5 years and Illuvien® which delivers fluocinolone acetonide for 3 years.[168-170] Ozurdex® is a biodegradable implant which delivers dexamethasone for up to 6 months.[171] Stimuli responsive implants are currently being investigated, which are light activated, mini pump or magnetically modulated.[172-176] Implants that are not placed intravitreally include punctal plugs which are implants that are inserted in the tear duct to prevent liquid drainage from the eye.[177]

Gene therapy is an option where genetically modified cells release different therapeutic proteins and growth factors; these cells are isolated within a device and inserted intravitreally. NT-501 is a device currently undergoing phase II clinical trials within the EU and US, in which genetically modified cells are grown onto a poly(ethylene terephthalate) scaffold to secrete ciliary neurotrophic factor, for the potential treatment of retinitis pigmentosa and age-related macular degeneration.[178]

1.6.4.1 Microparticles and Nanoparticles

Microspheres, microcapsules and their nanoscale equivalents are made from micro/nano particles, respectively. They have been investigated for ocular drug

delivery *via* implantation into the vitreal cavity. Micro/nano spheres involve the physical homogeneous dispersion of drug within a polymer matrix whereas micro/nano capsules consist of a drug core surrounded by a polymer coating (Figure 1.12). These colloidal drug carriers were initially used to prolong release of topically applied drugs and overcome solubility issues, however, with the use of microspheres the increase in bioavailability was insignificant,[147] therefore, research progressed to intraocular administration.
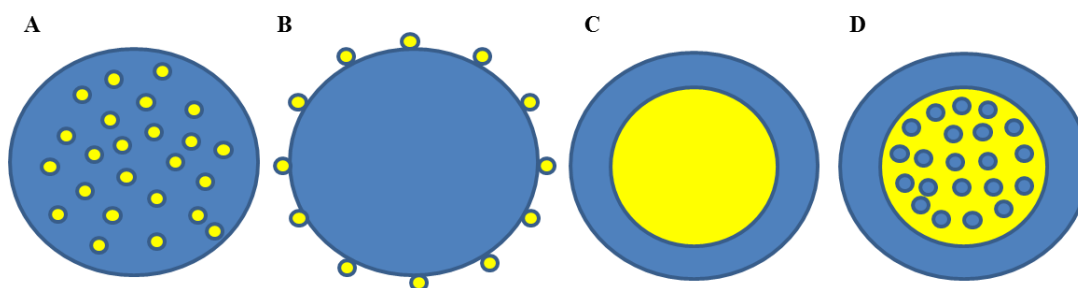
Figure 1.12 Schematic of micro/nanoparticles. From left to right: A: sphere with drug dispersed B: sphere with drug absorbed, C: capsule, D: capsule with drug dispersed.

Biodegradable polymers with bio-adhesive properties such as PLA, polyglycolic acid (PGA) and the PLGA have been used in this context. They attach to biological tissues leading to the drug being released close to the target area and have been shown to be intravitreally biocompatible over a 12 week period.[179] The encapsulation technique used to synthesise micro/nano-spheres depends on the hydrophilic/lipophilic nature of the drug.[180] Drug release can then occur by two different mechanisms: diffusion through the polymer matrix and polymer hydrolysis/bulk erosion. For PLGA, drug release is affected by drug solubility, fast degradation of short polymer chains and change in water content of PLGA. These result in a burst release followed by a lag phase then a pulsatile flow as erosion occurs. A 24-hour burst release of sodium fluorescein, which is highly hydrophilic, was observed,[181] whereas RA, a lipophilic drug, had a constant release from PLGA microspheres over 30 days.[138] The release profile from PLGA can be tailored upon variation of MW and degrees of polymerisation (DP_n).[159] The ratio of PLA to PLG within a 5,000 gmol^{-1} PLGA copolymer has been investigated using rhodamine as a model drug over a 30 day time period. It was observed that a 50/50 copolymer led to a much faster burst release with 80 % of the rhodamine released after 15 days whilst the 25/75 copolymer had only released 60 % at 30 days.

There have been many animal studies investigating the use of colloidal carriers injected intravitreously which provided non-toxic, therapeutic amounts of drug to suppress inflammation, proliferation and infection.[182-185] Evidence for potential intracellular drug delivery to RPE cells has been shown using a rat model where nanoparticles were found to be in the cytoplasm of the RPE cells, 4 months after an intravitreal injection.[154] In another study, microspheres coated in gelatine have been phagocytosed by RPE cells (phagocytosis is one of the functions of RPE cells, see Section 1.1.4).[186] A particular concern of utilising nanotechnology for drug delivery in the eye is that the nanoparticles may be cleared relatively quickly *via* the periocular circulation route, even before drug release has occurred. It has been found that nanoparticles of 20 nm have a very rapid clearance whilst those of 200 nm are cleared only after several weeks.[187]

1.6.4.2 Liposomes

Liposomes are biocompatible, amphiphilic vesicles made of a lipid bilayer as depicted in Figure 1.13. They can transport both hydrophilic and lipophilic drugs in the aqueous compartment and membrane respectively. Liposome properties can be tailored to different size, lipid content and surface charge; it is the surface charge which seems to determine uptake by the cornea.[188] Liposome uptake by the cornea is greater for positively charged liposomes and least for neutral materials. It has been reported that transport within a liposome helps increase drug efficacy up to 10 fold, while leading to a better control of release rate at the same time.[189-192] Habib *et al.* reported a 36 % increase in the delivery of fluconazole across the cornea when liposome drug carriers were used.[193] The inclusion of markers and receptors within the liposome membrane is currently being investigated to allow active targeting of different cells as well as laser or heat induced release.[194, 195]

Hydrophobic Region/ Membrane

Hydrophilic Region / Aqueous Compartment
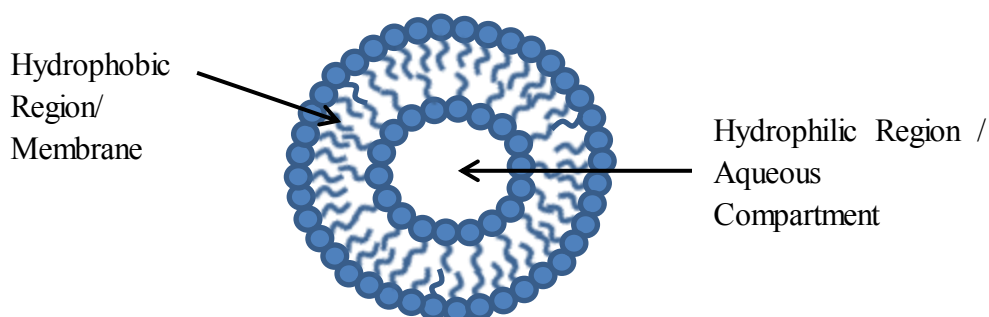
Figure 1.13 Schematic of a liposome.

1.6.5 Explants

Explants are DDDs attached to the outside of the eye, an example of which is a scleral buckle modified to release drugs; a solid non-biodegradable silicone band which can be removed after 1 year has been used.[196, 197] A hydrogel buckle made from poly(methyl acrylate-co-2-hydroxyethyl acrylate) which has the advantage of swelling in water, therefore, can act as a reservoir for hydrophilic drugs could also be used.[197-199]

1.6.6 Vitreous Substitute

An ideal vitreous substitute must meet a number of requirements: be transparent, have long term biocompatibility, have a high water/tamponade interface surface tension, be able to conform to irregular surfaces, have a low viscosity and properties which lead to low (if any) emulsification; many of these properties are often mutually incompatible.[44] Lin *et al.* saw a synthetic foldable vitreous substitute go to a 3 month clinical trial with positive results in flexibility, effectiveness and safety.[200] A vitreous substitute could also be used as a drug reservoir. Zheng *et al.* loaded a foldable vitreous substitute with 5-FU and saw a sustained release for up to 56 days both *in vivo* and *in vitro*.[201]

An alternative to vitreous substitutes are tamponade agents such as gas and SiO which were discussed in Section 1.2.3.3 for the treatment of RD. A SiO tamponade could be an ideal candidate for drug delivery to the posterior of the eye, as it could act as a drug reservoir. However, the majority of drugs such as triamcinolone and daunomycin as well as antigrowth factors and growth factor inhibitors are water soluble, therefore, do not have high (if any) solubility in SiO. Studies investigating the use of SiO as a reservoir for the extended delivery of many lipophilic drugs such as 5-FU, RA, α-tocopherol and acetylsalicylic acid have been carried out. Lipophilic 5-FU has been shown to rapidly clear from SiO with $t_{1/2} < 3.5$ hours for 1 mg.[107] N_1-alkoxycarbonyl prodrugs with 5-FU which are soluble in SiO have been synthesised. A prodrug is a compound that upon administration must undergo chemical conversion by a metabolic process to become an active pharmacological agent, ideally at efficacious levels without adverse effects (prodrugs will be discussed in more in detail in Section 1.8).[202] The release of drug is prolonged in this case as the

prodrug has to diffuse to the edge of the bubble and hydrolyse to release the drug; release of 5-FU was prolonged but was still under 2 days.[107] Co-drugs of 5-FU and RA have also been developed which have a $t_{1/2\ release}$ of 5.8 days which is promising but would need further modification to reach the desired 6-8 week treatment period for PVR.[203] Animal studies with α-tocopherol[204] and acetylsalicylic acid[205] dissolved in SiO have resulted in higher and prolonged retinal concentration of both drugs compared to delivery *via* a intravitreal injection.

1.6.7 Limitations of DDDs

Although all the DDDs discussed have many advantageous properties, there are still some disadvantages and more developments which need to be made. The limitations of the DDDs are summarised in Table 1.1.

Table 1.1 Table to summarise the limitations of different drug delivery devices.

Drug Delivery Device	Disadvantage	Reference
Contact Lens	Limitations in drug content and release amounts	151
	Diminished visual acuity	195
	Diminshed drug delivery to anterior segment	144
Liposome	Release of drug too quickly if burst or damaged	85
	Cloudiness in visual field	156
	Cataracts and inflammation	196
Micro- and Nano-particles	Clearance can occur before drug delivered	172
	Incorporation into RPE *via* phagocytosis	185
	Blockage of trabecular meshwork which leads to increased intraocular pressure and glaucoma	205
	Difficult to reverse if adverse effects after incorporation, may need to remove cells which might lead to a condition more severe than that being initially treated	166
Insert	Can leak drug	206
	Can dislocate and become lost which causes blurred vision and discomfort	207
Implant	Invasive procedure	195
	May need removal	208
Explant	Can cause infections	196
	May need removal	209
Vitreous substitute	Invasive procedure	43
	May need removal	43

1.6.8 Current PVR DDD Research

PVR requires a treatment period of 4-6 weeks which makes it an ideal candidate for treatment using a DDD.[87] This section will discuss some of the DDDs previously discussed with the aim of prevention/treatment of PVR.

Rabbit models with antiproliferative drugs encapsulated in liposomes have shown a significant improvement of the intravitreal drug half-life, therefore, improving drug efficacy as well as generating a decrease in toxicity. These studies also showed flaws in liposomal drug delivery such as cloudiness in the vision due to the size of the liposomes, possible cause of cataracts as well as risks of infection when administered and inflammation, which could induce PVR. Sustained delivery of RA from microspheres of 50/50 PLGA was seen in a rabbit model for up to 40 days.[138] Giordano *et al.* also demonstrated that the same amount of drug injected directly would have a toxic effect whereas when injected within the microspheres there were no histological abnormalities or cytotoxic effects.[138]

Scleral plug implants have been used to release drugs with beneficial impacts of reducing PVR within rabbit models. Yasukawa *et al.* investigated the use of a scleral plug synthesised with PLGA incorporating the antiproliferative drug cishydroxy proline for the treatment of PVR in rabbits. After 28 days they found a 48 % decrease in the prevalence of PVR compared with equivalent intravitreal injections of the drug.[105]

Utilising a SiO tamponade as a drug reservoir for treatment would be ideal as it is usually used in complicated RD where PVR is more likely to occur or already exists. It has also been suggested that the ideal drug delivery system is not only intravitreal but has a double benefit as it acts as a tamponade agent.[206] Many studies have already taken place solubilising lipophilic drugs into SiO (see Section 1.6.6), including 5-FU and RA, where the drug diffuses to the interface of SiO and is released into the surrounding aqueous.[107, 137] However, 98 % of RA, and the majority of 5-FU, is cleared from SiO within 1 week,[137, 207] therefore, drug modification is required to develop a truly sustained release.

1.7 RESEARCH OBJECTIVES

The work presented here focuses on developing a sustainable drug delivery system for the treatment of PVR utilising the SiO tamponade agent as a drug reservoir. SiO is the only long term tamponade agent clinically available, therefore, can be present in the eye for the 4-6 week treatment time PVR requires. Lipophilic drugs must be chosen for this project as water soluble drugs do not have high (if any) solubility in

oil. The two drugs chosen to be investigated throughout this research are Ibu and atRA. Ibu was chosen as its characteristic anti-inflammatory response may be able to reduce PVR, and Ibu has yet to be studied in the context of PVR. atRA was chosen due to the promising results previously reported by others in the literature in reducing PVR and RPE proliferation, as well as previously being administered *via* a SiO tamponade.[125-127] To develop a long term release system prodrugs will also be studied, and these are discussed in Section 1.7.1.

1.7.1 Prodrugs

Albert[208] and Harper[209] introduced the concept of a prodrug as a compound that on administration must undergo chemical conversion by a metabolic process to become an active pharmacological agent ideally at efficacious levels and without adverse effects (see Figure 1.14).[202] The model involves a parent drug molecule attached to a pharmacologically inactive pro-moiety deeming the whole system inactive. Prodrugs aim to overcome pharmaceutical problems (poor solubility, chemical instability of drug molecule, unacceptable taste or odour), pharmacokinetic issues (insufficient absorption/permeability, dosing frequency, toxicity) and pharmacodynamics problems such as lack of selectivity at the site of requirement.[210, 211]
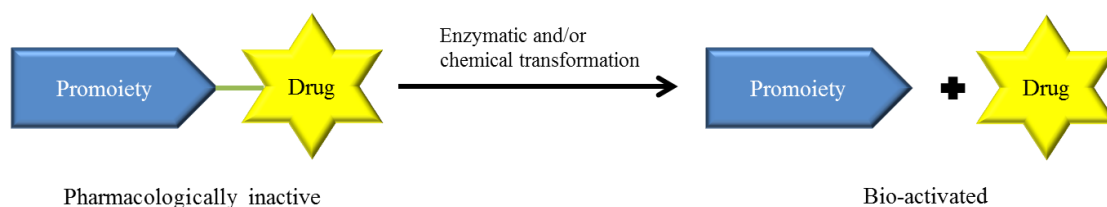
Figure 1.14 A schematic illustration of the prodrug concept.

The prodrug can be bio-activated either intracellularly or extracellularly by an enzymatic or chemical transformation.

1.7.2 Prodrug Bond

Release of drugs solubilised in SiO is primarily determined by the diffusion rate of drugs through the oil. Araiz *et al.* reported 98 % clearance of atRA from the eye (using a rabbit model) within 7 days.[137] Prodrugs could prolong drug release as the

rate of release will be determined by the cleavage of the bond linking the drug to the non-drug component.[212]   Many different bonds are currently used in prodrug synthesis and the most common bonds used with drugs such as atRA and Ibu, that contain carboxylic acid functional groups are shown below in Figure 1.15.
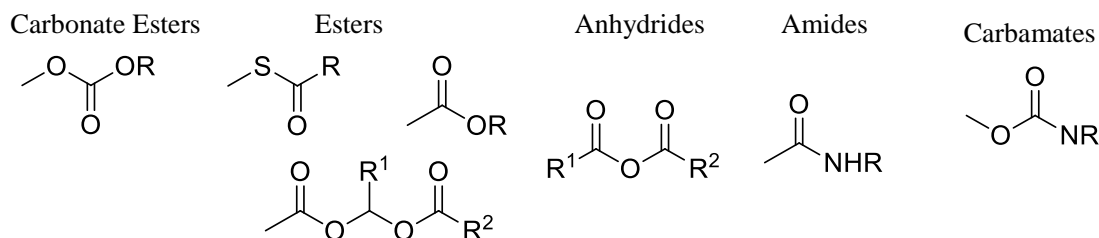
Figure 1.15 Common functional groups within prodrugs when a carboxylic acid is present on parent drugs.

As well as those shown above, some other linkages which can be utilised in various prodrugs include:

i.   Schiff Bases - Müller *et al*[213] investigated acid sensitive Schiff bases which are stable at pH 7.4 but for which acid-catalysed hydrolysis occurs at pH 5 to release drug.[210]   Kratz *et al* reviewed acid-sensitive drug-polymer conjugates recently developed and future aims within this research field.[214]

ii. Peptide linkers - enzymatically degraded to parent drug molecule and carrier.[215]

iii. Disulphide bridges - Bio-activate *via* intracellular disulphide exchange with a thiol such as glutathione.[216, 217]

iv. Hydrazone linkers - Display stability under a wide range of conditions yet undergo covalent exchange reactions in the presence of an acid or nucleophile catalyst such as in endosomal and lysosomal compartments which have a pH of 4 - 6.5.[218]

v.   Hydrolysable Linkers - amide[212, 219, 220], anhydride[221-224] and ester[211, 212, 225-227] bonds bio-activate when they are exposed to water.

In this project, prodrugs bio-activated extracellularly will be investigated, as activation is hypothesised to take place at the SiO/aqueous humour interface and within the aqueous humour itself.   Figure 1.16 shows the proposed drug release mechanisms for this project when a hydrophilic pro-moiety (poly ethyleneoxide

[PEO]) is used. The PEO will drive the diffusion of the drug towards the aqueous interface, the rate of the bio-activation (cleavage of the bond) will then determine the rate of release of drug from SiO into the aqueous humour, or within the aqueous humour with the hope of a prolonged time period.
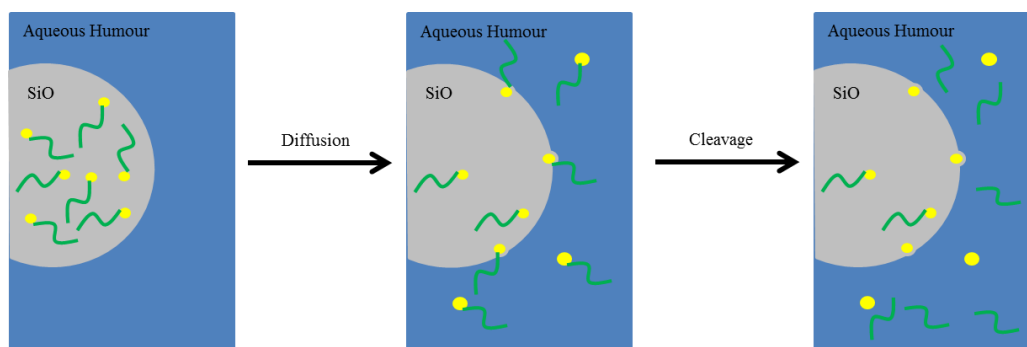
Figure 1.16 Proposed mechanism of the PEO prodrug and the bio activation of the drug at the SiO/aqueous humour interface and within the aqueous humour.

As the cleavage of the covalent bonds is expected to take place at the SiO/aqueous humour interface and within the aqueous humour it is important to try and determine the composition of the aqueous humour and determine the potential cleavage factors present.

1.7.2.1 Aqueous Humour

Aqueous humour flows around the eye and contributes to the homeostasis of the eye by providing nutrients, removing metabolites, transporting neurotransmitters and stabilising the ocular surface (see Figure 1.1).[228] There are very limited reports in the literature about the composition of aqueous humour, due to a general reluctance to take samples of aqueous humour from patients in case harm is caused; unfortunately the information which is available is contradictory.[229] General consensus of composition is: amino and ascorbic acid, bicarbonates, carbohydrates, carbon dioxide, chlorides, glucose, glutathione, inorganic ions, lactic acid oxygen, proteins, urea and water.[228, 230-233] Flow rates of approximately 3 μL/min in the morning and 2.4 μL/min in the afternoon have been reported, while during sleep it slows to 1.5 μL/min.[234] This may affect the cleavage of bonds within prodrugs if the presence of a certain concentration of cleavage factor is required. The literature also states that aqueous humour is different in healthy eyes and eyes with pathological

diseases,[235] in particular those with PVR.[236] As the amount of information available for the composition of aqueous humour for patients with PVR is minimal and contradictory, it was decided a simple ester linkage would be used within these prodrug studies. This allows solely the presence of water to bio activate the prodrug.

An ester is usually prepared by reacting an hydroxyl functional group with an acid group. While both our drugs bear a carboxylic acid, the polymers chosen as the pro-moiety either contain a hydroxyl function by nature, like PEO, or can be purchased already functionalised, like polydimethylsiloxane (PDMS), which removes the need for any modification prior to the esterification step. Ester prodrugs are also the most common ophthalmic prodrugs, as esterases (types of enzymes responsible for cleaving ester bonds within the body) are known to be present in the eye.[227] The use of an anhydride as the linker was not considered as these bonds are extremely water sensitive (more so than an ester bond), therefore making it difficult to carry out future experiments without degradation; this would become particularly problematic if the prodrug was chosen to be used clinically, as sterilisation (see Chapter 2, Section 2.3 autoclave degradation) may also need to be carried out.

1.7.3 PEO

The ideal polymer to incorporate into a prodrug should be biocompatible (non-toxic, non-immunogenic, contained within FDA approved medicines for internal consumption and preferably biodegradable), able to transport required drug dosage, inexpensive, protect the drug against premature metabolism, display active/passive targeting and be able to bio-activate at a rate appropriate to the desired dosing frequency.[237, 238] PEO is a "popular" polymer with a broad range of uses in everyday products, industrial applications and within biomedical drug delivery systems and its structure is presented below in Figure 1.17.
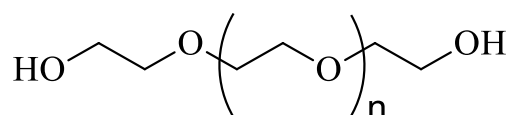
Figure 1.17 Structure of poly(ethylene oxide) (PEO).

PEO products have been on the market for 25 years and it is the most commonly used non-ionic polymer in the field of polymer based drug delivery.[239] Table 1.2 gives some examples of PEO based prodrugs currently available on the market including Macugen and Zioptan™ which are used ophthalmically.

Table 1.2 PEO based prodrugs currently available on the market and some being developed. Includes ophthalmic prodrugs Macugen and Zioptan™. Table adapted from refs: [239, 240]

Product Name	Prodrug	Disease	Company	Stage
Adagen	PEO-Adenosine deminase	Severe combined immune deficienct syndrome	Enzon Inc.	Market (1990)
Cimzia ™	PEO-anti - tumor necrosis factor - α	Rheumatoid arthritis, Crohn's disease	UCB S. A.	Market (2008)
Macugen	PEO-aptamer	Age-related macular degeneration	Amgen	Market (2004)
Mircera®	PEO-erythropoietin	Anaemia associated with chronic kidney disease	Roche Products Ltd.	Market (2007)
Neulasta™	PEO-granulocyte-colony stimulating factor	Chemotherapy- induced neutropenia	Amgen Inc.	Market (2002)
NKTR-102	PEO-irinotecan	Cancer- metastatic breast	Nektar Therapeutics	Phase III
Nalexogel	PEO-naloxone	Opioid-induced constipation	AstraZeneca	Market (2015)
Oncaspar®	PEO-Asparaginase	Acute lymphotcytic leukaemia	Enzon Inc.	Market (1994)
Pegasys®	PEO-interferon –α,ß- Hepatitis C	Hepatitis C	Hoffmann- La Roche	Market (2002)
PEGIntron	PEO-interferon-α,ß- Hepatitis C	Hepatitis C	Schering-Plough Corp.	Market (2000)
PEG-SN38	Multiarm PEO-camptothecan derivative	Cancer- various	Belrose Pharma Inc.	Phase III
Puricase	PEO-uricase	Gout	Savient Pharmaceuticals Inc.	Market (2007)
Zioptan™	PEO-tafluprost	Increased intraocular pressure due to glaucoma	Merck	Market (2012)

PEO is synthesised by an anionic polymerisation of ethylene oxide, initiated by nucleophilic attack of a hydroxide ion on the epoxide ring, resulting in a very narrow dispersity polymer.[240] The narrow dispersity is important for reproduction of the polymer and examination of clearance pathways. Low number average molecular weight (M_n) PEO is preferred, below 40,000 $gmol^{-1}$ but above 400 $gmol^{-1}$, as oxidation leads to a diacid and hydroxyl-acid metabolites, which can cause toxicity problems and clearance issues.[239] PEO has been shown to be removed from the body *via* a combination of renal and hepatic pathways as long as it is below

40,000 - 50,000 $gmol^{-1}$; above this M_n it would compromise the renal filtration system.[241, 242]   When using a hydrophobic drug, the hydrophilic-lipophilic balance of a polymer conjugate can be varied depending on the M_n of the PEO. Increasing M_n increases solubility in water and most organic solvents,[243] and the terminal hydroxyl groups provide a labile site for covalent attachment to drugs as discussed in Section 1.7.1.

1.7.4 atRA in Prodrugs

atRA is susceptible to degradation in light, air, high temperatures and when in solution, therefore, synthesising an atRA prodrug can be problematic.   Currently there are a number of methods in the literature to synthesise atRA-conjugates with condensation reactions, however, only a 40-48% yield is achieved,[244] also reported are acyloxyalkyl[245] and acyl chloride esterifications.[246]   The Steglich esterification method (discussed in more detail in Chapter 3, Section 3.3.2) was used by Wang *et al.*[247]   to   synthesise   a   methoxy-poly(ethylene   glycol)-*b*-poly(lactide-co-2,2-dihydroxymethyl propylene/atRA/cisplatin) esters and drug release was investigated. Micelles were prepared at a 1:1 ratio of atRA and cisplatin conjugates and release was measured *via* UV-Vis spectroscopy.   Although both atRA and cisplatin were released at neutral, acidic and basic pH, release of atRA was always slower.

1.7.5 Ibuprofen in Prodrugs

Ibu has been used to produce anhydride and ester linked prodrugs.[224, 248, 249]   Abu Zanat *et al.*[249] synthesised two Ibu prodrugs: Ibu-2-hydroxylethyl ester and the co-drug: 2-(2-(4-isobutylphenyl) propanoyloxy) ethyl nicotinate hydrochloride *via* an acyl chloride esterification. It was observed that the rate of hydrolysis of co-drug and Ibu-2-hydroxyethyl ester is influenced by pH. The co-drug's susceptibility to hydrolysis increased as pH increased toward the alkaline range, however, the opposite was true for the hydrolysis of Ibu-2-hydroxyethyl ester which was more reactive at low pH values. A prodrug of PEO-Ibuprofen was synthesised utilising the coupling agent 1,1'-carbonyldiimidazole (CDI) to form a diester (Ibu was attached to both ends of the PEO) with various M_n of PEO including 1,000 and 2,000 $gmol^{-1}$, with yields of 75 and 88 % respectively.[248]

1.7.6 Project Challenges

Key principles requiring investigation during this project include: toxicity of drugs on RPE, determination of an accurate method to measure drug solubility within SiO and release of drugs, and development of a tailored release of therapeutic amounts of drug over a prolonged treatment period of 4-6 weeks.

Drug characterisation and biological evaluation of atRA and Ibu on RPE to determine toxic thresholds and antiproliferative effects of the drugs will require studying using cultured RPE cells.

Synthetic aims include the investigation of linear end group modification of polymers to form prodrugs. The use of both a hydrophilic and lipophilic pro-moiety within prodrugs will be investigated as well as different amounts of substitution and different DP_n of the pro-moiety. The solubility of the prodrugs will be investigated as well as the cleavage of drugs from the prodrugs and release from SiO. Solubility of both atRA and Ibu in SiO will need to be accurately determined to be able to compare the effects of using the prodrugs to free drug. The objectives of this project are illustrated in Figure 1.18.
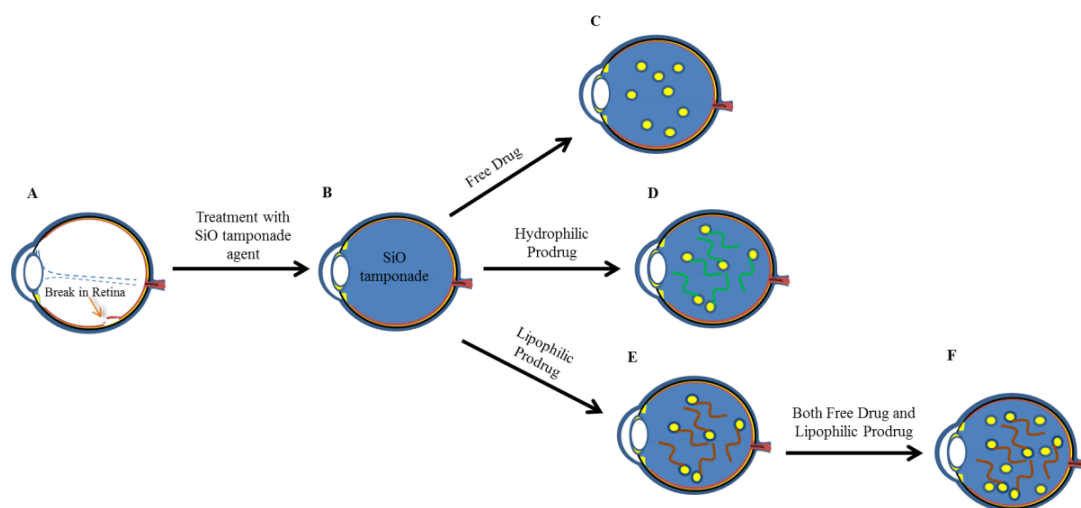
Figure 1.18 Illustration of the objectives of this project A: detached retina, B: treatment with SiO tamponade, C: drug dispersed within SiO, D: Prodrug with hydrophilic (PEO) pro-moiety dispersed within SiO, E: Prodrug with hydrophobic (PDMS) pro-moiety dispersed within SiO, F: mixture of drug and prodrug with PDMS pro-moiety within SiO tamponade.

As discussed, a detached retina (Figure 1.18 A) can be treated with a vitrectomy followed by insertion of a SiO tamponade (Figure 1.18 B). The solubility of drug on

its own within SiO (Figure 1.18 C) will be investigated so a comparison can be made when prodrugs are used, with the aim to determine if drug concentration increases or decreases when attached to both a hydrophilic and hydrophobic pro-moiety. Release profiles of free drug from SiO will also be determined so effects of prodrug on release can be investigated. Figure 1.18 D represents the prodrug with a PEO pro-moiety; the proposed mechanism for the bio-activation of the drug was shown in Figure 1.16. The PEO will drive the drug to the SiO/aqueous interface where it will either cleave leaving some drug within the SiO to diffuse out, or cleavage will occur within the aqueous humour. In both of these scenarios PEO would be a side-product of the drug delivery system within the aqueous humour. The rationale to use a hydrophobic pro-moiety came from this as a hydrophobic component would remain within the oil, and cleave at the interface, leaving only the drug to travel into the aqueous humour. The pro-moiety would then surgically be removed along with the SiO tamponade. Figure 1.18 E represents the lipophilic prodrug, and Figure 1.18 F represents drug dispersed within SiO in the presence of the prodrug; the effects of the hydrophobic pro-moiety with respect to solubility of drug will be investigated as well as the effects on release.

1.8 REFERENCES

1. R. L. Gregory, in *Eye and Brain: The Psychology of Seeing*, Princeton University Press, New Jersey, Fifth edn., 2015, pp. 24-67.

2. U. Welge-Lüen, C. A. May, A. S. Neubauer and S. Priglinger, *Current Opinion in Ophthalmology*, 2001, **12**, 94-99.

3. H. Kolb, in *Webvision The Organisation of the Retina and Visual System*, University of Utah, http://webvision.med.utah.edu/book/part-i-foundations/simple-anatomy-of-the-retina/, Accessed 17.1.2015.

4. J. V. Forrester, A.D. Dick, P. G. McMenamin and W. R. Lee, in *The Eye: Basic Sciences in Practice*, W. B. Saunders, London, 2nd edn., 2002, pp. 15-58.

5. Z. Chaudhuri, in *Postgraduate Ophthalmology*, ed. M. Vanathi, Jaypee Brothers Medical Publishers, New Delhi, 2012, vol. 1, pp. 21-29.

6. O. Strauss, *Physiological Reviews*, 2005, **85**, 845-881.

7.   B. S. Winkler, M. E. Boulton, J. D. Gottsch and P. Sternberg, *Molecular Vision*, 1999, **5**, 32-32.

8.   S. Beatty, H.-H. Koh, M. Phil, D. Henson and M. Boulton, *Survey of Ophthalmology*, 2001, **45**, 115-134.

9.   U. Schraermeyer and K. Heimann, *Pigment Cell Research*, 1999, **12**, 219-236.

10.   M. H. Levin and A. S. Verkman, *The Journal of Membrane Biology*, 2006, **210**, 105-115.

11.   S. S. Miller and R. H. Steinberg, *Experimental Eye Research*, 1977, **25**, 235-248.

12.   J. Immel and R. Steinberg, *The Journal of Neuroscience*, 1986, **6**, 3197-3204.

13.   T. D. Lamb, *Philosophical Transactions of the Royal Society Biological Sciences*, 2009, **364**, 2911-2924.

14.   J. C. Saari, *Annual Review of Nutrition*, 2012, **32**, 125-145.

15.   S. Patricia Becerra, R. N. Fariss, Y. Q. Wu, L. M. Montuenga, P. Wong and B. A. Pfeffer, *Experimental Eye Research*, 2004, **78**, 223-234.

16.   A. N. Witmer, G. F. J. M. Vrensen, C. J. F. Van Noorden and R. O. Schlingemann, *Progress in Retinal and Eye Research*, 2003, **22**, 1-29.

17.   H. Wenkel and J. W. Streilein, *Investigative Ophthalmology & Visual Science*, 2000, **41**, 3467-3473.

18.   L. J. M. Relvas, C. Bouffioux, B. Marcet, D. Communi, M. Makhoul, M. Horckmans, D. Blero, C. Bruyns, L. Caspers, J.-M. Boeynaems and F. Willermain, *Investigative Ophthalmology & Visual Science*, 2009, **50**, 1241-1246.

19.   V. Shah, N. Hall and M. J. Goldacre, *British Journal of Ophthalmology*, 2014, **99**, 639-643.

20.   J. A. Rowe, J. C. Erie, K. H. Baratz, D. O. Hodge, D. T. Gray, L. Butterfield and D. M. Robertson, *Ophthalmology*, 1999, **106**, 154-159.

21.   X. Li, *Ophthalmology*, 2003, **110**, 2413-2417.

22.   M. A. J. Van de Put, J. M. M. Hooymans and L. I. Los, *Ophthalmology*, 2013, **120**, 616-622.

23.   H. Ideta, J. Yonemoto, S. Tanaka, A. Hirose, C. Oka and K. Sasaki, *Graefe's Archive for Clinical and Experimental Ophthalmology*, 1995, **233**, 772-776.

24.   L. Mowatt, G. Shun-Shin and N. Price, *Eye*, 2003, **17**, 63-70.

25. D. Mitry, J. Chalmers, K. Anderson, L. Williams, B. W. Fleck, A. Wright and H. Campbell, *British Journal of Ophthalmology*, 2011, **95**, 365-369.

26. M. Ivanišević, L. Bojić and D. Eterović, *Ophthalmic Research*, 2000, **32**, 237-239.

27. S. Go, C. B. Hoyng and C. W. Klaver, *Archives of Ophthalmology*, 2005, **123**, 1237-1241.

28. T. Hikichi and C. L. Trempe, *Eye*, 1995, **9**, 64-66.

29. S. J. Haug and R. B. Bhisitkul, *Current Opinion in Ophthalmology*, 2012, **23**, 7-11.

30. N. Feltgen and P. Walter, *Deutsches Ärzteblatt International*, 2014, **111**, 12-22.

31. H. K. Kang and A. J. Luff, *The British Medical Journal*, 2008, **336**, 1235-1240.

32. H. Helbig, *Klin Monatsbl Augenheilkd*, 2002, **219**, 186-190.

33. New Orleans Academy of Ophthalmology, in *To the Macula and Beyond*, ed. I. R. Batlle, Kugler Publications, Gilsum, USA, 2005, p. 157.

34. L. S. Brunner, S. C. O. C. Smeltzer, B. G. Bare, J. L. Hinkle and K. H. Cheever, in *Brunner & Suddarth's Textbook of Medical-Surgical Nursing*, ed. H. Surrena, Wolters Kluwer Health/Lippincott Williams & Wilkins, Philadelphia, 12 edn., 2010, p. 1779.

35. C. K. Chan, S. G. Lin, A. S. D. Nuthi and D. M. Salib, *Survey of Ophthalmology*, 2008, **53**, 443-478.

36. W. I. Sabates, G. W. Abrams, D. E. Swanson and E. W. D. Norton, *Ophthalmology*, 1981, **88**, 447-454.

37. M. Stefaniotou, *Acta Ophthalmologica*, 2009, **87**, Supplement s244.

38. R. F. Lam, W. W. Lai, B. T. O. Cheung, C. Y. F. Yuen, T.-h. Wong, M. P. Shanmugam and D. S. C. Lam, *American Journal of Ophthalmology*, 2006, **142**, 938-944.

39. T. Banaee, S. M. Hosseini, H. Ghooshkhanei, M. Moosavi and S. Khayyatzadeh-Kakhki, *Journal of Ophthalmic & Vision Research*, 2009, **4**, 90-96.

40. S. G. Schwartz, D. P. Kuhl, A. R. McPherson, E. R. Holz and W. F. Mieler, *Archives of Ophthalmology*, 2002, **120**, 325-329.

41.   D. Wong and R. Williams, in *Vitreo-retinal Surgery*, eds. B. Kirchhof and D. Wong, Springer Berlin Heidelberg New York, Hiedelberg, 2005, pp. 147-161.

42.   D. M. Marcus, D. J. D'Amico and S. Mukai, *International Ophthalmology Clinic*, 1994, **34**, 97-108.

43.   T. T. Kleinberg, R. T. Tzekov, L. Stein, N. Ravi and S. Kaushal, *Survey of Ophthalmology*, 2011, **56**, 300-323.

44.   S. Donati, S. M. Caprani, G. Airaghi, R. Vinciguerra, L. Bartalena, F. Testa, C. Mariotti, G. Porta, F. Simonelli and C. Azzolini, *BioMedical Research International*, 2014, **1**, 12.

45.   S. G. Honavar, M. Goyal, A. B. Majji, P. K. Sen, T. Naduvilath and L. Dandona, *Ophthalmology*, 1999, **106**, 169-177.

46.   S. P. Azen, I. U. Scott, H. W. Flynn, M.-Y. Lai, T. M. Topping, L. Benati, D. K. Trask and L. A. Rogus, *Ophthalmology*, 1998, **105**, 1587-1597.

47.   B. W. McCuen, S. P. Azen, W. Stern, M. Ying, J. S. Lean, K. L. P. Linton and S. J. Ryan, *Retina*, 1993, **13**, 279-284.

48.   V. Tanner, M. Minihan and T. H. Williamson, *British Journal of Ophthalmology*, 2001, **85**, 480-482.

49.   Y. Sheng, W. Sun, B. Mo, Y.-J. Yu, Y.-S. Gu and W. Liu, *International Journal of Ophthalmology*, 2012, **5**, 591-595.

50.   I. Kocak and H. Koc, *International Journal of Ophthalmology*, 2013, **6**, 81-84.

51.   G. N. Foulks, D. L. Hatchell, A. D. Proia and G. K. Klintworth, *Cornea*, 1991, **10**, 29-37.

52.   J. L. Federman and H. D. Schubert, *Ophthalmology*, 1988, **95**, 870-876.

53.   D. Borislav, *Documenta Ophthalmologica*, 1993, **83**, 79-82.

54.   M. Suzuki, T. Okada, S. Takeuchi, Y. Ishii, H. Yamashita and S. Hori, *Japanese Journal of Ophthalmology*, 1990, **35**, 282-291.

55.   D. Odrobina and I. Laudanska-Olszewska, *BioMedical Research International*, 2014, **1**, 1-5.

56.   M. Day, R. L. Blanchard, R. English, T. Dobbie, R. Williams, M. Garvey and D. Wong, *AIP Conference Proceedings*, 2008, **1027**, 1411-1413.

57.   R. L. Williams, M. J. Day, M. J. Garvey, G. Morphis, C. Irigoyen, D. Wong and T. Stappler, *British Journal of Ophthalmology*, 2011, **95**, 273-276.

58.   I. U. Scott, H. W. Flynn, Jr, T. G. Murray, W. E. Smiddy, J. L. Davis and W. J. Feuer, *Archives of Ophthalmology*, 2005, **123**, 473-478.

59.   D. Wong, R. Williams, T. Stappler and C. Groenewald, *Graefe's Archive for Clinical and Experimental Ophthalmology*, 2005, **243**, 474-477.

60.   J. Roider, H. Hoerauf, K. Kobuch and V.-P. Gabel, *Graefe's Archive for Clinical and Experimental Ophthalmology*, 2002, **240**, 965-971.

61.   C. Wetterqvist, D. Wong, R. Williams, T. Stappler, E. Herbert and S. Freeburn, *The British Journal of Ophthalmology*, 2004, **88**, 692-696.

62.   E. Herbert, T. Stappler, C. Wetterqvist, R. Williams and D. Wong, *Graefe's Archive for Clinical and Experimental Ophthalmology*, 2004, **242**, 250-254.

63.   M. F. Marmor and T. J. Wolfensberger, in *The Retinal Pigment Epithelium: Function and Disease*, Oxford University Press, Oxford, 1998, pp. 220-254.

64.   R. D. Jager, W. F. Mieler and J. W. Miller, *New England Journal of Medicine*, 2008, **358**, 2606-2617.

65.   P. T. De Jong, *New England Journal of Medicine*, 2006, **355**, 1474-1485.

66.   L. S. Lim, P. Mitchell, J. M. Seddon, F. G. Holz and T. Y. Wong, *The Lancet*, 2012, **379**, 1728-1738.

67.   R. C. Hsieh, B. S. Fine and J. S. Lyons, *Archives of Ophthalmology*, 1977, **95**, 429-435.

68.   I. Chowers, L. Tiosano, I. Audo, M. Grunin and C. J. F. Boon, *Progress in Retinal and Eye Research*, 2015, **47**, 64-85.

69.   P. Hiscott, C. Sheridan, R. M. Magee and I. Grierson, *Progress in Retinal and Eye Research*, 1999, **18**, 167-190.

70.   P. T. Khaw, N. L. Occleston, G. Schultz, I. Grierson, M. B. Sherwood and G. Larkin, *Eye*, 1994, **8**, 188-195.

71.   D. M. Pattwell, C. M. Sheridan, M. Le Goff, P. N. Bishop and P. Hiscott, *Experimental Eye Research*, 2010, **90**, 461-464.

72.   C. M. Sheridan, N. L. Occleston, P. Hiscott, C. H. Kon, P. T. Khaw and I. Grierson, *The American Journal of Pathology*, 2001, **159**, 1555-1566.

73.   A. Sadaka and G. P. Giuliari, *Clinical Ophthalmology*, 2012, **6**, 1325-1333.

74.   C. Chiba, *Experimental Eye Research*, 2014, **123**, 107-114.

75.   M. Weller, P. Wiedemann and K. Heimann, *International Ophthalmology*, 1990, **14**, 105-117.

76.   G. Hilton, *Ophthalmology*, 1983, **90**, 121-125.

77.   D. G. Charteris, C. S. Sethi, G. P. Lewis and S. K. Fisher, *Eye*, 2002, **16**, 369-374.

78.   C. Sheridan, P. Hiscott and I. Grierson, in *Vitreo-Retinal Surgery*, eds. B. Kirchhof and D. Wong, Springer Berlin Heidelberg, Heidelberg, 2005, pp. 101-119.

79.   P. Hiscott, I. Morino, R. Alexander, I. Grierson and Z. Gregor, *Eye*, 1989, **3**, 606-610.

80.   J. Z. Cui, A. Chiu, D. Maberley, P. Ma, A. Samad and J. A. Matsubara, *Eye*, 2006, **21**, 200-208.

81.   C.-M. Yang, K. Olsen, E. Hernandez and S. Cousins, *Graefe's Archive for Clinical and Experimental Ophthalmology*, 1992, **230**, 66-71.

82.   Y. Tano, D. Chandler and R. Machemer, *American Journal of Ophthalmology*, 1980, **90**, 810-816.

83.   J. B. Jonas, J. K. Hayler and S. Panda-Jonas, *British Journal of Ophthalmology*, 2000, **84**, 1064-1067.

84.   J. C. Pastor, E. Rodríguez and F. Martín, *Progress in Retinal and Eye Research*, 2002, **21**, 127-144.

85.   T. L. Jackson, P. H. Donachie, T. H. Williamson, J. M. Sparrow and R. L. Johnston, *Retina*, 2015, **35**, 1615-1621.

86.   E. J. Sigler, J. C. Randolph, J. I. Calzada and S. Charles, *Retina*, 2014, **34**, 1939-1944.

87.   B. Guidetti, J. Azema, M. Malet-Martino and R. Martino, *Current Drug Delivery*, 2008, **5**, 7-19.

88.   D. B. Chandler, G. Rozakis, E. de Juan, R. Machemer and E. de Juan, Jr., *American Journal of Ophthalmology*, 1985, **99**, 686.

89.   D. B. Chandler, T. Hida, S. Sheta, A. D. Proia and R. Machemer, *Graefe's Archive for Clinical and Experimental Ophthalmology*, 1987, **225**, 259-265.

90.   H. C. Liang, Y. N. Hui and Y. S. Cai, *Chinese Journal of Ophthalmology*, 1994, **30**, 122-124.

91.   C. S. Yang, J. A. Khawly, D. P. Hainsworth, P. Ashton, H. Guo and G. J. Jaffe, *Archives of Ophthalmology*, 1998, **116**, 69-77.

92.   F. Koerner, A. Merz, B. Gloor and E. Wagner, *Graefe's Archive for Clinical and Experimental Ophthalmology*, 1982, **219**, 268-271.

93. M. Sunalp, P. Wiedemann, N. Sorgente and S. J. Ryan, *Current Eye Research*, 1984, **3**, 619-623.

94. E. Bali, E. J. Feron, E. Peperkamp, M. Veckeneer, P. G. Mulder and J. C. van Meurs, *Graefe's Archive for Clinical and Experimental Ophthalmology*, 2010, **248**, 957-962.

95. W.-C. Wu, Y.-H. Kao and D.-N. Hu, *Journal of Ocular Pharmacology and Therapeutics*, 2002, **18**, 251-264.

96. D. S. Muckle, *Rheumatology*, 1974, **13**, 141-147.

97. T. A. Stiris, C. Suguihara, J. Flynn, J. Quero and E. Bancalari, *Biology of the Neonate*, 1996, **69**, 101-108.

98. M. E. Tilden, R. S. Boney, M. M. Gloldenberg and J. T. Rosenbaum, *Journal of Ocular Pharmacology*, 1990, **6**, 131-135.

99. G. W. A. Tjebbes, J. L. van Delft, E. R. Barthen and N. J. van Haeringen, *Prostaglandins*, 1990, **40**, 29-33.

100. T. B. Connor, Jr., A. B. Roberts, M. B. Sporn, D. Danielpour, L. L. Dart, R. G. Michels, S. de Bustros, C. Enger, H. Kato and M. Lansing, *The Journal of Clinical Investigation*, 1989, **83**, 1661-1666.

101. D. H. Anderson, C. J. Guerin, G. S. Hageman, B. A. Pfeffer and K. C. Flanders, *Journal of Neuroscience Research*, 1995, **42**, 63-79.

102. H. Kishi, H. K. Mishima and U. Yamashita, *Current Eye Research*, 1998, **17**, 483-486.

103. T. H. Tezel and L. V. Del Priore, *Ophthalmic Research*, 1999, **31**, 192-202.

104. S. Wang and G. Xu, *Fujian Medical Journal*, 2010, **32**, 3-6.

105. T. Yasukawa, H. Kimura, Y. Tabata, H. Miyamoto, Y. Honda and Y. Ogura, *Graefe's Archive for Clinical and Experimental Ophthalmology*, 2002, **240**, 672-678.

106. D. Salonga, K. Danenberg, M. Johnson, R. Metzger, S. Groshen, D. Tsao-Wei, H. Lenz, C. Leichman, L. Leichman, R. Diasio and P. Danenberg, *Clinical Cancer Research*, 2000, **6**, 1322-1327.

107. B. Steffansen, P. Ashton and A. Buur, *International Journal of Pharmaceutics*, 1996, **132**, 243-250.

108. H. Borhani, G. Peyman, M. Rahimy and H. Thompson, *International Ophthalmology*, 1995, **19**, 43-49.

109. V. Sundaram, A. Barsam and G. Virgili, *The Cochrane Library*, 2010.

110. R. H. Y. Asaria, C. H. Kon, C. Bunce, D. G. Charteris, D. Wong, P. T. Khaw and G. W. Aylward, *Ophthalmology*, 2001, **108**, 1179-1183.

111. L. Wickham, C. Bunce, D. Wong, D. McGurn and D. G. Charteris, *Ophthalmology*, 2007, **114**, 698-704.

112. P. Wiedemann, C. Leinung, R.-D. Hilgers and K. Heimann, *Graefe's Archive for Clinical and Experimental Ophthalmology*, 1991, **229**, 150-152.

113. A. Kumar, S. Nainiwal, I. Choudhary, H. K. Tewari and L. K. Verma, *Clinical & Experimental Ophthalmology*, 2002, **30**, 348-351.

114. P. Wiedemann, K. Lemmen, R. Schmiedl and K. Heimann, *American Journal of Ophthalmology*, 1987, **104**, 10-14.

115. J. Khawly, P. Saloupis, D. Hatchell and R. Machemer, *Graefe's Archive for Clinical and Experimental Ophthalmology*, 1991, **229**, 464-467.

116. P. Wiedemann, C. Leinung, R. D. Hilgers and K. Heimann, *Progress of ophthalmology : Journal of the German Society of Ophthalmology*, 1991, **88**, 613-615.

117. H. Mietz, R. Walshe, P. Wiedemann, K. Heimann and W. R. Green, *Retina*, 1994, **14**, 425-429.

118. U. H. Steinhorst, E. P. Chen, D. L. Hatchell, G. P. Samsa, P. T. Saloupis, J. Westendorf and R. Machemer, *Investigative Ophthalmology & Visual Science*, 1993, **34**, 1753-1760.

119. Y. S. Chan, J. H. Wong, E. F. Fang, W. Pan, T. B. Ng, C. Yau Sang, W. Jack Ho, F. Evandro Fei, P. Wenliang, N. Tzi Bun, Y. S. Chan, J. H. Wong, E. F. Fang, W. Pan, T. B. Ng and V. N. Uversky, *Public Library of Science One*, 2012, **7**, epub ahead of print DOI: 10.1371/journal.pone.0038961.

120. Y. H. Chang, C. T. Horng, Y. H. Chen, P. L. Chen, C. L. Chen, C. M. Liang, M. W. Chien and J. T. Chen, *Investigative Ophthalmology & Visual Science*, 2008, **49**, 5441-5449.

121. V. Chesnokov, C. Sun and K. Itakura, *Cancer Cell International*, 2009, **9**, 9-25.

122. J.-T. Chen, P.-L. Chen, Y.-H. Chang, M.-W. Chien, Y.-H. Chen and D.-W. Lu, *Experimental Eye Research*, 2006, **83**, 1052-1062.

123. C.-M. Liang, *Molecular Vision*, 2010, **16**, 2559-2571.

124. C. M. Liang, M. C. Tai, Y. H. Chang, Y. H. Chen, C. L. Chen, D. W. Lu and J. T. Chen, *Acta Ophthalmologica*, 2011, **89**, 505-514.

125. M. Nakagawa, M. F. Refojo, J. F. Marin, M. Doi and F. I. Tolentino, *Investigative Ophthalmology & Visual Science*, 1995, **36**, 2388-2395.

126. W.-C. Wu, D.-N. Hu, S. Mehta and Y.-C. Chang, *Journal of Ocular Pharmacology and Therapeutics*, 2005, **21**, 44-54.

127. J. W. Doyle, R. K. Dowgiert and S. M. Buzney, *Current Eye Research*, 1992, **11**, 753-765.

128. R. Blomhoff and H. K. Blomhoff, *Journal of Neurobiology*, 2006, **66**, 606-630.

129. K. Palczewski, *Trends in Pharmacological Sciences*, 2010, **31**, 284-295.

130. T. Ebrey and Y. Koutalos, *Progress in Retinal and Eye Research*, 2001, **20**, 49-94.

131. G. H. Travis, M. Golczak, A. R. Moise and K. Palczewski, *Annual Review of Pharmacology and Toxicology*, 2007, **47**, 469-512.

132. P. D. Kiser, M. Golczak and K. Palczewski, *Chemical Reviews*, 2014, **114**, 194-232.

133. W. Baehr, S. M. Wu, A. C. Bird and K. Palczewski, *Vision Research*, 2003, **43**, 2957-2958.

134. V. Giguere, E. S. Ong, P. Segui and R. M. Evans, *Nature*, 1987, **330**, 624-629.

135. M. Petkovich, N. J. Brand, A. Krust and P. Chambon, *Nature*, 1987, **330**, 444-450.

136. Y.-H. Du, K. Hirooka, O. Miyamoto, Y.-Q. Bao, B. Zhang, J.-B. An and J.-X. Ma, *Experimental Eye Research*, 2013, **109**, 22-30.

137. J. J. Araiz, M. F. Refojo, M. H. Arroyo, F. L. Leong, D. M. Albert and F. I. Tolentino, *Investigative Ophthalmology & Visual Science*, 1993, **34**, 522-530.

138. G. G. Giordano, M. F. Refojo and M. H. Arroyo, *Investigative Ophthalmology & Visual Science*, 1993, **34**, 2743-2751.

139. Y.-C. Chang, D.-N. Hu and W.-C. Wu, *American Journal of Ophthalmology*, 2008, **146**, 440-446.

140. S. Fekrat, E. de Juan Jr and P. A. Campochiaro, *Ophthalmology*, 1995, **102**, 412-418.

141. Y. Barak, Y. Wohl, Y. Greenberg, Y. B. Dayan, T. Friedman, G. Shoval and H. Y. Knobler, *International Clinical Psychopharmacology*, 2005, **20**, 39-41.

142. I. M. MacDonald, C. Peters and M. H. Chen, *Canadian Journal of Ophthalmology*, 1996, **31**, 175-178.

143. J. Rong and S. Liu, *Biochemical and Biophysical Research Communications*, 2011, **407**, 605-609.

144. I. M. Macdonald, P. Rajeet, K. Kovithavongs, C. Peters, E. E. Tredget and G. Aziz, *American Journal of Opthalmology*, 1995, **30**, 440-446.

145. W. Zhang, M. R. Prausnitz and A. Edwards, *Journal of Controlled Release*, 2004, **99**, 241-258.

146. S. A. Molokhia, S. C. Thomas, K. J. Garff, K. J. Mandell, B. M. Wirostko, S. A. Molokhia, S. C. Thomas, K. J. Garff, K. J. Mandell and B. M. Wirostko, *Journal of Ocular Pharmacology and Therapeutics*, 2013, **29**, 92-105.

147. A. Zimmer and J. Kreuter, *Advanced Drug Delivery Reviews*, 1995, **16**, 61-73.

148. Z. Šklubalová and Z. Zatloukal, *Drug Development and Industrial Pharmacy*, 2006, **32**, 197-205.

149. R. D. Jager, L. P. Aiello, S. C. Patel, J. Cunningham and T. Emmett, *Retina*, 2004, **24**, 676-698.

150. E. M. del Amo and A. Urtti, *Drug Discovery Today*, 2008, **13**, 135-143.

151. D. Sarraf and D. A. Lee, *Journal of Ocular Pharmacology and Therapeutics*, 1994, **10**, 69-81.

152. A. L. Church, M. Barza and J. Baum, *Investigative Ophthalmology & Visual Science*, 1992, **33**, 3543-3545.

153. M. O. Yoshizumi, A. Dessouki, D. A. Lee and G. Lee, *Journal of Ocular Pharmacology and Therapeutics*, 1997, **13**, 529-536.

154. T. Yasukawa, Y. Ogura, Y. Tabata, H. Kimura, P. Wiedemann and Y. Honda, *Progress in Retinal and Eye Research*, 2004, **23**, 253-281.

155. T. P. O'Brien, M. R. Sawusch, J. D. Dick, T. R. Hamburg and J. D. Gottsch, *Journal of Cataract & Refractive Surgery*, 1988, **14**, 505-507.

156. M. R. Sawusch, T. P. O'Brien, J. D. Dick and J. D. Gottsch, *American Journal of Ophthalmology*, 1988, **106**, 279-281.

157. P. B. Patel, D. H. Shastri, P. K. Shelat and A. K. Shukla, *Systematic Reviews in Pharmacy*, 2010, **1**, 113-120.

158. I. H. Pitman, *Australian Journal of Opthalmology*, 1977, **5**, 101-105.

159. V. R. Kearns and R. L. Williams, *Expert Review of Medical Devices*, 2009, **6**, 277-290.

160. J. LaMotte, E. Grossman and J. Hersch, *Journal of the American Optometric Association*, 1985, **56**, 298-302.

161. R. Pignatello and G. Puglisi, *Recent Patents on Nanomedicine*, 2011, **1**, 42-54.

162. A. W. Lloyd, R. G. A. Faragher and S. P. Denyer, *Biomaterials*, 2001, **22**, 769-785.

163. R. Menapace, C. Skorpik and A. Wedrich, *Journal of Cataract & Refractive Surgery*, **16**, 567-577.

164. T. Yasukawa, Y. Ogura, H. Kimura, E. Sakurai and Y. Tabata, *Expert Opinion on Drug Delivery*, 2006, **3**, 261-273.

165. S. Lee, P. Hughes, A. Ross and M. Robinson, *Pharmaceutical Research*, 2010, **27**, 2043-2053.

166. P. U. Fechner and M. U. Fechner, *British Journal of Ophthalmology*, 1983, **67**, 259-263.

167. A. L. Weiner and D. A. Marsh, in *Retinal and Choroidal Angiogenesis*, ed. J. Penn, Springer, Netherlands, 2015, pp. 419-444.

168. D. C. Musch, D. F. Martin, J. F. Gordon, M. D. Davis and B. D. Kuppermann, *New England Journal of Medicine*, 1997, **337**, 83-90.

169. G. J. Jaffe, D. Martin, D. Callanan, P. A. Pearson, B. Levy and T. Comstock, *Ophthalmology*, 2006, **113**, 1020-1027.

170. M. N. Yasin, D. Svirskis, A. Seyfoddin and I. D. Rupenthal, *Journal of Controlled Release*, 2014, **196**, 208-221.

171. N. Kuno and S. Fujii, *Drugs & Ageing*, 2010, **27**, 117-134.

172. M. N. Yasin, D. Svirskis, A. Seyfoddin and I. D. Rupenthal, *Journal of Controlled Release*, 2014, **196**, 208-221.

173. E. Meng and T. Hoang, *Advanced Drug Delivery Reviews*, 2012, **64**, 1628-1638.

174. R. Lo, P.-Y. Li, S. Saati, R. Agrawal, M. Humayun and E. Meng, *Biomedical Microdevices*, 2009, **11**, 959-970.

175. S. Saati, R. Lo, P.-Y. Li, E. Meng, R. Varma and M. S. Humayun, *Current Eye Research*, 2010, **35**, 192-201.

176. F. N. Pirmoradi, J. K. Jackson, H. M. Burt and M. Chiao, *Lab on a Chip*, 2011, **11**, 2744-2752.

177. V. K. Yellepeddi, R. Sheshala, H. McMillan, C. Gujral, D. Jones and T. Raghu Raj Singh, *Drug Discovery Today*, 2015, **20**, 884-889.

178. D. F. Emerich and C. G. Thanos, *Current Opinion in Molecular Therapeutics*, 2008, **10**, 506-515.

179. X. Rong, W. Yuan, Y. Lu, X. Mo, R. Xianfang, Y. Weien, L. Yi and M. Xiaofen, *International Journal of Nanomedicine*, 2014, **9**, 3057.

180. C. Wischke and S. P. Schwendeman, *International Journal of Pharmaceutics*, 2008, **364**, 298-327.

181. B. Khoobehi, M. Stradtmann, G. A. Peyman and O. Aly, *Ophthalmic Surgery*, 1991, **22**, 175-180.

182. C.-H. Chiang, S.-M. Tung, D.-W. Lu and M.-K. Yeh, *Journal of Ocular Pharmacology and Therapeutics*, 2001, **17**, 545-553.

183. L.-J. Cui, N.-X. Sun, X.-H. Li, J. Huang and J.-G. Yang, *Acta Pharmacologica Sinica*, 2008, **29**, 1021-1028.

184. K. Adibkia, Y. Omidi, M. R. Siahi, A. R. Javadzadeh, M. Barzegar-Jalali, J. Barar, N. Maleki, G. Mohammadi and A. Nokhodchi, *Journal of Ocular Pharmacology and Therapeutics*, 2007, **23**, 421-432.

185. C. A. Harper III, B. Khoobehi, G. A. Peyman, B. M. Gebhardt and W. A. Dunlap, *International Ophthalmology*, 1993, **17**, 337-340.

186. J.-L. Bourges, S. E. Gautier, F. Delie, R. A. Bejjani, J.-C. Jeanny, R. Gurny, D. BenEzra and F. F. Behar-Cohen, *Investigative Ophthalmology & Visual Science*, 2003, **44**, 3562-3569.

187. A. C. Amrite, H. F. Edelhauser, S. R. Singh and U. B. Kompella, *Molecular Vision*, 2008, **14**, 150-160.

188. S. K. Sahoo, F. Dilnawaz and S. Krishnakumar, *Drug Discovery Today*, 2008, **13**, 144-151.

189. H. E. Schaeffer and D. L. Krohn, *Investigative Ophthalmology & Visual Science*, 1982, **22**, 220-227.

190. A. Bochot, P. Couvreur and E. Fattal, *Progress in Retinal and Eye Research*, 2000, **19**, 131-147.

191. O. N. El-Gazayerly and A. H. Hikal, *International Journal of Pharmaceutics*, 1997, **158**, 121-127.

192. R. Khalil, S. El-Nahhas, S. Omar and M. El-Ridy, *Egyptian Journal of Pharmaceutical Sciences*, 1992, **33**, 667-667.

193. F. S. Habib, E. A. Fouad, M. S. Abdel-Rhaman and D. Fathalla, *Acta Ophthalmologica*, 2010, **88**, 901-904.

194. S. Ebrahim, G. A. Peyman and P. J. Lee, *Survey of Ophthalmology*, 2005, **50**, 167-182.

195. R. Zeimer and M. Goldberg, *Advanced Drug Delivery Reviews*, 2001, **52**, 49-61.

196. P. C. Ho, I. M. Chan, M. F. Refojo and F. I. Tolentino, *Ophthalmic surgery*, 1984, **15**, 511-515.

197. F. D'Hermies, J.-F. Korobelnik, M. Savoldelli, D. Chauvaud and Y. Pouliquen, *Retina*, 1995, **15**, 62-67.

198. K. I. Hwang and J. I. Lim, *Archives of Ophthalmology*, 1997, **115**, 1205-1206.

199. M. Roldán-Pallarés, J. del Castillo Sanz, S. Awad-El Susi and M. Refojo, *Archives of Ophthalmology*, 1999, **117**, 197-201.

200. X. Lin, J. Ge, Q. Gao, Z. Wang, C. Long, L. He, Y. Liu and Z. Jiang, *Investigative Ophthalmology & Visual Science*, 2011, **52**, 374-381.

201. H. Zheng, Z. Wang, P. Wang, Y. Liu, Z. Jiang and Q. Gao, *Graefe's Archive for Clinical and Experimental Ophthalmology*, 2012, **250**, 751-759.

202. J. Stella, W. N. Charman and V. H. Naringrekar, *Drugs*, 1985, **29**, 455-473.

203. P. Jolimaître, M. Malet-Martino and R. Martino, *International Journal of Pharmaceutics*, 2003, **259**, 181-192.

204. J. M. Larrosa, J. Veloso, Amadeo A.S., F.-L. Leong and M. F. Refojo, *Current Eye Research*, 1997, **16**, 1030-1035.

205. M. T. Kralinger, G. F. Kieselbach, M. Voigt and J.-M. Parel, *Retina*, 2001, **21**, 513-520.

206. M. J. Colthurst, R. L. Williams, P. S. Hiscott and I. Grierson, *Biomaterials*, 2000, **21**, 649-665.

207. M. S. Blumenkranz and M. K. Hartzer, in *Proliferative Vitreoretinopathy (PVR)*, eds. H. MacKenzie, M. Freeman and F. I. Tolentino, Springer, New-York, 1988, pp. 81-87.

208. A. Albert, *Nature*, 1958, **182**, 421-423.

209. N. Harper, in *Progress in Drug Research*, ed. E. Jucker, Birkhäuser Basel, 1962, vol. 4, pp. 221-294.

210. Y. Singh, M. Palombo and P. J. Sinko, *Current Medicinal Chemistry*, 2008, **15**, 1802-1826.

211. S.-D. Clas, R. I. Sanchez and R. Nofsinger, *Drug Discovery Today*, 2014, **19**, 79-87.

212. A. J. M. D'Souza and E. M. Topp, *Journal of Pharmaceutical Sciences*, 2004, **93**, 1962-1979.

213. I. A. Müller, F. Kratz, M. Jung and A. Warnecke, *Tetrahedron Letters*, 2010, **51**, 4371-4374.

214. F. Kratz, U. Beyer and M. T. Schutte, *Critical Reviews in Therapeutic Drug Carrier Systems*, 1999, **16**, 245-288.

215. S. O. Doronina, B. E. Toki, M. Y. Torgov, B. A. Mendelsohn, C. G. Cerveny, D. F. Chace, R. L. DeBlanc, R. P. Gearing, T. D. Bovee, C. B. Siegall, J. A. Francisco, A. F. Wahl, D. L. Meyer and P. D. Senter, *Nature Biotechnology*, 2003, **21**, 778-784.

216. S. Jaracz, J. Chen, L. V. Kuznetsova and I. Ojima, *Bi-Organic & Medicinal Chemistry*, 2005, **13**, 5043-5054.

217. M. L. Rodrigues, L. G. Presta, C. E. Kotts, C. Wirth, J. Mordenti, G. Osaka, W. L. T. Wong, A. Nuijens, B. Blackburn and P. Carter, *Cancer Research*, 1995, **55**, 63-70.

218. G. D. Stefano, M. Lanza, F. Kratz, L. Merina and L. Fiume, *European Journal of Pharmaceutical Sciences*, 2004, **23**, 393-397.

219. V. R. Guarino, V. Karunaratne and V. J. Stella, *Bio-Organic & Medicinal Chemistry Letters*, 2007, **17**, 4910-4913.

220. H. Bundgaard and G. J. Rasmussen, *Pharmaceutical Research*, 1991, **8**, 1238-1242.

221. O. Shaaya, A. Magora, T. Sheskin, N. Kumar and A. Domb, *Pharmaceutical Research*, 2003, **20**, 205-211.

222. B. S. Lele and A. S. Hoffman, *Journal of Controlled Release*, 2000, **69**, 237-248.

223. L. Erdmann and K. Uhrich, *Biomaterials*, 2000, **21**, 1941-1946.

224. O. Shaaya, A. Magora, T. Sheskin, N. Kumar and A. J. Domb, *Pharmaceutical Research*, 2003, **20**, 205-211.

225. L. D. Lavis, *ACS Chemical Biology*, 2008, **3**, 203-206.

226. A. Rephaeli, R. Zhuk and A. Nudelman, *Drug Development Research*, 2000, **50**, 379-391.

227. M. Barot, M. Bagui, M. R. Gokulgandhi and A. K. Mitra, *Medicinal Chemistry (Shariqah (United Arab Emirates))*, 2012, **8**, 753-768.

228. M. Goel, R. G. Picciani, R. K. Lee and S. K. Bhattacharya, *The Open Ophthalmology Journal*, 2010, **4**, 52-59.

229. E. de Berardinis, O. Tieri, A. Polzella and N. Iuglio, *Experimental Eye Research*, 1965, **4**, 179-186.

230. J. C. C. Brown, P. J. Sadler, D. J. Spalton, S. M. Juul, A. F. Macleod and P. H. Sönksen, *Experimental Eye Research*, 1986, **42**, 357-362.

231. R. C. Tripathi, J. Li, W. A. Chan and B. J. Tripathi, *Experimental Eye Research*, 1994, **59**, 723-728.

232. R. C. Tripathi, C. B. Millard and B. J. Tripathi, *Experimental Eye Research*, 1989, **48**, 117-130.

233. U. R. Chowdhury, B. J. Madden, M. C. Charlesworth and M. P. Fautsch, *Investigative Ophthalmology & Visual Science*, 2010, **51**, 4921-4931.

234. R. F. Brubaker, *Investigative Ophthalmology & Visual Science*, 1991, **32**, 3145-3166.

235. J. Troger, G. Kieselbach, W. Göttinger, R. Metzler, C. Kähler and A. Saria, *German Journal of Ophthalmology*, 1994, **3**, 245-247.

236. J. Troger, B. Kremser, T. Stöckl, M. Kralinger, E. Schmid, C. Kunze and G. F. Kieselbach, *Graefe's Archive for Clinical and Experimental Ophthalmology*, 2000, **238**, 237-242.

237. J. Khandare and T. Minko, *Progress in Polymer Science*, 2006, **31**, 359-397.

238. B. Testa, *Biochemical Pharmacology*, 2004, **68**, 2097-2106.

239. K. Knop, R. Hoogenboom, D. Fischer and U. S. Schubert, *Angewandte Chemie International Edition*, 2010, **49**, 6288-6308.

240. S. S. Banerjee, N. Aher, R. Patil and J. Khandare, *Journal of Drug Delivery*, 2012, **2012**, 1-17.

241. H. Soyez, E. Schacht and S. Vanderkerken, *Advanced Drug Delivery Reviews*, 1996, **21**, 81-106.

242. R. B. Greenwald, Y. H. Choe, J. McGuire and C. D. Conover, *Advanced Drug Delivery Reviews*, 2003, **55**, 217-250.

243. J. M. Harris, in *Poly(ethylene glycol) Chemistry: Biotechnical and Biomedical Applications*, Springer Science & Business Media, New York, 2013, pp. 1-12.

244. G. H. Hakimelahi, T. W. Ly, S.-F. Yu, M. Zakerinia, A. Khalafi-Nezhad, M. N. Soltani, M. N. Gorgani, A. R. Chadegani and A. A. Moosavi-Movahedi, *Bioorganic & Medicinal Chemistry*, 2001, **9**, 2139-2147.

245. R. Roduit and D. F. Schorderet, *Apoptosis*, 2008, **13**, 343-353.

246. A. Nudelman and A. Rephaeli, *Journal of Medicinal Chemistry*, 2000, **43**, 2962-2966.

247. R. Wang, H. Xiao, H. Song, Y. Zhang, X. Hu, Z. Xie, Y. Huang, X. Jing and Y. Li, *Journal of Materials Chemistry*, 2012, **22**, 25453-25462.

248. R. Cecchi, L. Rusconi, M. C. Tanzi, F. Danusso and P. Ferruti, *Journal of Medicinal Chemistry*, 1981, **24**, 622-625.

249. F. Z. Abu Zanat, A. M. Qandil and B. M. Tashtoush, *Drug Development and Industrial Pharmacy*, 2011, **37**, 1090-1099.

CHAPTER 2

Drug Characterisation and Biological
Evaluation

2.1 INTRODUCTION

As mentioned in Chapter 1 the drugs of choice for use throughout this thesis are atRA (all-trans retinoic acid) and Ibu (ibuprofen). atRA has been proven to be sensitive to light, air and temperature, and will isomerise/oxidise under these conditions,[1-3] whereas Ibu is stable. A full characterisation of atRA was carried out in order to confirm the purity of the product commercially obtained. [1]H and ^{13}C nuclear magnetic resonance (NMR) spectroscopy, mass spectroscopy, high-performance liquid chromatography (HPLC) and melting point analysis were utilised to assess purity. The degradation of atRA, under conditions which would be used in subsequent work, was also studied.

The cytotoxicity of the two different drugs was evaluated using MTT, Resazurin, Phalloidin and BrdU assays on ARPE-19 cells (ATCC® Number: CRL-2302™, adult retinal pigment epithelium cells from the normal eyes of a 19 year old male donor, who died in a motor vehicle accident). This cell line was chosen because ARPE-19 cells are an established but non-immortalised human cell line which model the structure and functionality of RPE cells *in vivo* and as such provide a good system to study interactions of drugs encountering the RPE.[4, 5] BrdU incorporation was also used to investigate the anti-proliferative effects of atRA and Ibu on ARPE-19 cells.

Overall the aims of this chapter are to characterise and evaluate the degradation of the sensitive atRA, under conditions relevant to the subsequent research that will be carried out, as well as the biological evaluation of both atRA and Ibu, in order to determine toxic thresholds and antiproliferative effects of both drugs.

2.1.1 Cellular Assays

There are many different assays that can be carried out to determine the cytotoxicity and antiproliferative effects of a drug to a cell. In this section the assays used throughout this research to biologically evaluate the drugs are discussed.

2.1.1.1 MTT Assay

The 3-(4,5-dimethylthiazol-2-yl)-2,5-diphenyltetrazolium bromide (MTT) assay measures the mitochondrial activity of a cell, and is therefore indicative of cytotoxicity. Mitochondria have many functions with the most prominent being energy conversion and regulation of cell metabolism.[6] MTT is a colorimetric assay where the mitochondria metabolise MTT *via* the reduction to formazan crystals, which reside within the cell, therefore the metabolic activity of the cell can be monitored (Scheme 2.1).

Mitochondial reductase

3-(4,5-dimethylthiazol-2-yl)-2,5-diphenyltetrazolium bromide
(MTT)

(E,Z)-5-(4,5-dimethylthiazol-2-yl)-1,3-diphenylformazan
(Formazan)

Scheme 2.1 MTT reduction to formazan.

The cells are broken down and the formazan crystals solubilised in acid then measured on a spectrophotometer. The more active the mitochondria are within the cell, suggesting the cell is healthy, the more formazan will be produced; therefore a stronger absorbance will be seen on the spectrophotometer (See Figure 2.1).

Figure 2.1 MTT plate showing variation of formazan crystal formation, typical of healthy cells with deep purple colour (left) and unhealthy/dead with a lilac colour (right).

2.1.1.2 Resazurin Assay

The resazurin assay is similar to the MTT assay in that it measures the mitochondrial activity of a cell. In this assay the mitochondria reduce resazurin to the fluorescently active resorufin presented in Scheme 2.2; the fluorescence is then measured on a fluorescent plate reader. The advantages of this assay over MTT is that the cells remain alive after the assay is performed, therefore, further studies can be carried out on the same samples, including staining.

7-Hydroxy-3H-phenoxazin-3-one 10-oxide
(Resazurin)

7-Hydroxy-3H-phenoxazin-3-one
(Resorufin)
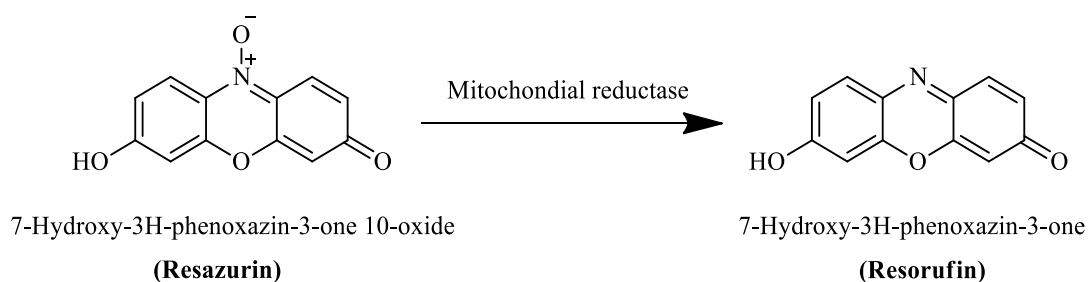
Scheme 2.2 Resazurin reduction to resorufin.

2.1.1.3 Phalloidin Assay

Phalloidin belongs to a family of phallotoxins that are derived from the death cap mushroom which, as the name suggests, is highly toxic and is responsible for most fatal mushroom poisoning worldwide.[7] Phalloidin is conjugated to a fluorophore and used to stain the F-actin of the cellular cytoskeleton so the structural integrity can be determined *via* fluorescent microscopy. Figure 2.2 shows an image of ARPE-19 cells stained with phalloidin. The nuclei of the cells have also been stained with dianidine-2-phenylindole (DAPI). DAPI is a blue fluorescent DNA stain which binds to DNA base pair adenine-thymine rich areas, so is ideal for nuclei staining.[8] Another advantage of using DAPI is that it can pass through membranes without causing any damage.
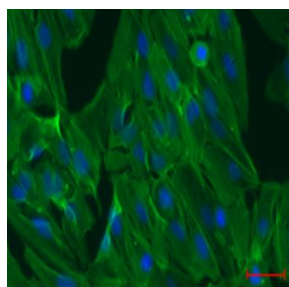
Figure 2.2 ARPE-19 cell stained with phalloidin (green) and the nuclei 4', 6-diamidino-2-phenylindole (DAPI) (blue). Scale bar represents 50 μm.

2.1.1.4 BrdU Assay

Bromodeoxyuridine (BrdU) is a synthetic analogue of thymidine (Figure 2.3) and is usually used to determine the rate of cellular proliferation.[9-11] BrdU replaces thymidine in newly developed DNA of replicating cells. To stain the incorporated BrdU, the cells need to be fixed into an immobile biological state, the membrane permeabilised, as well as the nuclei, to allow penetration of the dye. A blocking agent is then applied and antibody staining for BrdU (anti-BrdU) is performed. Only the nuclei of cells which have incorporated BrdU are stained during this process which indicates the rate of proliferation of the cells. Another dye, such as Hoechst 33342 which has been used in ARPE-19 cells previously[12] and is similar to DAPI as it is a blue fluorescent DNA stain, is used to stain the nuclei of all the cells which did not incorporate BrdU.
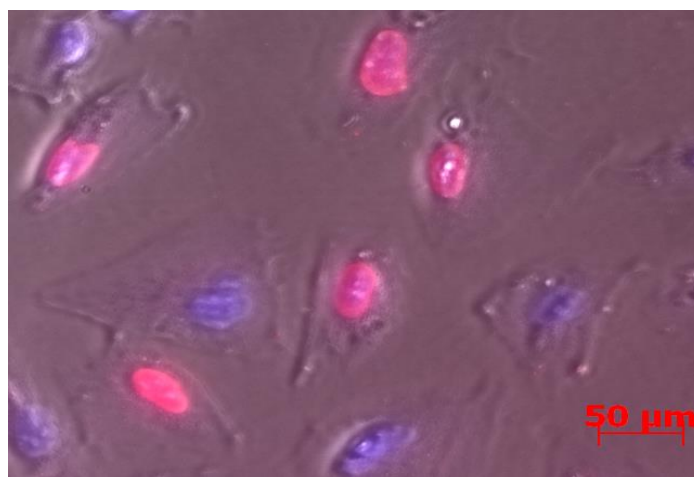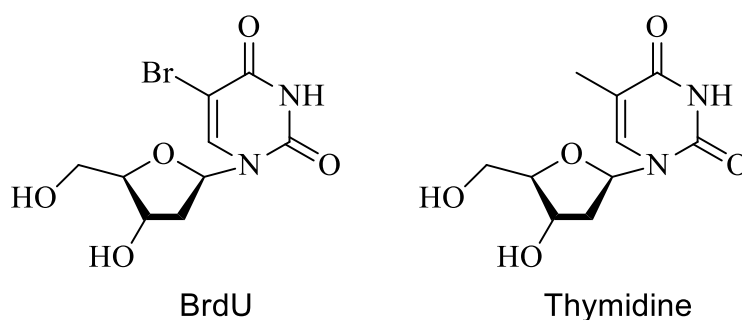
Figure 2.3 BrdU and thymidine structures and an image of ARPE-19 cells which have been incubated with BrdU for 4h. The nuclei which have incorporated BrdU are stained red and the nuclei of cells which didn't stained with Hoechst (blue).

2.2 RETINOIC ACID CHARACTERISATION

atRA was analysed by ^{1}H and ^{13}C NMR spectroscopy, chemical ionisation (CI) mass spectroscopy, HPLC and melting point analysis to determine isomeric purity. It is possible for each double bond in the hydrocarbon chain to undergo isomerisation to mono-cis or multiple-cis forms of RA. However, due to steric hindrance some of these isomers are not thermodynamically stable at ambient temperature and, therefore, isomerise into a stable form.[2] Possible isomers of atRA and oxidation products can be seen in Figure 2.5.

Mass spectrometry analysis (Figure 2.4) confirms the MW of RA; however, this technique cannot differentiate the isomers but can confirm no oxidation products are present.
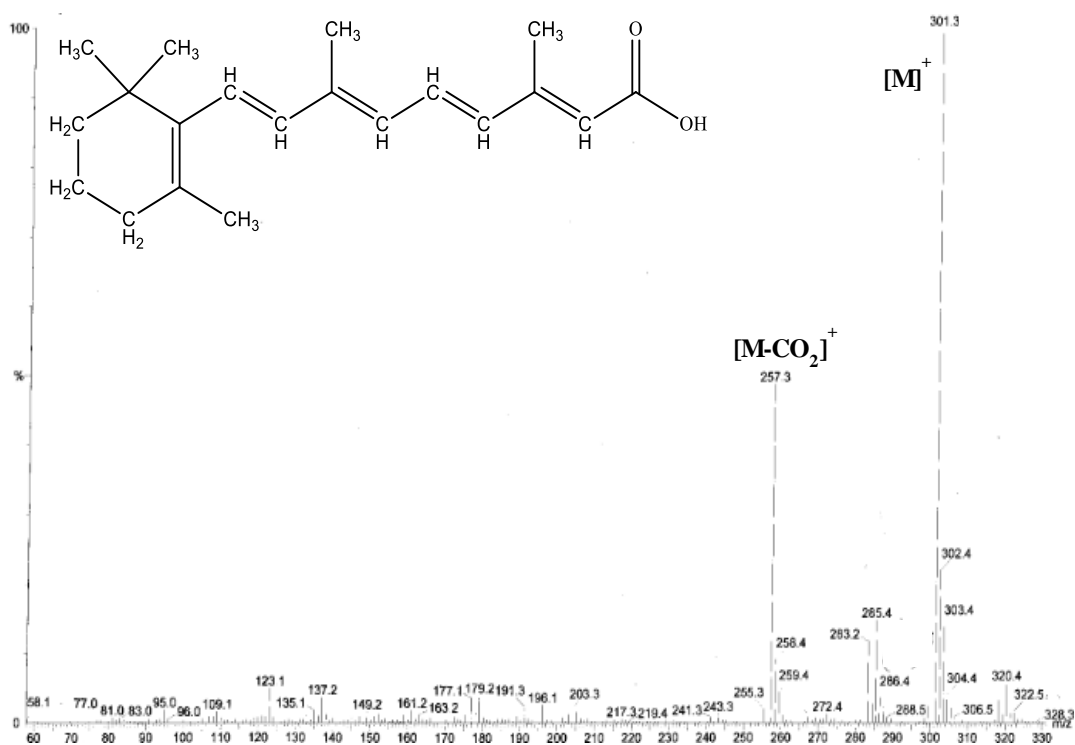
Figure 2.4 Mass Spectra (CI-MS) of atRA.

all-trans retinoic acid

13-cis retinoic acid

11-cis retinoic acid

9-cis retinoic acid

11,13-dicis retinoic acid

9,13-dicis retinoic acid

all-trans 5,6-epoxy retinoic acid

13-cis 5,6-epoxy retinoic acid
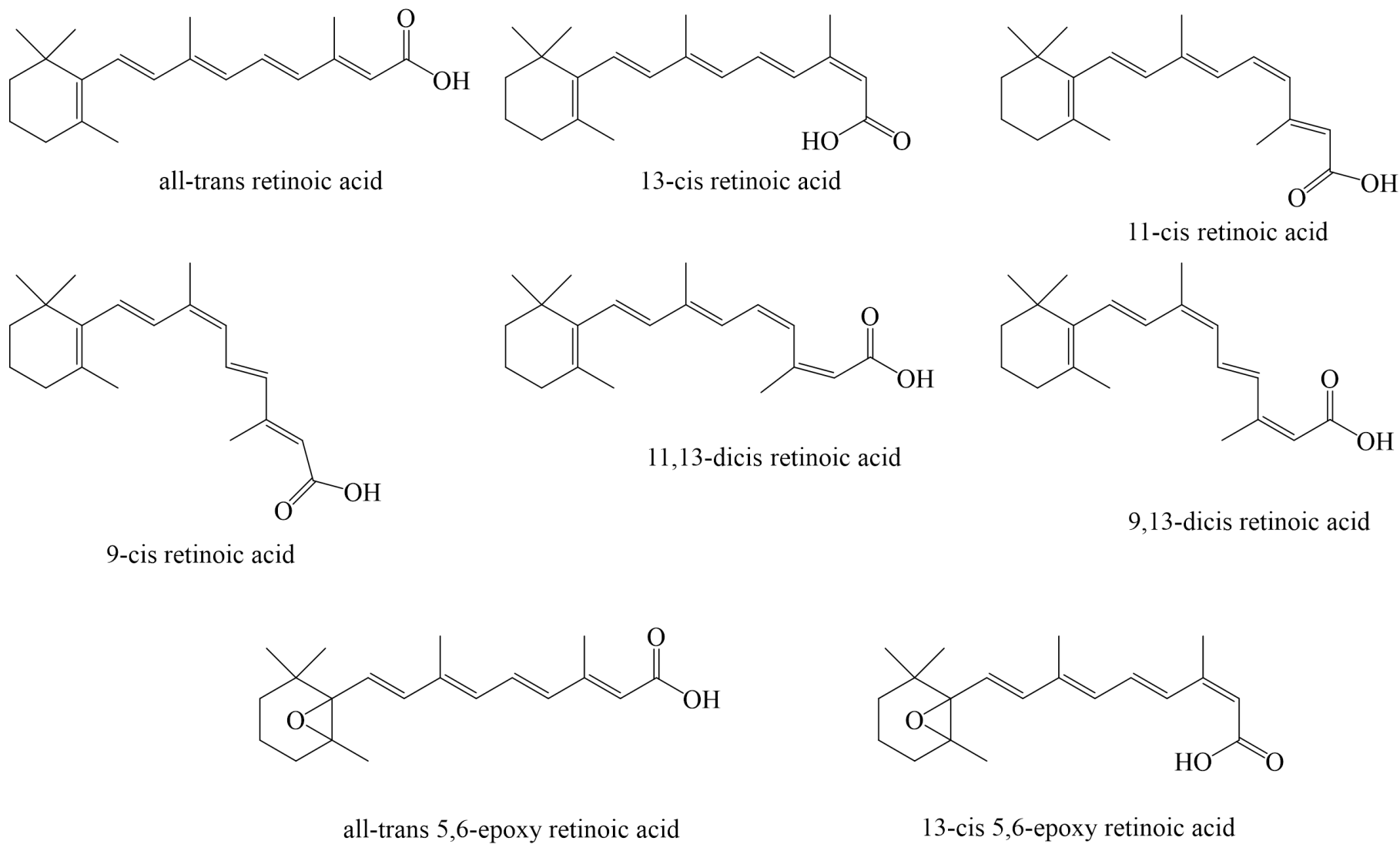
Figure 2.5 Isomers of retinoic acid and oxidation products all-trans epoxy retinoic acid and 13-cis 5,6 epoxy retinoic acid.[2]

The ^{1}H NMR spectrum of RA is shown in Figure 2.6 with all peaks assigned. Only the chemical shifts characteristic of the all-trans isomer are present indicating isomeric purity. In particular, there is absolutely no trace of the most common 13-cis isomer (see Figure 2.5) for which the chemical shift attributed to the CH named (l) would be shifted to 7.73 ppm.[13]
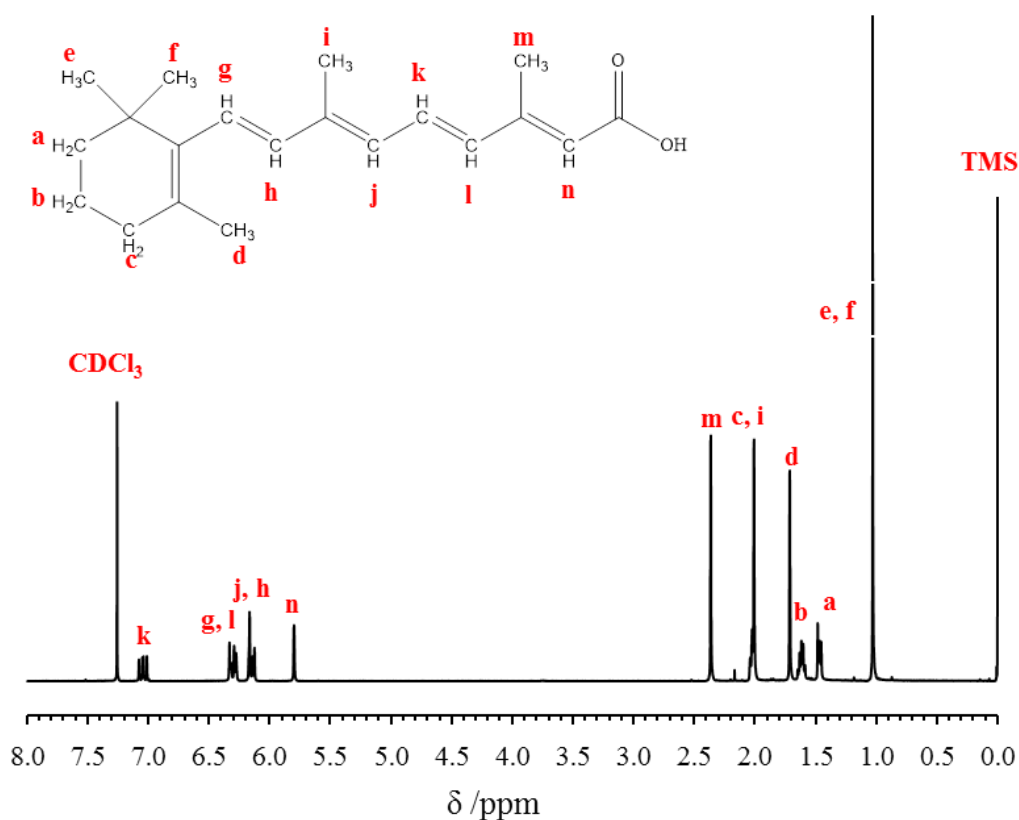
Figure 2.6 ^{1}H NMR (CDCl$_3$, 400 MHz) of atRA.

Further confirmation that no other isomer is present was obtained from the ^{13}C NMR spectrum of the RA sample (presented in Figure 2.7), where no carbon environment characteristic of isomers other than atRA was observed. Similar to ^{1}H NMR, there is no trace of the most common 13-cis isomer for which the chemical shift attributed to the carbon labelled (18) would be shifted to 168.6 ppm compared to 172.7 ppm observed.[14]
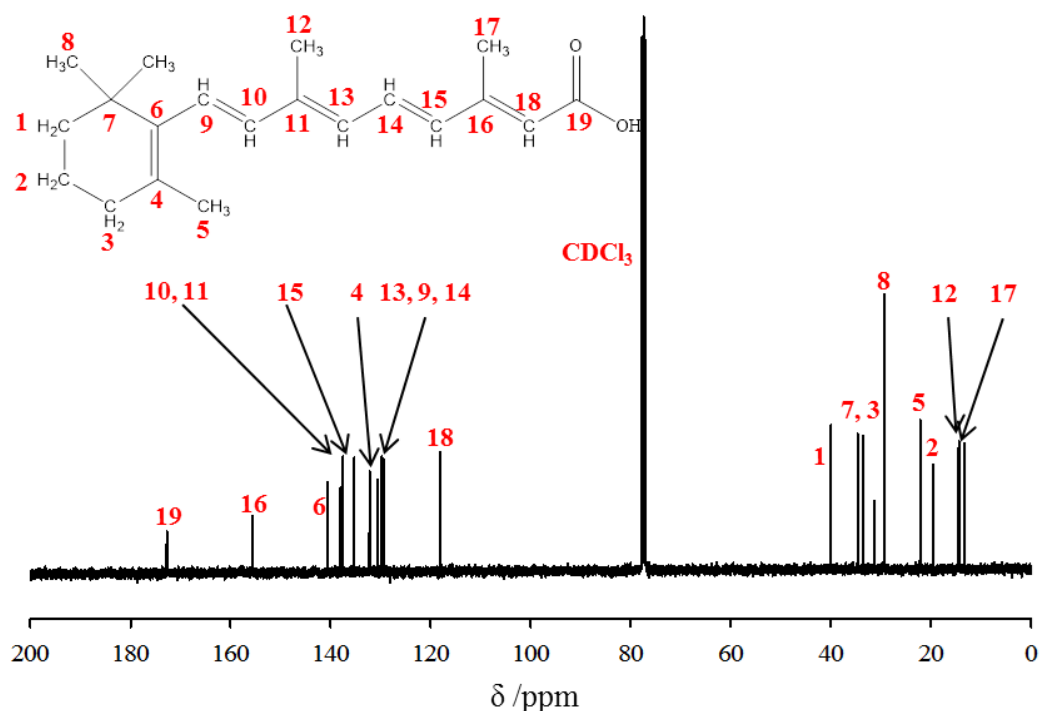
Figure 2.7 ^{13}C NMR (CDCl$_3$, 400 MHz) of atRA.

The melting point of RA was measured *via* an Optimelt Automatic Melting Point System. The melting temperature range was determined to be 179.8-181.5 °C which is characteristic of atRA whereas, 9-cis RA and 13-cis RA are characterised by melting points of 184-187 °C and 175 °C respectively.[15]

Finally RA was characterised by HPLC (UV-Vis detection: details in Section 6.1.4). The separation of RA cis- and trans- isomers by HPLC has been the subject of many investigations.[2, 13, 16] Using an eluent composed of 95% acetonitrile (ACN), 5% methanol (MeOH) and 0.6% acetic acid, a narrow peak was observed, with no lagging or tailing (see Figure 2.8). The presence of a single narrow peak confirms that only one isomer is present, concluding the atRA purity for later experiments. The peak located at 1.2 minutes is due to the detectors response to the mobile phase within the sample.
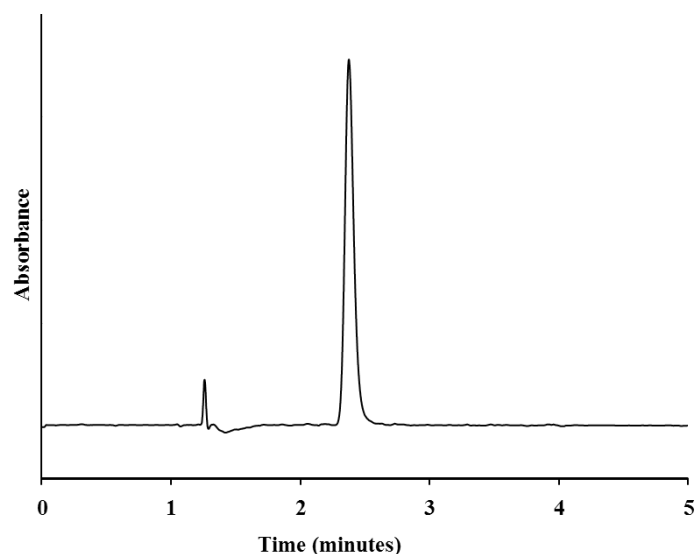
Figure 2.8 HPLC chromatogram of atRA (Eluent: 95% ACN; 5% MeOH; 0.6% Acetic Acid).

2.3 RETINOIC ACID DEGRADATION

As atRA has been proven to be light, heat and oxygen sensitive, it was essential to the project to study its degradation under the proposed experimental conditions which would be utilised throughout this research. The different conditions tested are summarised in Table 2.1.

Table 2.1 Various conditions and time points at which the degradation of atRA was studied.

	Solid atRA	atRA in EtOH (1mg/mL)	atRA in DMSO (66.6mg/mL)	atRA in SiO (suspension)	atRA in DCM (1mg/mL)
-20 °C Argon	1, 7, 28, 548d	1, 7, 28d	-	-	-
-20 °C Air	1, 7, 28d	1, 7, 28d	1, 7d	-	-
37 °C Light, Air	-	-	1, 7d	1, 7, 28d	-
37 °C Dark, Air	-	-	1, 7d	1, 7, 28d	-
Ambient T, Light, Argon	1, 7d	-	-	-	-
Ambient T, Light, Air	1, 7d	1, 7d	-	1, 7, 28d	-
Ambient T, Dark, Argon	1, 7d	-	-	-	1, 4, 7d
Ambient T, Dark, Air	1, 7d	1, 7d	-	1, 7, 28d	-

The possible and expected atRA degradation products (isomers, photoisomers and oxidation induced epoxide formation) can be seen in Figure 2.5. Degradation of atRA was monitored by HPLC, ^{1}H NMR and mass spectroscopy (CI for solid samples and electrospray (ES) for solutions) for all conditions apart from atRA in SiO due to incompatibility of the SiO with these methods.

As a yellow solid powder, atRA is normally stored under argon at -20 °C in the dark. Under these conditions no degradation was observed and atRA stability was assessed up to 548 days (3.5 years) after receipt of the product (Appendix Figure A1 and A2). When a solid sample was stored under the same conditions (-20 °C, in the dark) but in the presence of air, oxidation products began to show in CI-MS after 28 days (Figure 2.9). Increasing temperature as well as exposure to light also leads to the presence of other isomers (Appendix Figure A3-A8).
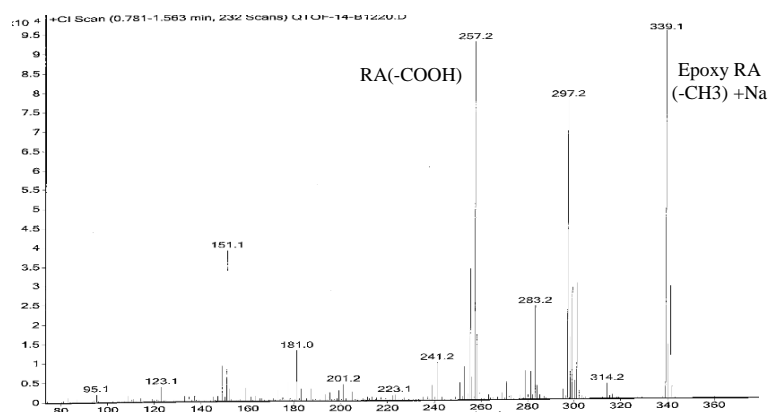
Figure 2.9 CI-MS of atRA stored at -20 °C under air for 28 days.

There was an increase in degradation when atRA was in solution, particularly upon exposure to light. Ethanol solutions were studied as EtOH would need to be used throughout the project. Samples were analysed at 1 and 7 days, and although some very minor degradation was observed upon storage at -20 °C (see Appendix Figure A9-A14), most degradation occurred when the temperature was increased and the samples were stored in the presence of light (see Appendix Figure A15-A17). Figure 2.10 shows the HPLC chromatograms of the ethanol solutions stored at ambient temperature, under air, in both light and dark. The appearance of a signal at 2 minutes elution compared to the atRA peak at 2.4 minutes indicates the presence of an impurity. This signal is much stronger when the sample is exposed to light and increases from 1 to 7 days.
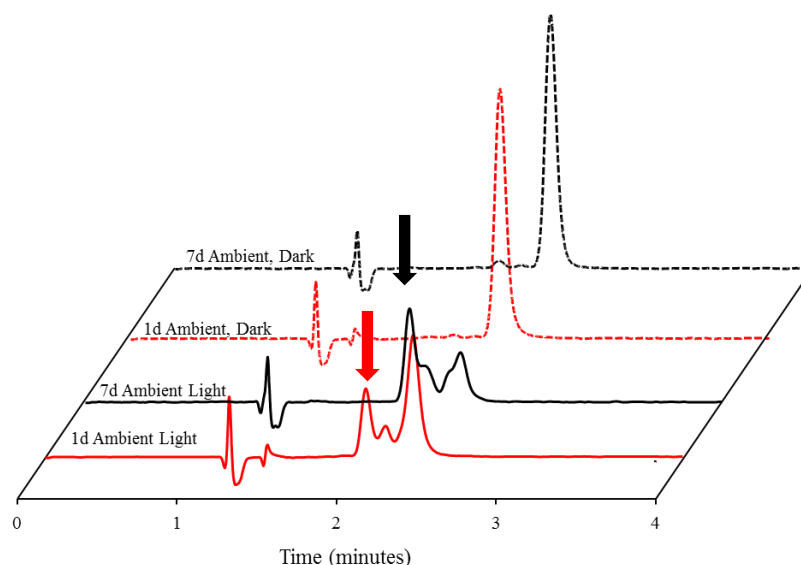
Figure 2.10 HPLC chromatograms of ethanol solutions of retinoic acid stored at ambient temperature in both light and dark, at 1 and 7 days.

atRA degradation was also investigated in DMSO solutions, as DMSO would be used later in the project to help solubilise atRA into media. Oxidation occurred within these samples when stored in the freezer after only one day, as evidenced by ES-MS, where an MH+ peak at 315 m/z, indicative of a 5,6-epoxide, can be seen (Figure 2.11).
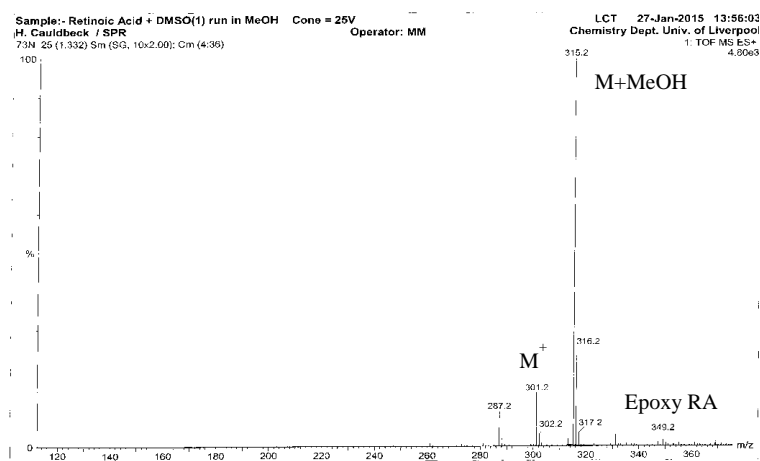
Figure 2.11 ES-MS of atRA stored in a DMSO solution at -20 °C in air for 1 day.

^{1}H NMR analysis in DMSO-d_6 showed a change of the multiplicity of the peak at 6.15 ppm attributed to C**H**-CH(CH$_3$)-C**H**-, (highlighted in Figure 2.12), as well as an increase of the integration values compared to the ^{1}H NMR of atRA (peaks **j,k** in Figure 2.6). This clearly indicates that isomerisation has occurred as well as oxidation.
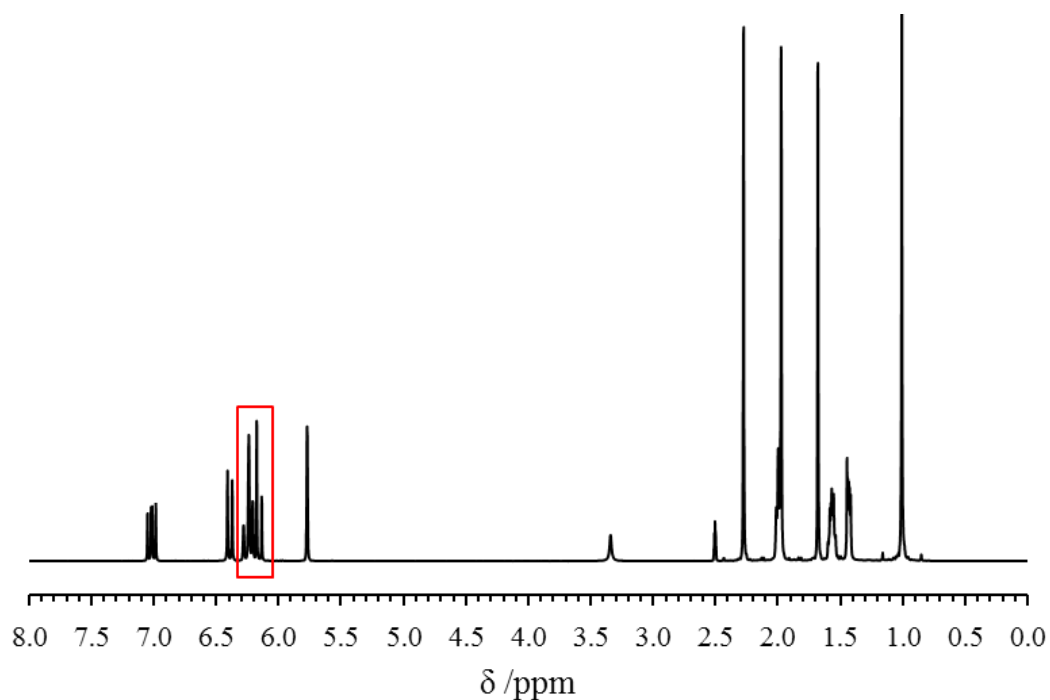
Figure 2.12 ^{1}H NMR (DMSO-*d6*, 400MHz) of atRA after storage in a DMSO solution at -20 °C in the presence of air for 1 day.

As anticipated, samples stored in DMSO at 37 °C degraded to a greater extent than those stored at -20 °C, particularly in the presence of light (see Appendix Figure A18-A23). Furthermore, visual inspection showed a colour change from a yellow to orange solution.

For DCM, which is the solvent of choice for the synthetic reactions that were planned for this project, degradation was assessed under argon and in the dark. Isomerisation occurred under these conditions after 4 days, as evidenced by the presence of new peaks in the HPLC chromatograms (see Figure 2.13). Furthermore, as the ^{1}H NMR spectra was unchanged (see Appendix Figure A24) for that period of time, the extent of degradation was considered to be at a level acceptable for further study. Time periods of future reactions in DCM will be kept in mind.
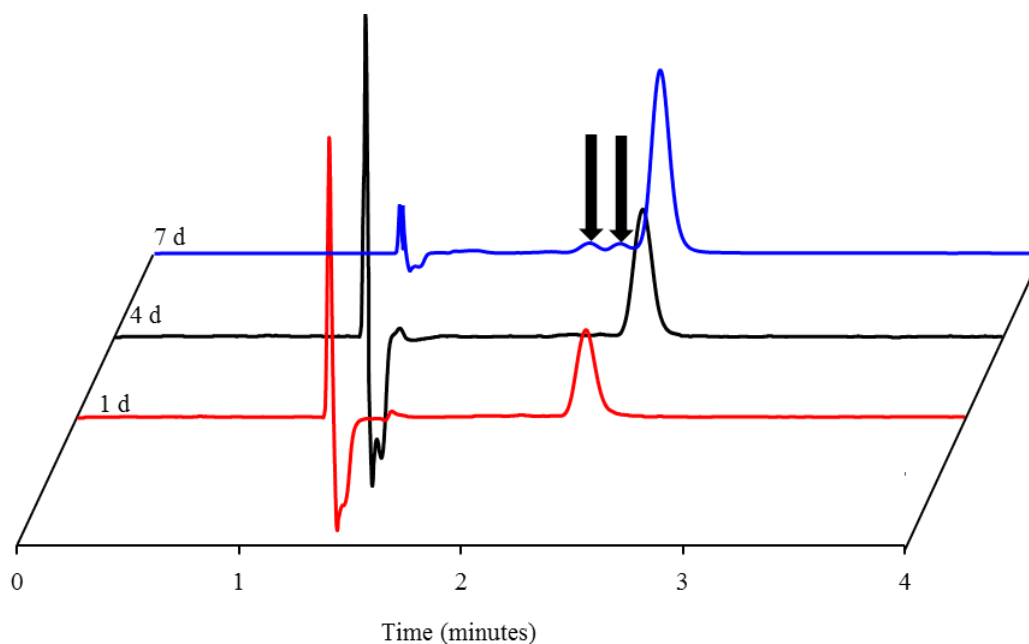
Figure 2.13 HPLC chromatograms of atRA stored in DCM at ambient temperature in the dark for 1 (red), 4 (black) and 7 (blue) days. (Eluent: 95% ACN; 5% MeOH; 0.6% Acetic Acid).

Studying the degradation of atRA in SiO was essential as the ultimate aim of the project is to solubilise atRA into SiO for the treatment of PVR. Only ^{1}H NMR was used to analyse this as neither HPLC nor mass spectroscopy can be carried out in the presence of SiO, and extraction methods of atRA from the SiO could potentially lead to degradation, therefore, making it impossible to determine whether degradation occurred before or after extraction. Studies of atRA in SiO was not carried out at concentrations where atRA is solubilised, as even at the saturation concentration, signals in the ^{1}H NMR spectra were not intense enough to analyse atRA compared to the SiO peaks. Instead samples of 1 mg/mL atRA in SiO were used. The ^{1}H NMR spectra of the samples exposed to the harshest conditions, i.e light, air and 37 ℃, can be seen in Figure 2.14. From the ^{1}H NMR analysis there was no degradation of atRA over 28 days in SiO.
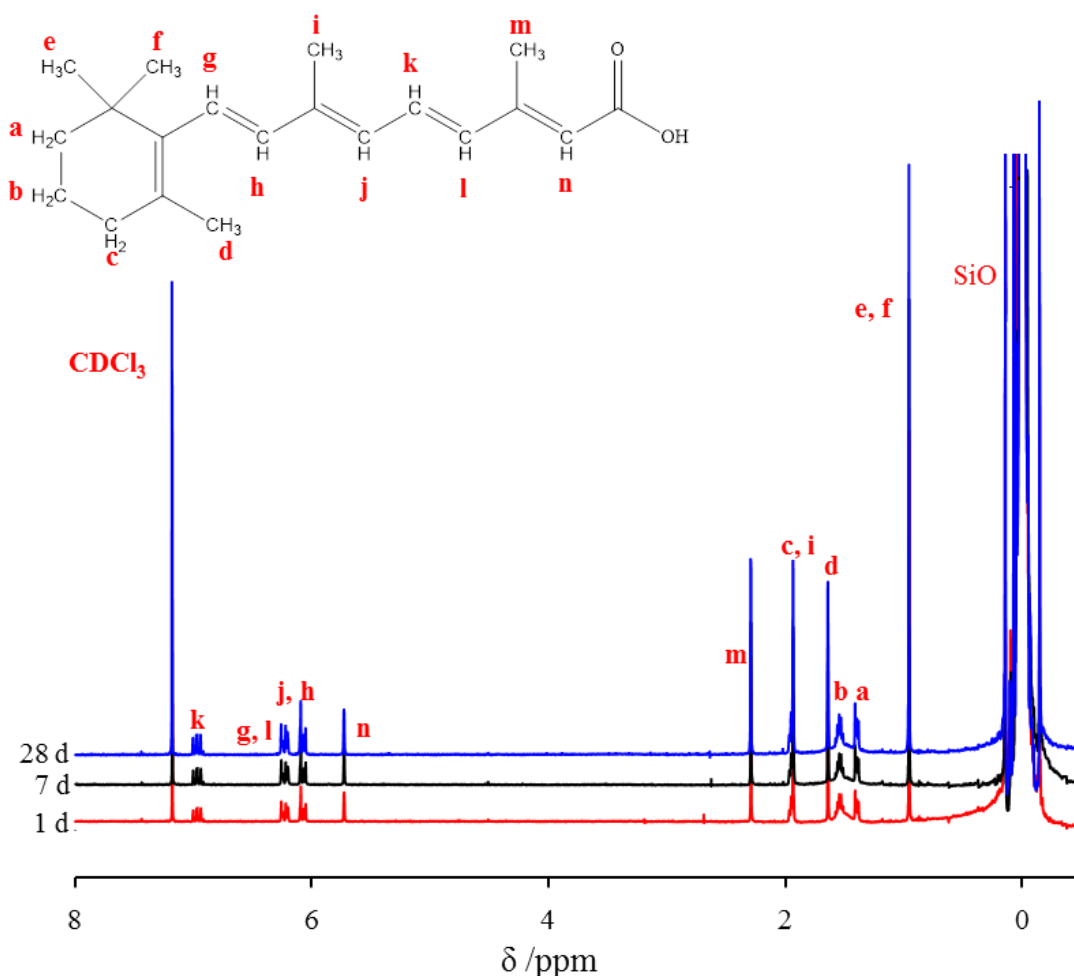
Figure 2.14 ^{1}H NMR (CDCl$_3$, 400MHz) of atRA in SiO at 1 mg/mL after 1, 7 and 28 days, upon storage under light, air and at 37°C.

2.3.1 Degradation in Media

Cell culture experiments will be carried out in this project, therefore the effects of culture media on atRA needed to be studied. The classic conditions for incubating ARPE-19 cells were used, i.e. 37 °C with 5 % CO$_2$ and in the dark. Direct analysis of atRA in media could not be carried out, as media is not a suitable solvent for any of the analytical techniques available, therefore, atRA had to be extracted (see Section 6.4.1 for details). To ensure the extraction method was not degrading the atRA and confounding the results, a t=0 time point was taken which included extraction. Solutions of atRA in media were prepared at a concentration of 10^{-3} M (using DMSO at 1 % to achieve solubility) as this is the maximum concentration currently dosed in the literature.[17] Figure 2.15 shows the HPLC chromatograms of samples taken at different time points along with the sample at t=0. A degradation

product eluting at 1.9 minutes is present after day 1 (absent at t=0) and increases from 7.9 % of the atRA peak after 1 day to 18.6 % at 7 days study.
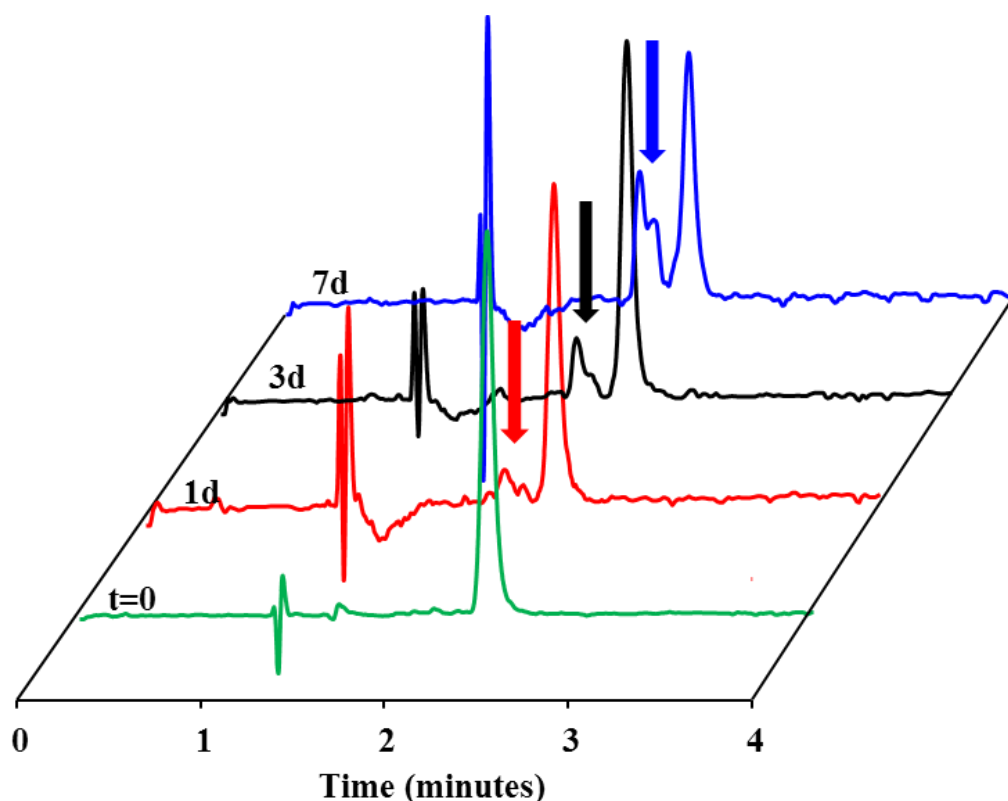
Figure 2.15 HPLC chromatograms of RA extracted from media at t=0 (green), 1 (red), 3 (black) and 7 (blue) day. (Eluent: 95 % ACN; 5 % MeOH; 0.6 % Acetic Acid).

The media is usually changed every 3-4 days when cultivating ARPE-19 cells, however, this degradation study suggests that when studying release of atRA, samples must be taken more frequently, preferably every day.

2.3.2 Autoclave Degradation

One of the companies which currently supplies medical grade SiO for eye tamponades is Fluoron GmbH.[18] The commercial oil is subjected to sterilisation by autoclave at a temperature of 121 °C for 21 minutes. Solutions of atRA in SiO (1 mg/mL) were prepared, then autoclaved under the same conditions. ^{1}H NMR and UV-Vis spectroscopy were carried out to analyse degradation by solubilising the SiO solutions in CDCl$_3$ and THF respectively. No isomerisation was observed in either spectrum (^{1}H NMR spectrum in Appendix Figure A25). Figure 2.12 shows the comparison between the UV-Vis traces of SiO, atRA and atRA solution in SiO

before and after treatment by autoclave. There is no difference in absorbance of atRA in THF or atRA in SiO solubilised in THF before and after being autoclaved. The difference in intensity observed is due to samples being at different concentrations. Overall the treatment by autoclave doesn't seem to affect atRA when in SiO.
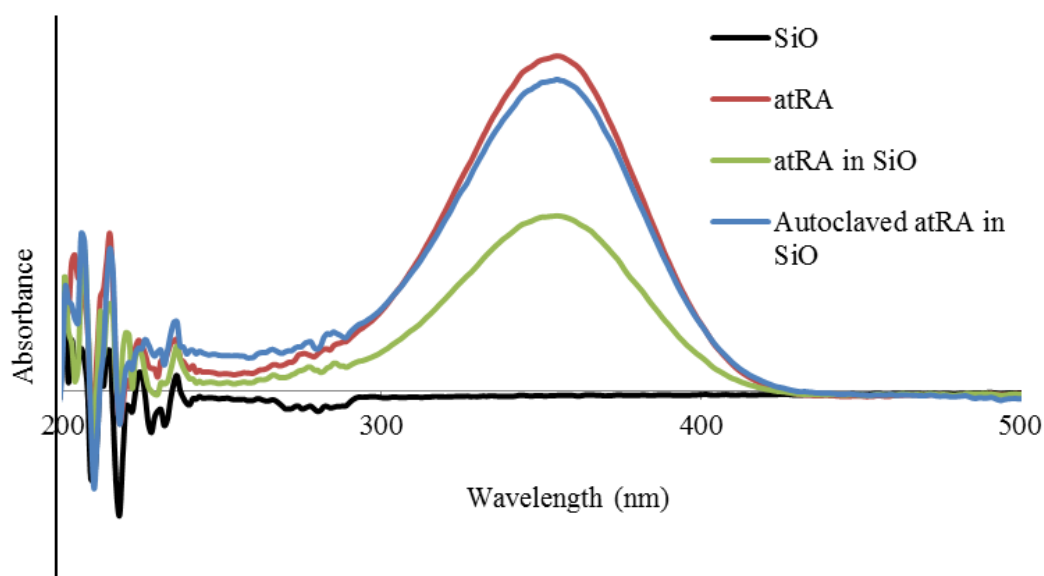
Figure 2.16 UV-Vis spectra of atRA compared to atRA in SiO before and after autoclave; all solubilised in THF.

2.4 BIOLOGICAL EVALUATION

As discussed in Section 2.1, the assays used to determine drug toxicity were MTT, resazurin, phalloidin staining and BrdU. BrdU assays were also used to investigate the anti-proliferative effects of atRA and Ibu on ARPE-19 cells. Various conditions of both culture time (pre- and post-confluent; cells cultured for 1 and 7 days respectively) and drug exposure times (1 and 7 days) were studied.

2.4.1 Controls

For each assay three technical replicates of each condition were carried out as well as controls, to confirm the assay was working correctly and ensure the validity of the experiment. These included:

- Negative Control- represents healthy cells solely treated with culture media, expecting to observe no adverse effects

- Positive Control- cells treated with 20 % DMSO to induce cell death

- 1 % DMSO- higher concentrations of drug require the presence of 1 % DMSO to become soluble in culture media.

For MTT and Resazurin assays, the above controls were studied as well as the following additional experiments to ensure no background signals were observed in the spectrophotometer or fluorescent plate reader:

- Media

- Media plus cells

- Media plus MTT/resazurin.

Results from both MTT and resazurin assays are presented in Figure 2.17 where no significant difference between the negative controls and cells treated with 1 % DMSO was observed. This indicates that this concentration of DMSO does not affect the metabolic activity of the mitochondria and is not toxic to RPE cells. Therefore, the drugs can be solubilised in 1 % DMSO and put into the media without affecting cytotoxicity studies. There was a significant difference between both the negative control and 1 % DMSO dosage, against the positive control, and the background measurements of media, cells and MTT/resazurin, therefore indicating no interference from these additional components and resulting in confidence of a good experimental set up.
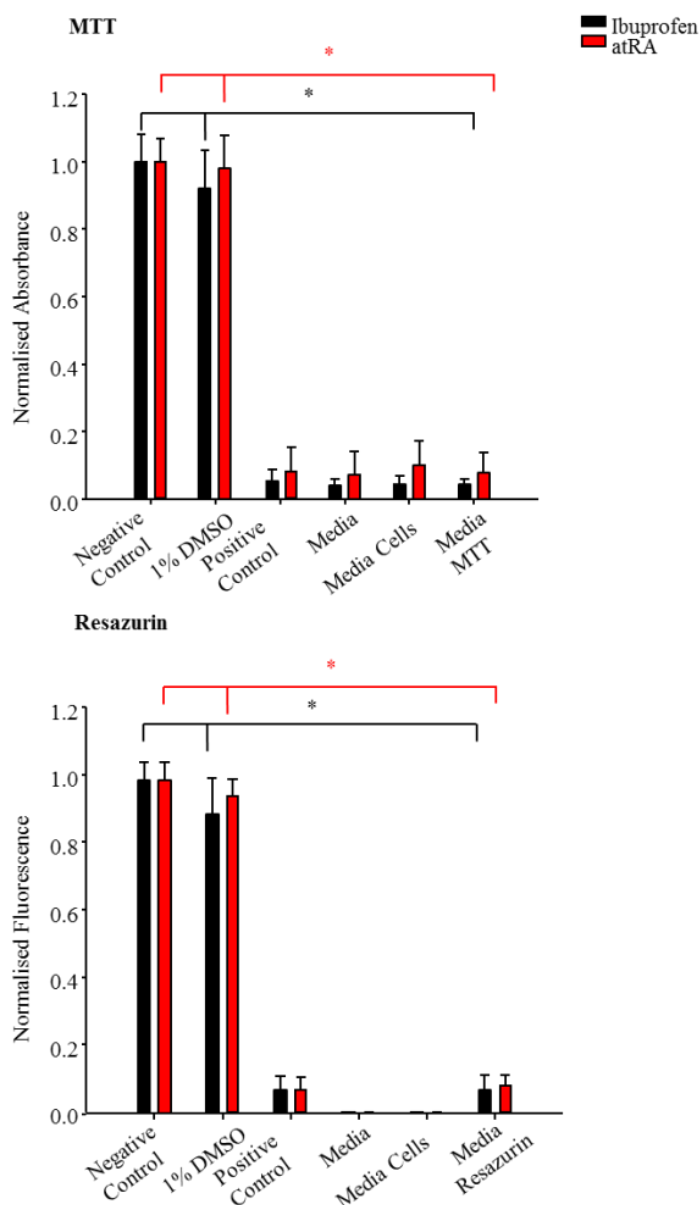
Figure 2.17 Controls studied by MTT (top) and resazurin (bottom) assays (mean, error bars represent ± 1 standard deviation); n=3 . *, Significance by ANOVA and Dunnett's T3 post-hoc evaluation (p≤0.05).

Phalloidin staining was carried out on the negative and positive control samples as well as cells treated with 1 % DMSO (representative images of the controls are presented in Figure 2.18). Staining confirmed that the cellular structure was intact for the negative control and cells treated with 1 % DMSO. However, the majority of cells in the positive control had died, those that were still attached to the base of the well were stained and could be seen to be rounded and/or not resembling a healthy cell.
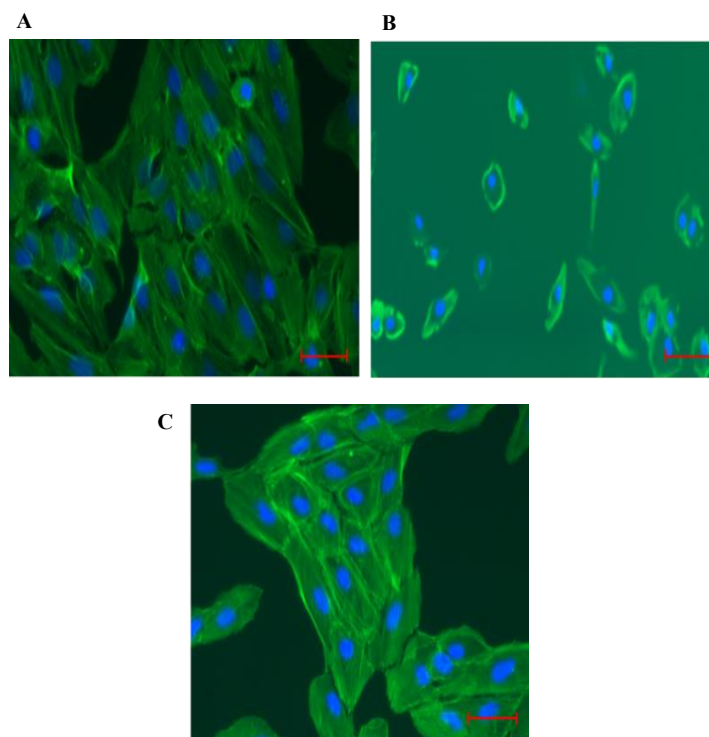
Figure 2.18 Fluorescent phalloidin (green) marked F-actin in ARPE-19 cells and DAPI (blue) stained nuclei. A: Negative control, B: positive control and C: cells exposed to 1 % DMSO. Scale bar represents 50 µm.

2.4.2 Retinoic Acid

The metabolic activity and morphology of ARPE-19 cells were studied at multiple time scales. Both pre- and post-confluent cells (1 day and 7 days growth respectively) were exposed to atRA for 1 and 7 days. MTT and resazurin were the initial assays carried out followed by phalloidin staining on the cells from the resazurin assays. Finally cell counts were performed to assess the toxicity.

MTT and resazurin assays were in concordance with one another with respect to the amount of atRA that affected the metabolic activity of the cell (Figure 2.19). For pre- and post-confluent cells after 1 day exposure to atRA, cytotoxicity was observed at concentrations above 10^{-5} M. After 7 days exposure, cytotoxicity for post-confluent cells was also observed for concentrations above 10^{-5} M, however, for pre-confluent cells the toxic limit decreased by a factor of ten, to concentrations above 10^{-6} M.

MTT
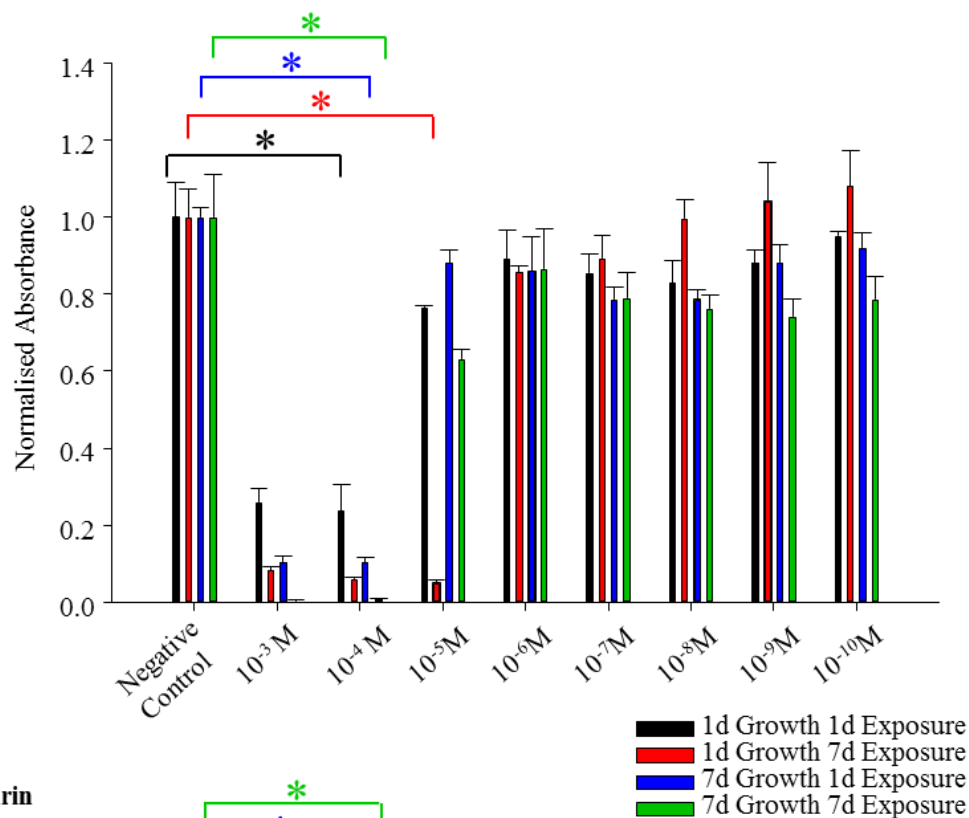
Resazurin
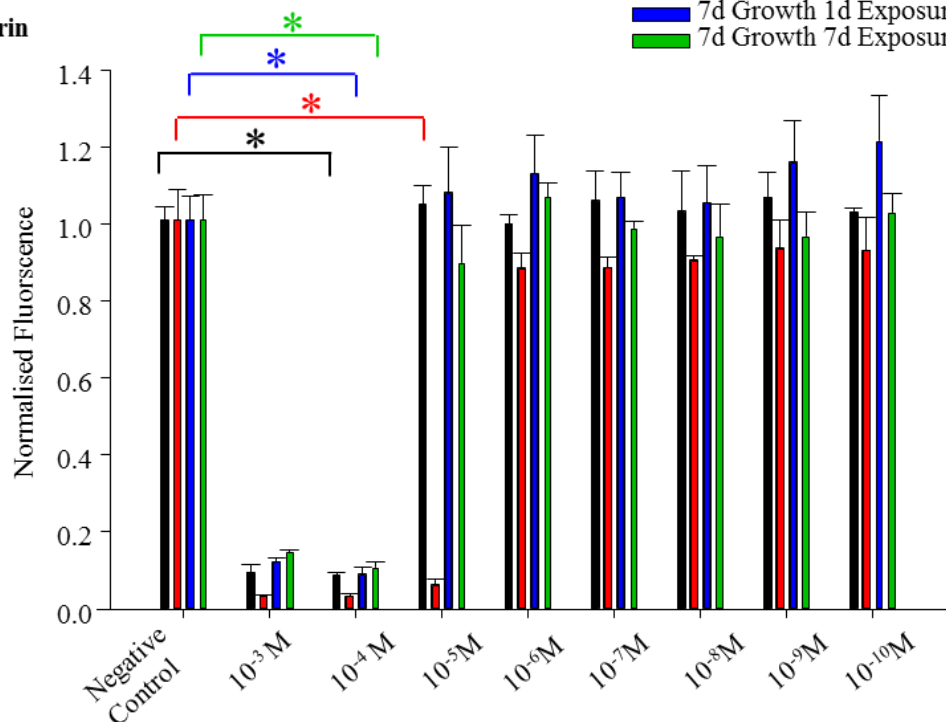
Figure 2.19 Overall cytotoxicity of atRA determined from MTT and resazurin assays. ARPE-19 cells were exposed to different concentrations of atRA, from $10^{-3} - 10^{-10}$ M, grown and treated for different time scales. Pre-confluent cells (grown for 1 d) were exposed to atRA for 1 d (black) and 7 d (red). Post-confluent cells (grown for 7 d) were also exposed to atRA for 1 d (blue) and 7 d (green). (mean, error bars represent ± 1 standard deviation); n=3. *, Significance by ANOVA and Dunnett's T3 post-hoc evaluation (p≤0.05).

Phalloidin staining confirmed these cytotoxic concentrations with images of healthy cytoskeletons when pre-confluent cells were exposed to atRA for 7 days at concentrations 10^{-5} M or 10^{-6} M. Figure 2.20 shows pre-confluent cells exposed to different concentrations of atRA for 1 day. Many cells exposed to 10^{-3} M atRA have died, therefore, there were very few cells to image. Cells exposed to 10^{-4} M still look unhealthy whereas cells exposed to 10^{-5} M are comparable to those imaged in the negative control (healthy cells).
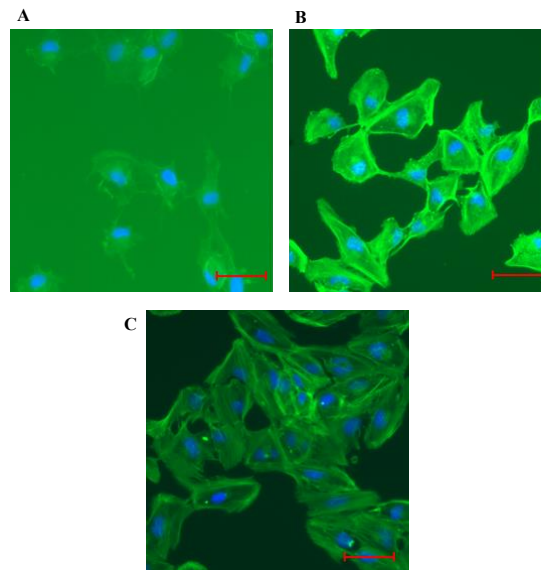
Figure 2.20 Images of pre-confluent ARPE-19 cells with F-actin stained by phalloidin (green) and nuclei by DAPI (blue) exposed to different concentrations of atRA. A: 10^{-3}, B: 10^{-4} and C: 10^{-5} M. Scale bar represents 50 μm.

BrdU incorporation assays allow for both cytotoxicity and anti-proliferative effects to be studied. Cell number was determined as all nuclei were stained after drug exposure and counted; a decreased cell number compared to the negative control indicated an increase in drug toxicity. This assay followed the same trend as the previous assays (see Figure 2.21); no cytotoxic effects were observed below 10^{-5} M for post- and pre-confluent cells when exposed for 1 day or 10^{-6} M for pre-confluent cells with a longer exposure time of 7 days. However, the cell number is approximately 25 % of the cell number usually seen when cells are cultured for 8 days. Also the samples subjected to longer culture time (8 days) present larger variations, as evidenced by the standard deviation; this is because the cells grow in clusters and for analysis random areas of wells are counted to determine overall cell number. Therefore, some images would have a larger number of cells than others where there were large areas devoid of cells.
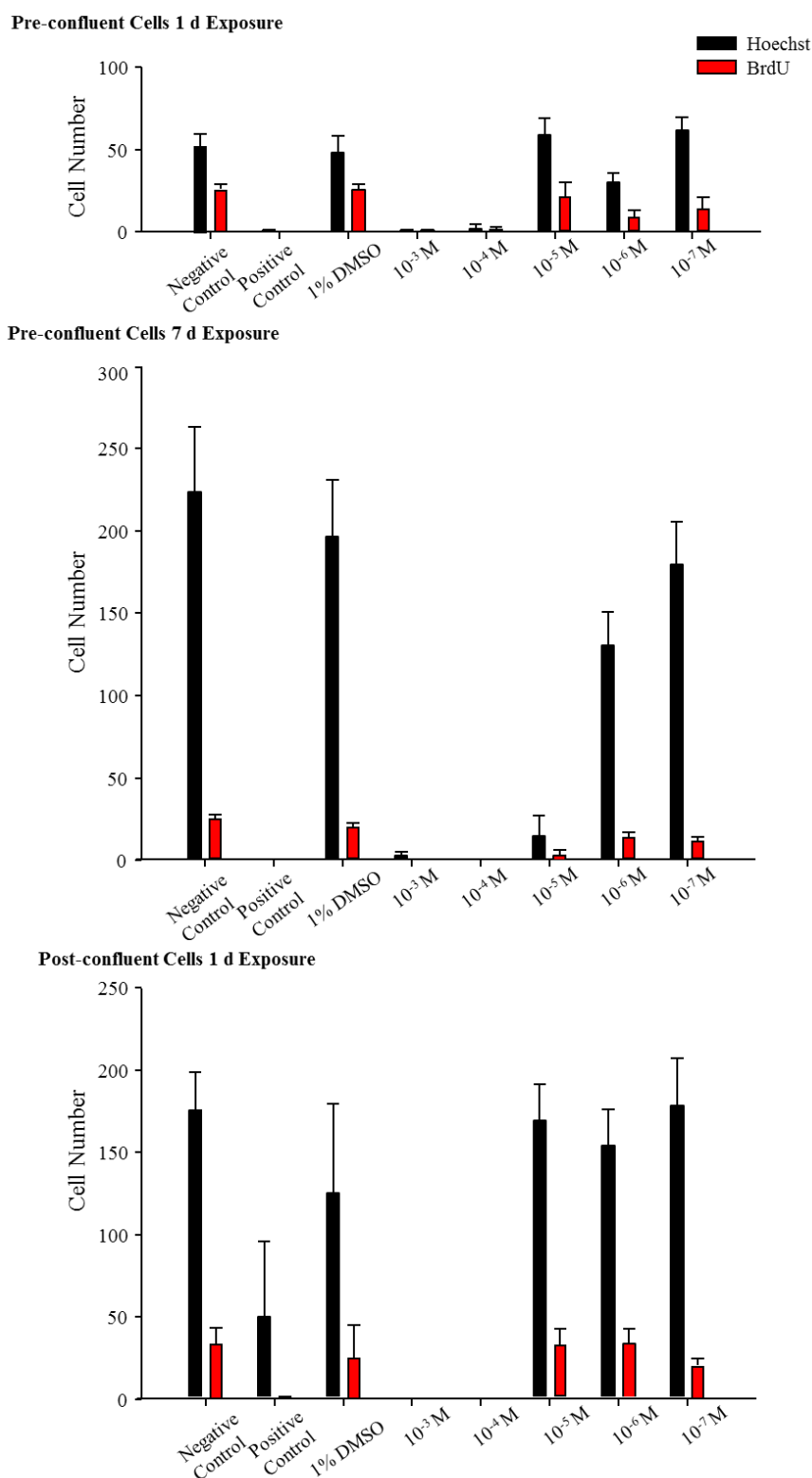
Figure 2.21 Cell number upon exposure to atRA determined from BrdU assay. ARPE-19 cells were exposed to different concentrations of atRA, from $10^{-3} - 10^{-7}$ M, grown and treated for different time periods. Pre-confluent cells (grown for 1 day) were exposed to atRA for 1 day (top) and 7 days (middle). Post-confluent cells (grown for 7 days) were also exposed to atRA for 1 day (bottom). Bars represent mean number of BrdU-positive cells per field of view. (Error bars represent ± 1 standard deviation); n=9.

The anti-proliferative effect of atRA was also studied using this assay (see Section 2.1.1.4). After the cells were exposed to atRA for the desired time they were incubated with BrdU for 4 hours. Only the cells which proliferated during this time incorporated BrdU. Cells were fixed and stained, then imaged by fluorescence microscopy. Both the Hoechst stained nuclei and anti-BrdU stained nuclei were counted and a percentage of proliferation determined. Table 2.2 summarises the percentage of proliferation observed for all the different concentrations tested. A decrease in proliferation was observed when cells were exposed to increasing concentrations of atRA. Pre-confluent cells exposed to atRA for 1 day showed the most dramatic effect. In this particular case the cells were still proliferating at a faster rate to form a monolayer, compared to subsequent assays when cells were cultured for 8 days and a monolayer had already formed. Proliferation percentage went from 49 % in the negative control (where proliferation should be consistent with normal cellular rate) to 22 % when exposed to 10^{-5} M atRA. No BrdU incorporation was observed within the 4 hour incubation period for post-confluent cells when exposed to atRA for 7 days as a monolayer of ARPE-19 cells had already formed and proliferation was no longer occurring at a steady rate.

Table 2.2 Proliferation calculated as a percentage of cell nuclei with incorporated BrdU compared to Hoechst stained nuclei, when cells were exposed to atRA 10^{-5}-10^{-7} M (10^{-5} M excluded for pre-confluent cells with 7 days exposure as this concentration determined to be toxic) as well as controls where proliferation shouldn't be affected.

| Exposure Conditions	% Proliferation of Pre-confluent Cells		% Proliferation Post-Confluent Cells
	1 d Exposure	7 d Exposure	1 d Exposure
Negative Control	49	11	20
1 % DMSO	54	10	21
10^{-5} M atRA	22	-	12
10^{-6} M atRA	30	6	21
10^{-7} M atRA	37	11	19

2.4.3 Ibuprofen

Cytotoxic responses of ARPE-19 cells were also studied upon exposure to varying amounts of Ibu, from 10^{-3} to 10^{-10} M. The same time scales and experimental set-up

were used as in Section 2.4.2 to study both pre- and post-confluent cells at different exposure times.

MTT and resazurin assays were in concordance with one another with respect to the amount of Ibu which affected the metabolic activity of the cell, see Figure 2.23. For pre-and post-confluent cells and 1 day exposure to Ibu, cytotoxicity was observed at concentrations above 10^{-4} M. Upon 7 days of exposure, cytotoxicity for post-confluent cells was also observed at concentrations above 10^{-4} M. However, for pre-confluent cells the toxic limit decreased to concentrations above 10^{-5} M. All cytotoxicity observed for Ibu occurred at a concentration a factor of 10 higher than atRA for the same culture and exposure times.

Phalloidin staining confirmed these cytotoxic amounts with images of healthy cytoskeletons in the case of pre-confluent cells exposed to Ibu for 7 days, at concentrations below 10^{-4} M or 10^{-5} M. Figure 2.22 shows pre-confluent cells exposed to Ibu for 1 day; cells exposed to 10^{-3} M Ibu have died and those that remain do not exhibit a healthy epithelial morphology, therefore, there were not as many cells to image whereas cells exposed to 10^{-4} M Ibu are comparable to those imaged in the negative control (healthy cells).
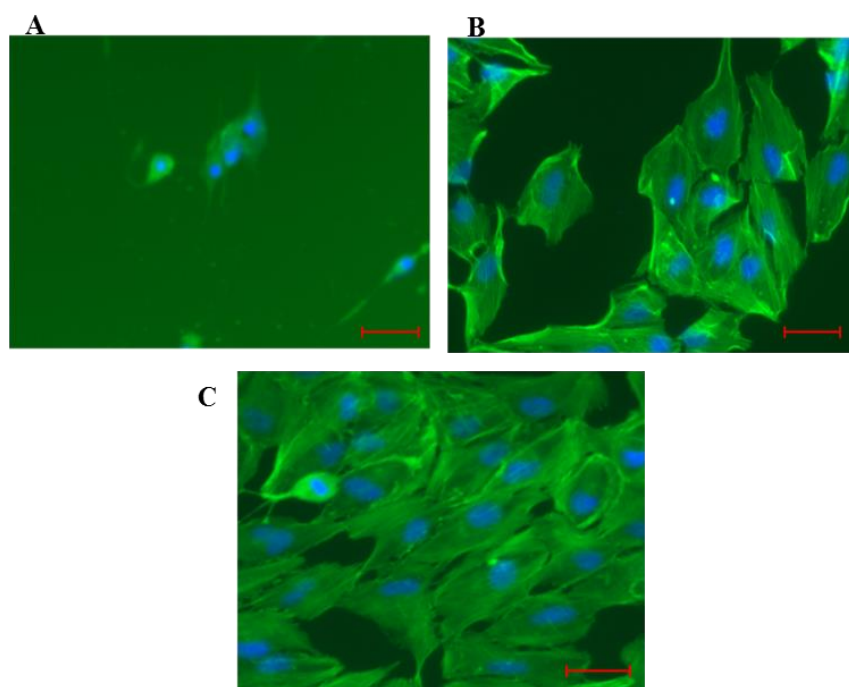

Figure 2.22 Fluorescent imaging of pre-confluent ARPE-19 cells with F-actin stained by phalloidin (green) and nuclei by DAPI (blue) exposed to different concentrations of Ibu. A: 10^{-3}, B: 10^{-4} and C: 10^{-5} M. Scale bar represents 50 μm.

MTT
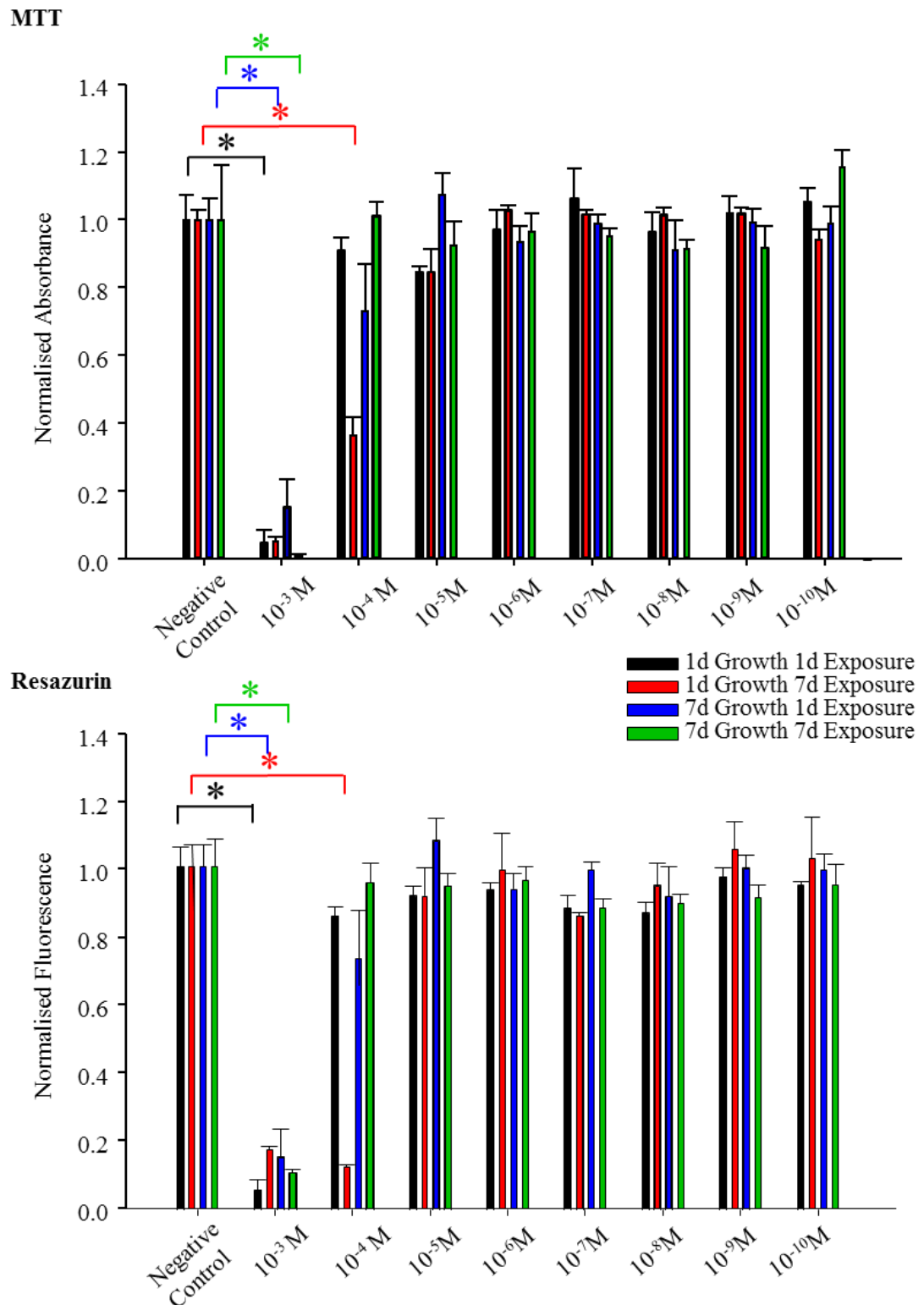
Resazurin

Figure 2.23 Overall cytotoxicity for Ibu determined from MTT and resazurin assays. ARPE-19 cells were exposed to different concentrations of Ibu, from $10^{-3} - 10^{-10}$ M, grown and treated for different time scales. Pre-confluent cells (grown for 1 day) were exposed to Ibu for 1 day (black) and 7days (red). Post-confluent cells (grown for 7 days) were also exposed to Ibu for 1 day (blue) and 7 days (green). (mean, error bars represent $\pm$ 1 standard deviation); n=3. *, Significance by ANOVA and Dunnett's T3 post-hoc evaluation (p$\leq$0.05).

BrdU incorporation assay allowed for both cytotoxicity and anti-proliferative effects to be studied. Cell number was determined and followed the same trend as the previous assays (see Figure 2.24). No cytotoxic effects were observed below 10^{-4} M for post- and pre-confluent cells upon 1 day exposure, or 10^{-5} M for pre-confluent cells with a longer exposure time of 7 days.
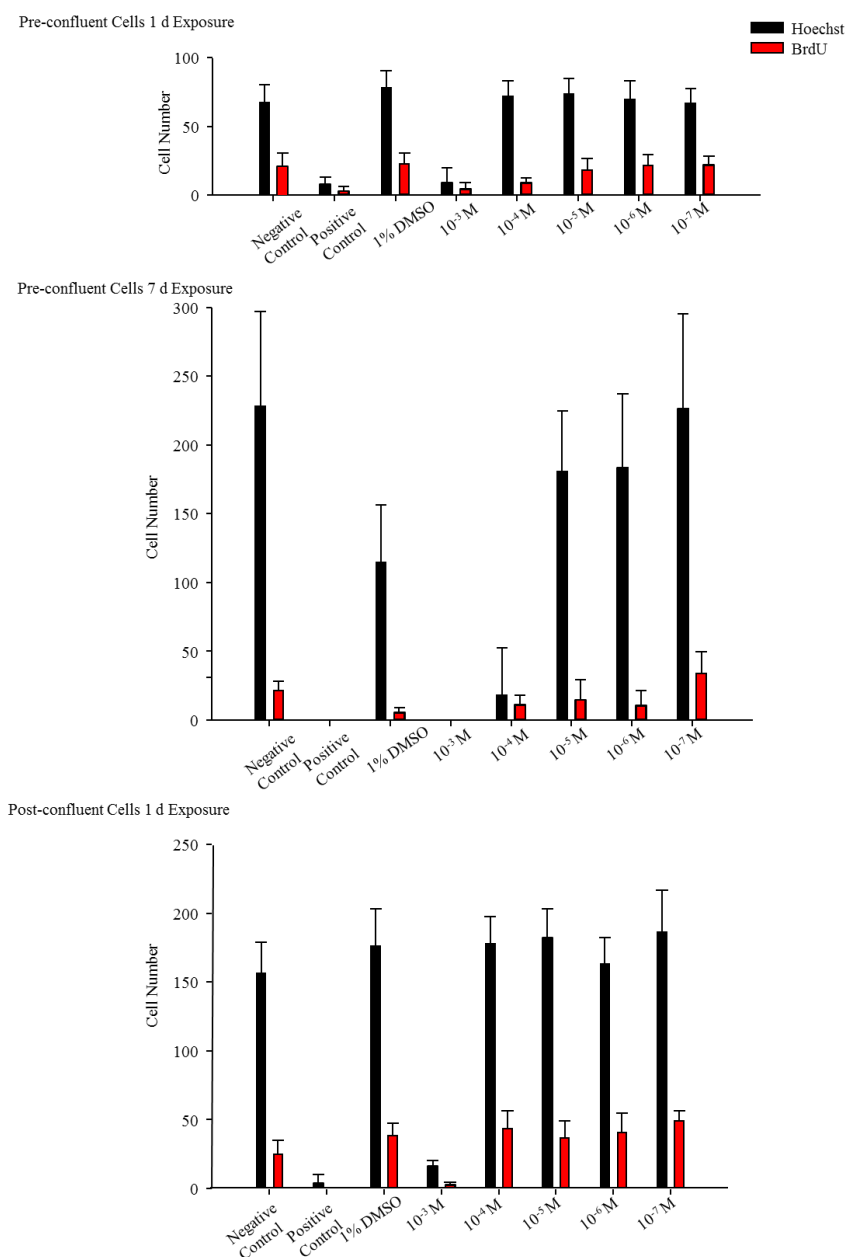
Figure 2.24 Cell number upon exposure to Ibu, determined from BrdU assay. ARPE-19 cells were exposed to different concentrations of Ibu, from 10^{-3} – 10^{-7} M, grown and treated for different time scales. Pre-confluent cells (grown for 1 day) were exposed to Ibu for 1 day (top) and 7 days (middle). Post-confluent cells (grown for 7 days) were also exposed to Ibu for 1 day (bottom). Bars represent mean number of BrdU-positive cells per field of view. (Error bars represent ± 1 standard deviation); n=9.

The anti-proliferative effect of Ibu was also studied. After the cells were exposed to Ibu for the desired time period they were incubated with BrdU for 4 hours. Table 2.3 shows Ibu had no effect on proliferation, apart from when pre-confluent cells were exposed to Ibu for 1 day at 10^{-4} M. Here the proliferation rate was less than half of what was seen for the controls and the other treatment concentrations.

Table 2.3 Proliferation calculated as a percentage of cell nuclei with incorporated BrdU compared to Hoechst stained nuclei, when cells were exposed to Ibu 10^{-4} – 10^{-7} M (10^{-4} M excluded for pre-confluent cells with 7 d exposure as this concentration determined to be toxic) as well as controls where proliferation shouldn't be affected.

Exposure Conditions	% Proliferation of Pre-confluent Cells		% Proliferation Post-Confluent Cells
	1 d Exposure	7 d Exposure	1 d Exposure
Negative Control	31	10	16
1 % DMSO	29	5	22
10^{-4} M Ibu	12	-	25
10^{-5} M Ibu	25	8	20
10^{-6} M Ibu	31	6	25
10^{-7} M Ibu	33	15	27

2.5 CONCLUSION

The characterisation of atRA was accomplished by ^{1}H and ^{13}C NMR spectroscopy, CI mass spectroscopy, HPLC and melting point analysis, all of which confirmed isomeric purity of the sample as being the all-trans material. A degradation study of the atRA isomer was carried out under various conditions relevant to experimental conditions to be used within the thesis. The ideal storage conditions were determined to be atRA as a solid at -20 °C in the dark with an inert argon atmosphere so no degradation can occur.

Biological evaluation of both atRA and Ibu was carried out on ARPE-19 cells *via* MTT, resazurin, phalloidin and BrdU assays. For pre-and post-confluent cells and 1

day exposure to atRA, cytotoxicity was observed at concentrations above 10^{-5} M whilst exposure to Ibu under the same conditions resulted in cytotoxic results above 10^{-4} M. Upon 7 days exposure, cytotoxicity in the case of post-confluent cells was observed at the same concentrations, however, for pre-confluent cells the toxic limit decreased by a factor of ten for both atRA and Ibu to concentrations above 10^{-6} M and 10^{-5} M respectively. All cytotoxicity observed for Ibu occurred at a concentration a factor of 10 higher than atRA for the same culture and exposure times, therefore it was determined that Ibu is less toxic to ARPE-19 cells than atRA. Overall, the cytotoxic limits of atRA and Ibu on ARPE-19 cells determined from these assays will lead to the concentrations of drug used for future loading and release studies within the project.

2.6 REFERENCES

1. X. Tan, N. Meltzer and S. Lindenbaum, *Pharmaceutical Research*, 1992, **9**, 1203-1208.

2. D. K. Bempong, I. L. Honigberg and N. M. Meltzer, *Journal of Pharmaceutical and Biomedical Analysis*, 1995, **13**, 285-291.

3. J. J. Araiz, M. F. Refojo, M. H. Arroyo, F. L. Leong, D. M. Albert and F. I. Tolentino, *Investigative Ophthalmology & Visual Science*, 1993, **34**, 522-530.

4. K. Dunn, A. Aotaki-Keen, F. Putkey and L. Hjelmeland, *Experimental Eye Research*, 1996, **62**, 155-170.

5. K. C. Dunn, A. D. Marmorstein, V. L. Bonilha, E. Rodriguez-Boulan, F. Giordano and L. M. Hjelmeland, *Investigative Ophthalmology & Visual Science*, 1998, **39**, 2744-2749.

6. G. M. Cooper, in *The Cell: A Molecular Approach*, Sinauer Associates Incorporated, Sunderland, Massachusetts, 2nd edn., 2000, pp. 373-421.

7. J. Ramsbottom, *Proceedings of the Nutrition Society*, 1953, **12**, 39-44.

8. S.-Y. Chiang, J. Welch, F. J. Rauscher and T. A. Beerman, *Biochemistry*, 1994, **33**, 7033-7040.

9. H.-C. Chen, Y.-T. Zhu, S.-Y. Chen and S. C. Tseng, *Laboratory Investigation*, 2012, **92**, 676-687.

10. R. E. King, K. D. Kent and J. A. Bomser, *Chemico-Biological Interactions*, 2005, **151**, 143-149.

11. Y. Krishna, C. Sheridan, D. Kent, V. Kearns, I. Grierson and R. Williams, *British Journal of Ophthalmology*, 2011, **95**, 569-573.

12. R. Roduit and D. F. Schorderet, *Apoptosis*, 2008, **13**, 343-353.

13. M. Motto, K. Facchine, P. Hamburg, D. Burinsky, R. Dunphy, A. Oyler and M. Cotter, *Journal of Chromatography A*, 1989, **481**, 255-262.

14. A. Barua and H. Furr, *Molecular Biotechnology*, 1998, **10**, 167-182.

15. C. V. Planta, U. Schweiter, L. Chopard-dit-Jean, R. Ruegg, M. Kofler and O. Islet, *Helvetica Chimica Acta*, 1962, **45**, 548-561.

16. C. Eckhoff and H. Nau, *Journal of Lipid Research*, 1990, **31**, 1445-1454.

17. M. Nakagawa, M. F. Refojo, J. F. Marin, M. Doi and F. I. Tolentino, *Investigative Ophthalmology & Visual Science*, 1995, **36**, 2388-2395.

18. http://www.cbmedical.com/Certificati/Fluoron/Fluoron%20Sterilizzazione.pdf, Fluoron GmbH, (accessed June 2015).

CHAPTER 3

Linear Polymer End Group Modification

3.1 INTRODUCTION

The synthesis of a drug delivery system (DDS) which releases non-toxic concentrations of drug (determined in chapter 2) over a prolonged period of time, for the prevention and treatment of PVR, drives the research throughout this chapter. The main criterion for the DDS is that it is soluble in SiO as the treatment will be administered *via* a SiO tamponade acting as a drug reservoir. The use of a prodrug to control the release was investigated. Poly(ethylene oxide) (PEO) was used as a hydrophilic non-drug component to drive the attached drug (Ibu and atRA which is hydrophobic) to the SiO/aqueous humour interface and into the aqueous humour, where the cleavage of the bond and the bio-activation occur, this then determines the release rate of the pharmacologically active drug (Figure 3.1).
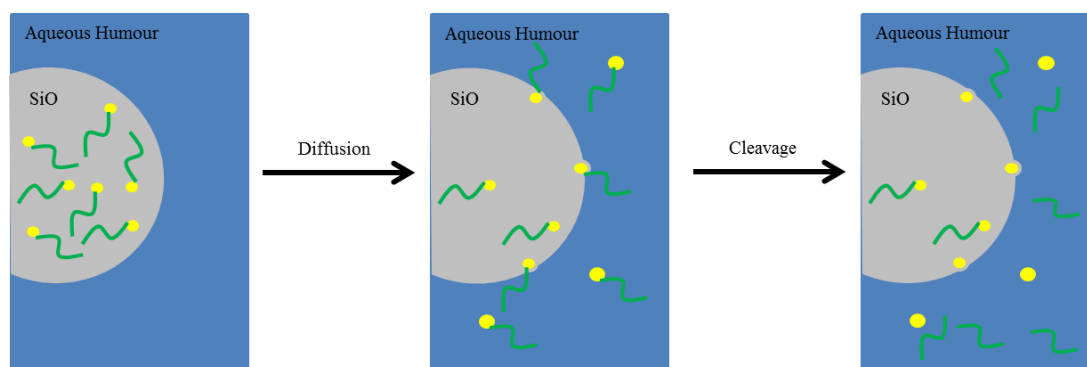
Figure 3.1 Proposed mechanism of the PEO prodrug approach and the bio-activation of the drug at the SiO/aqueous humour interface and within the aqueous humour.

A lipophilic prodrug with PDMS as the promoiety was also studied in terms of the effect on solubility of drugs and release profiles from SiO. The use of PDMS as the promoiety is advantageous due to the chemical similarity of side products and the SiO tamponade.

3.2 PEO Prodrug

3.2.1 Synthesis

Throughout this section the synthesis of both PEO-atRA and PEO-Ibu prodrugs is described. Different number average molecular weight (M_n) PEO materials were used to tailor the degree of lipophilicity-hydrophilicity present within the prodrug. Both mono-functional and di-functional linear PEO were used, which allowed the

incorporation of either one or two drug molecules per polymer chain. Initially a conjugation route using 1,1-carbonyl diimidazole (CDI) was undertaken to synthesise the prodrugs, and other strategies (such as the Steglich esterification method) were also evaluated.

3.2.1.1 CDI Chemistry

CDI chemistry is a useful method for the synthesis of esters[1, 2] but was first used in peptide synthesis for the coupling of carboxylic acid and amine groups.[3] CDI can also be used to prepare urethane, carbonate, amide and urea linkages.[4] The different synthetic routes possible using CDI chemistry are shown in Scheme 3.1, with specific highlight for the route used within this project.
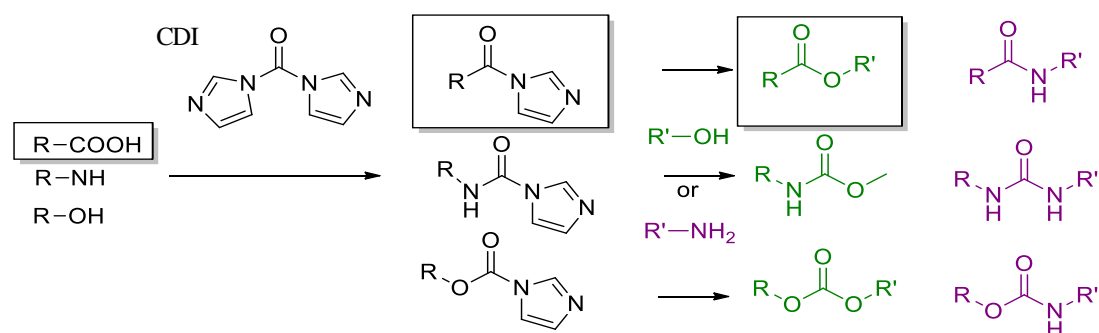
Scheme 3.1 Possible chemistries using CDI as a coupling agent including esterification with a carboxylic acid (highlighted).

The mechanism of esterification *via* CDI coupling is shown below in Scheme 3.2. CDI reacts with a carboxylic acid to give an imidazole carboxamide intermediate. This intermediate selectively reacts with primary alcohols or amines, due to steric hindrance around the carbonyl group, leading to the formation of an ester. This method was the original choice of esterification because the expected reaction time is much shorter than traditional routes (3 hours compared to over 24 hours), therefore minimising atRA exposure to conditions that may lead to degradation.
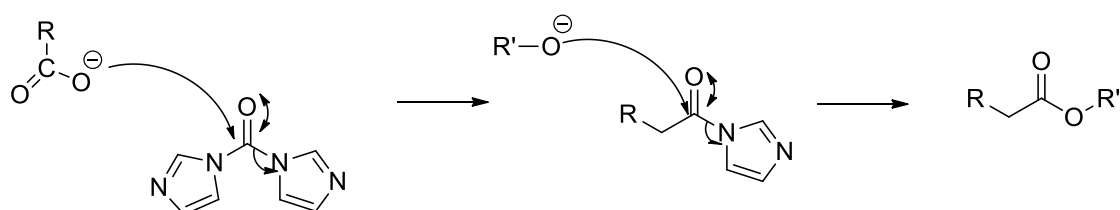
Scheme 3.2 Mechanism of esterification *via* CDI coupling.

A model reaction was carried out using benzoic acid (BA) and methyl terminated poly(ethylene oxide) (Me-PEO) (M_n 750 gmol^{-1}). The desired poly(ethylene oxide) benzoate (PEO-BA) was successfully synthesised with an average yield of 61 % and fully characterised by ^{1}H and ^{13}C NMR and IR spectroscopies (see appendix Figure A26-28). When BA was substituted by atRA, under the same conditions, the reaction failed. The intermediate (Scheme 3.3) was successfully formed, as evidenced by the appearance of two peaks in ^{1}H NMR spectroscopy at δ ppm 8.20 (s) and 8.09 (s), attributed to NCHN and NCHCHN respectively, with integration proportional to atRA (see appendix Figure A27).
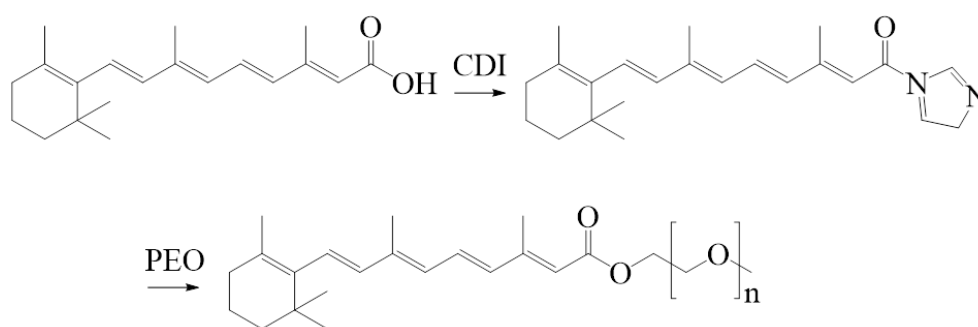
Scheme 3.3 Esterification of atRA and PEO reacting *via* a CDI intermediate.

Usually the intermediate is readily reactive to an alcohol, however, this wasn't the case with atRA. p-Toluenesulfonic acid was added as a catalyst to try and drive the reaction, but even under these aggressive conditions the intermediate remained unreacted. As the model reaction with BA was successful but the reaction with atRA was not, it was assumed that the structure/chemistry of atRA was causing the problem. To get further confirmation, a reaction with atRA and benzyl alcohol was carried out, which was also unsuccessful. It is possible that the conjugation in the atRA is stabilising the intermediate, making it unsusceptible to the reaction.

3.2.1.2 Steglich Esterification

Another approach to synthesise atRA and Ibu esters is the Steglich esterification method. This procedure offers a convenient method for the esterification of alcohols, thiols and carboxylic acids including very labile acids such as vitamin A.[5] The reaction takes place at room temperature, under mildly basic conditions and its mechanism is shown in Scheme 3.4.
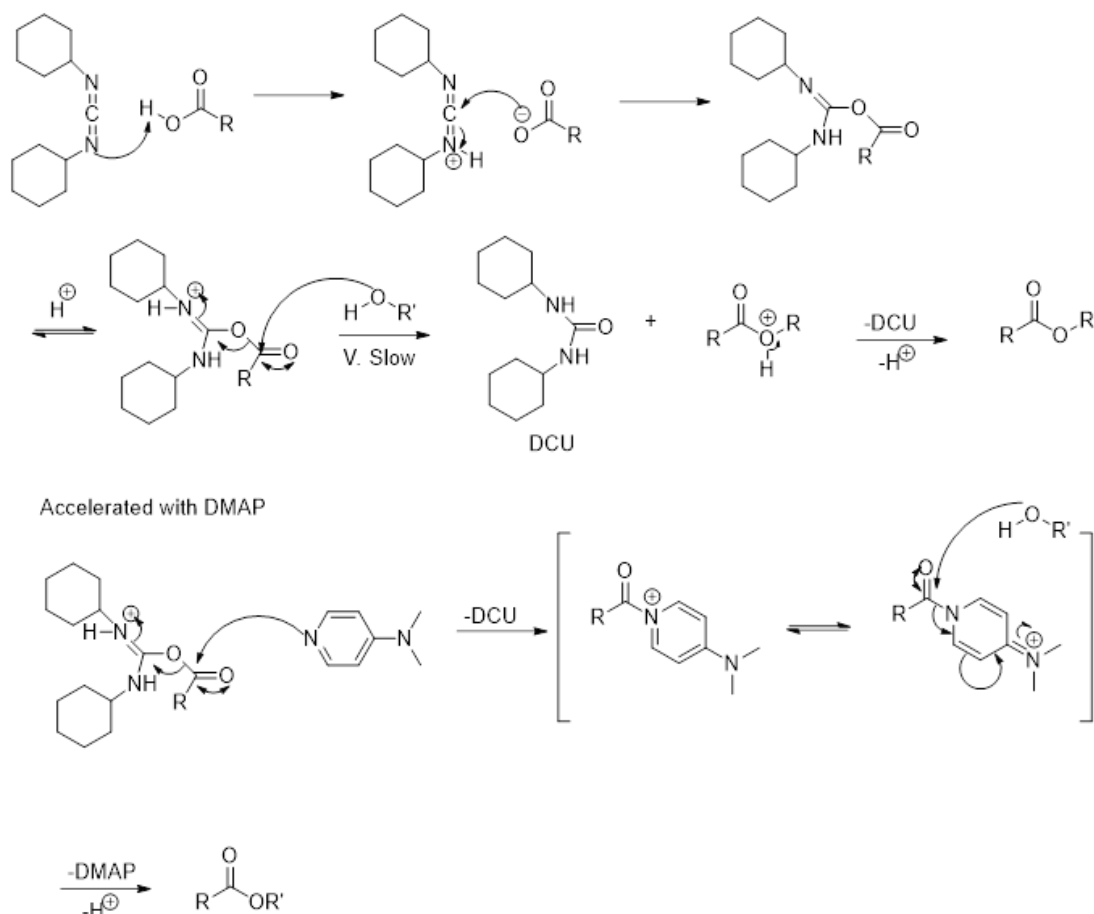
Scheme 3.4 Mechanism of a Steglich esterification.

The Steglich esterification is a variation of a classic esterification, using dicyclohexylcarbodiimide (DCC) as a coupling reagent and 4-dimethylaminopyridine (DMAP) as a catalyst. DCC and the carboxylic acid form an *O*-acylisourea intermediate, which offers reactivity similar to the corresponding deprotonated carboxylic acid. The alcohol can then be added to the activated carboxylic acid to liberate the stable dicyclohexylurea (DCU) and the ester; however this reaction is very slow in comparison to esterifications where strong nucleophiles such as amines are used. The reaction with alcohol is slow enough that it allows the isolation of the *O*-acylisourea which then remains as a side product. The reaction's success comes from the addition of DMAP, a stronger nucleophile than an alcohol, which acts as an acyl transfer agent to form an activated amide ("active ester").[6] The alcohol then reacts quickly with this intermediate to form the desired ester.

The synthesis of mono-substituted methyl terminated poly(ethylene oxide) retinoates (Me-PEO-atRA) *via* Steglich esterification was completed without any complications

of intermediate stabilisation, as previously seen with CDI chemistry. After filtration of the DCU by-product, and precipitation of the crude product (petroleum ether at approximately -70 °C), a yellow wax was recovered and fully characterised by NMR (^{1}H, ^{13}C and 2D) and IR spectroscopies, all of which were in agreement with the desired product. The ^{1}H NMR spectra of a purified Me-PEO-atRA (1,050 gmol^{-1}, n = 16) is presented in Figure 3.2. The appearance of a peak at 4.31 ppm attributed to the C$\underline{H}_2$OCO from Me-PEO (labelled o) indicates the formation of an ester, also confirmed by the shifts of the peaks at 2.35 (m) and 5.82 ppm (n) corresponding to C$\underline{H}_3$CCHOO and C$\underline{H}$COO respectively. The attribution was confirmed by 2D NMR spectroscopy (^{1}H-^{1}H and ^{1}H-^{13}C); the correlation between the protons (o, m and n) and the carbonyl was observed, confirming the ester formation (see Appendix Figure A28 and A29).
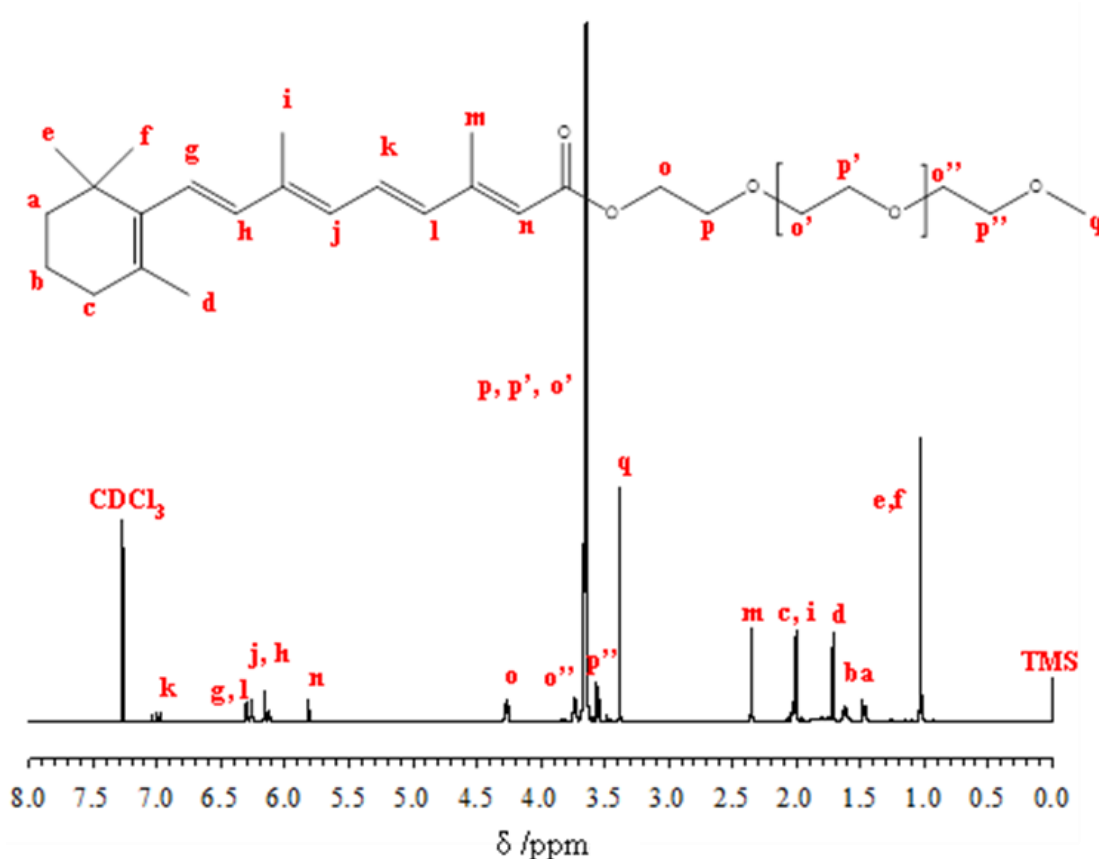
Figure 3.2 ^{1}H NMR (CDCl$_3$, 400 MHz) of Me-PEO$_{(16)}$-atRA.

Mass spectroscopy was also carried out and displayed a shift of the Me-PEO MW distribution by a factor of 300 gmol^{-1} compared to unreacted Me-PEO, indicating the addition of an atRA molecule and the formation of the ester moiety (see Appendix Figure A30). The IR spectrum confirmed the ester functionality with a peak at

$1,707 \text{ cm}^{-1}$, characteristic of a carbonyl in an ester (see appendix Figure A31). Me-PEO-atRA and Me-PEO-Ibu were successfully synthesised using Me-PEO of three different M_n values (750, 2,000 and 5,000 gmol^{-1}; $DP_n = 16$, 45 and 113 monomer units respectively), all of which were fully characterised and determined to be the desired product. Bi-functional PEO conjugates were also synthesised when hydroxyl groups were present at both ends of the PEO chain. A summary of the prodrugs synthesised can be seen below in Scheme 3.5.

A

n=16, 50 % Conversion

n=45, 59 % Conversion

n=113, 68 % Conversion

=R
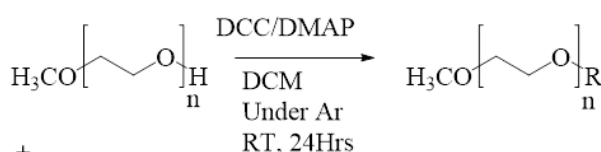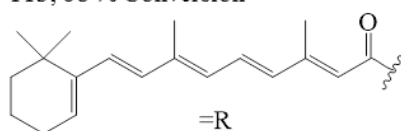
B

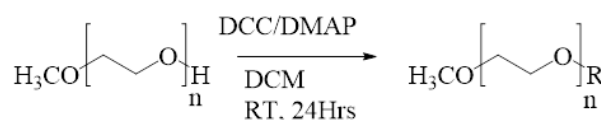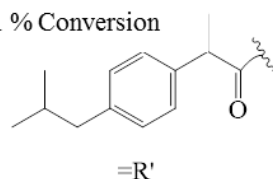n=14, 72 % Conversion

n=23, 74 % Conversion

n=45, 68 % Conversion
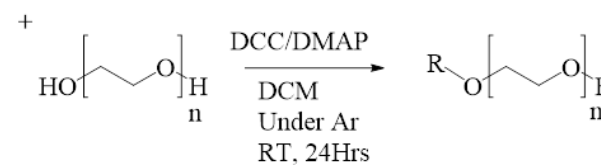
C

n=16, 94 % Conversion

n=45, 91 % Conversion

n=113, 91 % Conversion

=R'

D

n=14, 100 % Conversion

n=23, 100 % Conversion

n=45, 100 % Conversion

Scheme 3.5 Schematic of prodrugs synthesised (A, B: atRA and C, D: Ibu) with different PEO functionality (A, C: Me-PEO and B, D: PEO) and conversions reached.

When Me-PEO was the reactant, the peak at 3.38 ppm corresponding to the C$\underline{H}_3$ from Me-PEO chain end (labelled q in Figure 3.2) could be used as a reference peak

to determine conversion *via* comparison of the new peak (o) and peak (q). Unfortunately, the conversion for di-substituted PEO prodrugs could not be determined by ^{1}H NMR spectroscopy as the reference peak at 3.38 ppm was no longer available. Determination of conversion and drug content was attempted with UV-Vis analysis, however, it was concluded that this was not the appropriate technique to determine concentration of drug when it is bilaterally attached to PEO. This was due to varying trends of calibration curves when PEO/Me-PEO of different chain lengths are attached, possibly due to the micellisation of the hydrophobically-modified water-soluble polymer chains.

To determine the conversion by ^{1}H NMR spectroscopy, an approximation of the PEO chain length close to the nominal reported value was taken; for example when an M_n of 600 gmol^{-1} was given, the number of ethylene oxide repeat units was determined to be 14, therefore the PEO peak at 3.45-3.85 ppm was calibrated to 56 protons (the number of hydrogens present within the PEO chain) then compared to the ester peak at 4.31 ppm. To confirm this, drug content within the prodrug was determined *via* a new methodology of ^{1}H NMR spectroscopy using an external reference. Anisole was chosen as its unique signals do not interfere with any of the PEO-drug peaks. Using precise volumes of NMR solvent (DMSO-d_6), and an accurate concentration of anisole and drug, it was possible to determine the concentration of drug for all di-substituted PEO materials. Initially ^{1}H NMR spectra of free atRA and Ibu were acquired with a known mass of materials present. The signal at 7.1 ppm from anisole was normalised, and subsequently compared to the signal at approximately 1.0 ppm for atRA which corresponds to the protons of the methyl groups for both free and attached atRA (2 x –C$\underline{H}_3$) and 0.8 ppm for Ibu which represents the CH(C$\underline{H}_3$)$_2$. This allowed the precise concentration of drug to be calculated per mass of sample. ^{1}H NMR analysis of all PEO retinoates and PEO-Ibu synthesised were carried out in the exact same conditions, i.e. volume of DMSO-d_6 and concentration of anisole. The concentration of drug could be calculated by comparing the amount of atRA and Ibu conjugated to PEO to the free atRA and Ibu reference spectra. This confirmed the correct conversions were calculated.

The Ibu prodrugs were all successfully synthesised with high conversions, above 90 %. However, atRA prodrugs had lower conversion rates, between 50 and 74 %.

An explanation of the relatively low conversion (c.f. Scheme 3.5 A and B) comes from the conjugation of atRA. Conjugation determines the electron distribution throughout the drug, therefore, affects the reactivity. Computational modelling was performed by E. Eden (University of Liverpool) to investigate the reactivity of atRA with respect to the conjugated system, and confirmed this hypothesis by showing the size of the p(z) coefficient at the carbonyl carbon decreasing with increasing conjugation (see appendix Figure A38). In other words, the space available for the hydroxyl group to attack decreased, therefore, caused the carbon to be less available to react throughout the esterification reaction. The size of the PEO chain was also investigated; it was found that this was not expected to affect the reaction.

3.2.2 Cleavage of Ester Bond

The cleavage of the ester bond *in vivo* is anticipated to occur at the interface between the SiO and aqueous humour and within the aqueous humour (see Figure 3.1); therefore, the composition of the aqueous humour plays a key role. As discussed previously (section 1.7.2.1) this is not precisely characterised and the nature of the possible cleaving agents/factors is not known. Any cleavage experiment run *in vitro* won't be a perfect model of the *in vivo* situation, therefore, will be carried out mainly as a proof of concept.

Strong acidic or basic conditions were initially studied as conditions to cleave the ester bond. Table 3.1 summarises the different conditions used to cleave atRA from both mono- and di- substituted PEO and Ibu from di-substituted PEO. The cleavage was performed in deuterated solvents, so it could be directly monitored by NMR spectroscopy. Controls were also measured in the solvents as well as with the addition of 0.2 equivalents of acid (deuterium chloride; DCl) and base (sodium deuteroxide; NaOD). The decrease of the ester linkage is presented in terms of percentage of the original ester functionality.

Table 3.1 Different conditions used for the cleavage of PEO prodrugs *in vitro* with amount of cleaved drug given as a percentage.

Solvent	Time (Days)	Conditions	PEO$_{16}$-atRA	atRA-PEO$_{14}$-atRA	Ibu-PEO$_{14}$-Ibu	Comment
D$_2$O (37 °C)	7	-	52%	45%	56%	Poor solubility atRA/Ibu led to poor spectra
	7	0.2eq. DCl	50%	81%	87%	Poor solubility atRA/Ibu led to poor spectra
	7	0.2eq. NaOD	45%	66%	56%	
	7	Porcine Liver Esterase	-	-	-	Unable to Analyse *via* ^{1}H NMR
Dioxane-d_8 (37 °C)	3	-	0%	0%	0%	
	1	0.2eq. DCl	99%	95%	98%	
	3	0.2eq. NaOD	48%	62%	71%	No clear degradation of drugs, but decrease of signal intensity. Ester function reduced
Acetone-d_6 (37 °C)	1	-	0%	0%	0%	
	1	0.2eq. DCl	76%	88.5%	92%	
	1	0.2eq. NaOD	18%	30.4%	69%	

Experiments were initially planned to be carried out in deuterium oxide (D$_2$O) to hydrolyse the ester bonds; however, due to poor solubility of drugs in D$_2$O poor spectra were observed. Therefore, although the decrease of ester functionality was observed, degradation of the drugs could not be accurately monitored. Porcine liver esterase (PLE) was used to determine if enzymatic release occurred, however, the ^{1}H NMR spectra of PLE in D$_2$O was also extremely complicated and no signals could be confidently assigned.

Deuterated dioxane and acetone were finally chosen for these studies as both solubilised the prodrugs and gave clear spectra. Also, no degradation of the parent drugs was observed when solubilised at 37 °C (dark) for 3 and 1 day(s) respectively. Acidic conditions were observed to reduce the ester signals much more dramatically than basic conditions; however, both successfully cleaved the parent drug from the PEO effectively without degradation. Figure 3.3 shows the assigned spectra of PEO$_{(14)}$ di-substituted with Ibu, before and after treatment with DCl for 24 hours. The complete disappearance of the ester signal (3) was observed as well as no degradation of Ibu.
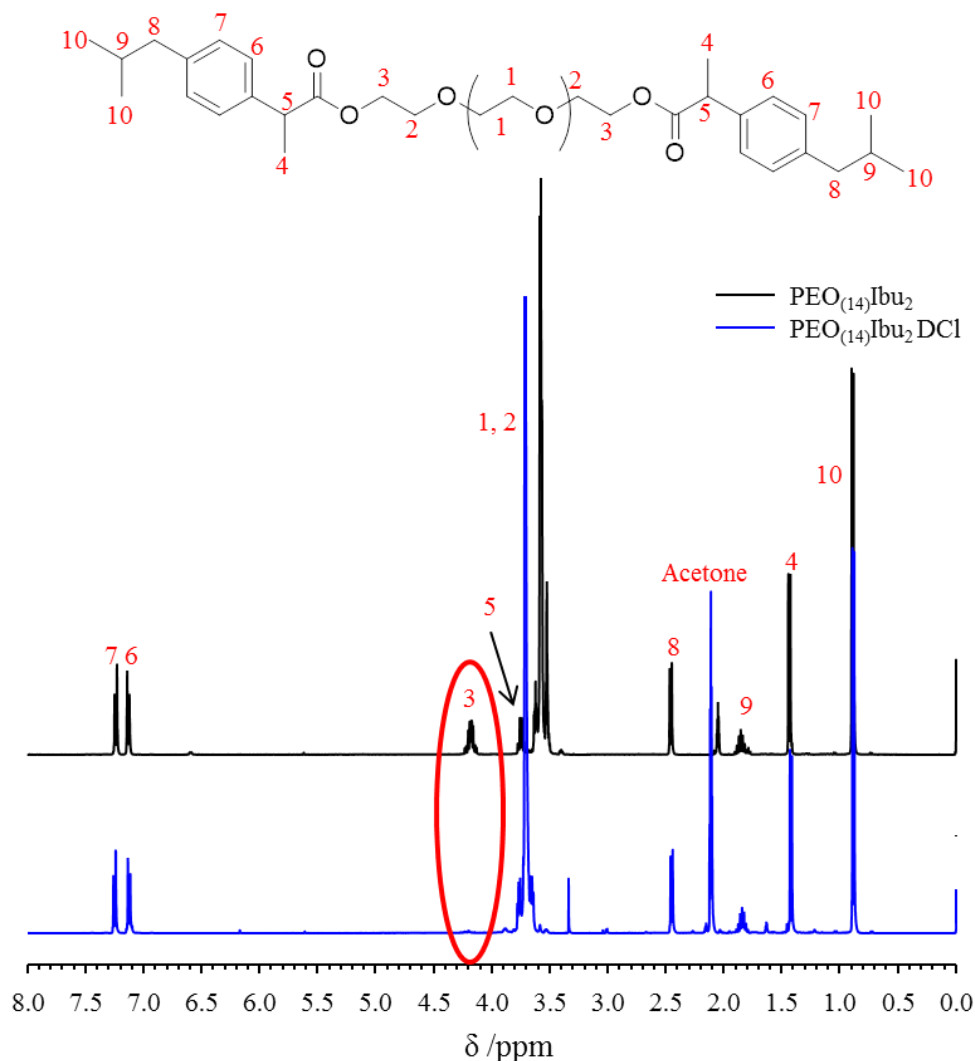
Figure 3.3 ^{1}H NMR spectra (Acetone-d_6, 400 MHz) of Ibu-PEO$_{14}$-Ibu before (black) and after (blue) treatment with DCl (0.2eq.) at 37 °C for 1 day.

Overall it was determined that atRA from both mono- and di- substituted PEO, and Ibu from di-substituted PEO, could be successfully cleaved without degradation of the parent drug. Acidic conditions at 37 °C were the most efficient particularly in dioxane-d_8, however, these conditions were not indicative of actual physiological environments.

3.2.3 Biological Evaluation

Preliminary MTT and resazurin assays were conducted for cells treated with mono-substituted PEO$_{(48)}$ attached to both atRA and Ibu because these incorporated the most PEO. Metabolic activity of ARPE-19 cells was studied at multiple time-points resulting in both pre-confluent (1 day growth) and post-confluent (7 day growth)

cells being exposed to the prodrugs for 1 and 7 days. MTT and resazurin assays were in concordance with one another and showed the same toxicity levels were observed as when cells are exposed to free drug (see appendix Figure A39 and A40). In the case of retinoates, cytotoxicity was observed at concentrations above 10^{-5} M atRA content for pre- and post-confluent cells and 1 day prodrug exposure. With 7 days exposure, cytotoxicity for post-confluent cells was also observed at concentrations above 10^{-5} M, however, for pre-confluent cells the toxic limit decreased by a factor of ten to concentrations above 10^{-6} M. In the case of Ibu prodrugs, cytotoxicity was observed at concentrations above 10^{-4} M Ibu content for pre- and post-confluent cells and 1 day Ibu exposure. With 7 days exposure, cytotoxicity for post-confluent cells was also observed at concentrations above 10^{-4} M, however, for pre-confluent cells the toxic limit decreased to concentrations above 10^{-5} M. Overall it was observed that PEO didn't affect the metabolic activity of the cells, and that cytotoxicity was solely dependent on drug content.

### 3.2.4 Solubility in SiO using UV-Vis Spectroscopy

The solubilisation of PEO prodrugs in SiO is a crucial aspect to the project as the route of administration of this DDS to the eye is through a SiO tamponade. The hydrophilic pro-moiety is necessary to help draw the hydrophobic drug to the SiO/aqueous interface and into the aqueous humour so cleavage of the ester bond and bio-activation of the prodrug can occur. While PEO is expected to have a limited solubility in SiO, it was anticipated that once a lipophilic drug was attached, the PEO conjugate solubility would increase in a hydrophobic environment such as SiO. SiO_{1000} was used throughout these investigations unless otherwise stated.

3.2.4.1 atRA

Initially, the saturation concentration of free atRA in SiO needed to be determined so the effect, if any, that the prodrug has on solubility can be deduced. A protocol reported in the literature was used[7] where a saturated solution of atRA in SiO was prepared and stirred gently in the dark at ambient temperature. Samples were taken at different time-points over a 2 week period and filtered using a syringe pump (4 mL/h) through 0.45 μm PTFE filters to remove un-dissolved material. To determine the amount of atRA dissolved in SiO, the drug was extracted from the SiO

three times with acetone (1:2 v/v). The acetone layers were combined and the solvent was evaporated with the remaining solid dried at ambient temperature. The samples were solubilised in 2 mL of a mixture of DMSO/H_2O (8/2) and subsequently analysed by UV-Vis spectroscopy. A standard curve previously determined for atRA (see Experimental 6.5.4.1) was used to determine the drug concentration.

To test the accuracy of the extraction method, a known mass of atRA was solubilised in SiO and 93 % was recovered; this was deemed an acceptable error. The experiment was repeated several times and an atRA solubility profile in SiO was determined under these conditions (Figure 3.44); the solubility reported in the literature (20 µg/mL, 6.66×10^{-5} M) is also depicted on the graph (red line). After 14 days, the average amount of atRA solubilised was 28.5 µg/mL (9.5×10^{-5} M), a value that is >40 % higher than literature values. Both of these saturation concentrations (literature and experimental) are lower than the cytotoxicity limits of ARPE-19 cells as investigated in Chapter 2.
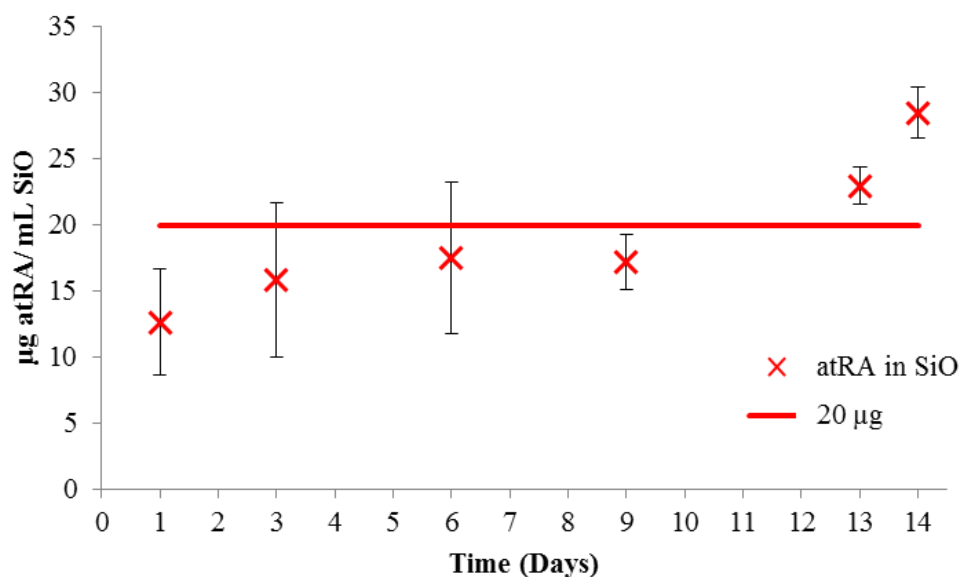
Figure 3.4 UV-Vis analysis of atRA solubility in SiO over 2 weeks (mean ± SD); n=3. 20 µg line shows solubility of atRA reported in the literature.[7]

3.2.4.2 Ibu

The same methodology exploited in atRA studies was used to determine the Ibu saturation concentration in SiO but phosphate buffered saline (PBS) was used as the solvent for UV-Vis spectroscopy analysis; Ibu saturation concentration in SiO was

determined to be 220 μg/mL (1.07 x 10^{-3} M) *via* this methodology. While the concentration of atRA solubilised in SiO was not high enough to allow us to perform an NMR analysis directly on the oil sample, in order to confirm the number determined by UV-Vis, this was possible with Ibu. 0.2 mL of the saturated oil (after filtration) was solubilised in 0.7 mL CDCl$_3$ containing 2 mg/mL anisole as an internal reference, allowing for the quantification of Ibu. The ^{1}H NMR analysis showed that although UV-Vis and ^{1}H NMR measurement of the extracted product gave similar values, the amount recovered by this technique was only 57 % of Ibu solubilised (~1 mg/mL, n = 3). The solubility of Ibu in SiO was then determined by ^{1}H NMR of the SiO after filtration to be 2.05 mg/mL (9.94 x 10^{-2} M, n = 2), which was a much higher concentration than that determined by the UV-Vis method adapted from the literature. Extraction of Ibu from SiO with acetone may, therefore, not be as effective as for atRA.

Overall, the saturation concentration of both atRA and Ibu were determined to be 28.5 μg/mL and 1.81 mg/mL respectively. Although the methodology in the literature led to an incomplete extraction of Ibu from SiO (57 %), atRA extraction was determined to be successful with a 93 % extraction. This is possibly due to acetone acting as a better solvent for atRA than Ibu.

3.2.4.3 PEO Prodrugs

Saturated solutions of all the prodrugs synthesised in SiO were prepared, following the same methodology as for free drug (see experimental, Section 6.5.4). Rather than extracting SiO and using UV-Vis to determine the amount of prodrug solubilised, the solutions were analysed by ^{1}H NMR spectroscopy. Anisole was used as an internal reference, and the prodrug saturation concentrations were determined using the resonance at 3.1 ppm assigned to the PEO chain; no drug peaks were visible because of the low concentration solubilised.

The solubility profile of the prodrugs can be seen below in Figure 3.5. There is a definite trend for both the mono- and di- substituted PEO prodrugs; as the PEO chain length increases, the solubility in SiO decreases. There is also an increase in the amount of prodrug solubilised when PEO is di-substituted compared with Me-PEO

prodrugs. In all cases, the maximum solubility in SiO for both mono and di-substituted materials was seen with the shortest chain length PEO (n = 14).
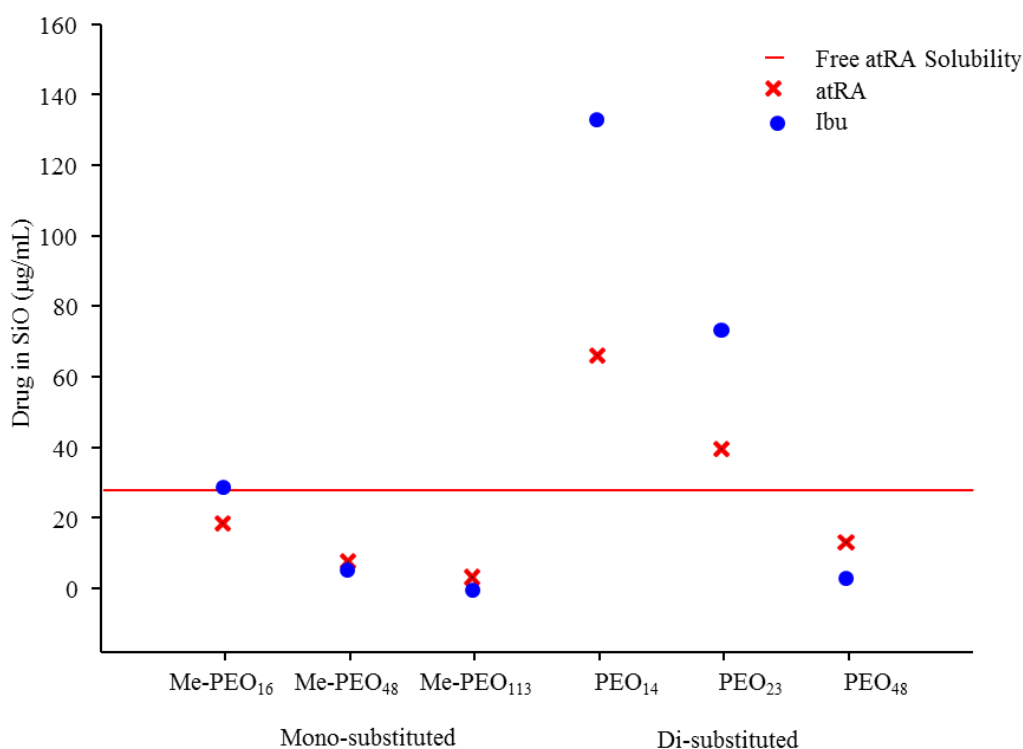
Figure 3.5 Solubility of drug attached to PEO prodrugs, in SiO. atRA (x) and Ibu (•). Measured value of free atRA in SiO (red line).

The solubility of the different atRA prodrugs in SiO (i.e. either PEO-atRA or Me-PEO-atRA), decreased with increased PEO chain length. This led to the maximum concentration of atRA that was solubilised when attached to the pro-moiety being lower than the saturation concentration of the free drug in SiO, apart from for the two smaller di-substituted PEO prodrugs. Therefore, these were no longer considered to be a good candidate to achieve prolonged drug delivery to treat PVR. The level of Ibu attached to the hydrophilic pro-moieties solubilised in SiO, particularly the di-substituted low M_n PEO, was considered to be high enough to investigate the release from SiO.

3.2.5 Release of Prodrugs from SiO into Culture Media

The release of free Ibu as a control, along with Me-PEO$_{16}$-Ibu and di-substituted PEO$_{14}$, from SiO into culture media was investigated. ^{1}H NMR spectroscopy of Ibu remaining in the oil could be analysed to determine the concentration as

distinguishable peaks were visible within the spectra. The release of Ibu, PEO-Ibu mono- and di-substituted from SiO was investigated with culture media being replenished daily or left stationary over 4 days. Figure 3.6 shows the cumulative percentage which was released under these conditions, however, it was not determined whether the Ibu was still attached to the pro-moiety or not; a percentage was used to allow Ibu and pro-drug comparison with ease as saturated solubility is much higher. Figure 3.6A shows the release when the media is replenished daily; overall the release rate follows the trend Ibu>Me-PEO$_{14}$-Ibu>PEO$_{16}$-Ibu, however, more of the di-substituted prodrug is released initially than the mono-substituted prodrug but the amount is always lower than free Ibu. Over the 4 day experiment, 93 % of Ibu was released from the SiO compared to 73 % and 61 % of the mono- and di-substituted prodrugs respectively. When the media is not changed over the 4 day experiment, the same trend is observed, again with a faster release of the di-substituted initially than the mono-substituted prodrug, however, the overall difference of amounts released is much smaller. The same 93 % of Ibu is released but this time more of the prodrugs are released than seen previously; 86 % and 78 % for the mono- and di-substituted respectively.

Overall, the use of PEO prodrugs does slow down the release of Ibu from SiO into culture media with the di-substituted version being the most effective in prolonging release. However, the majority of drug/prodrug is released after only 4 days, which does not meet the 4-6 week treatment period criteria aimed for.

A

B
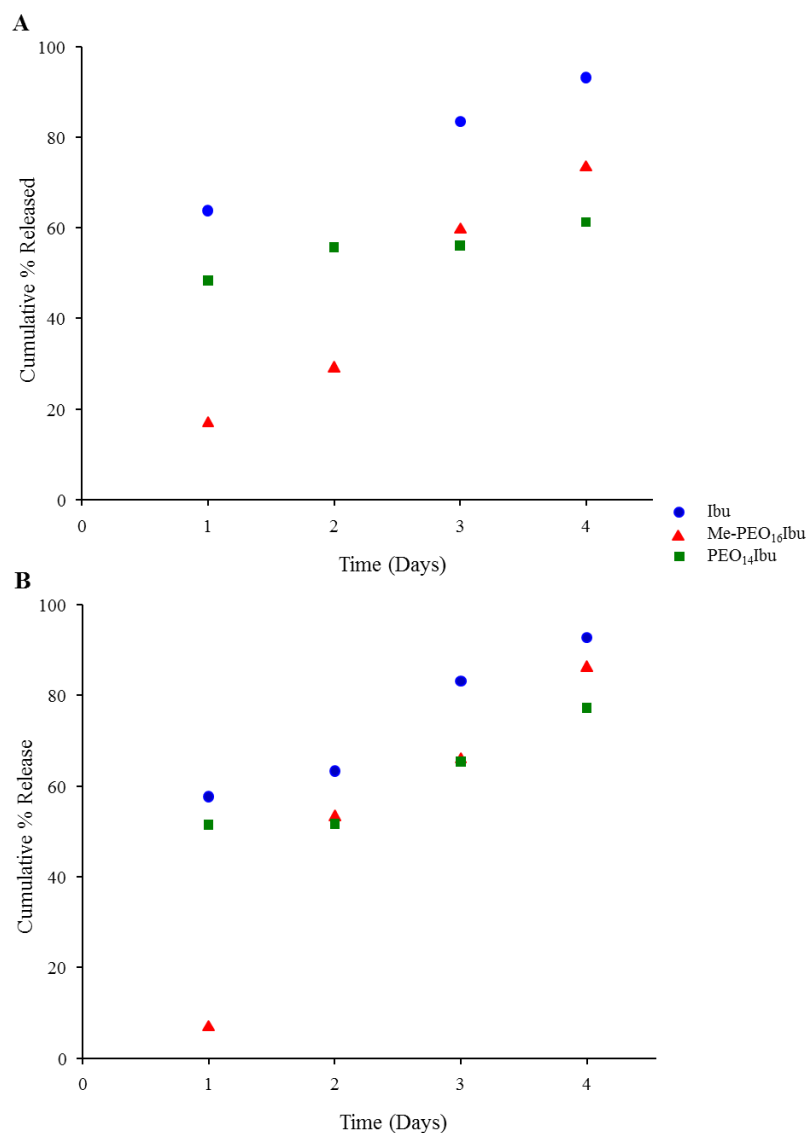
Figure 3.6 Release of free Ibu (●), Me-PEO$_{16}$-Ibu (▲) and PEO$_{14}$-Ibu (■) from SiO into A: replenished media and B: unchanged culture media.

3.3 PDMS PRODRUGS

As the solubility of PEO prodrugs resulted in a much lower saturation concentration drug equivalent in SiO than free drug, the use of a hydrophobic pro-moiety was investigated. End-functionalised poly(dimethylsiloxane) (PDMS) appears to be the ideal candidate as it is almost identical to the SiO tamponade. This reduces solubility issues and also contributes to lowering the effect of side products, as the pro-moiety left after the cleavage would be chemically very similar to the surrounding SiO.

3.3.1 Synthesis – Steglich Esterification

The PDMS-prodrugs were synthesised *via* the Steglich esterification method. The commercially available bis(hydroxyalkyl) terminated poly(dimethylsiloxane) (PDMS-diOH, Figure 3.7) was reacted with both atRA and Ibu individually, at ambient temperature in dichloromethane (DCM). These conditions had been investigated with respect to the degradation of atRA (see Chapter 2, Section 2.3) and found to be acceptable. The working concentrations of reactants were based on the maximum solubility of atRA in DCM determined previously (i.e. 12 mg/mL, see Experimental 6.5.6.1 and 6.5.6.2).
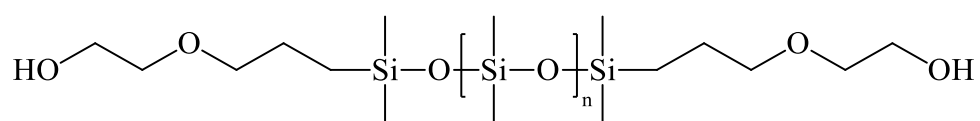
Figure 3.7 Poly(dimethylsiloxane), bis(hydroxyalkyl) terminated (4,700 gmol^{-1}).

The formation of prodrug was monitored by ^{1}H NMR spectroscopy (see Figure 3.8) with the formation of the ester bond characterised by the appearance of a peak at 4.31 ppm (labelled 2'), as well as a chemical shift of all the signals of the protons close to both the acid function of the drug (e.g. 11, 12, 13 and 14) and the hydroxyl function of PDMS-diOH (e.g. 3). The chemical shifts after the reaction are highlighted by red arrows in Figure 3.8. In this particular case, the conversion reached 72 % after 4 days, therefore, the PDMS-atRA obtained contains 72 % of atRA as chain-ends. The remaining 28 % of available chain-ends remained as hydroxyl groups as seen by the residual signals labeled 2 and 3 in Figure 3.8.
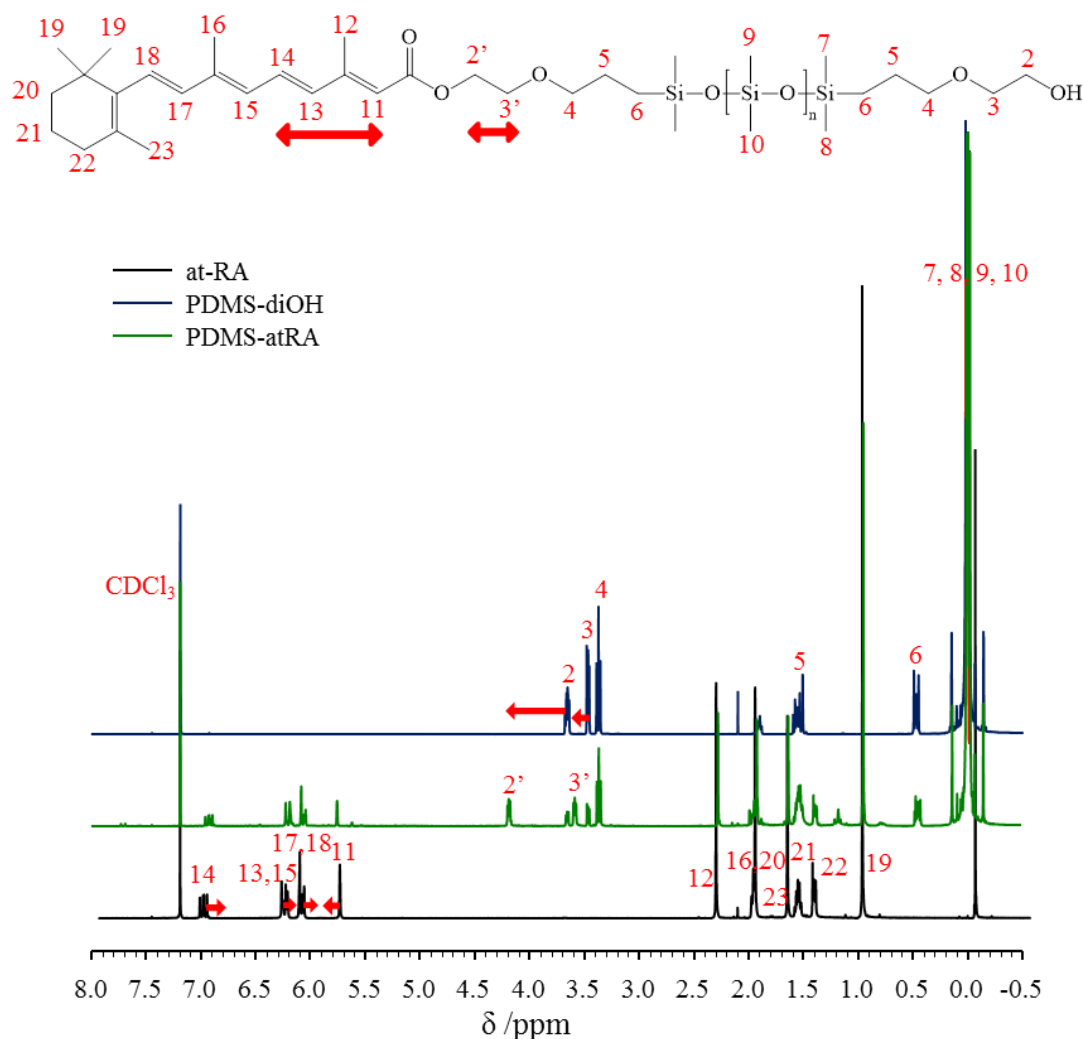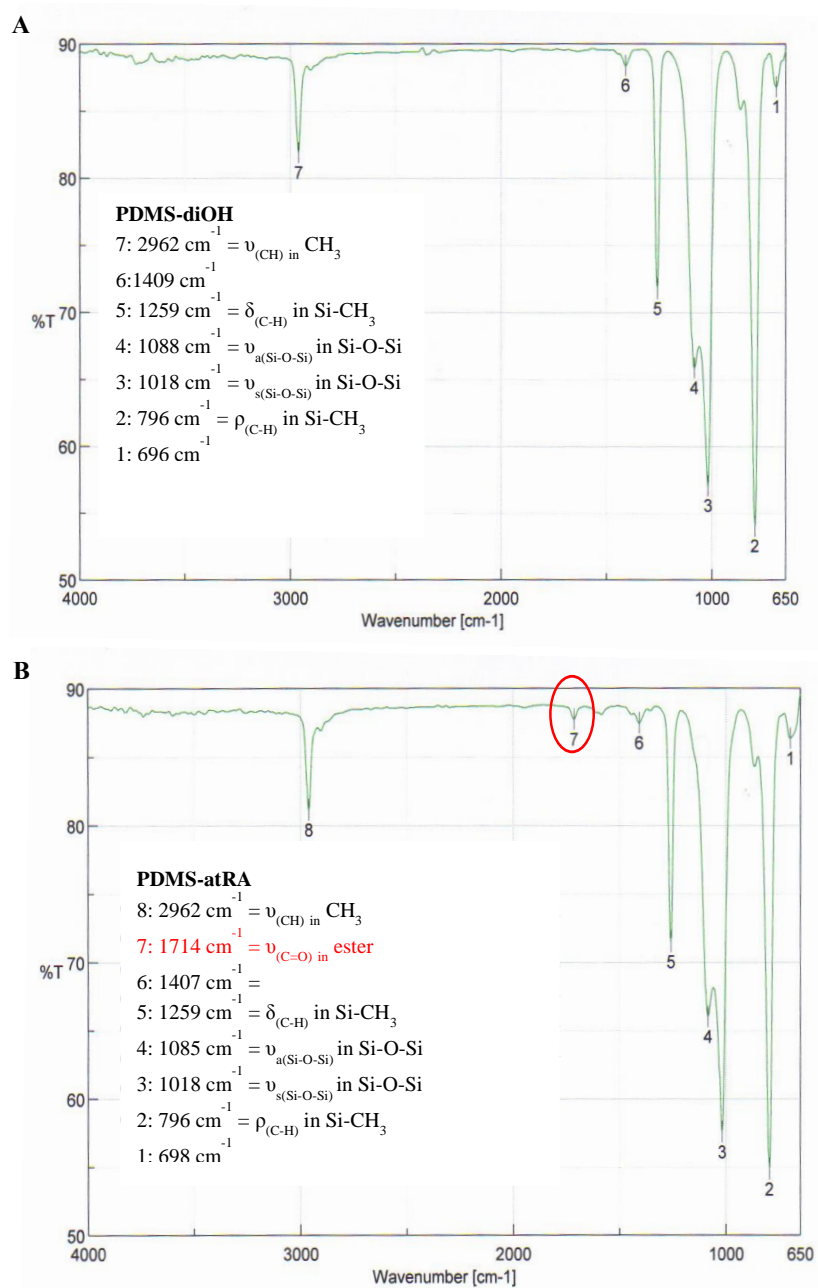
Figure 3.8 ^{1}H NMR spectra (CDCl$_3$, 400 MHz) of starting PDMS-diOH (blue) and atRA (black) along with PDMS-atRA (green) after purification.

This classic esterification reaction usually requires no longer than 24 hours to achieve completion, as seen for the PEO-Ibu prodrug syntheses, but this depends on the nature of the acid and alcohol involved in the reaction. For atRA the reaction was much slower, reaching only 40 % conversion after 2 days, and usually less than 70 % after 4 days (n = 4). The conjugation throughout atRA stabilises the acid function by making the carbonyl function less available to react, as was observed *via* computational modelling of the Me-PEO-atRA prodrug. Leaving the reaction for more than 4 days did not lead to higher conversions, therefore, all reactions were stopped at 4 days to limit degradation of atRA. Complete conversion was reached after 1 day in the case of PDMS-Ibu, further confirming that the limiting factor during the esterification between atRA and PDMS-diOH was the nature of the acid.

The final products were purified by repeated washes in methanol (MeOH), allowing for the removal of unreacted atRA or Ibu. This purification process involves the loss of some of the shorter PDMS chains within the molecular weight distribution, therefore, leading to a higher average M_n within the final products than the initial starting material. PDMS prodrugs were fully characterised by ^1H and ^{13}C NMR spectroscopy (see Appendix Figure A42), as well as FT-IR spectroscopy which confirmed the formation of an ester bond, with the appearance of a characteristic ester signal at 1,714 cm^{-1}.

A

PDMS-diOH
7: 2962 cm^{-1} = $\upsilon_{(CH)\ in}$ CH$_3$
6: 1409 cm^{-1}
5: 1259 cm^{-1} = $\delta_{(C-H)}$ in Si-CH$_3$
4: 1088 cm^{-1} = $\upsilon_{a(Si-O-Si)}$ in Si-O-Si
3: 1018 cm^{-1} = $\upsilon_{s(Si-O-Si)}$ in Si-O-Si
2: 796 cm^{-1} = $\rho_{(C-H)}$ in Si-CH$_3$
1: 696 cm^{-1}

B

PDMS-atRA
8: 2962 cm^{-1} = $\upsilon_{(CH)\ in}$ CH$_3$
7: 1714 cm^{-1} = $\upsilon_{(C=O)\ in}$ ester
6: 1407 cm^{-1} =
5: 1259 cm^{-1} = $\delta_{(C-H)}$ in Si-CH$_3$
4: 1085 cm^{-1} = $\upsilon_{a(Si-O-Si)}$ in Si-O-Si
3: 1018 cm^{-1} = $\upsilon_{s(Si-O-Si)}$ in Si-O-Si
2: 796 cm^{-1} = $\rho_{(C-H)}$ in Si-CH$_3$
1: 698 cm^{-1}

Figure 3.9 FTIR analysis of A: PDMS-diOH and B: PDMS-atRA after purification.

Table 3.2 summarises the characteristics of the different PDMS prodrugs prepared and used throughout the project.

Table 3.2 Characteristics of the PDMS prodrugs synthesised and used throughout the project.

Parent Drug	Conversion (%) ‡	Average M_n‡ (gmol⁻¹)	DP_n‡	[Drug] 10^{-4} (mol/g)
atRA	72	6,810	82	2.11
	63	7,060	86	1.78
	59	7,040	86	1.67
	60	6,960	85	1.72
Ibu	83	6,820	83	2.43
	100	6,520	78	3.06
	100	6,120	73	3.27

3.3.1.1 Synthesis of PDMS-atRA - Anhydride Method

Due to the Steglich esterification reaching only 40 % conversion after 2 days, and less than 70 % after 4 days for the synthesis of PDMS-atRA, an alternative route was investigated. This involved the use of a two-step mechanism in which the first step consists of the synthesis of the atRA anhydride through a self-condensation reaction. The acid was mixed with 0.55 equivalents of the dehydrating agent DCC in DCM for 2 days. The reaction was followed using both ^{1}H and ^{13}C NMR spectroscopy; however, ^{13}C NMR analyses were more useful to monitor the reaction as there was a shift of the peak assigned to the carbonyl environment, which resonates at 173 ppm in the acid form and 163 ppm as the anhydride (see appendix Figure A43). After 2 days, ^{13}C NMR confirmed the loss of the acid resonance and the crude product was filtered to remove the DCU by-product, prior to solvent removal *in vacuo*. Yellow crystals were obtained with a 67 % yield and the solid was used immediately for the synthesis of PDMS-atRA to try and prevent any hydrolysis of the anhydride or atRA. The synthesis of PDMS-atRA was carried out by reacting PDMS-diOH in DCM with 2 equivalents of anhydride-atRA, in the presence of 4 equivalents of pyridine and 0.2 equivalents of DMAP per hydroxyl group, at ambient temperature in the dark for 4 days. The excess anhydride was quenched with water for 3 hours and the crude product diluted with DCM and extracted with 1 M $NaHSO_4$ followed by 1 M $NaHCO_3$ and brine to remove the DMAP and pyridine. Precipitation in MeOH to remove the excess acid yielded a yellow oil with 65 % yield. As this was similar to

the yields obtained with the steglich esterification method, all further reactions were carried out under the DCC/DMAP one-pot/one-step conditions described previously.

3.3.2 Biological Evaluation of PDMS Prodrugs

The metabolic activity and morphology of ARPE-19 cells was studied for pre-confluent cells (1 day growth) which were exposed to SiO_{1000} and blends of PDMS-atRA and PDMS-Ibu with SiO_{1000} at 10 % (v/v) for 1 day. A resazurin assay was subsequently carried out, followed by phalloidin staining of the cells from the assay (see experimental Section 6.4.2).

The resazurin assay contained positive (healthy cells) and negative controls (cells exposed to 20 % DMSO) as well as media with no resazurin present to determine background signals. As seen in Figure 3.10, these controls confirmed the validity of the assay, as there was a significant difference between the negative control and both the positive control and media without resazurin. However, no significant difference was observed between the positive control and cells exposed to SiO_{1000}, PDMS-atRA and PDMS-Ibu blends at 10 % v/v in SiO_{1000}, indicating that the oil and blends have no cytotoxic effect on the ARPE-19 cells.
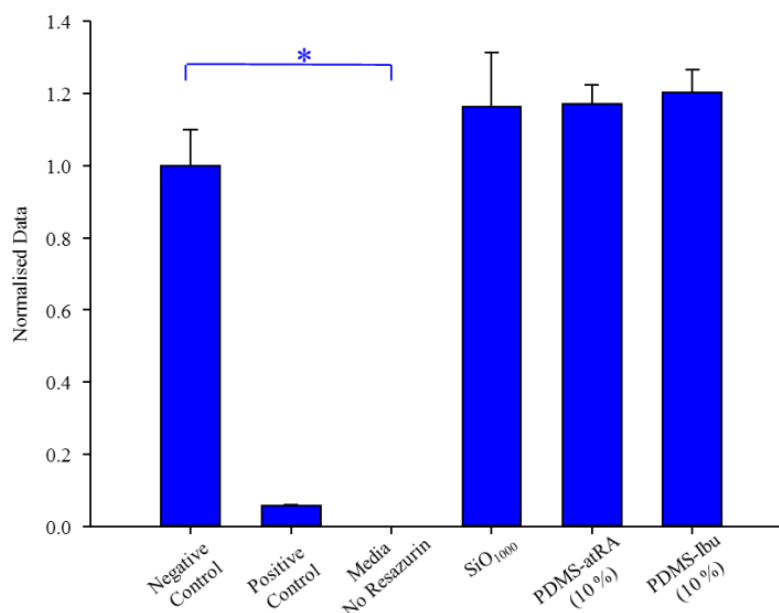
Figure 3.10 Resazurin assay with appropriate controls to determine the cytotoxicity of SiO_{1000} and blends of PDMS-atRA and PDMS-Ibu with SiO_{1000} at 10 % (v/v). Pre-confluent ARPE-19 cells (grown for 1 d) were exposed to the oils for 1 d. (mean, error bars represent $\pm$ 1 standard deviation); n=3. *, Significance by ANOVA and Dunnett's T3 post-hoc evaluation ($p \leq 0.05$).

Phalloidin staining confirmed no cytotoxic effects with images of healthy cytoskeletons when cells were exposed to the oil and blends. Images of phalloidin stained cells exposed to SiO_{1000} and the 10 % blends, are presented in Figure 3.11, alongside negative control (healthy cells). All four images represent healthy cytoskeletons.
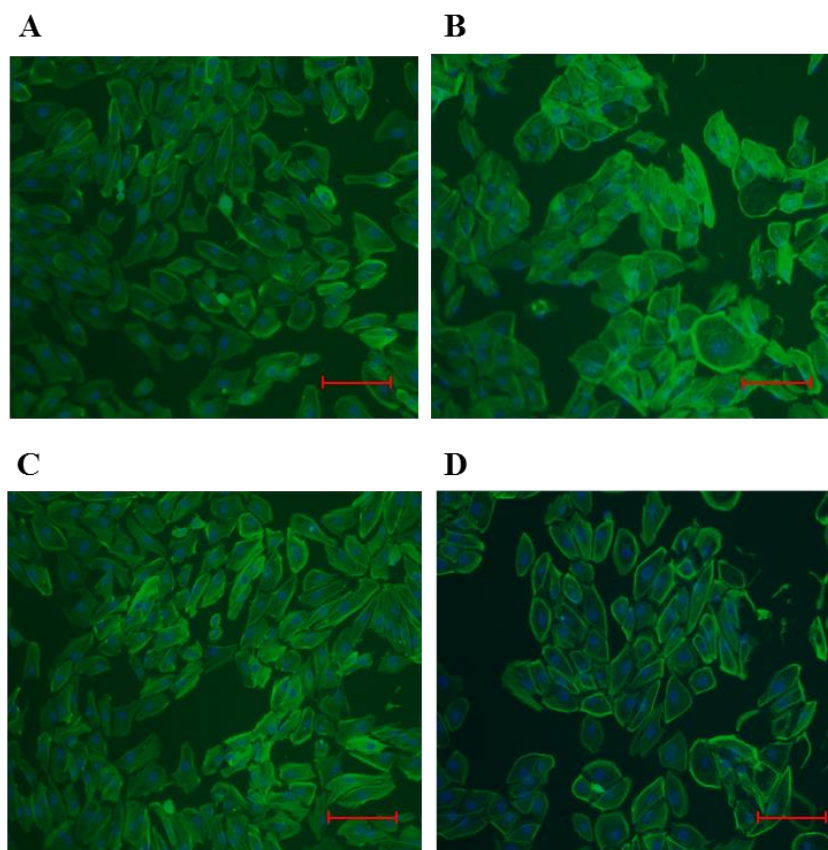
Figure 3.11 Fluorescent phalloidin (green) marking F-actin in ARPE-19 cells and DAPI (blue) stains the nuclei. Negative control (A), cells exposed to SiO_{1000} (B), blends of PDMS-atRA (C) and PDMS-Ibu (D) with SiO_{1000} at 10 % (v/v). Scale bars represent 50 μm.

3.3.3 Cleavage of Ester Bond

Similarly to the PEO prodrugs, the cleavage of the ester bond was investigated under conditions that do not fully represent conditions *in vivo* and as a proof-of-concept study.

PDMS is known to be sensitive to decomposition under strong acidic or basic conditions; however, these conditions were shown to cleave the ester bonds within PEO-prodrug systems previously and were investigated. PDMS is immiscible with water, but water is required when an acid or base is to be used, therefore, a good

solvent of PDMS that is miscible with water was required. While both acetone and THF are good solvents for PDMS, upon the addition of water, THF was the only solvent able to solubilise PDMS, providing that the ratio of water in THF did not exceed 8 % (v/v). Quantities of NaOH, KOH and HCl had to be adapted and solutions prepared in that respect. See Section 6.5.3 for an example of a typical experiment.

3.3.3.1 Cleavage of PDMS-atRA

To cleave atRA from PDMS, mild basic conditions were attempted using 2-5 equivalents of base per ester function. DMAP was also evaluated, with or without water, with no difference being observed. Acidic conditions were also studied, using 5-10 equivalents per ester function. Table 3.3 provides a summary of the various conditions studied to cleave the atRA from the PDMS chains and the effects on PDMS and atRA under these conditions.

Table 3.3 Conditions used to attempt the cleavage of the PDMS-atRA *in vitro* and their effects on PDMS and atRA. X = no cleavage or degrades PDMS/atRA. ✓ = PDMS/atRA stable.

Solvent	Time (Hours)	Conditions	Ester Cleaved	PDMS Stable	atRA Stable
THF (40°C)	22	2 eq. KOH	X	X	Partial degradation
	22	5 eq. KOH	X	X	
	22	2 eq. NaOH	X	X	Partial degradation
	22	5 eq. NaOH	X	X	
	312 (13 d)	2 eq. DMAP	X	✓	Partial degradation
	168 (7 d)	5 eq. DMAP	X	✓	
	312 (13 d)	2 eq. DMAP with H_2O	X	✓	Partial degradation
	168 (7 d)	5 eq. DMAP with H_2O	X	✓	
	24	5 eq. HCl	X	✓	✓*
	24	1 0 eq. HCl	X	✓	✓*
Dioxane (40°C)	24	5 eq. HCl	X	✓	✓*
	9	1 0 eq. HCl	X	✓	✓*
Dioxane (60°C)	9	5 eq. HCl	X	✓	X
	6	1 0 eq. HCl	X	✓	X
Stabilised Dioxane (60°C)	9	5 eq. HCl	X	✓	X

✓* No clear degradation but decrease of signal intensity in ^1H NMR

The use of both NaOH and KOH, even at low concentrations, led to the clear decomposition of the PDMS chains. While ^{1}H NMR analyses displayed no change of the ester peak or atRA signals, the integration of the PDMS main chain signal diminished by a factor of 3-4 (integrations decreased from 507 to 165 protons when Si-C$\underline{H}_2$-CH$_2$, labelled 6, was taken as a reference for integration) as illustrated in Figure 3.12.

Figure 3.12 ^{1}H NMR spectra (CDCl$_3$, 400 MHz) of PDMS-atRA before and after exposure to KOH in THF at 40 °C for 22 h.

Gel permeation chromatography (GPC) was also used to characterise the prodrugs before and after exposure to NaOH and KOH. The traces obtained (Figure 3.13) confirmed the decomposition of the main polymer chain.

Figure 3.13 GPC RI chromatogram overlays of PDMS-atRA (black) before and after exposure to KOH (2 and 5 equivalents) and NaOH (2 and 5 equivalents) in THF at 40 °C for 22 h.

The use of DMAP as a base did not affect the PDMS chain and the atRA seemed to degrade partially under these conditions, but the ester linkage remained unchanged. Conducting the experiments with water or without water led to identical results.

The use of acidic conditions (5-10 equivalents of HCl) in either THF or dioxane at 40 °C led to comparable results. No decomposition of the PDMS chain was observed, the ester function remained unchanged, and no clear degradation of atRA was observed, as there was no change in the appearance of the ^{1}H NMR spectra; however, there was a decrease of the signal intensities (see Appendix Figure A44 and A45). When the temperature of a cleavage study in dioxane was increased from 40 to 60 °C, severe degradation of atRA was seen, shown by the complete disappearance of the signals in ^{1}H NMR spectrum (see Appendix Figure A46); while the ester function remained unchanged and was still visible on the spectrum. In order to check that dioxane itself was not involved in side reactions due to the presence of peroxide, an inhibitor (methoxyphenol at 100 ppm) was added to the solvent. The reaction was repeated with 5 equivalents of HCl at 60 °C and samples were taken at 3, 6 and 9 hours (9 hour time-point stated on Table 3.3), purified and analyzed by ^{1}H NMR spectroscopy. The same results were obtained, with the degradation of atRA and the ester function remaining unchanged concluding it was not the solvent that led to degradation. Overall, conditions required for the cleavage of atRA from PDMS-atRA were not found and degradation of atRA was observed.

3.3.3.2 Cleavage of PDMS-Ibu

As previously discussed, Ibu is not as susceptible to degradation as atRA, therefore, it was possible to further investigate the prodrug cleavage using stronger/harsher conditions in the particular case of PDMS-Ibu to determine whether cleavage of the drug from the PDMS pro-moiety was possible. Acidic conditions were used in either THF or dioxane, at various temperatures using concentrated HCl up to 40 equivalents per ester function. Table 3.4 summarises all conditions studied to cleave Ibu from the PDMS chain-ends.

Table 3.4 Conditions used to attempt the cleavage of the PDMS-Ibu *in vitro* and their effects on the ester functionality, PDMS and Ibu.

Solvent	Time (Hours)	Conditions	Comment
THF (40 °C)	24	5 eq. KOH	
Dioxane (85 °C)	20	15 eq. HCl	No Change
Dioxane (Ambient T)	20	40 eq. HCl	

All three experiments led to no change of the chemical structure of the PDMS-Ibu; no cleavage of the ester function and no degradation of Ibu or the PDMS chain were observed. Due to cleavage of ester functions being well established, and because the cleavage of the hydrophilic PEO prodrugs was successful, it was suspected that the hydrophilicity/hydrophobicity of the PDMS prodrugs with the cleavage conditions was the reason for this. As PDMS is highly hydrophobic, the polymer chain is most probably in a collapsed configuration in the presence of water, even at ratios as low as 8 vol%. Due to the parent drug being attached at the chain ends, they are most likely to be inaccessible for reaction as illustrated in Figure 3.14.
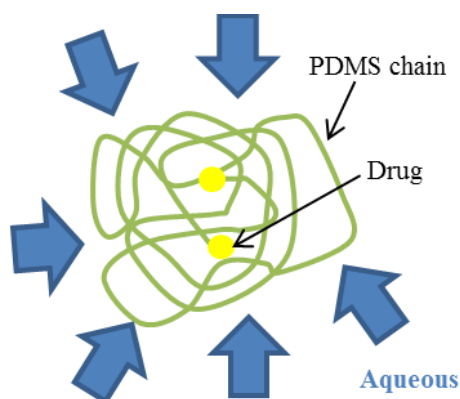
Figure 3.14 Probable configuration of the PDMS-drug polymer chains in the presence of water.

3.3.3.3 PDMS Prodrug with PEO Spacer

Carl *et al.* introduced the concept of a tripartite prodrug design with a spacer in between the parent drug and pro-moiety to overcome stability issues of hydrolysis of the prodrug bond.[8]   As the cleavage of the drug from the polymer chain was successful using a hydrophilic polymer chain (PEO), the addition of a hydrophilic spacer between the PDMS chain and the drug molecule was considered. In this section, solely Ibu was used as the parent drug in order to prevent any possible interference arising from potential atRA degradation when harsh conditions were to be used for cleavage experiments.

3.3.3.3.1 Synthesis of PDMS-PEO Prodrug

PDMS-PEO-Ibu was synthesised following a 3-step procedure as shown in Scheme 3.6.
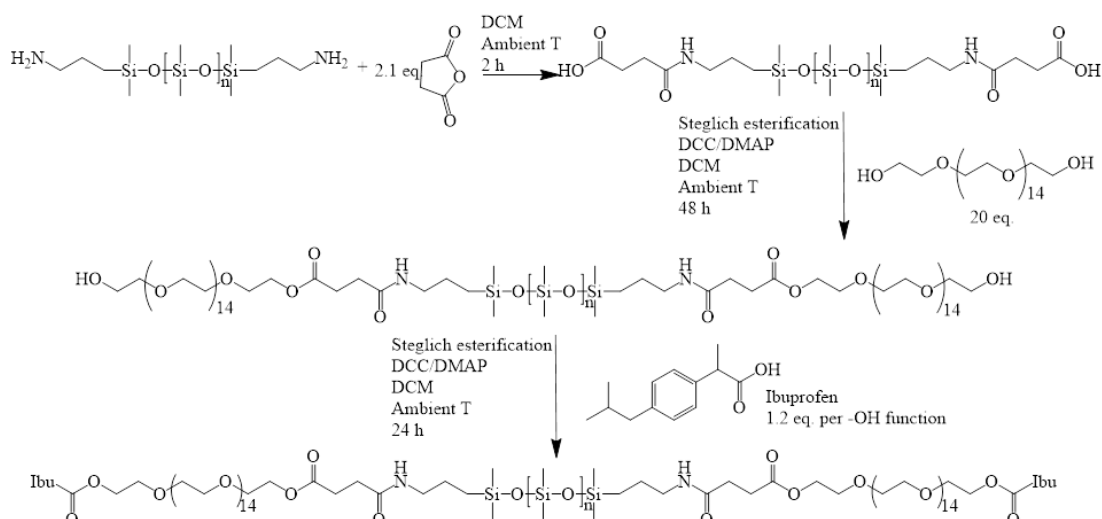
Scheme 3.6 Preparation of PDMS-PEO-Ibu following a 3 step procedure.

The first step involved the preparation of PDMS functionalized with acid groups (COOH), in order to react further with PEO *via* esterification. The reaction between the commercial bis(3-aminopropyl)-terminated poly(dimethylsiloxane) (H$_2$N-PDMS-NH$_2$, 3,000 gmol^{-1}) and succinic anhydride gives the expected HOOC-PDMS-COOH with 100 % conversion in just a few hours (see Figure 3.15). The product can be used straight away, without any purification, in the next step which consists of an esterification with PEO (600 gmol^{-1}, n = 14). The use of a large excess of PEO (approximately 20 equivalents per acid function) is combined with a very slow addition of acid onto the excess alcohol, allowing for the preparation of HO-PEO-PDMS-PEO-OH as the main product (see Figure 3.15). As both polymers (PDMS and PEO) are bi-functional, the excess PEO is necessary to prevent further reactions with any free HOOC-PDMS-COOH that would remain. The purification of the obtained polymer, which is essential for further reactions with Ibu in a new esterification reaction, is the most challenging part of the synthesis. Finding a good protocol to eliminate the entire remaining unreacted PEO without losing too much product is very difficult as the different polymer chains are in the range of "low molecular weight" polymers, therefore, even purification based on solubility differences leads to the loss of an important amount of the final product (see experimental, Section 6.5.8). HO-PEG-PDMS-PEG-OH was successfully synthesised and purified as highlighted by ^{1}H NMR and the appearance of a new ester signal at 4.12 ppm attributed to COO-C$\underline{H}_2$-CH$_2$-O (assigned 10 in Figure 3.15). The last step, the esterification with Ibu, was successful and led to the expected Ibu-

PEG-PDMS-PEG-Ibu, confirmed by ^{1}H NMR analyses (Figure 3.15). The ^{1}H NMR spectra display the appearance of a new ester signal at 4.15 ppm attributed to OCOC$\underline{H}$(CH$_3$) (14).
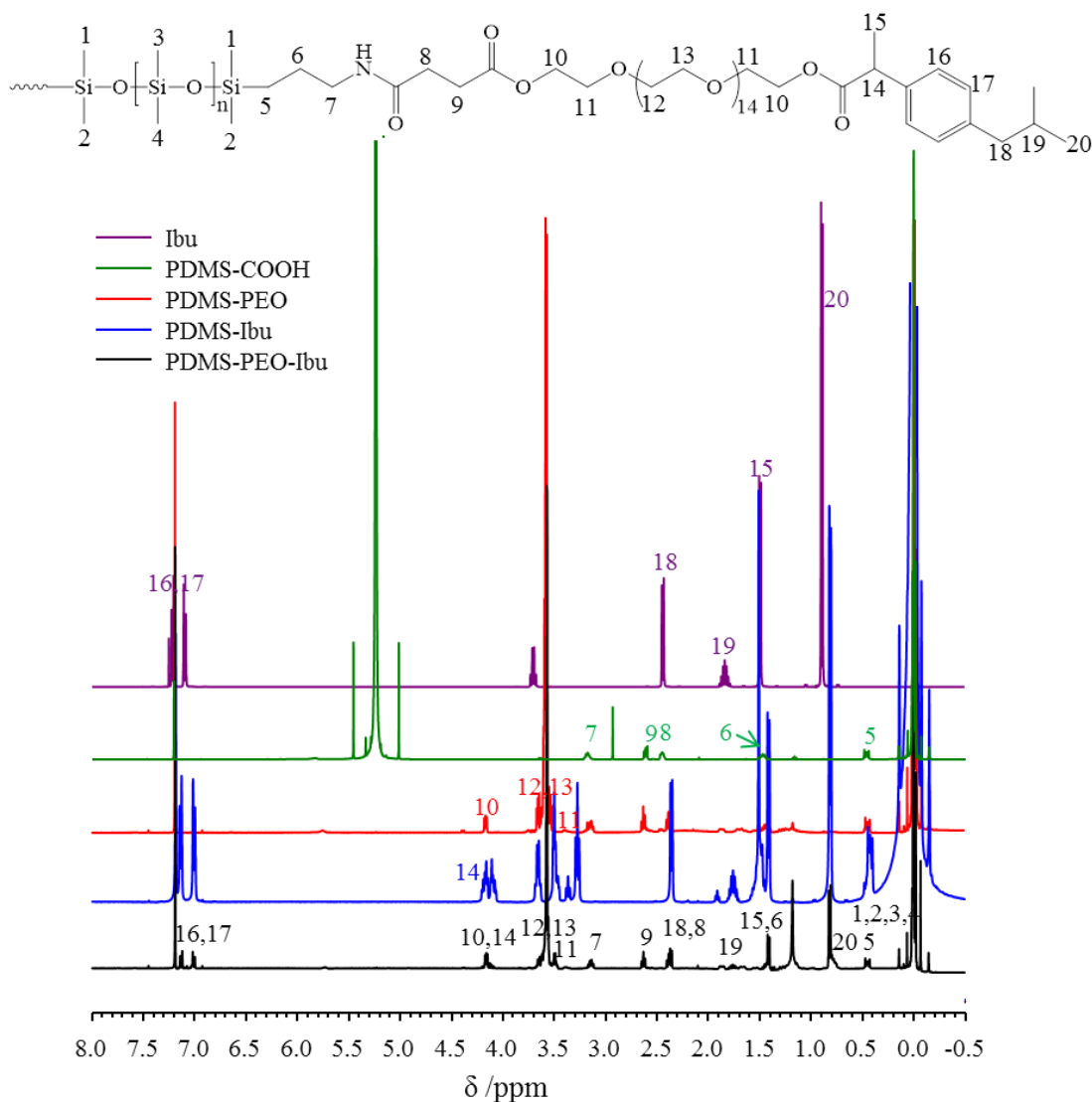
Figure 3.15 ^{1}H NMR spectra (CDCl$_3$, 400 MHz) of PDMS-PEO-Ibu at different steps of the synthesis: PDMS-COOH (green), PDMS-PEO (red) then PDMS-PEO-Ibu (black), along with Ibuprofen (purple) and PDMS-Ibu (blue) as a comparison.

3.3.3.3.2 Cleavage of PDMS-PEO Prodrug

PDMS-PEO-Ibu was treated with HCl (15 eq.) in dioxane at 85 °C. ^{1}H NMR analyses of the crude product after 16 hours reaction (see Figure 3.16), displays the disappearance of both ester signals (10) and (14), as well as (9) and (8) which confirms the complete cleavage of the polymer chain between PDMS and PEO and between PEO and Ibu. A purification step (washing with aqueous solution to

neutrality) allowed for the recovery of isolated PDMS and Ibu without any trace of PEO, as shown in Figure 3.16. The overlay of PDMS-PEO-Ibu, and both starting PDMS-NH$_2$ and Ibu spectra, clearly shows that the organic layer obtained after purification only contains free Ibu and PDMS-NH$_2$.
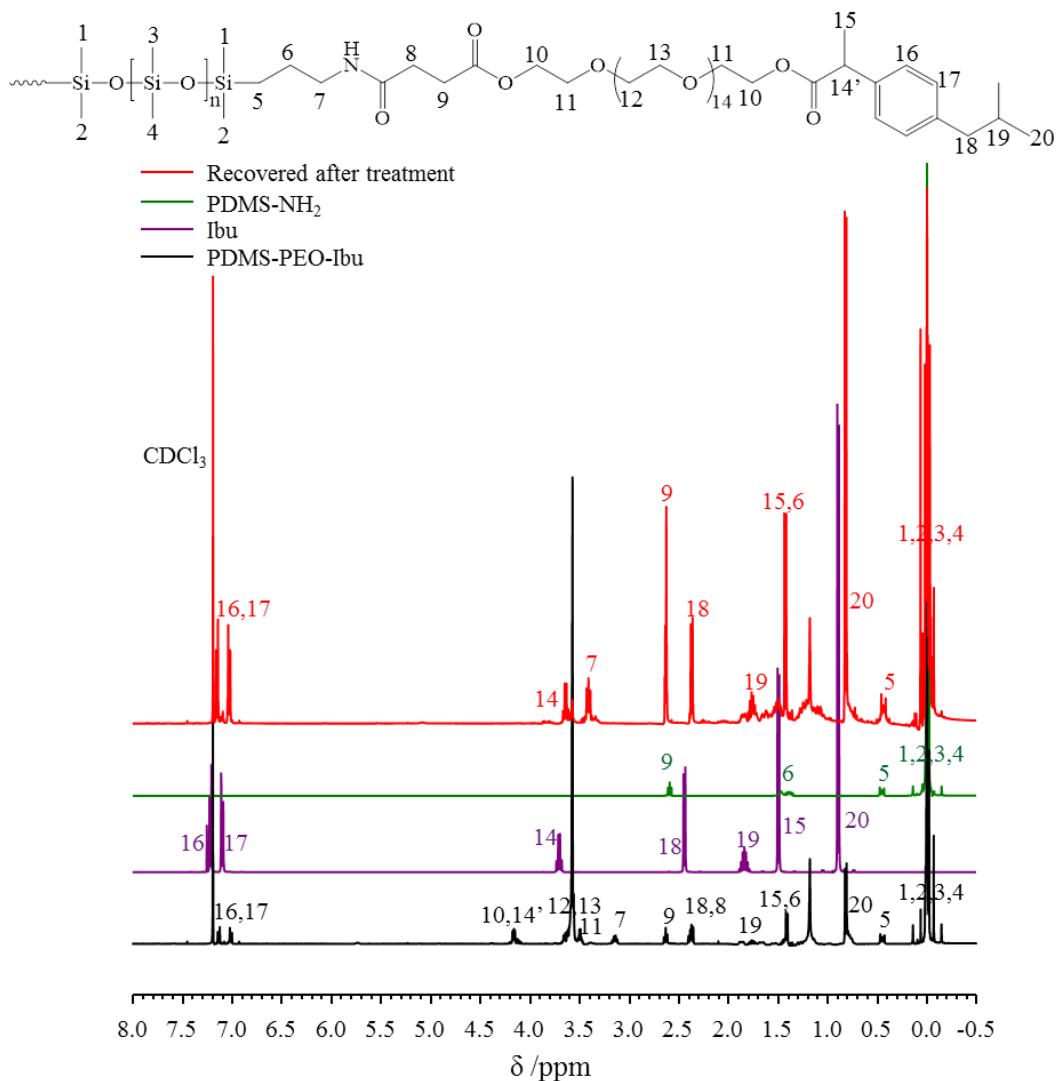
Figure 3.16 ^{1}H NMR spectra (CDCl$_3$, 400 MHz) of PDMS-Ibu before (black) and after (red) exposure to 15 equivalents of HCl in dioxane at 85 °C for 16 h, as well as starting materials Ibuprofen (purple) and PDMS-NH$_2$ (green).

To summarise, the cleavage of the drug from the PDMS polymer chain was achieved *in vitro*, using strong acidic conditions, providing that a hydrophilic spacer was present between PDMS and the drug. The added PEO spacer appears to balance the hydrophobicity of the polymer chain and, therefore, allow access to the chain-ends in the presence of water.

3.4 PDMS-DRUG AND SIO BLENDS

Due to the solubility of PDMS-atRA and PDMS-Ibu in SiO, the potential for these materials to act as "additives", and modify the release and solubilisation behavior of SiO, was studied with free drug.

As shown in Figure 3.17, when only free drug is present in SiO, release appears to be driven solely by diffusion through the oil, and has been reported to occur in an uncontrolled manner within a week *in vivo*.[7] When using the newly synthesised PDMS-drug as a prodrug, the release of drug should be controlled by a combination of diffusion and the cleavage of the bond between the PDMS and the drug molecule. The latter is quite unpredictable *in vivo*, as the factors for cleavage are not identified, thereby leading to little control of the release. On the other hand, by mixing free drug in a blend of SiO and PDMS-drug, the release of drug may be modified as diffusion of the free drug and cleavage of the drug from the PDMS chain may be affected by the presence of the modified PDMS. Moreover, the presence of PDMS-drug may provide a positive effect on the solubility of the free drug and allow higher concentrations to be achieved in SiO. Both atRA and Ibu solubility in blends, containing different ratios of PDMS-drug, was investigated in addition to their release pattern from blends into culture media.
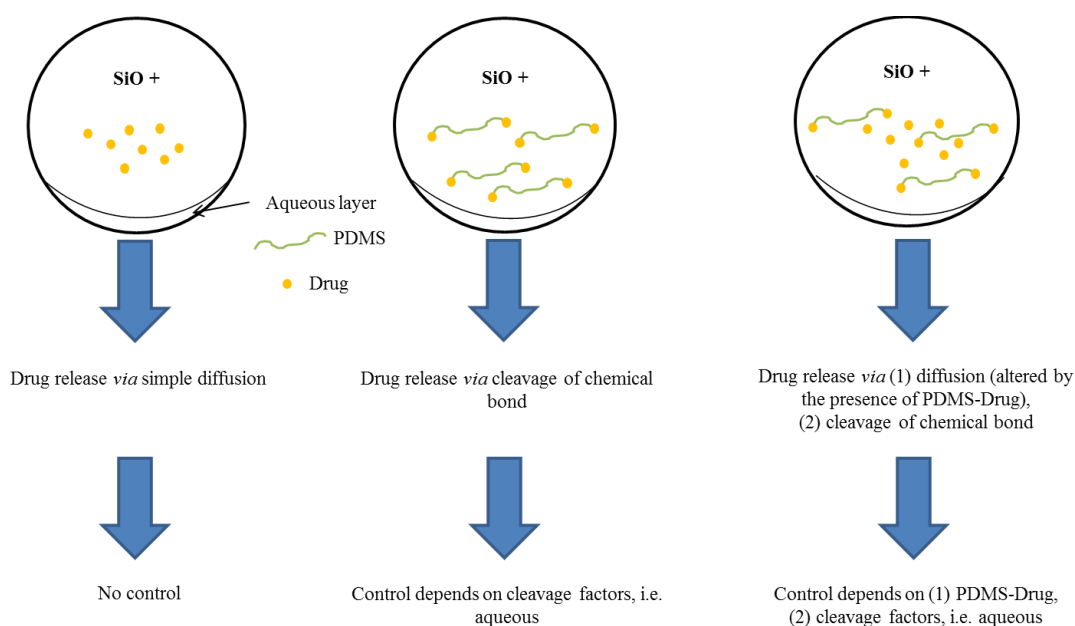
Figure 3.17 Different possible routes of drug release from SiO tamponade.

The measurement of atRA by UV-Vis spectroscopy presents important limitations such as low accuracy of the extraction method and the inability to measure release into culture media directly as there is an overlap of absorption peaks of atRA and an essential media component, foetal calf serum (see Appendix Figure A47). It is also not possible to measure solubility of atRA in SiO by ^{1}H NMR spectroscopy of the oil directly, as achievable concentrations are too low. As measuring atRA is essential to the project and analyses by traditional routes were not sufficient, the use of tritiated (^{3}H) atRA was investigated. Analysing the release of Ibu via ^{1}H NMR of the oil directly also has its limitations when measuring small concentrations, and UV-Vis spectra of Ibu is distorted in media to the extent that no calibration curve could be obtained, therefore, the use of tritiated Ibu was also investigated. The main advantages of using a radioactive isotope is the ease of detection, even at extremely small amounts, as well as the relatively simple protocol compared to other analyses; by selecting the ^{3}H containing drug, the chemistry of the compound is essentially unchanged and the measured behaviour can be related to expected free drug behaviour *in vivo*.

3.4.1 Introduction and use of Radioactive Isotopes

Isotopes of an element have the same number of protons in the nucleus but a different number of neutrons, therefore, the same atomic number but a different mass number. Isotopes can either be stable or radioactive (radioisotopes) and unstable due to an imbalance of protons and neutrons which emit particles/energy to improve stability. In 1889, Ernest Rutherford recognised that radioisotopes undergo nuclear decay/disintegration which involves the release of energy *via* emission of ionising radiation.[9] Rutherford named two modes of radioactive decay based on their penetrating power (see Table 3.5): heavier alpha and lighter beta radiations. A third type of radiation was discovered by Villard in 1900 and is called gamma rays,[10] later recognised as electromagnetic radiation. Table 3.5 shows some of the properties of these types of radiation.

Table 3.5 Types of radioactivity and their properties. Adapted from ref:[11]

Radiation	Form	Range of Maximum Energy (MeV*)	Penetration Range in Air (m)	Shielding Material
Alpha (α)	Particulate Helium Nuclei	4 – 8	0.025 - 0.080	Paper or even the dead cells in the outer layer of human skin
Beta (ß)	Particulate Electron	0.01 - 3	0.150 – 16	Plastic or few mm aluminium
Gamma (γ)	Electromagnetic	0.03 - 3	1.3 – 13**	Heavy metal e.g. barium or lead

* 1 MeV = 1.6 x 10^{-13} J
** Distance which radiation intensity halved

During nuclear decay of a radioisotope, more than one type of radiation may be emitted. Alpha decay is a form of spontaneous fission, a reaction where a nucleus lowers its mass and atomic number by splitting and the emission of a large alpha particle (2 protons and 2 neutrons), equivalent to a helium nucleus. As such, alpha particles are relatively large, are likely to collide with surrounding atoms, do not travel far and do not require much shielding (see Table 3.5).

Beta decay involves the transmutation of a neutron, which can occur *via* three routes represented in Figure 3.18.
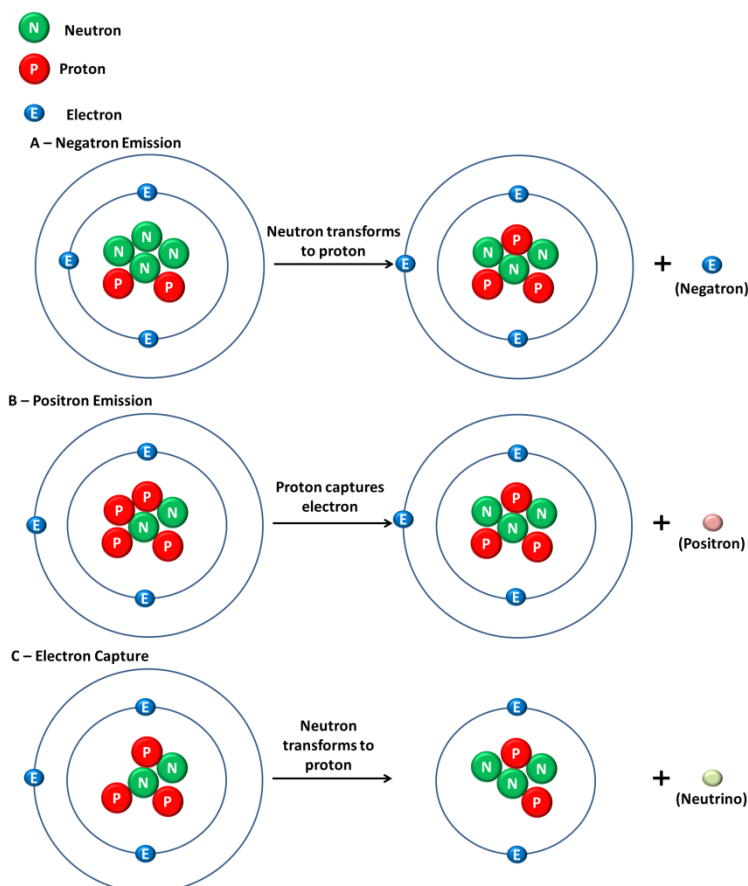
Figure 3.18 Illustrated representation of the different types of beta decay A: negatron emission, B: Positron emission and C: electron capture.

A. Negatron emission: Emits a negatively charged beta particle in the form of an electron. Negatron emission occurs in nuclei that contain more neutrons than stable isotopes of the same element. These "proton deficient" nuclides can be identified by their mass number being significantly higher than their atomic number, such as ^{3}H and ^{14}C. To regain some stability, the nucleus can transform one of its extra neutrons into a proton leading to the emission of an electron (negative beta particle) and an antineutrino (v).

B. Positron emission: Emits a positively charged beta particle in the form of a positron (the antiparticle of an electron, which has the same mass as an electron but with the opposite charge). Positron emission occurs in proton rich nuclei (nuclei which contain more protons than neutrons); nuclear decay takes place in order to restore balance by transforming a proton into a neutron. This leads to the emission of a positron and a neutrino, which can be identified by the atonic number decreasing by 1 while the mass number remains constant. Positron emission may develop into gamma rays if the positron is annihilated by collision with an electron.

C. Electron capture: Emits only a neutrino. Electron capture occurs most often in the heavier neutron-deficient elements such as ^{231}U. A neutrino is emitted when an orbital electron is captured by a proton in the nucleus and transformed into a neutron

Gamma radiation is electromagnetic radiation and not particulate like alpha and beta emission, however, it is always sub-sequential to initial alpha or beta decay. Gamma radiation involves the discharge of a high-energy photon from an over-excited nucleus, therefore, it does not change the identity of the atom from which it originates. As the gamma rays are not particulate they have only a small chance of colliding with surrounding atoms and, therefore, have a long range through air (see Table 3.5).

Tritium Labelling

Radioisotopes can be used to study the properties, behaviour and reactions of non-radiolabelled compounds and throughout this project tritiated atRA and Ibu supplied by ARC were used (see Appendix Figure A50). The tritium isotope was first

produced in 1934 by Rutherford and co-workers[12] from deuterium and has the same properties as hydrogen with respect to charge and electrostatic repulsion with other atomic nuclei. The only difference between tritium and hydrogen is that the nuclei contains an extra neutron and, therefore, undergoes beta decay to become stable. Tritium emits negative beta particles by negatron emission, and was chosen as it has a long half-life (12.43 years) and decay during experimental time periods would not need to be accounted for. Also tritium is a relatively safe beta emitter as it produces a maximum energy of 0.0186 MeV which only penetrates 4 mm of air and is incapable of passing through the dead outermost layer of skin (0.05 mm). Due to this weak signal it can only be detected *via* liquid scintillation counting (see Section 6.17).

3.4.2 Drug Solubility Measurement in SiO and Blends Utilising Radioisotopes

The process of using radiolabelled drugs to determine solubility concentration within SiO is a much simpler protocol than that used when UV-Vis was utilised as there is no longer the need for the extraction step, see Figure 3.19.
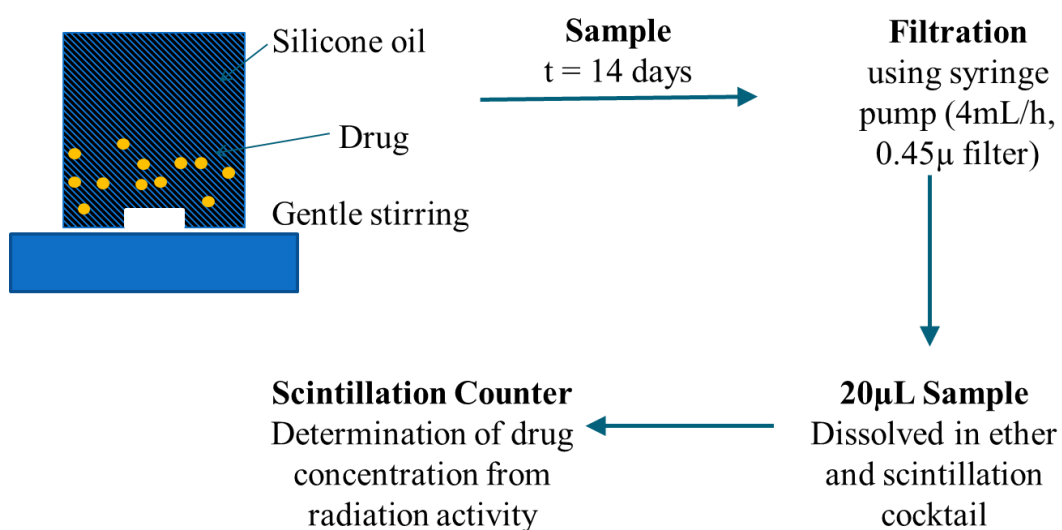
Figure 3.19 Process of determining solubility of drug in SiO when utilising radiolabelled drugs.

3.4.2.1 atRA Solubility Studies

The saturation concentration of free atRA in SiO was investigated using the tritiated atRA. A saturated solution of atRA, spiked with tritiated atRA, in SiO was prepared and stirred gently. Samples were taken at different time-points then filtered using a

syringe pump (4 mL/h) and 0.45 μm PTFE filters. To determine the amount of atRA dissolved in SiO, a 20 μL sample of oil was taken, which was insoluble in the scintillation cocktail, therefore, a co-solvent was needed to fully solvate the material for accurate analysis. After several tests using a known activity of sample, it was determined that a ratio of diethyl ether/scintillation cocktail (8:10 mL) allowed accurate activity measurement by liquid scintillation.

While the solubility reported for atRA in SiO in the literature is 20 μg/mL, higher concentrations, in the order of 28 μg/mL (9.5×10^{-5} M, s.d.= 1, n = 6). were measured when the same protocol was used.[7] Using the tritiated atRA, the solubility measured was over 20 times higher than the previous values, reaching 450.6 μg/mL (1.5×10^{-3} M, s.d. = 39.9, n = 4).

The solubility of atRA in SiO_{5000} was also investigated as a simpler protocol was now in place to deal with such a viscous substance. Saturation was determined to be higher than in SiO_{1000} at 610 μg/mL (2.03×10^{-3} M, n=1) in SiO_{5000}.
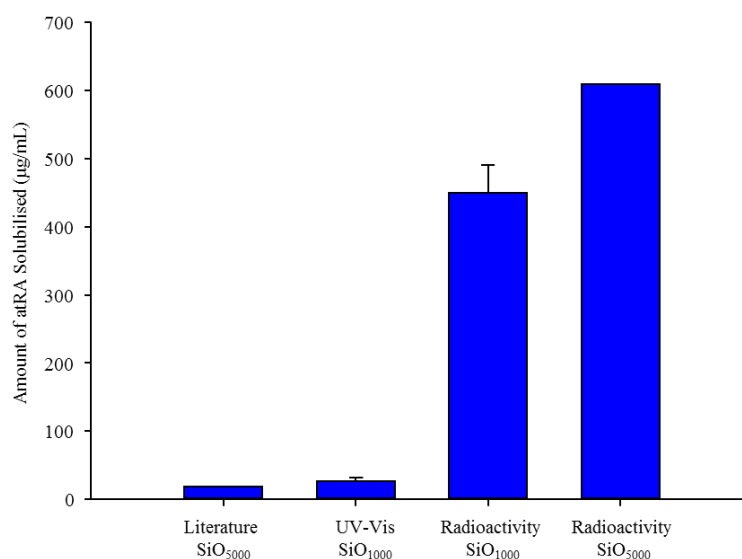
Figure 3.20 Comparison of saturation concentration of atRA measured in SiO *via* UV-vis or radioactivity measurements. Literature value taken from Araiz et al.[7] Error bars ±1 standard deviation.

The use of radiolabelled isotopes has provided a much more accurate method to measure small drug concentration in SiO compared to the classic extraction combined with traditional instrumentation e.g. UV-Vis spectroscopy. However, such a large difference between methods was not anticipated. When the literature value

was further analysed, it was noticed that the calibration curve used was in the range 0.5×10^{-4} M to 1×10^{-6} M, with the reported 20 μg/mL (0.6×10^{-4} M) being on the cusp of the maximum value; therefore, higher concentrations need extrapolation from the curve, leading to potential errors. Overall an accurate method to measure solubility of atRA in SiO has been established using radiolabelling techniques and a fundamental inaccuracy in the published literature has been identified.

3.4.2.2 atRA in SiO Blends

The same protocol used to determine accurate atRA solubility in SiO was employed to determine free atRA concentration in blends of PDMS-atRA in SiO at 1, 5 and 10 % (v/v). As the amount of PDMS-atRA present in the blend increased so did the measured saturation concentration of atRA (see Table 3.6). An increase from 450.6 μg/mL to 812.7 μg/mL was observed when a blend of 10 % PDMS-atRA in SiO blend was used. This indicated the blends have a positive effect on the solubility of the free drug, increasing its saturation concentration in the oil possibly due to the presence of attached drug and its affinity towards free drug.

Table 3.6 Saturation amounts of atRA (μg/mL) in SiO and SiO blended with PDMS-atRA at 1, 5 and 10 % (v/v) for 2 weeks at ambient temperature, in air.

	SiO	1 % PDMS-atRA	5 % PDMS-atRA	10 % PDMS-atRA
atRA (μg/mL oil)	450.6	651.0	699.8	812.7
atRA (M)	1.50×10^{-3}	2.17×10^{-3}	2.33×10^{-3}	2.71×10^{-3}

The shear viscosity of SiO_{1000} and SiO_{5000}, as well as the blends with end-modified PDMS, were measured at 37 °C (the temperature of cell culture within the project) and calculated from the gradient of the plot of shear stress against shear rate; graphs are shown below in Figure 3.21.
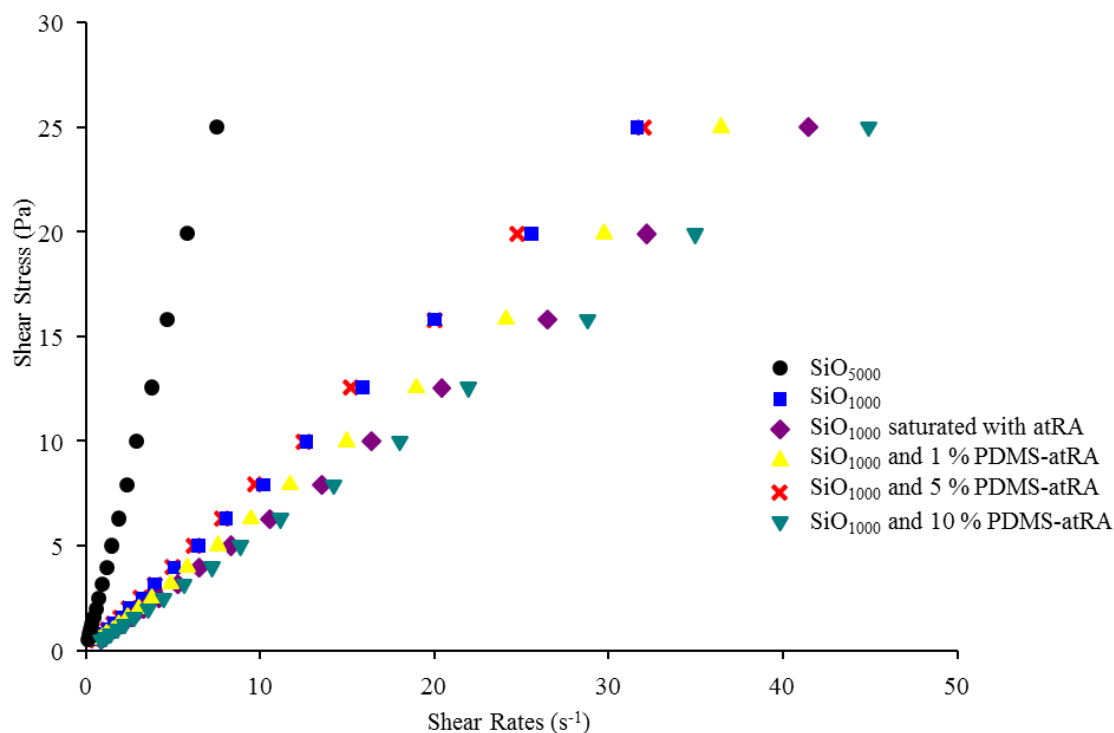
Figure 3.21 Graph of shear stress against shear rate for SiO_{5000} (●), SiO_{1000} (■), SiO_{1000} saturated with atRA (♦), SiO_{1000} blends with 1 (▲), 5(x) and 10 (▼) % (v/v) PDMS-atRA from which the shear viscosity was calculated.

The measured viscosities show that there is a negligible effect of saturating SiO_{1000} with atRA, and the viscosity of the blends do not follow a trend of decreasing or increasing viscosity, therefore, it is not characteristic variation in viscosity that is affecting the observed saturation concentration change within the blends, Table 3.7.

Table 3.7 Shear viscosities (mPa/s) calculated from the gradient of the plot of shear stress against shear rate at 37 °C.

Material	Shear Viscosity (mPa/s) at 37 °C
SiO_{5000}	3.35
SiO_{1000}	0.79
SiO_{1000} saturated with atRA	0.79
SiO_{1000} with 1 % PDMS-atRA	0.61
SiO_{1000} with 5 % PDMS-atRA	0.68
SiO_{1000} with 10 % PDMS-atRA	0.56

3.4.2.3 Ibu Solubility Studies

The same radiolabelling methodology was used to determine Ibu saturation in SiO, using tritiated Ibu, over 7 days and at ambient temperature. Ibu saturation in SiO was found to be 0.22 mg/mL *via* UV-Vis spectroscopy, and ^{1}H NMR spectroscopy determined the saturation concentration to be 2.05 mg/mL ($9.94.10^{-2}$ M, n = 2). When tritiated Ibu was used, a similar value was obtained *via* liquid scintillation counting (2.26 mg/mL).
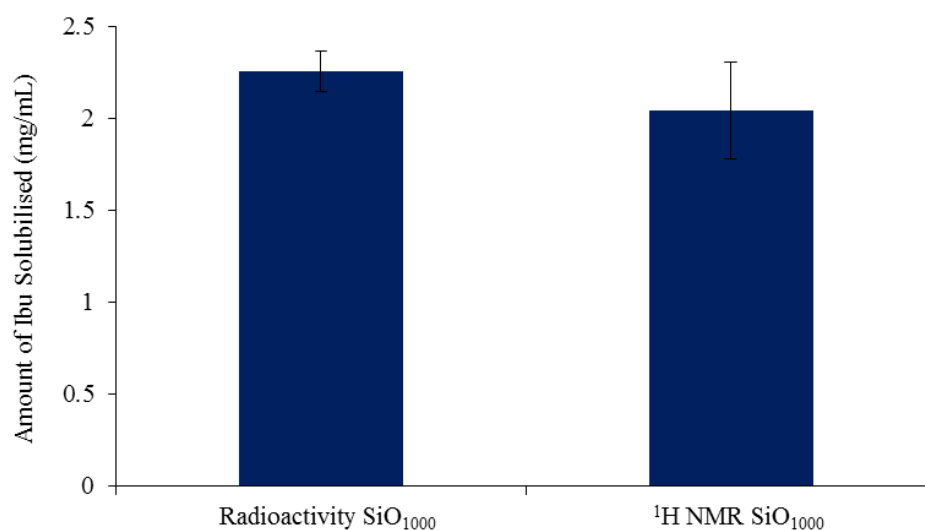
Figure 3.22 Comparison of saturation concentration of Ibu measured in SiO$_{1000}$ *via* radioactivity and ^{1}H NMR analyses. Error bars ± 1 standard deviation.

3.4.2.4 Ibu in SiO Blends

The radiolabelling protocol used to determine Ibu solubility in SiO was used to determine Ibu concentration in blends of PDMS-Ibu in SiO at 1, 5 and 10 % (v/v). Unlike atRA, the amount of PDMS-Ibu present in the blend did not have any significant effect on the solubility of Ibu, see Table 3.8.

Table 3.8 Saturation concentration of Ibu (mg/mL) in SiO and SiO blended with PDMS-Ibu at 1, 5 and 10 % (v/v).

	SiO	1 % PDMS-Ibu	5 % PDMS-Ibu	10 % PDMS-Ibu
Ibu (mg/mL oil)	2.13	2.04	2.00	1.98

Although the solubility of Ibu had not increased when using the blends, the concentration solubilised was still high. Therefore, it was still important to investigate the blends further, as well as exploring the release of Ibu from SiO and see if release was affected in any way.

3.4.3 Release of drug from SiO and Blends

The effect of the presence of PDMS-drug on the release pattern of free drug was investigated within the Ibu and atRA systems, with the potential that the affinity of the blend to the drug would result in a slower release compared to the short time periods stated in the literature; that is 98 % clearance of atRA administered to the eye *via* a SiO tamponade, within a 7 day time period.[7] This time period also needed to be confirmed, as the literature had already proven to be inaccurate in measuring atRA solubility in SiO and subsequent measurements could also be affected by inaccuracies. The optimum time period for release, targeted by this research, is 6 weeks as this is the clinical treatment period for PVR. Appropriate conditions of temperature, CO_2 content, and presence/absence of cells for these experiments were investigated.

3.4.3.1 Experimental Design for Drug Release Studies

The release of atRA and Ibu from SiO_{1000} and SiO_{1000} blends with PDMS-drug (using solutions containing various initial concentrations) into culture media was monitored using tritiated versions of the drugs as prepared in Section 3.4.2.1. The experiments were designed as follows: 1 mL of oil or blend containing free drug was placed over 0.5 mL of culture media in a 24 well plate. The culture media was exchanged with fresh culture media when samples were taken (see Figure 3.23), and the amount of drug in the media determined directly *via* liquid scintillation counting.
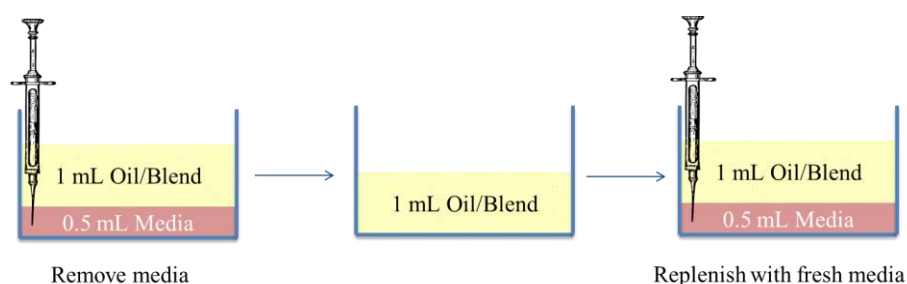
Figure 3. 23 Illustration of how media samples were taken throughout drug release studies.

3.4.3.1.1 Quenching Effect of Culture Media in Liquid Scintillation

It is known that highly coloured samples can interfere with the scintillation counting process *via* quenching. The colour of the sample interferes with the light signals produced by the scintillant, therefore, leading to discrepancies in the data collected. To rule out potential inaccuracies, the effect of 250 μL of culture media within the scintillant cocktail (10 mL) was tested and showed no significant effect on the counts due to the solution being very dilute (see Table 3.9). For each 0.5 mL culture media sample collected throughout the experiments, 250 μL was analysed, and the total amount of drug released deduced from that.

Table 3.9 Decays per minute (DPM) of tritiated atRA solutions of both high and low concentration with and without media present.

	High Tritium Content (DPM)			Low Tritium Content (DPM)		
Without Media	11,702	12,361	12,282	308	458	348
With Media	11,566	12,521	12,237	281	429	306
Difference	-136	160	-45	-27	-29	-42

3.4.3.1.2 Effect of Temperature on SiO

The shear viscosities of SiO_{1000} were measured at 20, 30 and 37 °C (the approximate temperature of the eye) to determine if temperature would alter the rheological properties of the oil. The shear viscosities were calculated from the gradient of the plot of shear stress against shear rate. As a difference was observed (see Table 3.10), all release experiments were carried out at 37 °C as this is the temperature used to culture cells as well as a similar temperature observed in the eye.

Table 3.10 Shear viscosities (mPa/s) of SiO_{1000} calculated from the gradient of the plot of shear stress against shear rate at 20, 30 and 37 °C.

Temperature (°C)	Shear Viscosity (mPa/s) at 25 Pa
20	1.0879
30	0.9115
37	0.7912

3.4.3.1.3 Effect of CO$_2$ on Release

The effect of atmospheric CO$_2$ content within the experiments on the release rate of atRA from SiO and blends into culture media was evaluated. A release experiment was carried out at 10 % CO$_2$ (5 % CO$_2$ is used to culture the cells) due to lack of availability of incubators that could hold radioisotopes. The same experiment was carried out in air, and the different release rates observed were compared.

Figure 3.24 highlights differences in release from experiments conducted in air and within the presence of 10 % CO$_2$. On day 1, more atRA was observed to be released when the experiment was carried out in air, however, this difference decreased by day 2, and by day 8 the opposite effect was observed with more atRA released under a 10 % CO$_2$ atmosphere. Overall, this experiment showed that the atmospheric conditions for accurate release studies need to be kept constant to allow comparison.

As a consequence of the investigations of optimum experimental conditions, all following experiments were carried out at 37 °C in a 5 % CO$_2$ atmosphere (the same conditions used for ARPE-19 cell culture).
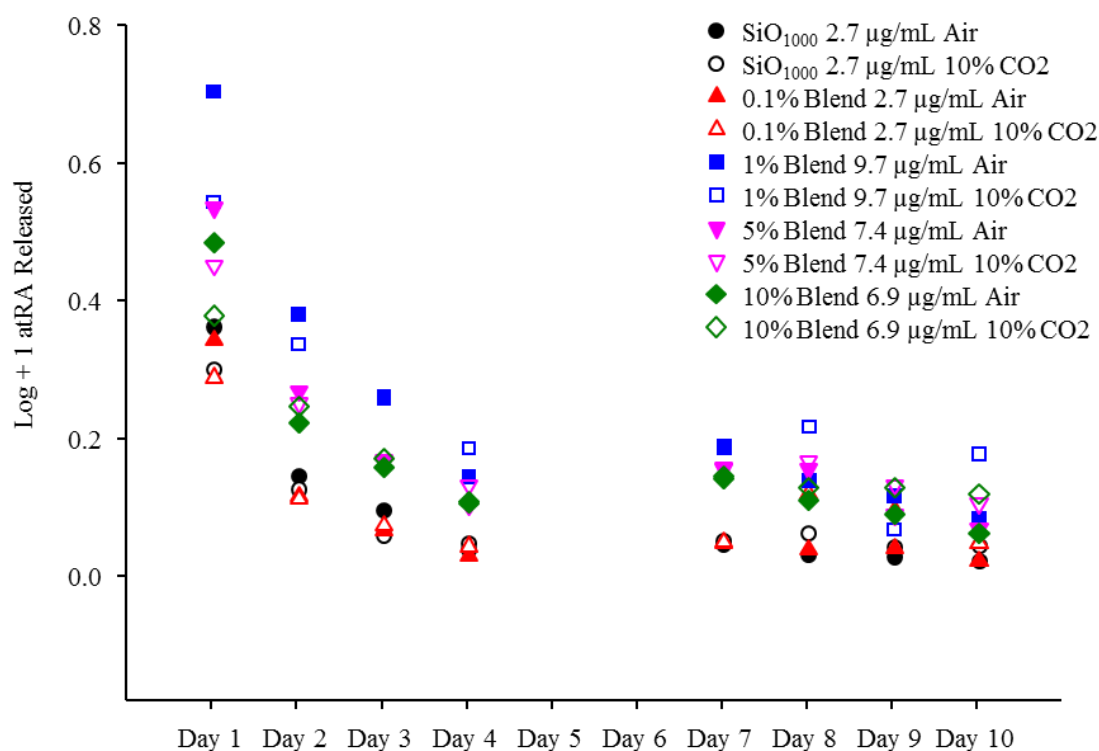
Figure 3.24 Release of atRA at a concentration below 10 μg/mL from SiO (black) and 0.1(red), 1 (blue), 5 (pink) and 10 % (green) blends (v/v) both in air (filled) and in a 10 % CO$_2$ atmosphere (unfilled) into media. All experiments were carried out at 37 °C.

3.4.3.1.4 Effect of the Presence of Cells

A release experiment of atRA in SiO into media in the presence of pre- and post-confluent cells (cultured for 1 day and 7 days respectively) was performed. This aimed to determine if the presence of cells had an impact on the drug release rate, as cells could act as a drain for released atRA and potentially affect the balance of concentrations. As seen in Figure 3.25 no obvious differences in release rates were observed, therefore, future experiments could be carried out in the absence of cells.
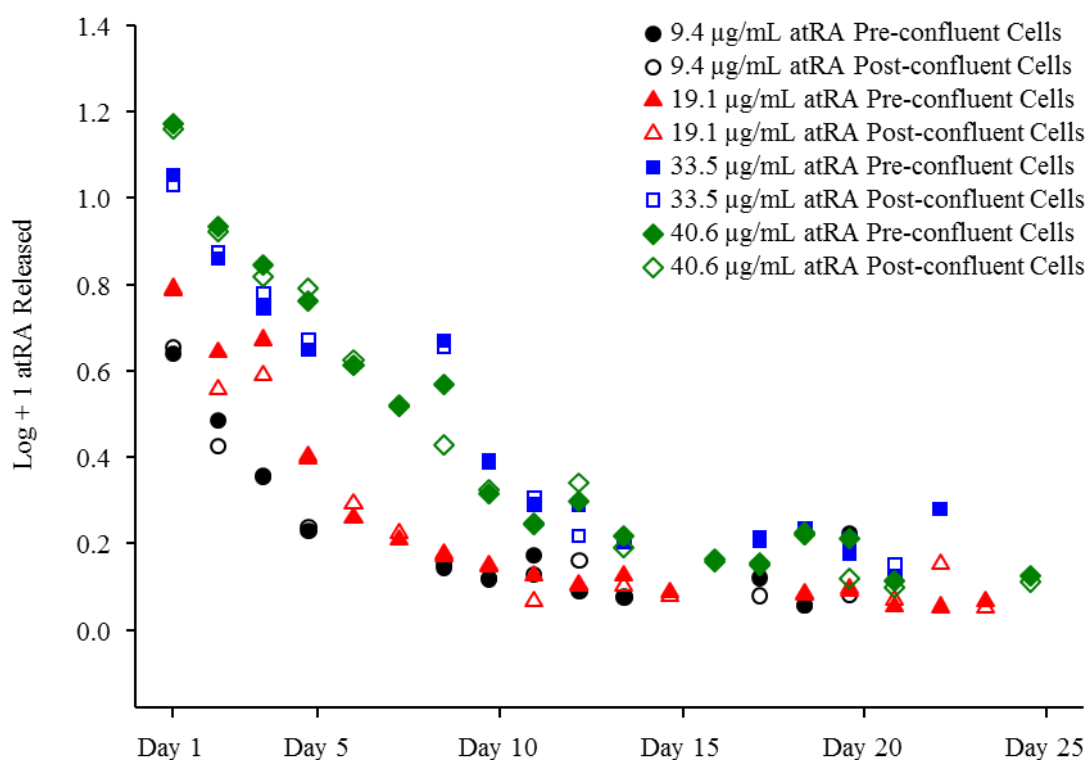
Figure 3.25 Release of atRA at various concentrations from SiO_{1000} into media in the presence of pre- and post-confluent cells (filled and unfilled respectively) presented in a log+1 scale. All experiments were carried out at 37 °C in a 5 % CO_2 atmosphere.

3.4.3.2 Release Studies of atRA

The release into culture media of atRA from saturated SiO_{1000} and blends (PDMS-atRA contents of 1, 5 and 10 % in SiO_{1000} (v/v)) was studied. As stated earlier, the saturation concentration of atRA increases with increasing amounts of PDMS-atRA, therefore, all starting concentrations within the experiments were slightly different as saturation conditions were employed. Figure 3.26 displays the amount of atRA released over a 50 day period, presented with a log plot + 1 scale; this scale was chosen so release points were easily comparable. A rapid release of atRA is

observed within the first few days, after which the release gradually slows and then becomes steady over the remaining 20 days. More atRA appears to be released from the blends, probably due to initial saturation concentrations being higher.
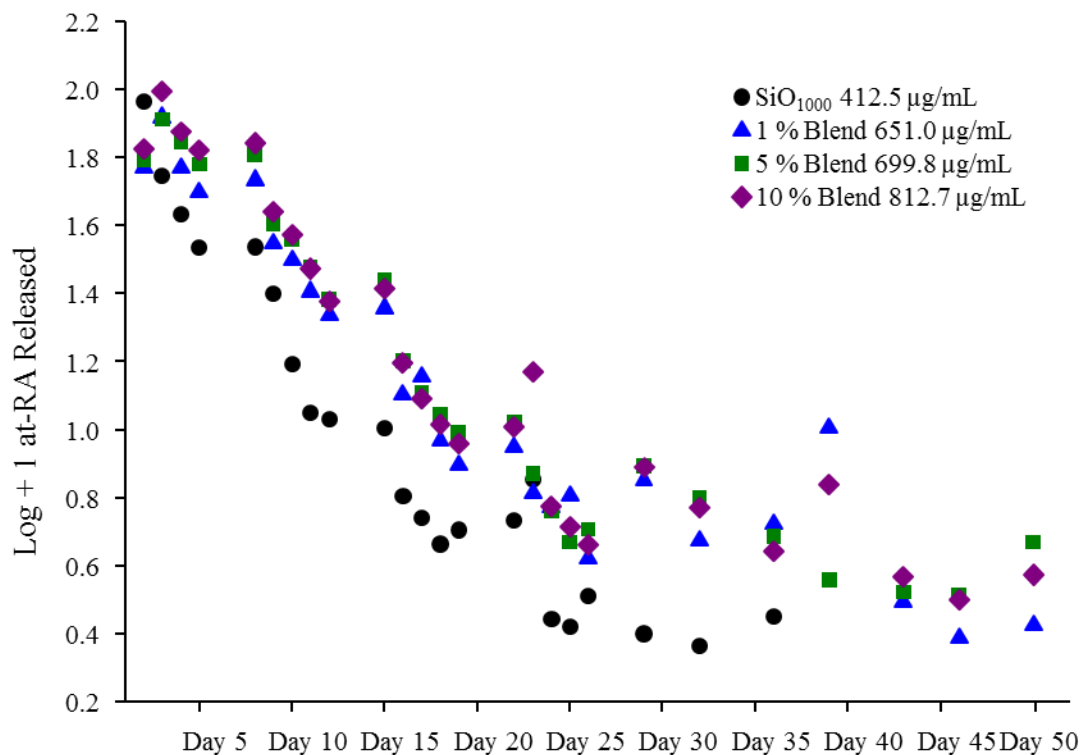
Figure 3.26 Release amounts of atRA from saturated SiO_{1000} (●), 1 (▲), 5 (■) and 10 (◆) % (v/v) blends of PDMS-atRA in SiO_{1000} into culture media presented on a log+1 scale.

When looking at the amount of atRA released from SiO and the blends as a cumulative percentage (Table 3.11 and Appendix Figure A48), it is very interesting to notice the difference in time taken for 80 % of the solubilised atRA to be released: 2 weeks for SiO_{1000} compared to nearly 7 weeks for the 10 % blend. This is also interesting as the literature value of 7 days to clear 98 % atRA from a saturated SiO_{1000} solution has been disputed (although the 7 d time point was taken from a rabbit model rather than an *in vitro* model).

Although promising release time periods were observed, the amounts of atRA being initially released was above the toxic range for ARPE-19 cells (10^{-4}-10^{-5} M). It was important to ascertain if the use of blends of SiO with PDMS-atRA could impact the release rate for lower concentrations of atRA to avoid the potential of toxicity, and if the longevity of the release period was dependant on the amount of atRA initially solubilised.

Table 3.11 Number of days needed to reach a certain percentage (cumulative) of release of atRA from saturated solutions of SiO_{1000} and 1, 5 and 10 % PDMS-atRA blends *Extrapolated values in italics.*

Cumulative Percentage	Days Taken to Reach Percentage of Release			
	SiO_{1000} (412.5 µg/mL)	1 % Blend (651.0 µg/mL)	5 % Blend (699.8 µg/mL)	10 % Blend (812.7 µg/mL)
10	<1	1.1	1.1	1.2
20	<1	1.9	1.8	1.8
30	1.6	2.9	2.9	3.1
40	2.4	4.2	4.1	4.2
50	3.3	7.2	6.8	7.2
60	5.4	9.8	9.2	9.9
70	8.2	15.2	12.8	16.4
80	14.0	30.9	21.9	48.2
90	35.0	*121.9*	*75.1*	*153.1*
100	*110.6*	*214.9*	*144.9*	*251.5*

3.4.3.3 Release Studies Using Non-Saturation Concentrations of atRA Within SiO and Blends

In the previous section it was observed that higher initial solubilised concentrations of atRA maintained the longest release profiles, however, the ability of the affinity of atRA to PDMS-atRA to slow the release rate was not shown conclusively. To investigate this further, a series of release experiments where varying but similar amounts of atRA were solubilised into SiO and blends with PDMS-atRA was carried out. The cumulative percentage release values are presented in Table 3.12 (graph in Appendix Figure A49). No noticeable release differences were observed between the SiO and the SiO/PDMS-atRA blends, apart from when 10 % PDMS-atRA was

present within the blend. The time needed to release 80 % of the atRA solubilised in SiO_{1000} and the 1 and 5 % blends is on average 16 days (2 weeks) whereas for the 10 % blend, this increases to nearly 51 days (>three times longer, ~7 weeks).

Table 3.12 Number of days needed to reach a certain percentage (cumulative) of release of atRA from SiO_{1000} and 1, 5 and 10 % blends containing approximately the same initial amount of atRA, i.e. 50 µg/mL. *Extrapolated values in italics.*

Cumulative Percentage	Days Taken to Reach Percentage of Release			
	SiO_{1000} (49.2 µg/mL)	1 % Blend (58.3 µg/mL)	5 % Blend (48.4 µg/mL)	10 % Blend (46.2 µg/mL)
10	<1	<1	<1	<1
20	<1	1	<1	<1
30	1.7	1.7	1.8	1.6
40	2.2	2.3	2.3	2.4
50	3.1	3.1	3.8	4.6
60	5.1	4.9	6.2	7.9
70	8.7	8.6	8.9	15.3
80	16.2	14.8	17.1	50.8
90	59.0	39.1	65.5	*150.8*
100	*175.8*	*172.0*	*159.7*	*244.0*

3.4.3.4 Different Amounts of atRA from SiO and Blends

An underlying problem with the release observed for the desired time range (seven weeks) was that the initial burst release took the concentrations above the toxic range

for the ARPE-19 cells (10^{-4} – 10^{-5} M). To ensure that the release period were definitely independent of the initial amounts of atRA, an experiment utilising varying amounts of atRA in SiO_{1000} (ranging from 13.2 to 412.5 µg/mL) was carried out. From this it was determined that the release period was independent of atRA starting concentration (see Table 3.13).

Table 3.13 Number of days needed to reach a certain percentage (cumulative) of release of atRA from SiO_{1000} and 1, 5 and 10 % blends containing approximately various initial concentrations of atRA. *Extrapolated values in italics.*

Cumulative Percentage	Days Taken to Reach Percentage of Release From SiO_{1000}				
	13.2 µg/mL	32 µg/mL	41 µg/mL	49.3 µg/mL	412.5 µg/mL
10	<1	<1	<1	<1	<1
20	<1	<1	<1	<1	<1
30	1.0	1.2	1.4	1.8	1.6
40	1.9	1.8	2.1	2.3	2.4
50	2.6	2.6	2.7	3.1	3.3
60	6.6	4.4	4.6	5.1	5.4
70	14.0	8.3	6.8	8.7	8.2
80	*35.4*	14.9	10.3	16.2	14.0
90	*77.2*	25.0	19.2	*59.0*	35.0
100	*128.2*	*37.9*	*76.2*	*171.0*	*110.6*

After determining that the release rates were independent of atRA starting concentration in SiO_{1000}, the impact of the presence of PDMS-atRA blends was also studied. When the release from saturated blends was compared with the release from a blend with an approximate starting concentration of 50 µg/mL, it appeared that the amount of PDMS-atRA present in the blend controlled the release time as shown in Table 3.14. If we compare SiO_{1000} with a SiO_{1000} blend with PDMS-atRA

(10 vol %), 80 % of the atRA initially present within SiO_{1000} containing 40 or 400 µg/mL was released in 10 and 14 days respectively, whereas 80 % of the atRA within a SiO_{1000}/PDMS-atRA 10 % blend containing either 45 or 800 µg/mL was released in 51 and 48 days respectively. This suggests that the presence of the blends may extend the release period into the 6 week period that is required clinically.

Table 3.14 Table to show time (days) taken to reach certain percentages of cumulative release of atRA from solutions of 1, 5 and 10 % blends of PDMS-atRA in SiO_{1000} (v/v) with various initial concentration of atRA. *Extrapolated values in italics.*

Cumulative Percentage	Days Taken to Reach Percentage of Release					
	1% Blend 58.3µg/mL	1% Blend 651µg/mL	5% Blend 48.4µg/mL	5% Blend 700µg/mL	10% Blend 46.2µg/mL	10% Blend 813µg/mL
10	<1	1.1	<1	1.1	<1	1.2
20	1	1.9	<1	1.8	<1	1.8
30	1.7	2.9	1.8	2.9	1.6	3.1
40	2.3	4.2	2.3	4.1	2.4	4.2
50	3.1	7.2	3.8	6.8	4.6	7.2
60	4.9	9.8	6.2	9.2	7.9	9.9
70	8.6	15.2	8.9	12.8	15.3	16.4
80	14.8	30.9	17.1	21.9	50.8	48.2
90	39.1	*121.9*	65.5	*75.1*	*150.8*	*153.1*
100	*172.0*	*214.9*	*159.7*	*144.9*	*244.0*	*251.5*

This is an exciting prospect as the potential to tailor the initial starting concentration to avoid the toxicity of the burst release ARPE-19 cells and maintain the sustained release amounts above the therapeutic level for an antiproliferative effect may be achievable.

3.4.3.5 atRA Release from SiO_{5000}:SiO_{1000} Blends

Whilst some surgeons prefer using SiO_{1000} as a tamponade agent, some prefer to use SiO_{5000} (see Chapter 1 Section 1.2.3.3.3). Due to SiO_{5000} having a higher viscosity, it reduces the risk of emulsion formation within the eye after administration. A preliminary comparative experiment was carried out in which the release profile of atRA from a SiO_{1000} solution was evaluated against the release from a 50/50 SiO_{1000}/SiO_{5000} solution. To achieve the same starting concentration of atRA in both of the oils, a solution of atRA in SiO_{1000} was prepared, stirred for 2 weeks and filtered following the same protocol as described previously. Once filtered, the solution was divided into two vials and the appropriate volume of SiO_{5000} was added to one to create a 50/50 blend of SiO_{1000}/SiO_{5000}, while the second one was diluted with SiO_{1000}. The resulting oils had an initial concentration of 32 µg/mL of atRA.
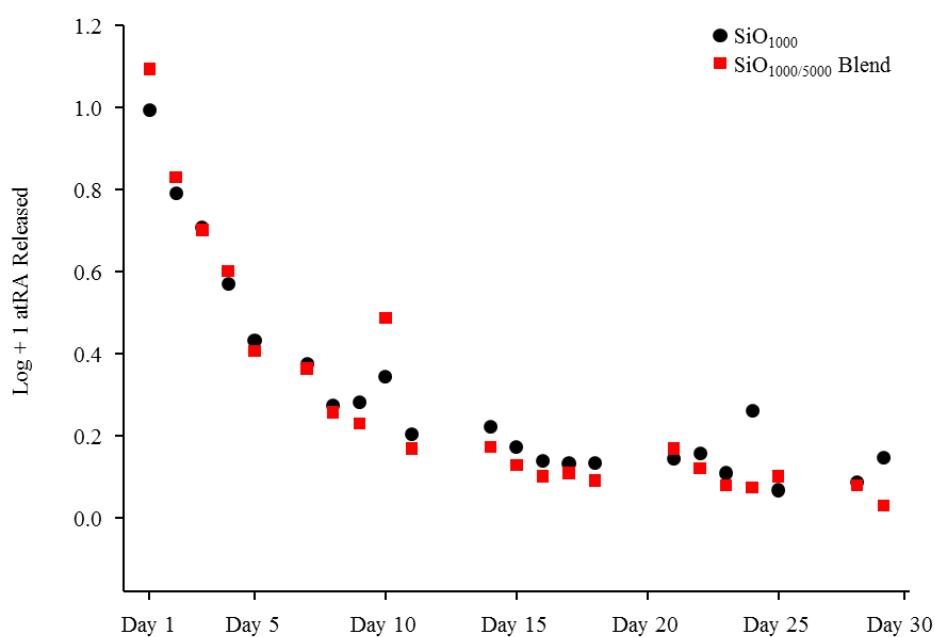
Figure 3.27 Release of atRA (starting concentration 32 µg/mL) from SiO_{1000} (●) and $SiO_{1000/5000}$ blend (■) into culture media presented on a log+1 scale. Experiments were carried out at 37 °C in a 5 % CO_2 atmosphere.

Figure 3.27 shows there is no apparent difference in atRA release from either SiO_{1000} or a $SiO_{1000/5000}$ 50/50 vol % blend. It appears, therefore, that the viscosity of the oil does not seem to affect atRA release.

3.4.4 Release of Ibuprofen from SiO and Blends

The release of Ibu from saturated SiO_{1000} and SiO/PDMS-Ibu blends, containing 1, 5 and 10 vol % PDMS-Ibu, into culture media was investigated. Figure 3.28 shows the observed release rates determined by both ^{1}H NMR spectroscopy and liquid scintillation measurements.

While burst release is also observed within the first day, the majority of Ibu is released over several days, with 90 % being released after only 3 days. The same release profiles were observed for SiO_{1000} and the 3 different blends, therefore, it can be concluded that the presence of PDMS-Ibu did not affect the release rates of Ibu from SiO_{1000} as seen for the atRA systems.
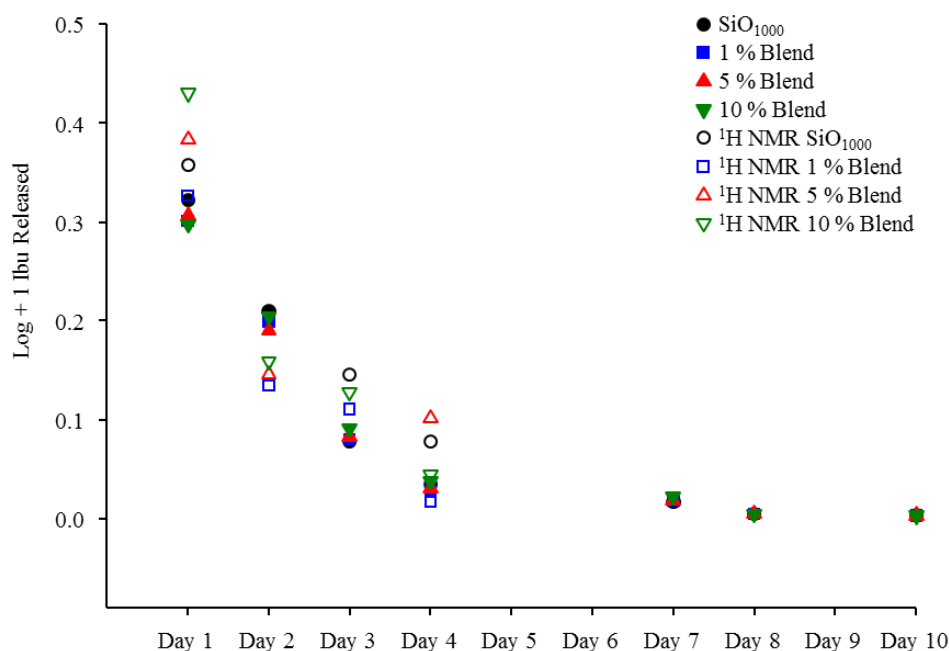
Figure 3.28 Release of Ibu from saturated solutions of SiO_{1000} (black) and 1 (red), 5 (red) and 10 % (green) blends (v/v) measured both by ^{1}H NMR spectroscopy (unfilled) and by liquid scintillation (filled) into culture media, presented on a log+1 scale. All experiments were carried out at 37 °C in 5 % CO_2.

3.5 CONCLUSION

The synthesis of PEO prodrugs with atRA and Ibu was achieved, with successful cleavage without observable degradation of the drugs. Biological evaluation concluded PEO did not affect metabolic activity of ARPE-19 cells and cytotoxicity

was dependant on drug content. Due to inefficient solubility of the PEO prodrugs in SiO compared to free drug, all investigations were ceased apart from studies using PEO$_{14}$-Ibu which had the highest solubility in SiO. Release studies of PEO$_{14}$-Ibu with Me-PEO-Ibu and free Ibu from SiO into culture media concluded that the PEO prodrug did prolong release; however, the majority was released over 4 days which falls short of the target 4-6 week treatment period criteria.

The synthesis of PDMS prodrugs with both drugs was successful; however, cleavage of drug *via* breakage of the ester bond was not readily achieved. It was hypothesised that this was due to a hydrophilicity/hydrophobicity issue of the prodrugs within the cleavage conditions. The synthesis of a tripartite PDMS prodrug with a PEO spacer supported this as cleavage was then observed when this was present. Biological evaluation of the PDMS prodrugs at 10 % (v/v) in SiO indicated no cytotoxicity occurred at this concentration.

Due to the unsuccessful cleavage of the PDMS prodrugs, they were studied as additives to SiO to ascertain any impact on drug solubility and release. Different methodologies were tested to investigate drug solubility in SiO; the development and use of radioisotope techniques was required to achieve accurate measurements, and a fundamental inaccuracy of atRA solubility in SiO reported in the literature was identified. The presence of PDMS-atRA in SiO had a positive effect on atRA solubility, possibly due to the affinity of attached drug to free drug in the blend. PDMS-atRA also had a positive effect on release, with the release period being independent of atRA starting concentration and dependant on the PDMS-atRA concentration in the blend. Excitingly, a release period of atRA from a SiO blend with PDMS-atRA over 7 weeks was observed and it was found there would be a possibility to tailor initial starting concentrations of atRA so the burst release was below the toxic range but the sustained release was above the therapeutic level for an antiproliferative effect to be observed. Unfortunately, the presence of PDMS-Ibu in a SiO blend did not have any significant effect on Ibu solubility nor did it affect the release rates of Ibu from SiO.

3.6 REFERENCES

1. H. Yano, F. Hirayama, H. Arima and K. Uekama, *Journal of Pharmaceutical Sciences*, 2001, **90**, 493-503.

2. S. P. Rannard, S. Rogers and R. Hunter, *Chemical Communications*, 2007, **4**, 362-364.

3. G. W. Anderson and R. Paul, *Journal of the American Chemical Society*, 1958, **80**, 4423-4423.

4. S. P. Rannard and N. J. Davis, *Organic Letters*, 1999, **1**, 933-936.

5. B. Neises and W. Steglich, *Angewandte Chemie International Edition*, 1978, **17**, 522-524.

6. E. Boden and G. E. Keck, *Journal of Organic Chemistry*, 1985, **50**, 2395-2395.

7. J. J. Araiz, M. F. Refojo, M. H. Arroyo, F. L. Leong, D. M. Albert and F. I. Tolentino, *Investigative Ophthalmology & Visual Science*, 1993, **34**, 522-530.

8. P. L. Carl, P. K. Chakravarty and J. A. Katzenellenbogen, *Journal of Medicinal Chemistry*, 1981, **24**, 479-480.

9. E. Rutherford, J. Chadwick and C. D. Ellis, in *Radiations from Radioactive Substances*, Cambridge University Press, New York, 2010, pp. 1-38.

10. L. Gerward, *Physics in Perspective*, 1999, **1**, 367-383.

11. J. R. Dean, A. M. Jones, D. Holmes, R. Reed, J. Weyers and A. Jones, in *Practical Skills in Chemistry*, Pearson Education, Essex, England, 2002, pp. 235-240.

12. M. L. E. Oliphant, P. Harteck and L. Rutherford, *Proceedings of the Royal Society of London A*, 1934, **144**, 692-703.

CHAPTER 4

Branched Amphiphilic Polymer Architectures as Potential Additives for SiO Tamponades

4.1 INTRODUCTION

The aim of this investigation was the evaluation of the synthesis of branched amphiphilic copolymers as additives for SiO tamponades and the potential for drug (atRA or Ibu) to be covalently bound to the hydrophilic component of the copolymer (Figure 4.1).
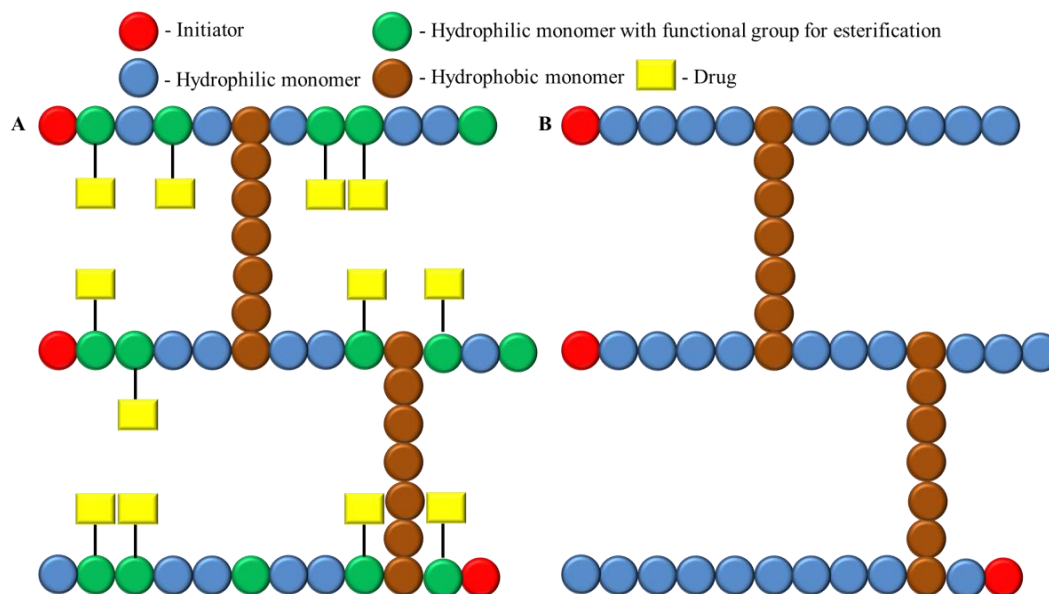
Figure 4.1 A: Branched amphiphilic copolymer with drug attached to a hydrophilic component. B: Branched amphiphilic copolymer.

The main criterion for the DDS envisaged within this Chapter is that it is soluble in SiO as any future therapy will employ a SiO tamponade acting as a drug reservoir. By incorporating both hydrophilic and hydrophobic monomers into a statistical copolymer, it was hypothesised that previous low solubilities of hydrophilic polymers in SiO (see Chapter 3) would be modified. Different degrees of polymerisation (chain length) of both the hydrophilic and hydrophobic components were studied and evaluated to establish their effects on solubility within SiO.

4.1.1 Controlled Radical Polymerisation

The development of controlled radical polymerisation (CRP) has provided materials chemists with a highly flexible approach to construct polymers *via* methods that allow the number of monomer units and the polymer architecture to be predetermined prior to synthesis. Such techniques have led to a diverse range of

multifunctional polymers with well-defined M_n and low dispersity (Đ) across the molecular weight distribution. The three leading CRP methods that have been adopted globally are atom transfer radical polymerisation (ATRP),[1] nitroxide mediated polymerisation (NMP)[2] and reversible addition-fragmentation chain transfer (RAFT).[3]

All three CRP methods present a very similar mechanistic principle (see Scheme 4.1) where an active species (P●), capable of monomer addition, is in dynamic equilibrium with its dormant state (P-X) which is inert to polymerisation. Each method ensures that the concentration of the active species remains low throughout polymerisation thus minimising undesirable reactions such as chain transfer and chain termination.[4] Only when this is achieved does the polymerisation react in a controlled manner; slow monomer addition is ensured allowing the polymer chains to grow in a more uniform manner, therefore, minimising dispersity within the molecular weight distribution.

$$X{-}P \underset{k_{deact}}{\overset{k_{act}}{\rightleftharpoons}} X + P\bullet \quad \circlearrowright$$

Monomer
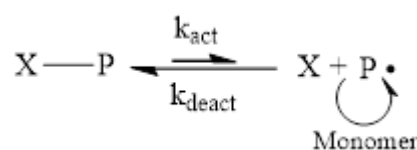
Scheme 4.1 A general representation of the reversible deactivation process responsible for maintaining a low radical concentration throughout controlled radical polymerisation processes where (X-P) is the dormant species and (P●) is the active species.

NMP, although a useful technique for some monomers, is limited to the functionality that it can tolerate,[5] whereas ATRP and RAFT provide excellent techniques capable of polymerising a wide range of monomer functionalities within a range of solvent environments.[6, 7] It is for this reason that they have been selected as the CRP methods to be used throughout this project.

4.1.2 Atom Transfer Radical Polymerisation

Following the discovery of ATRP at the end of the 20th century it has become a widely used CRP method around the world.[6] As for all CRP methods, a controlled polymerisation is facilitated by ensuring a low concentration of the active species by establishing a dynamic equilibrium with a dormant state. The term ATRP comes from the atom transfer step which is the key elementary reaction responsible for the

controlled nature of the polymerisation. In ATRP the active species (R•) is generated by a reversible redox process catalysed by a transition metal complex (M_t^n-Y/Ligand with Y being another ligand or counter ion) which undergoes a one electron oxidation process by abstraction of a (pseudo)halogen atom from a dormant species (R-X).[6] Initiators are typically alkyl halides, although the use of a number of (pseudo)halogen compounds has been reported.[8-10] The reversible redox process occurs with an activation rate constant (k_{act}) and deactivation constant (k_{deact}). A general mechanism for the ATRP process can be seen in Scheme 4.2.
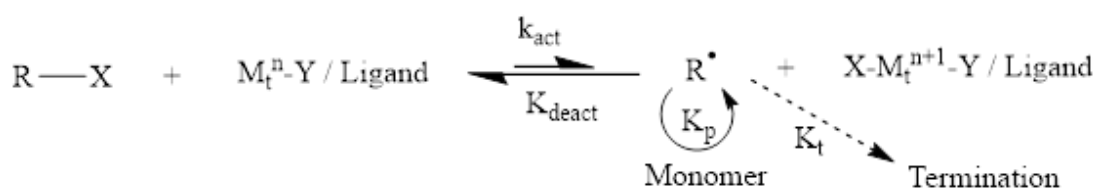
Scheme 4.2 The general mechanism of ATRP, as described by Matyjaszewski and Xia. Figure recreated from ref: [6]. An alkyl halide (RX) is under dynamic equilibrium with its active species (R•), which can undergo propagation with monomer at a rate of k_p to increase the length of the polymer chain, or termination processes at a rate k_t.

The active species (R•) undergoes monomer addition in a similar way to conventional free radical polymerisation, with the propagation rate constant (k_p). Undesirable reactions such as chain termination (k_t) also occur in ATRP, however, this is controlled due to the low concentration of the active species throughout the polymerisation. In the initial non-stationary stage of polymerisation a small number (<5 %) of growing chains will undergo termination while generation of a sufficient amount of the oxidised metal complex (X-M_t^{n+1}) is formed.[11, 12] This ensures a low active radical species throughout the polymerisation, therefore, minimising termination reactions. Ideally an ATRP reaction will not only minimise the number of terminated polymer chains but ensure that surviving chains grow in a controlled and uniform manner.

4.1.2.1 Reaction and Kinetics for ATRP

ATRP allows a number average polymer chain length to be targeted *via* the concentration ratio of monomer:initiator in the initial stages of the polymerisation. This allows well defined polymers of M_n = 1,000 – 150,000 gmol^{-1} to be synthesised with narrow dispersity (1.0 <Đ< 1.5).[13, 14] However, as higher M_n polymers are

targeted, chain termination reactions become more prevalent, therefore, increasing polymer dispersity.[15] ATRP also allows for the production of end-functionalised polymers by controlling initiator structure, which creates one chain end of each polymer formed.[16]

The rate of polymerisation is dependent on the concentration of the active species throughout the polymerisation. This is governed by the magnitude of the equilibrium constant ($K_{eq} = k_{act} / k_{deact}$) of the reversible redox process by which the active species is generated.[17] If K_{eq} is very small then the active species concentration will be low, therefore, giving a slow polymerisation rate.[18] In contrast, if K_{eq} is high, the active species concentration will also be higher therefore giving a faster rate of polymerisation. However, an increased active radical concentration will also increase the probability of undesirable reactions such as chain termination which will negatively impact on the dispersity of the polymer chains.

The propagation rate can be derived using the rate law outlined in Equation 4.1 which makes the following two assumptions: firstly, the contribution of termination is negligible once steady state is achieved due to the persistent radical effect[12] and, secondly, a fast equilibrium approximation is generated without which it would be impossible to obtain polymers of low dispersities.[19]

$$R_p = k_p[M][R\bullet] = k_p \, K_{eq} \, [M][I]_0 * [Cu^I]/[X - Cu^{II}]$$

Equation 4.1 Rate law of ATRP. The rate of propagation (R_p) is dependent upon the propagation rate constant (k_p), monomer concentration ([M]) and the concentration of the active species ([R$\bullet$]). Further derivation reveals that (R_p) is dependent upon the equilibrium constant of the reversible redox process (K_{eq}), initial initiator concentration ([I]$_0$) and the concentrations of both copper species ([Cu^I]/[X-Cu^{II}]).

A plot of monomer conversion against time on a semi-logarithmic scale reveals a linear plot which indicates that the polymerisation obeys first order kinetics with respect to monomer.[20-22] This also shows that the concentration of the active species remains constant throughout the polymerisation. An example of a kinetic profile from an ATRP can be seen in Figure 4.2. Typically a small number of polymer chains will terminate during the early stages of polymerisation, however, this can be

greatly reduced by the addition of a small amount of the Cu(II) species which acts as a radical deactivator to minimise termination during the early stages.[23]
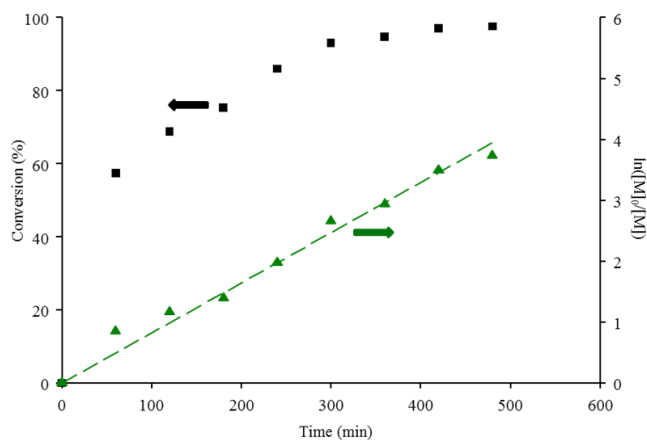
Figure 4.2 A kinetic plot from a typical ATRP of p(OEGMA$_{30}$) in IPA:H$_2$O (92.5:7.5) at 55.5 % w/v (monomer:solvent) with CuCl:bipyridyl (bpy) as the catalytic system and ethyl α-bromoisobutyrate (EBriB) as the initiator. When plotted on a semi-logarithmic scale a linear increase in conversion over time is observed. Conversion (■) and ln([M]$_0$/[M]) (▲).

Typically throughout an ATRP reaction a linear increase in the number average molecular weight (M$_n$) is observed when plotted against monomer conversion, as monomers add to growing polymer chains during propagation (see Figure 4.3).[23] During the early stages of ATRP there will be differences in chain lengths of growing polymer chains due to multiple monomer additions occurring each time the active species is formed.[24]   However, as the reaction progresses, chains will become more uniform due to continuous exchange reactions, thus a decrease in dispersity is normally observed with conversion.
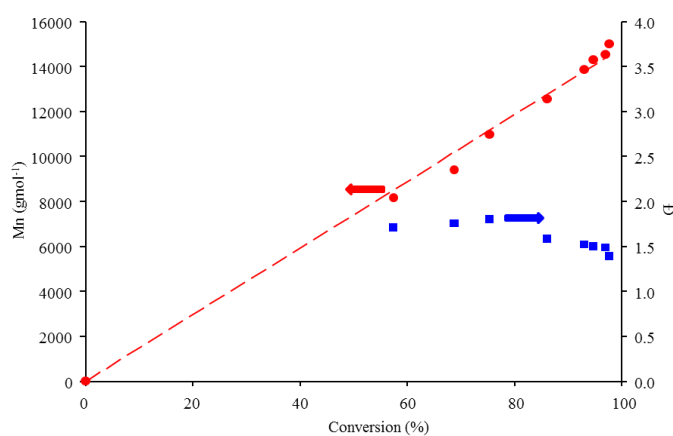
Figure 4.3 The evolution of M$_n$ (●) and Đ (■) with monomer conversion of p(OEGMA$_{30}$) in IPA:H$_2$O (92.5:7.5) at 55.5 % w/v (monomer:solvent) with CuCl:bpy as the catalytic system and EBriB as the initiator.

4.1.2.2 Branched Polymers *via* ATRP

One method of producing branched polymers by ATRP involves the incorporation of a divinyl monomer during the polymerisation of traditional vinyl monomers.[25] The enhanced control offered by ATRP means that, ideally, all propagating chains grow at the same rate. Such branched polymerisations, therefore, proceed by an alternate mechanism to the formation of branched polymers using divinyl monomers *via* conventional free radical polymerisation mechanism, which utilise thiol chain transfer agents to provide a controlled and non-crosslinking reaction by what is known as the 'Strathclyde route'.[24, 26-28] The mechanism of branched polymer synthesis using low concentrations of divinyl monomers in an ATRP polymerisation was investigated by Bannister *et al.*[29] Three stages of polymerisation were identified from analysis of both monomer conversion and evolution of molecular weight during the copolymerisation of HPMA and EGDMA (Scheme 4.3).
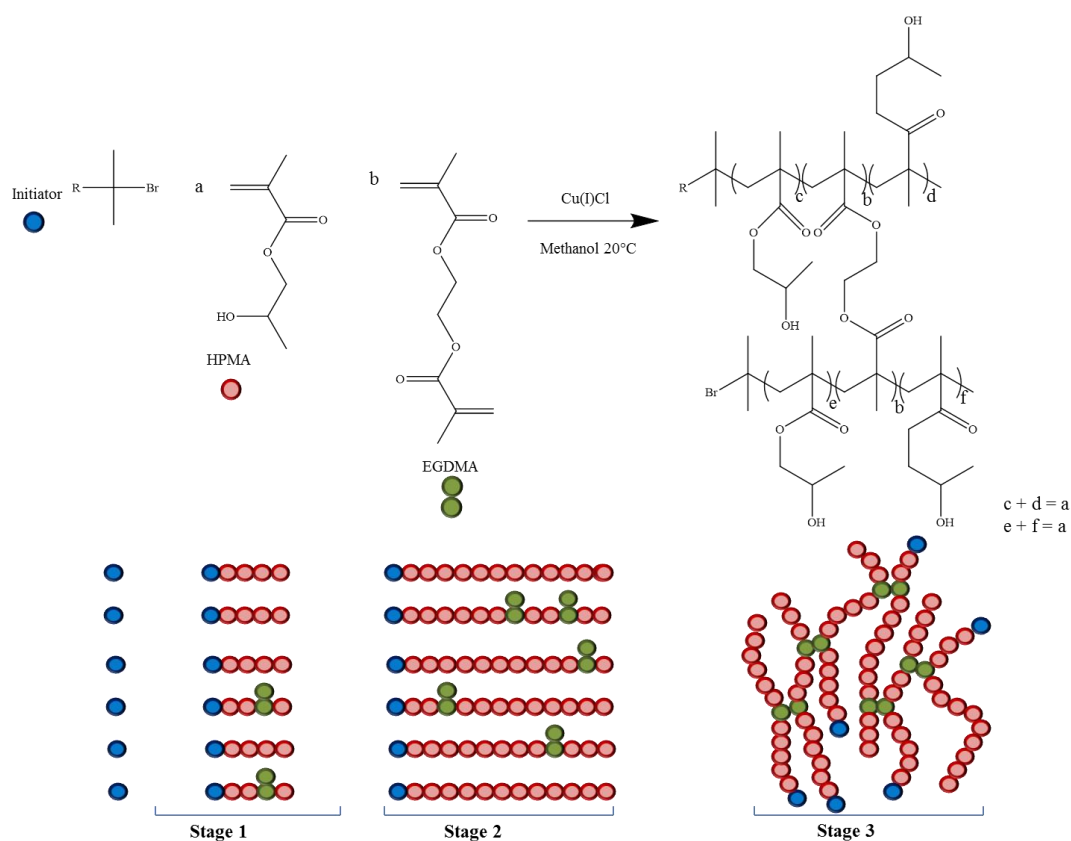
Scheme 4.3 The stages of polymerisation during the production of branched polymers by ATRP as identified by Bannister *et al.*[29] Stage 1 involves the initiation and propagation stages which are apparent in ATRP of traditional vinyl monomers. Statistical incorporation of the divinyl monomer occurs in stage 2 and stage 3 involves intermolecular branching of polymer chains to give a soluble branched polymer.

The first stage of the polymerisation includes the statistical copolymerisation of the mono and divinyl monomers at a ratio to give primary chains containing less than one potential branch point (i.e. pendant vinyl group) per chain. If there is more than one brancher per chain gelation can occur. In this stage the monomer concentration is relatively high compared to the pendant vinyl groups therefore branching is negligible. During the early stages of polymerisation, the evolution of M_n is identical to that of conventional CRP, showing a linear increase in M_n with monomer conversion. The number of branch points per chain increases in the second stage of the polymerisation, therefore, a deviation from CRP behaviour is observed. This is due to the formation of covalent bonds between growing chains as the pendant vinyl group is consumed *via* reaction with propagating chain ends. The third stage is dominated by the intermolecular coupling of polymer chains *via* reaction of the pendant vinyl groups. This occurs at high monomer conversion when there is an increased probability of reaction of the pendant vinyl groups due to a dramatic decrease in monomer concentration. This stage can be identified by a characteristic large increase in M_n and M_w due to chain growth being dominated by polymer chains coupling through pendant vinyl groups.

In order to produce soluble branched polymers it is important that the number of potential branch points is limited to less than one divinyl functionality per primary chain.[30, 31] This is known as the gel-point criterion; above this primary chains become highly cross-linked leading to macrogelation. The degree of branching is also highly dependent upon the final monomer conversion which can be accounted for by the step-growth polymerisation behaviour during the final stage of the polymerisation mechanism.[32]

4.1.3 Reversible Addition/Fragmentation Chain Transfer Polymerisation

Reversible addition/fragmentation chain transfer is a form of CRP which relies on the use of a chain transfer agent (CTA) to control the process of monomer addition. RAFT CTAs utilise sulphur chemistry to interact with propagating radicals. Due to recent advances in RAFT agent synthesis, a number of synthetic approaches are available to create CTAs.[33, 34] The general structure of a CTA is based around a thiocarbonylthio group capped at each side with what is commonly referred to as the

R and Z groups. Following polymerisation the α-terminus of the polymer chain is capped with the R group, while the Z group is capping the ω-end of the polymer chain. A generic CTA structure, along with that of a number of commonly used CTAs can be seen in Figure 4.4.
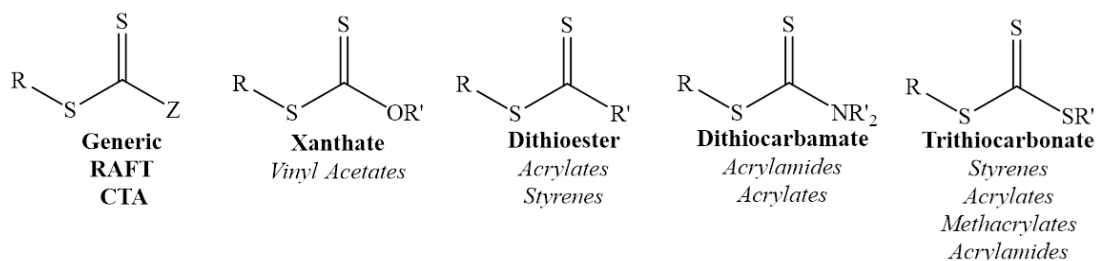
Figure 4.4 Structures of generic RAFT agents along with their compatible monomers.[35-40]

The main functionalities of RAFT agents are dithioesters, trithiocarbonates, dithiocarbamates and xanthates. The chemical nature of the RAFT agent dictates the monomer functionality to which it is best suited to polymerise, for example, highly activated RAFT agents such as xanthates are used to polymerise less activated monomers such as vinyl acetate. Alternatively, more activated monomers such as methacrylates can be polymerised with good control by less activated RAFT agents such as trithiocarbonates and dithioesters.

The mechanism of RAFT is yet to be fully understood, with a number of phenomena yet to be explained;[7, 41, 42] however, the most widely accepted proposed RAFT mechanism has been outlined in Scheme 4.4. As with all polymerisations, the reaction starts with an initiation step, which may happen through auto-initiation (for example styrene above 110 °C), or more conventionally through the thermal decomposition of an initiating species such as 2,2'-azobis(2-methylpropionitrile) (AIBN). Whichever method of initiation is used, the initiating species forms a radical (I$^\bullet$) which combines with multiple monomer units to form short polymeric chains (P$_n{}^\bullet$).

Once the concentration of (P$_n{}^\bullet$) has increased significantly, a pre-equilibrium is established with the RAFT agent (**1**) to form an intermediate species (**2**). Once formed, there are two ways that (**2**) can decompose: through a direct reversal to reform (**1**), or by fragmentation of the S-R bond to expel the R group as a radical species (R$^\bullet$), giving another intermediate species, (**3**). (R$^\bullet$) can then combine with

monomer units to form a second short polymeric chain ($P_m{}^\bullet$). Once this has occurred it quickly leads to the formation of the main equilibrium.

The main equilibrium is established following the addition of ($P_m{}^\bullet$) onto (**3**) to give the radical intermediate (**4**), which contains both of the propagating moieties attached to either of the sulphur atoms. It can be argued that (**4**) represents the dormant state in the reaction with both growing polymer chains locked into the RAFT agent. This species can undergo one of two possible fragmentation reactions to expel either of the growing polymer chains thus reforming the thiocarbonyl group (**3**) or (**5**) and the active species, allowing further propagation. As (**3**) and (**5**) are, in essence, indistinguishable, the decomposition of (**4**) has no preference as to which growing chain is released.

The fact that the growing polymer chains spend most of the time locked into the dormant state explains the control offered by RAFT. The ability to maintain a low concentration of active radical species in solution at any one time prevents undesirable chain termination occurring by polymer-polymer coupling processes.

Initiation

nM

Initiatior $\longrightarrow$ 2 x I$^{\bullet}$ $\xrightarrow{\quad k_{pi} \quad}$ P$_n^{\bullet}$

Propagation

P$_n^{\bullet}$ $\xrightarrow[k_p]{M}$ P$_{n+1}^{\bullet}$

Pre-equilibrium

P$_n^{\bullet}$ + R ... (**1**) $\underset{k_{-add1}}{\overset{k_{add1}}{\rightleftharpoons}}$ (**2**) $\underset{k_{\beta-1}}{\overset{k_{\beta1}}{\rightleftharpoons}}$ (**3**) + R$^{\bullet}$

Re-Initiation

R$^{\bullet}$ $\xrightarrow[k_{pr}]{mM}$ P$_m^{\bullet}$

Main Equilibrium

P$_m^{\bullet}$ + P$_n$ ... (**3**) $\underset{k_{-add}}{\overset{k_{add}}{\rightleftharpoons}}$ (**4**) $\underset{k_{-\beta}}{\overset{k_{\beta}}{\rightleftharpoons}}$ P$_n^{\bullet}$ + P$_m$ ... (**5**)

Termination

P$_m^{\bullet}$ + P$_n^{\bullet}$ $\xrightarrow{k_{tc}}$ P$_{n+m}$

$\xrightarrow{k_{td}}$ P$_n^{=}$ + P$_m^{H}$
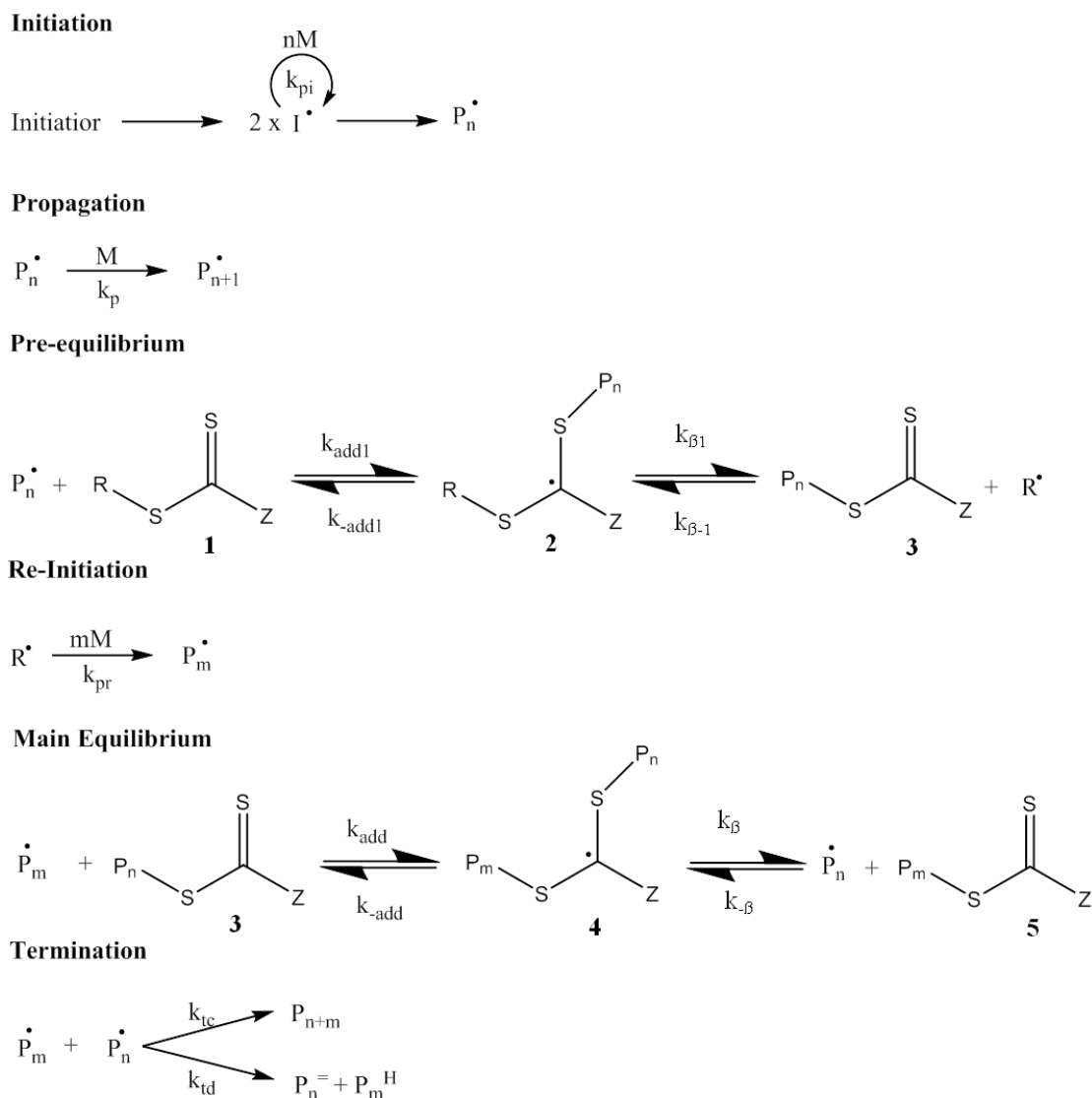
Scheme 4.4 The widely accepted mechanism of RAFT polymerisation.[7] Initiator decomposition gives a radical species (I$^{\bullet}$) which quickly propagates with monomer (M) at the rate constant k_{pi} to give short oligomer chains (P$_n^{\bullet}$). Addition of this species to (1) occurs under equilibrium with the addition occurring with a rate constant of (k_{add1}) to give (2) and the reverse process occurring with a rate constant of (k_{-add1}). Expulsion of the R group from (2) is under dynamic equilibrium and occurs with a rate constant of $k_{\beta1}$ and a reverse process occurring with a rate constant of $k_{\beta-1}$. This gives (3) and another active radical species, which undergoes propagation at rate of k_{pr} to give P$_m^{\bullet}$. Addition of P$_m^{\bullet}$ into (3) occurs with a rate constant of k_{add} to give (4). (4) can decompose to reform (3) at a rate constant of k_{-add} by expulsion of P$_m^{\bullet}$ or generate (5) by expulsion of P$_n^{\bullet}$ at a rate constant of k_{β}, which has a reverse process occurring at $k_{-\beta}$. Active radical species can undergo termination processes either by polymer coupling at k_{tc} or by disproportionation reaction with an hydrogen atom at a rate of k_{td}.

4.1.3.1 Branched Polymers by RAFT

Branched copolymers have also been produced by RAFT polymerisation using a method known as the 'grafting from approach'; which uses the polymer backbone as a scaffold from which polymer chains are grown. This process has been used to produce comb like structures *via* copolymerisation with a monomer that can easily be modified into a RAFT agent. This approach then allows for further polymerisation from the pendant RAFT functionality.[43] The 'grafting from approach' has been used for the preparation of branched polymers of polystyrene, by copolymerisation of styrene with a styrenic monomer containing a dithiobenzoate modification. Polymerisation resulted in the production of branched polystyrene compared with the lower M_n polymers produced in the absence of the modified monomer.[44]

Alternatively, similar structures have been produced by a different method in which polystyrene reinitiated in the presence of maleic anhydride resulted in the incorporation of one maleic anhydride unit per polymer chain (the chemistry limits the reaction to the addition of only one unit). Chain extension of styrene with the same targeted DP_n resulted in polystyrene-*co*-maleic anhydride with the maleic anhydride located in the middle of the polymer chain. Following multiple repetitions polystyrene-*co*-maleic anhydride was produced with maleic anhydride units spaced evenly along the polymer backbone. These functionalities were then targeted using poly(ethylene oxide) containing a terminal hydroxyl group, which yielded the graft copolymer.[45]

Branched polymers have also been produced *via* the copolymerisation of vinyl and divinyl functionalised monomers in the presence of a RAFT agent.[46] This method to synthesise branched architectures using RAFT involves the production of a macro RAFT agent from which chain extension can be carried out (see Figure 4.5). The production of branched polymers using this method was reported by Liu *et al.* who copolymerised MMA and EGDMA in the presence of 2-(2-cyanopropyl)dithiobenzoate.[47] The controlled nature of the polymerisation afforded preparation of controlled polymer architecture, furthermore end-group fidelity was proven through successful chain extension, yielding star like structures. Hyperbranched poly(MMA) polymers still containing their RAFT agent end groups

underwent chain extension with styrene to give star copolymers containing a branched PMMA core and styrene arms.

Figure 4.5 Branched polymer architecture obtained by RAFT showing dual functionality of the polymer chains.

4.2 COPOLYMERS OF OEGMA AND HEMA BRANCHED WITH PDMSDMA

The synthesis of a range of branched polymers was considered as providing potential benefits for the formation of soluble polymeric additives for SiO when used as a tamponade agent. Initially, ATRP was used to synthesise a linear statistical copolymer of the commercially available hydrophilic monomer oligo(ethylene glycol) methyl ether methacrylate (OEGMA, DP_n = 3-4 ethylene glycol units / M_n = 300 gmol^{-1}), with 2-hydroxylethylmethacrylate (HEMA) which is also hydrophilic and bears a hydroxyl pendant group (to be used to covalently bond atRA or Ibu and form pro-drug prototypes). The polymerisations of both OEGMA and HEMA under aqueous solvent conditions have been reported in the literature and it was the presence of water has been shown to dramatically accelerate the ATRP of OEGMA and HEMA.[48-50] Particularly, the use of mixtures of isopropanol/water (IPA:H$_2$O, 92.5:7.5 v/v) or methanol/water, (MeOH:H$_2$O, 50:50 v/v) as the polymerisation solvent for OEGMA and HEMA respectively, at ambient temperature that have previously been reported to lead to controlled polymerisations.[51, 52] The statistical copolymerisation of OEGMA and HEMA was targeted with an overall degree of polymerisation DP_n = 30 monomer units (DP_{30}) with molar ratios of the two monomers of 80/20 and 50/50 (Scheme 4.5). Similar conditions to those reported in

the literature were used including a temperature of 30 °C and an IPA:H$_2$O solvent mixture of 92.5:7.5 v/v at a concentration of 55.5 % w/v (monomer:solvent). A CuCl:bpy catalytic system was employed and the commercial EBriB was utilised as initiator. Removal of the copper was performed *via* a neutral alumina column and the polymers recovered by precipitation. The characteristics of the copolymers obtained are presented in Table 4.1.

n = 24 (80 %) or 15 (50 %)
q = 6 (20 %) or 15 (50 %)
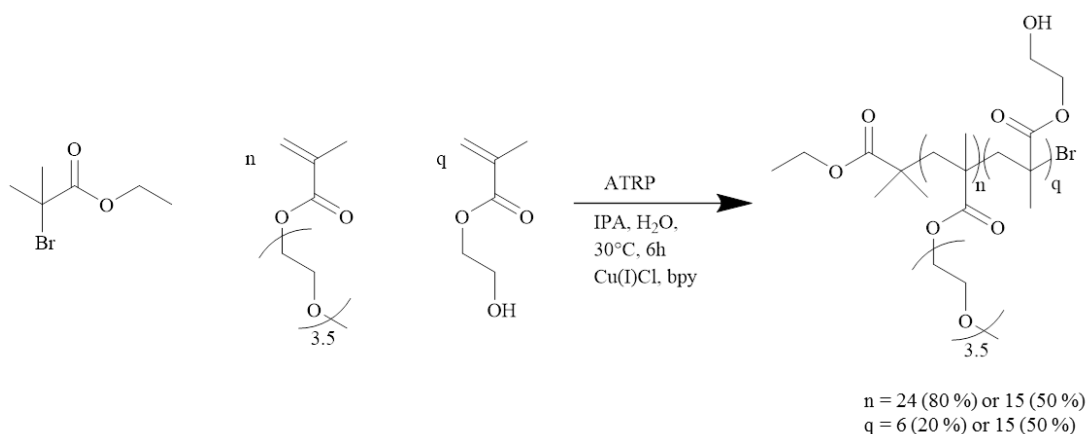
Scheme 4.5 Synthesis of statistical p(OEGMA-*co*-HEMA) *via* ATRP.

The incorporation of a low concentration of dimethacrylate monomer into this polymerisation can lead to soluble polymers with high M$_n$ and high M$_w$ with a branched architecture.[53] In an attempt to establish compatibility with the SiO tamponade, a hydrophobic dimethacryloxypropyl terminated PDMS (PDMSDMA) was utilised as the dimethacrylate branching agent (see Figure 4.6) and various chain-lengths of this macro-brancher (M$_n$) were used. In this initial scoping experiment, the shortest chain length (M$_n$ 390 gmol^{-1}, m=1) was used.

Table 4.1 Characteristics of the linear p(OEGMA-*co*-HEMA) and the branched equivalents with PDMSDMA n=1.

Target Polymer Composition	Theoretical Mn (gmol^{-1})	GPC[a] Mn (gmol^{-1})	Mw (gmol^{-1})	Đ	^{1}H NMR[b] DP$_n$ OEGMA	HEMA
p(OEGMA$_{24}$-*co*-HEMA$_6$)	8,200	10,350	13,100	1.27	24	6
p(OEGMA$_{15}$-*co*-HEMA$_{15}$)	6,650	14,350	20,500	1.43	15	15
p(OEGMA$_{24}$-*co*-HEMA$_6$-*co*-PDMSDMA$_{0.95}$)	-	27,000	102,900	3.81	24	6
p(OEGMA$_{15}$-*co*-HEMA$_{15}$-*co*-PDMSDMA$_{0.95}$)	-	29,500	296,500	10.05	15	15

[a] Determined by GPC (DMF eluent at 60°C) [b] Determined by ^{1}H NMR in CDCl$_3$

m = 1, 12 ,55 and 282
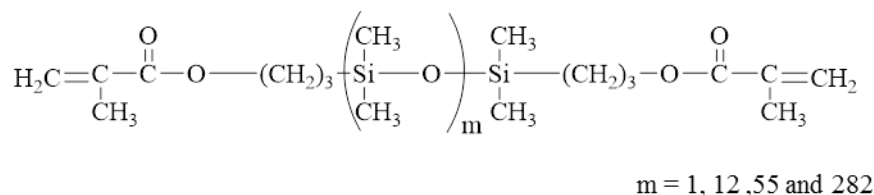
Figure 4.6 Chemical structure of dimethacrylate monomer PDMSDMA.

Gelation can occur during these reactions if the molar ratio of initiator to brancher is >1:1 due to cross-linking of polymer chains. Therefore, all reactions were carried out at a ratio of 1:0.95 initiator:brancher to achieve the desired highly branched architectures. The concentration of the polymerisation also affects the branching; the more dilute the reaction, the more likely intramolecular looping will occur,[54] however, ultimately branching becomes diffusion controlled within the reaction.[55] Therefore, it was important to ensure all polymerisations were carried out at a constant concentration, here 55.5 % w/v (monomer:solvent).

All the copolymers (linear and branched) were characterised by gel permeation chromatography (GPC) and ^{1}H NMR, and the results are collated in Table 4.1. The DP_n for each monomer was calculated *via* ^{1}H NMR for both OEGMA and HEMA as the vinyl peaks for each monomer were distinguishable to analyse separately. M_n determined by GPC was higher than the targeted theoretical values, which is not uncommon for ATRP and possibly due to initiator efficiency being less than 100 % within the early stage of the equilibrium definition, leading to longer chains than predicted. Effects of reduced initiator efficiency are well reported within the literature.[56, 57]

When comparing the two linear copolymers, it was observed that the dispersity of p(OEGMA-*co*-HEMA) 50/50 is higher than the 80/20 copolymer; Đ = 1.43 compared to Đ=1.27 respectively. The higher dispersity could be due to HEMA initiating and propagating faster than OEGMA. RI traces of the linear polymers presented in Figure 4.7 show a monomodal distribution; however, a slight shoulder can be seen on the lower retention volume (high M_w) side of the 50 % OEGMA copolymer. This could be due to coupling of chain ends at high conversions.[58] Both this and the higher Đ displayed in the 50/50 copolymer can be investigated by determining the kinetics of the polymerisations (see section 4.6.1). The dispersity

calculated via GPC for the branched copolymers is much higher than their linear equivalents which is consistent with the attainment of branched architectures.

The difference between the linear and branched polymers is clearly visible from the RI chromatograms shown in Figure 4.7: the incorporation of the PDMSDMA results in higher M_w branched polymers which elute at lower retention volumes. However, a broad distribution is detected within the branched polymers due to the statistical incorporation within the ATRP mechanism, therefore, both highly branched and linear materials are present.
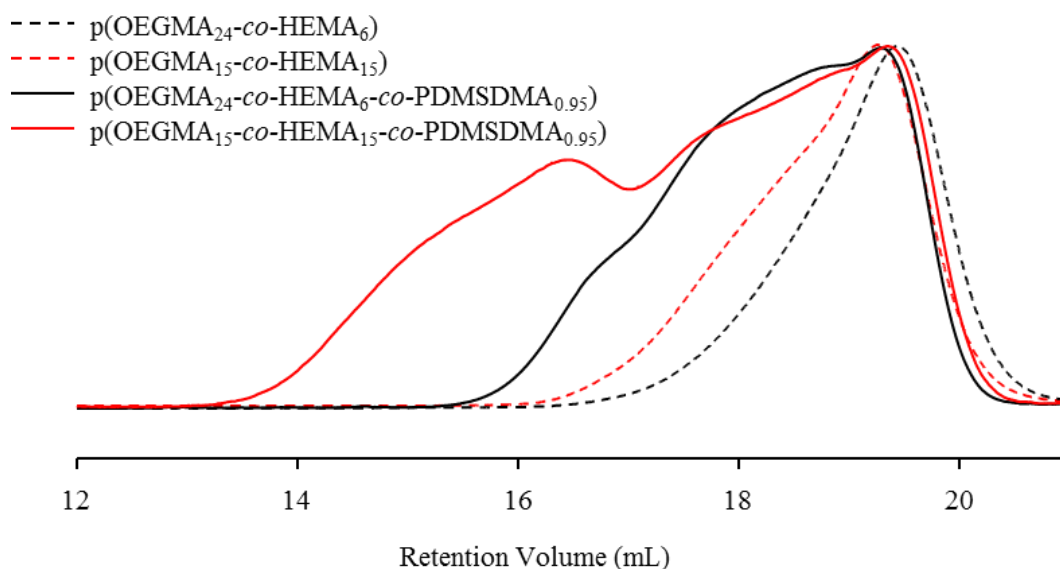
Figure 4.7 GPC RI chromatogram overlays of the branched copolymers p(OEGMA-*co*-HEMA-*co*-PDMSDMA) and their linear equivalents synthesised by ATRP.

4.2.1 Kinetic Evaluation of ATRP branching reactions

To determine if a polymerisation is controlled, time points are taken throughout the reaction and analysed to determine if the polymerisation follows first order kinetics with respect to the monomer concentration, and to observe the development of M_n compared to monomer conversion.

The kinetic plots for both linear copolymers, (Figure 4.8), show that high conversion was reached within 4-6 hours (Figure 4.8 A and C) and followed first order kinetics. The conversion of both monomers was determined by ^{1}H NMR spectroscopy with the use of an internal standard (anisole) with characteristic aromatic peaks at 7.21

and 6.84 ppm; these peaks remained constant throughout the polymerisation. The vinyl peaks at 6.05 and 5.49 ppm attributed to HEMA and 6.12 and 5.54 ppm attributed to OEGMA decrease as the monomer is consumed (see Appendix Figure A34). The ratio between the anisole aromatic peaks and monomer peaks therefore can be used to determine the conversion. The HEMA monomer reacted faster than the OEGMA monomer, this also resulted in a faster polymerisation when the higher ratio of HEMA (50 %) was used.
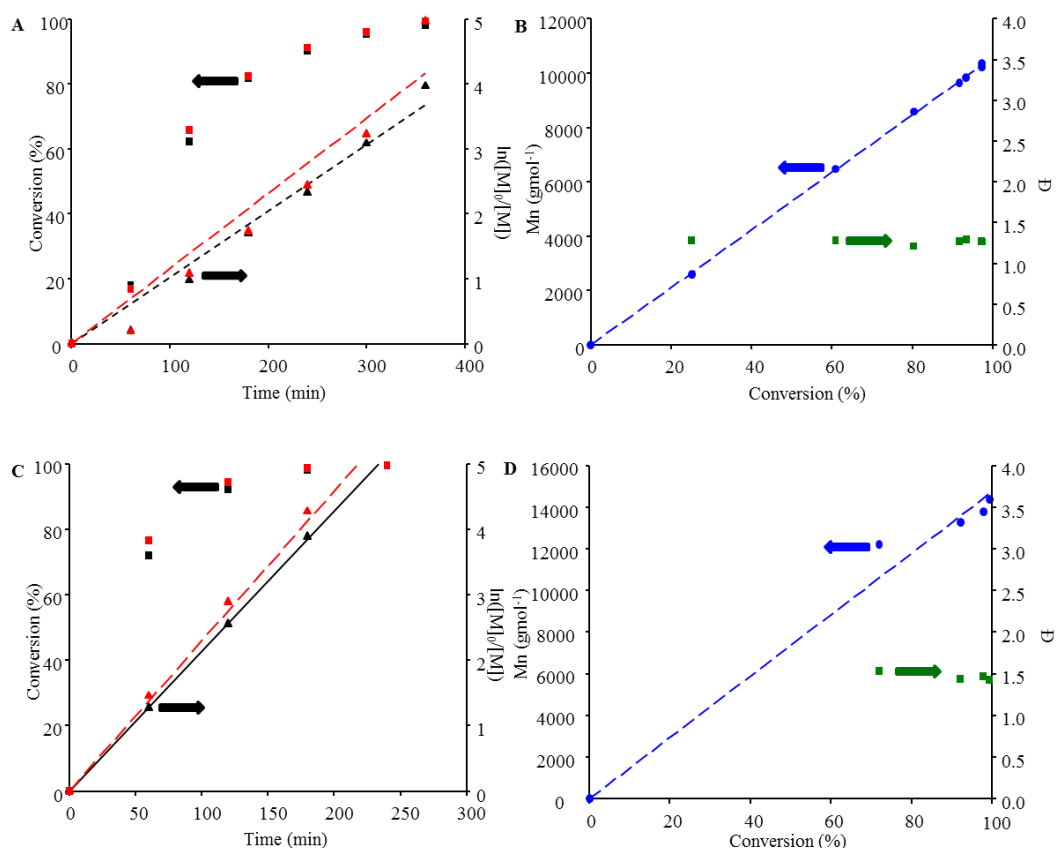
Figure 4.8 Kinetic plots for linear copolymers p(OEGMA$_{24}$-*co*-HEMA$_6$), (A and B) and p(OEGMA$_{15}$-*co*-HEMA$_{15}$), (C and D). ■/■ = conversion OEGMA/HEMA; ▲/▲ = ln([M]$_0$/[M]) OEGMA/HEMA; ● = M$_n$; ■ = Đ.

When investigating the kinetics for the branched polymers, the incorporation of the PDMSDMA led to the vinyl peaks in ^{1}H NMR spectra being indistinguishable from one another (i.e. they merged together as they are all in similar environments; see Appendix Figure A35). This resulted in the conversion being determined for the total monomer concentration rather than for each individual monomer. The kinetic plots for both branched polymerisation are shown in Figure 4.9.
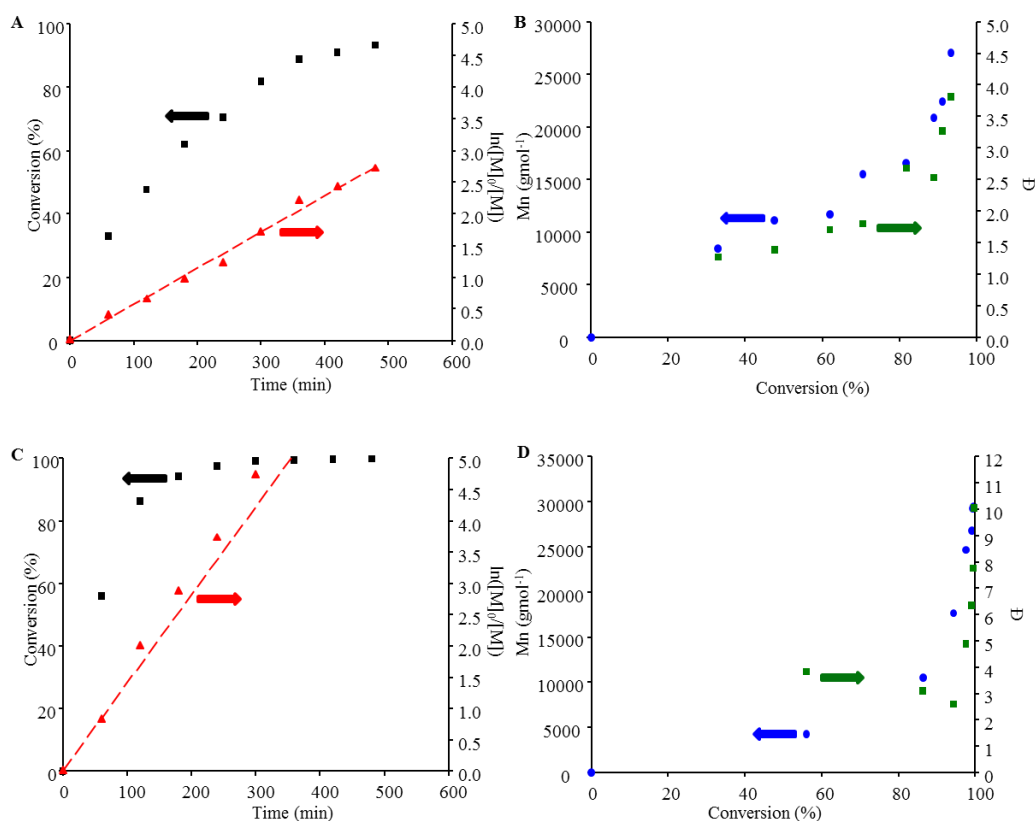
Figure 4.9 Kinetic plots for branched copolymers p(OEGMA$_{24}$-*co*-HEMA$_6$-*co*-PDMSDMA$_{0.95}$) (A and B) and p(OEGMA$_{15}$-*co*-HEMA$_{15}$-*co*-PDMSDMA$_{0.95}$) (C and D). Conversion (■), ln([M]$_0$/[M]) (▲), M$_n$ (●), Đ (■).

Again a faster polymerisation was observed when the ratio of HEMA was higher (50 %), but both polymerisations followed first order kinetics (Figure 4.9 A and C). The M$_n$ values were observed to increase relatively linearly in both polymerisations until high conversions were reached (>80 %); this is a typical characteristic of branched polymerisations of this type. Once high conversion is reached, the M$_n$ increases dramatically as large branched structures are being formed *via* intermolecular reactions joining individual linear polymers and structures containing many primary polymer chains.

4.2.2 Linear and Branched Copolymer Solubility Studies in SiO

The solubility of both OEGMA and HEMA monomers and copolymers were assessed in SiO$_{1000}$. It was determined that both monomers were practically immiscible with SiO, however, upon the incorporation of the hydrophobic PDMSDMA, both branched copolymers of p(OEGMA-*co*-HEMA), were soluble at 20 % (v/v).

4.2.3 Drug Attachment to Branched Copolymers

Once the branched amphiphilic copolymers were successfully synthesised and their solubility in SiO_{1000} confirmed, the functionalisation with drug molecules was investigated.

4.2.3.1 Functionalised Monomer

Both atRA and Ibu were successfully covalently bound to the HEMA monomer, however, polymerisation of the functionalised monomer resulted in some unexpected reactions. The Steglich esterification method (as described in Chapter 3) was utilised to react both atRA and Ibu to the HEMA monomer to form atRA-ethyl methacrylate (atRAEMA) and Ibu-ethyl methacrylate (IbuEMA) respectively, this is shown in Scheme 4.6.
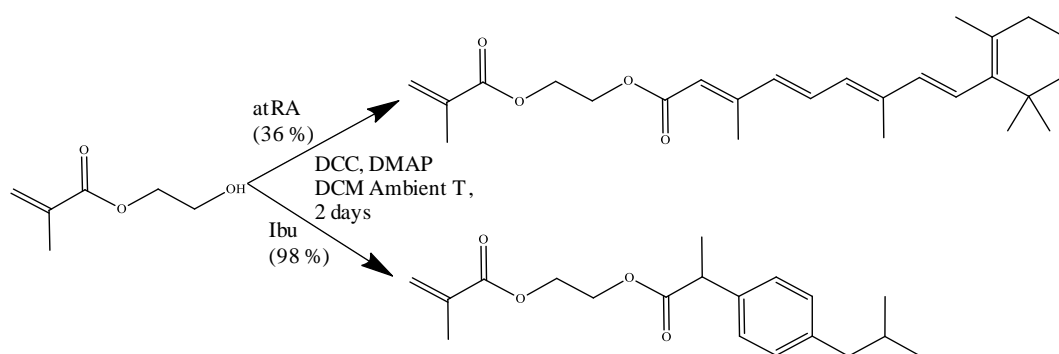
Scheme 4.6 Steglich esterification of both atRA and Ibu with HEMA monomer.

Similarly to the observations made in Chapter 3, the esterification of atRA with HEMA resulted in a lower yield than the Ibu esterification, most probably due to the conjugated nature of atRA. Both purified, modified monomers were analysed by ^{1}H NMR spectroscopy and compared to their starting materials (Figure 4.10). The modified HEMA monomer, covalently bound to the drugs atRA (Figure 4.10 A) and Ibu (Figure 4.10 B), showed agreement across all integrations with expected values, confirming the attainment of atRAEMA and IbuEMA (see Appendix Figure A36 and A37).
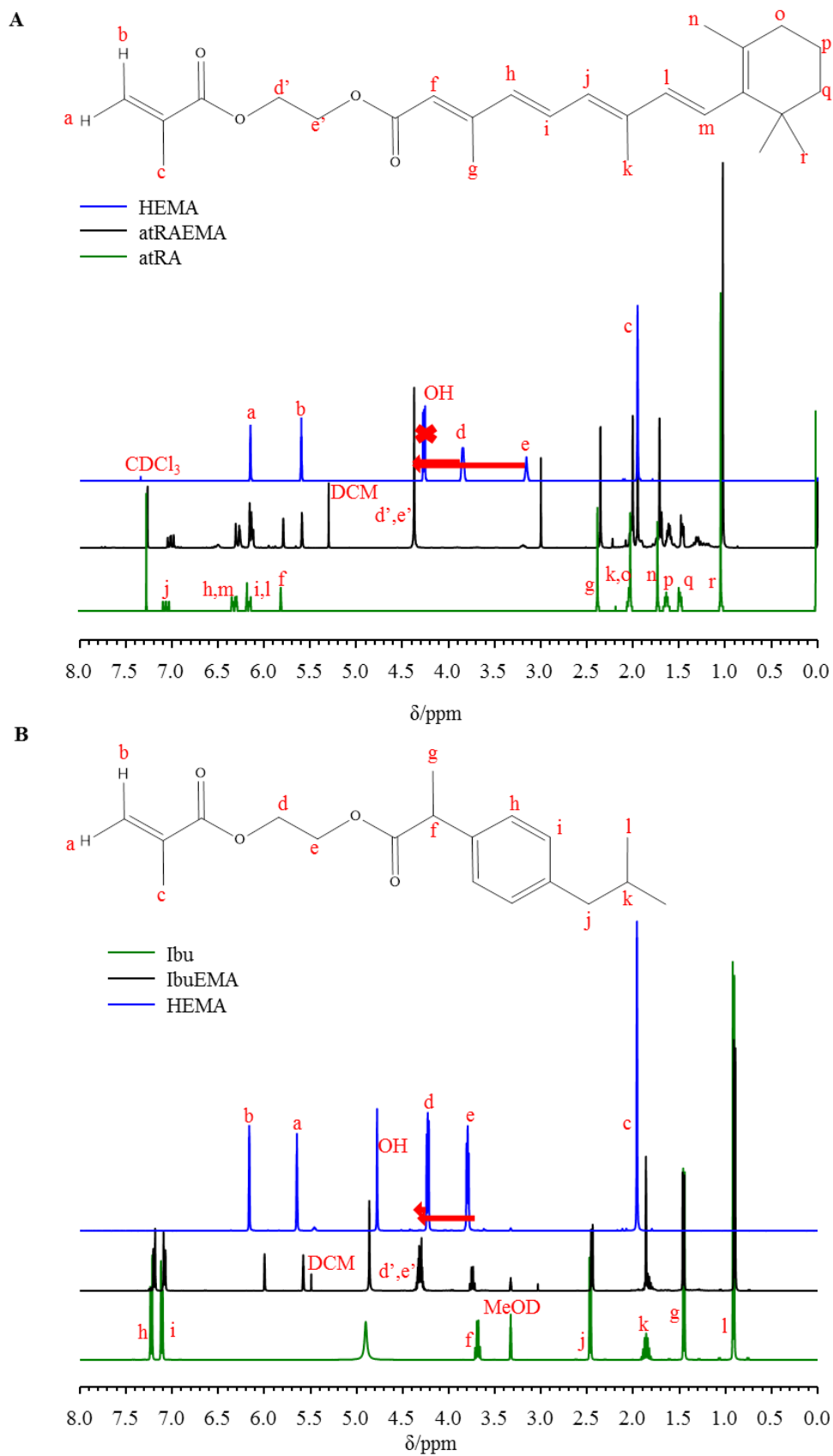
Figure 4.10 ^{1}H NMR spectra (A:CDCl₃, B: MeOD, 400 MHz) of starting HEMA and drug along with modified HEMA after purification.

4.2.3.1.1 atRAEMA Polymerisation and Copolymerisation by ATRP

The synthesis of the 50/50 and the 80/20 linear copolymers of OEGMA and HEMA was repeated under the identical conditions to those described previously, but replacing the HEMA with atRAEMA, however, after 8 hours no reaction had occurred. Following this, a linear homopolymerisation of the atRAEMA targeting a DP_{30} was carried out, again unsuccessfully. It appeared that the antioxidant nature of atRA was potentially acting as a terminator during the polymerisation, rendering this monomer-drug conjugate useless of the intended ATRP polymerisations.

To test this hypothesis, the kinetics of HEMA homopolymerisation were carried out in the presence of added atRA within the system, at 1 and 10 % (w/w), the kinetic plots are presented in Figure 4.11. The rate of conversion decreased in the presence of 1 % (w/w) atRA and decreased further when 10 % (w/w) was present (see Figure 4.11), confirming atRA was interacting with the radical concentration. Interestingly, the polymerisations still exhibited a linear semi-log plot, suggesting a slowing of the polymerisation rather than a loss of overall control.

GPC analysis also confirmed that atRA was interfering with the polymerisation as broader distributions were observed when atRA was present and the elution of a very high molecular weight species appeared when atRA 10 % (w/w) was present (see Figure 4.12). As such, the control that was potentially indicated through the initial analysis (Figure 4.11) was not seen in the final products.
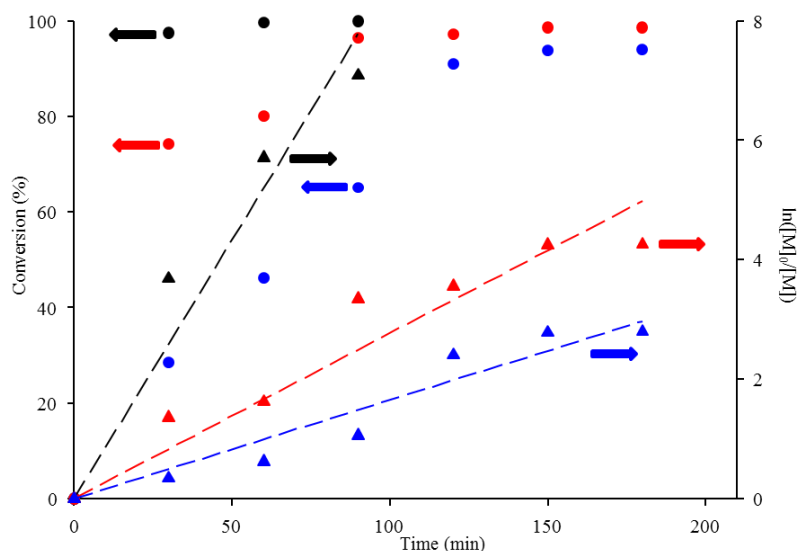
Figure 4.11 Kinetic plots for HEMA polymerisation in the presence of atRA 1 and 10 % (w/w) (red and blue respectively), and in the absence of atRA (black). Conversion (circles), ln([M]$_0$/[M]) (triangles).
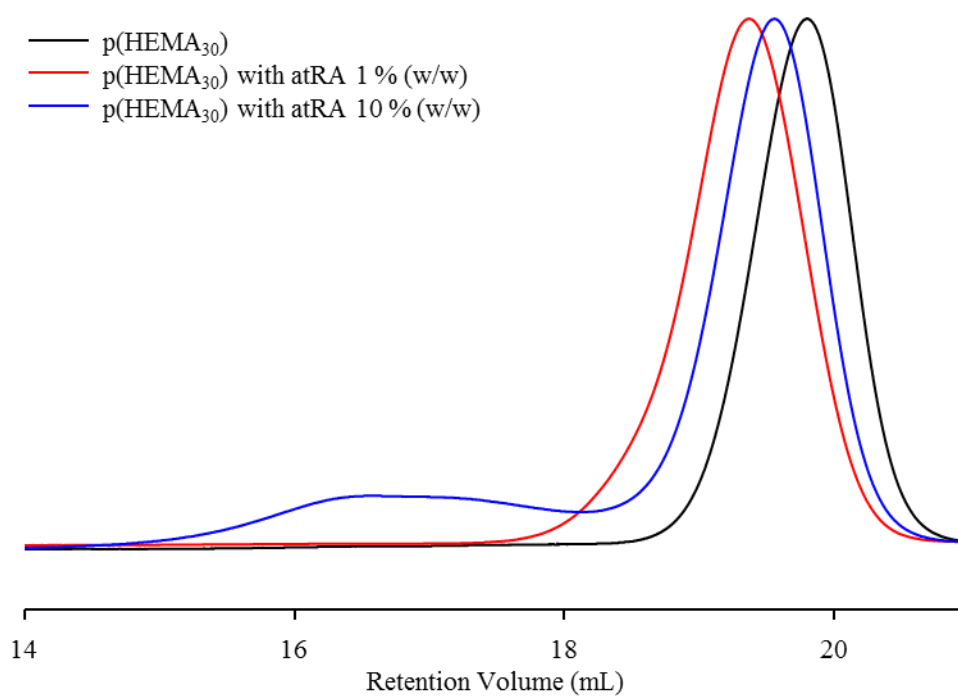
Figure 4.12 GPC RI chromatogram overlays of p(HEMA$_{30}$) synthesised in the presence and absence of atRA.

The interference of atRA with the ATRP reaction led to the conclusion that the use of a pre-functionalised monomer was not appropriate for the preparation of atRA functionalised amphiphilic branched p(OEGMA-*co*-atRAEMA-*co*-PDMSDMA).

4.2.3.1.1 Polymerisation and Copolymerisation of IbuEMA Using ATRP

Solubility issues arose with the Ibu-modified monomer whilst investigating the ATRP polymerisation in the IPA:H_2O solvent system previously used. A solvent system of MeOH:H_2O (92.5:7.5 v/v), which displays controlled ATRP reaction for pHEMA,[52] was successfully used while all other parameters were kept consistent with regards to the previous ATRP reactions. Polymerisations of HEMA targeting a chain length of DP_{30} were carried out under these conditions, in the presence of 1 and 10 % (w/w) Ibu and kinetic studies showed that, unlike atRA, Ibu did not affect the polymerisation (see Figure 4.13).
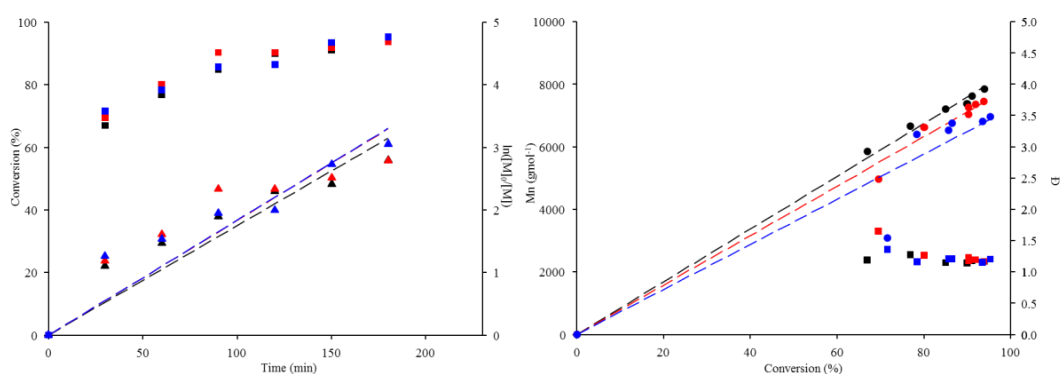
Figure 4.13 Kinetic plots for p(HEMA$_{30}$) (black) in the presence of Ibu 1 (red) and 10 % (blue) (w/w). Conversion (squares), ln([M]$_0$/[M]) (triangles) M_n (circles), Đ (squares).

The measured M_n values for all polymerisations were again higher than the targeted M_n as may be expected, however, the polymers obtained were consistent and almost identical when characterised by GPC and ^{1}H NMR spectroscopy (see Table 4.2), despite the varying concentrations of Ibu. The GPC RI chromatograms of the different polymers are overlaid in Figure 4.14.

Table 4.2 ^{1}H NMR and GPC data for all pHEMA synthesised in MEOH:H_2O (92.5:7.5) with and without the presence of Ibuprofen.

Target Polymer Composition	Ibu Content (% w/w)	Theoretical		GPC[a]			^{1}H NMR[b]	
		M_n (gmol^{-1})	M_n (gmol^{-1})	M_w (gmol^{-1})	Đ	DP_n	DP_n	
p(HEMA$_{30}$)	-	4,100	5,100	8,605	1.44	38	30	
p(HEMA$_{30}$)	1	4,100	5,750	8,205	1.43	43	30	
p(HEMA$_{30}$)	10	4,100	5,628	7,931	1.41	42	30	

^{a}Determined using GPC (DMF eluent at 60 °C) ^{b} Determined by ^{1}H NMR in MeOD.
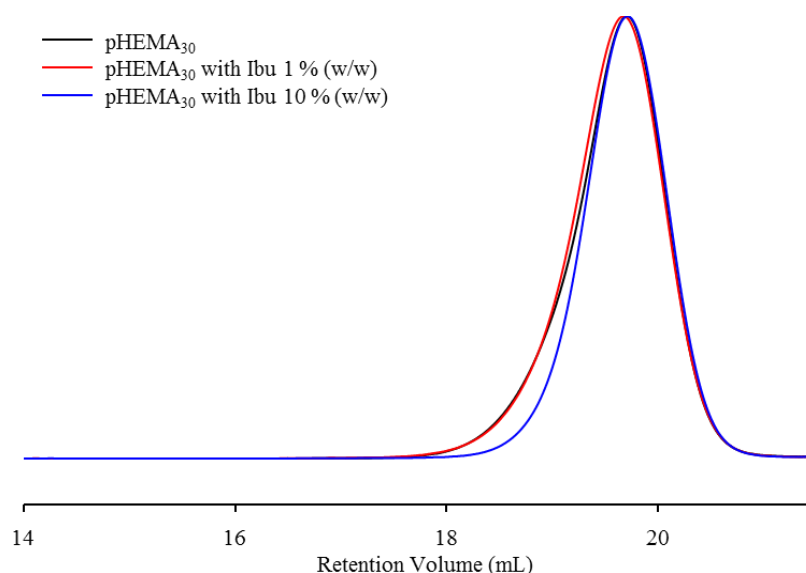
Figure 4.14 GPC RI chromatogram overlays of p(HEMA$_{30}$) synthesised in the presence or absence of Ibu.

The copolymerisation of OEGMA with IbuEMA in the presence of PDMSDMA brancher was attempted under the conditions described above, however, the brancher was not soluble in the MeOH:H$_2$O (92.5:7.5) solvent. A new solvent system in which all three components and the catalytic system was soluble needed to be found. Acetone was investigated as the solvent of choice, with the initial synthesis of p(IbuEMA$_{30}$).

The polymerisation of IbuEMA was carried out in MeOH:H$_2$O and in acetone in parallel, as a comparison and the ATRP reaction was observed to be uncontrolled in acetone. The GPC traces of the two polymers obtained are presented in Figure 4.15 and the RI chromatogram broadened considerably when acetone was employed as the reaction solvent, and high molecular weight species were apparent within the right angle light scattering (RALS) detector chromatograms (Figure 4.15 B). The difference between the two detectors is that the RI detector is dependent on the concentration of analyte, whereas the RALS detector response is dependent on the size in solution of the polymeric species under investigation (the larger the material the more light will be scattered). Therefore, although the RI response detected no material at an elution volume of 14 mL, the RALS detector response clearly indicates the presence of this impurity. The lack of control observed with acetone suggests that it is not an appropriate solvent to use for the synthesis of the targeted amphiphilic branched architectures.
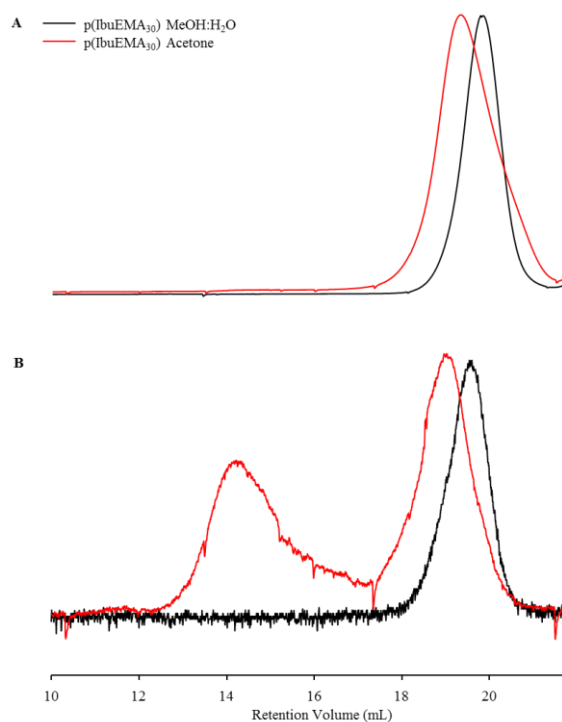
Figure 4.15 GPC chromatogram overlays of p(IbuEMA$_{30}$) polymerised in MeOH:H$_2$O (92.5:7.5) (black) and Acetone (red). A: RI chromatograms and B: RALS chromatograms.

The lack of a useful solvent system in which all monomers, brancher and catalytic system were soluble, leading to a controlled ATRP reaction, post functionalisation of the copolymers comprising HEMA was investigated.

4.2.3.2 Drug Incorporation *via* Post-Functionalisation of Polymers

As described earlier, linear p(HEMA$_{30}$) was synthesised *via* an ATRP reaction in a MeOH:H$_2$O solvent mixture to yield a polymer that was analysed by ^{1}H NMR spectroscopy (CDCl$_3$) and GPC (DMF eluent at 60 °C) to give an M$_n$ = 9,100 gmol^{-1}, Đ = 1.40. A Steglich esterification was carried out for both atRA and Ibu as before (see Chapter 3, Section 3.3.2), but on the pre-polymerised polymer using toluene at 40 °C (previously DCM at ambient temperature) to ensure solubility of p(HEMA). The reactions were left for 4 days, in the dark when using atRA, followed by dicyclohexylurea (DCU) by-product removal. The purified polymer was analysed by ^{1}H NMR spectroscopy (MeOD), as shown in Figure 4.16.

From the ^{1}H NMR spectra in Figure 4.16, it can be seen that atRA did not react with p(HEMA$_{30}$), while Ibu was successfully conjugated to the p(HEMA$_{30}$); but only with a yield of 14 % in 4 days. It is possible that this is due to steric hindrance between

p(HEMA$_{30}$) and the drug molecules. The successful p(IbuEMA) esterification is characterised by the merging of peaks at 4.16 and 3.90 ppm which represent the CH$_2$ groups within p(HEMA) (c and d in Figure 4.16 B) merging together at 4.06 ppm as they become part of the same environment, i.e. next to –O-C=O.
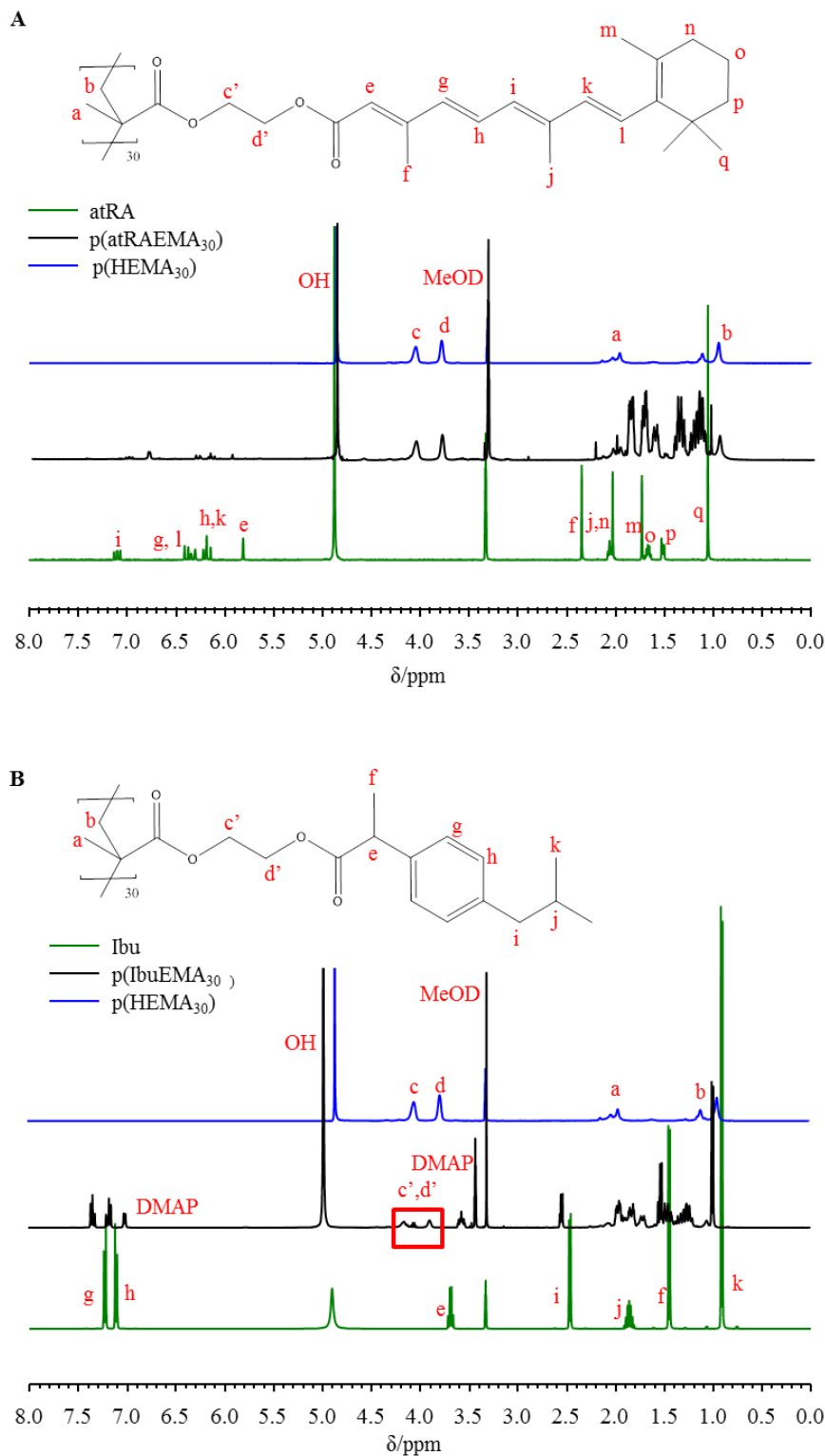
Figure 4.16 ^{1}H NMR spectra (MeOD, 400 MHz) of starting p(HEMA$_{30}$) and drug (A: atRA and B:Ibu) along with modified p(HEMA$_{30}$). A: p(atRAEMA$_{30}$) and B:p(IbuEMA$_{30}$).

Due to the unsuccessful post-modification of p(HEMA) with atRA and the low yields obtained for p(IbuEMA$_{30}$) after 4 days, the direct conjugation of drugs to p(HEMA) was abandoned.

4.3 BRANCHING OF OEGMA WITH PDMSDMA USING ATRP

Attaching atRA to the HEMA monomer led to poor polymerisation, whilst modifying HEMA with Ibu was successful; however, polymerisations with the Ibu-modified monomer became problematic when trying to find an appropriate solvent to carry out a controlled ATRP in which all components were soluble. Finally post modification of p(HEMA$_{30}$) with both atRA and Ibu could not obtain viable yields. Therefore, the synthetic strategy was modified to evaluate the formation of amphiphilic branched copolymers with the aim to investigate the improvement of drug solubility using the hydrophilic and hydrogen-bonding environment (in this case OEGMA) within SiO. The subsequent release of free drug and an analogous approach to that described in PDMS-drug blends in Chapter 3 will also be studied.
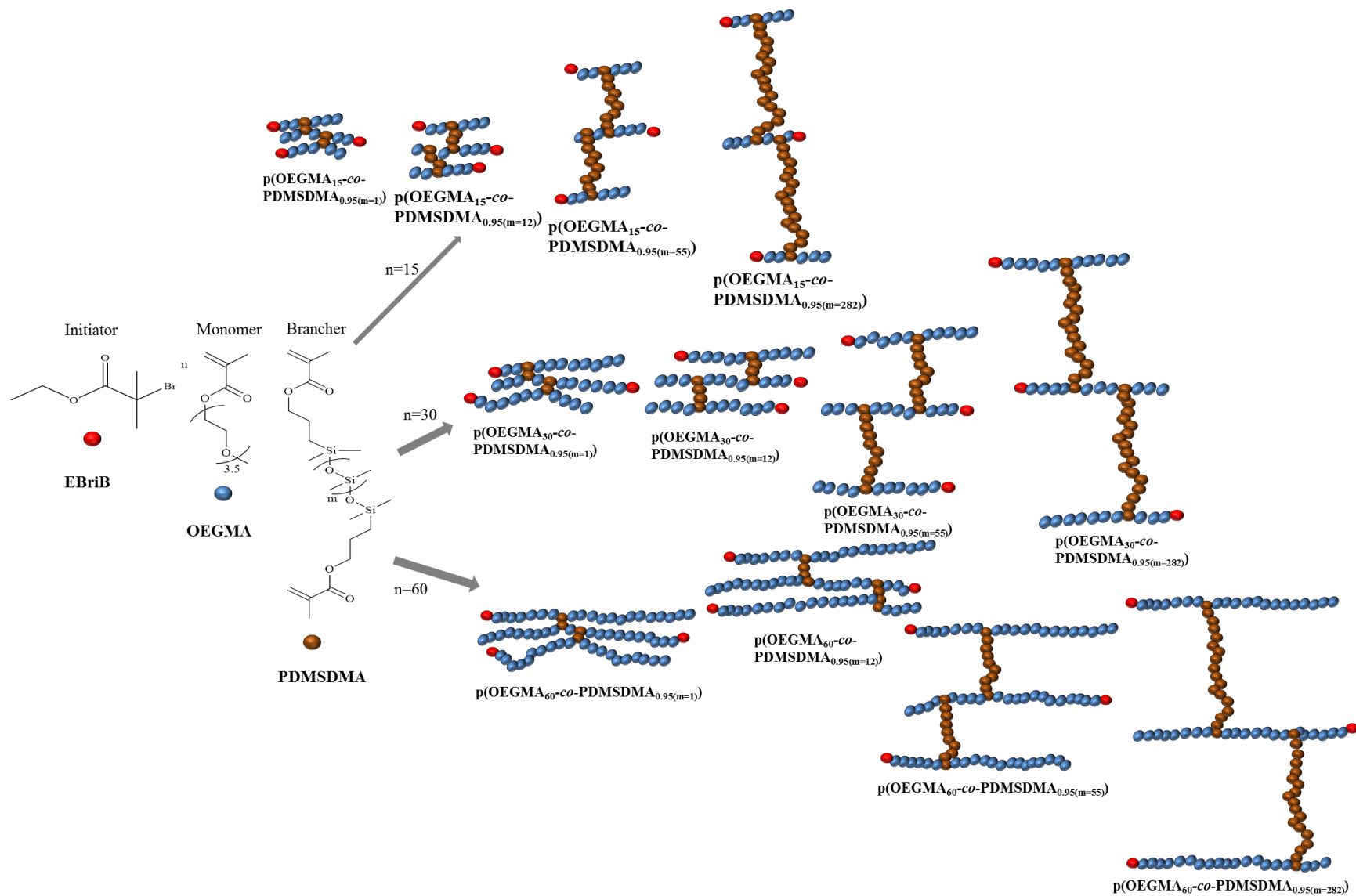
Scheme 4.7 Schematic representation of initiator, monomer and brancher and the different targeted DP branched polymers synthesised with different M_n branchers.

4.3.1 Kinetic Studies of Linear and Branched OEGMA ATRP Polymerisation

The absence of a strategy requiring covalent attachment of drugs to a SiO-soluble polymer removed the need for the HEMA segment which, although hydrophilic, has a much simpler structure than OEGMA. Studies, therefore, aimed to understand the homopolymerisation of OEGMA, a commercially available hydrophilic monomer with a DP_n = 3-4 monomer units (M_n = 300 gmol^{-1}). The main aim was to form a branched amphiphilic architecture of OEGMA at various DP_n values (15, 30 and 60 monomer units) for the primary structural polymer chains, but using four different chain lengths of PDMSDMA as the brancher, ranging from 390-21,250 gmol^{-1} (m = 1, 12, 55 and 282), Scheme 4.7. The polymerisation of OEGMA under aqueous solvent conditions have been reported in the literature, particularly the use of isopropanol:water, IPA:H$_2$O mixtures (92.5:7.5 % v/v).[51] Similar conditions to those reported in the literature for the homopolymerisation of OEGMA were employed for the following reactions, namely 30 °C using the IPA:H$_2$O mixture (92.5:7.5 % v/v) at a concentration of 55.5 % w/v (monomer:solvent) with CuCl: bpy as the catalytic system and EBriB as the initiator. Kinetic studies were investigated when a low molecular weight PDMSDMA (M_n 386 gmol^{-1}, m = 1), was employed in the branched copolymerisation. All polymers synthesised were characterised by ^{1}H NMR spectroscopy and GPC, Table 4.3.

Table 4.3 ^{1}H NMR and GPC data for all linear p(OEGMA) and branched equivalents with PDMSDMA (M_n 390 gmol^{-1}, n = 1) synthesised.

Target Polymer Composition	Theoretical M_n (gmol^{-1})	GPC[a] M_n (gmol^{-1})	GPC[a] M_w (gmol^{-1})	GPC[a] Đ	^{1}H NMR[b] Conversion (%)
p(OEGMA$_{15}$)	4,700	7,400	10,100	1.36	99
p(OEGMA$_{30}$)	9,200	15,000	20,900	1.39	97
p(OEGMA$_{60}$)	18,200	29,300	48,700	1.66	90
p(OEGMA$_{15}$-co-PDMSDMA$_{0.95}$)	-	159,000	537,600	3.38	99
p(OEGMA$_{30}$-co-PDMSDMA$_{0.95}$)	-	1,559,000	8,069,000	5.18	98
p(OEGMA$_{60}$-co-PDMSDMA$_{0.95}$)	-	45,350	175,700	3.87	99

^{a} Determined by GPC (DMF eluent at 60 °C) ^{b} Determined by ^{1}H NMR in CDCl$_3$

The GPC chromatogram overlays (RI Figure 4.17A; RALS Figure 4.17B) highlight the difference between linear and branched copolymerisations. As seen previously, the incorporation of PDMSDMA results in higher molecular weight branched polymers eluting at lower retention volumes with broad distributions.
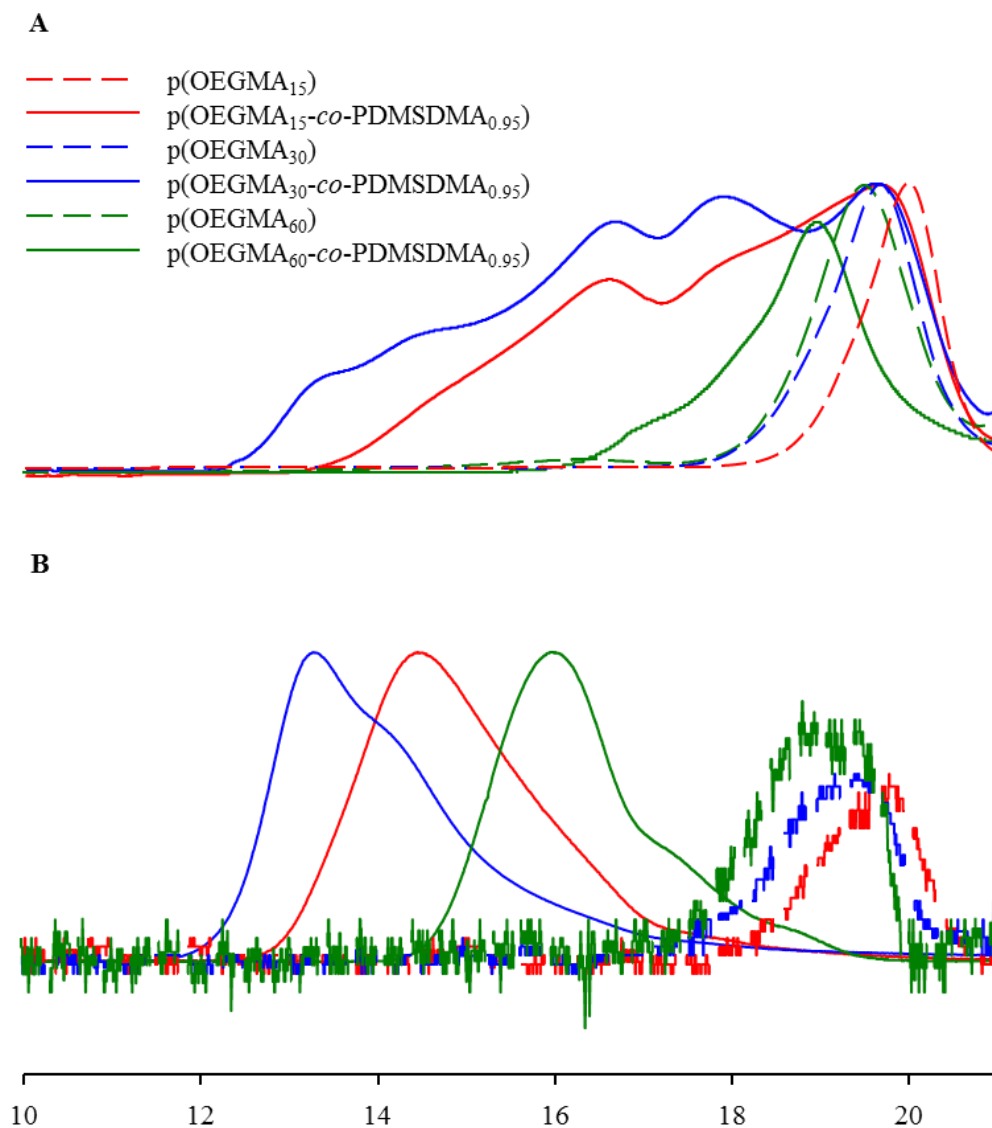
Figure 4.17 Overlaid GPC chromatograms showing linear and branched p(OEGMA) A: RI traces and B: RALS traces.

The kinetics of linear p(OEGMA) was also monitored by ^{1}H NMR spectroscopy, Figure 4.18, and overlaid spectra were obtained in the case of p(OEGMA$_{30}$) at different time points. As previously, the presence of an external reference, anisole, aided this analysis.
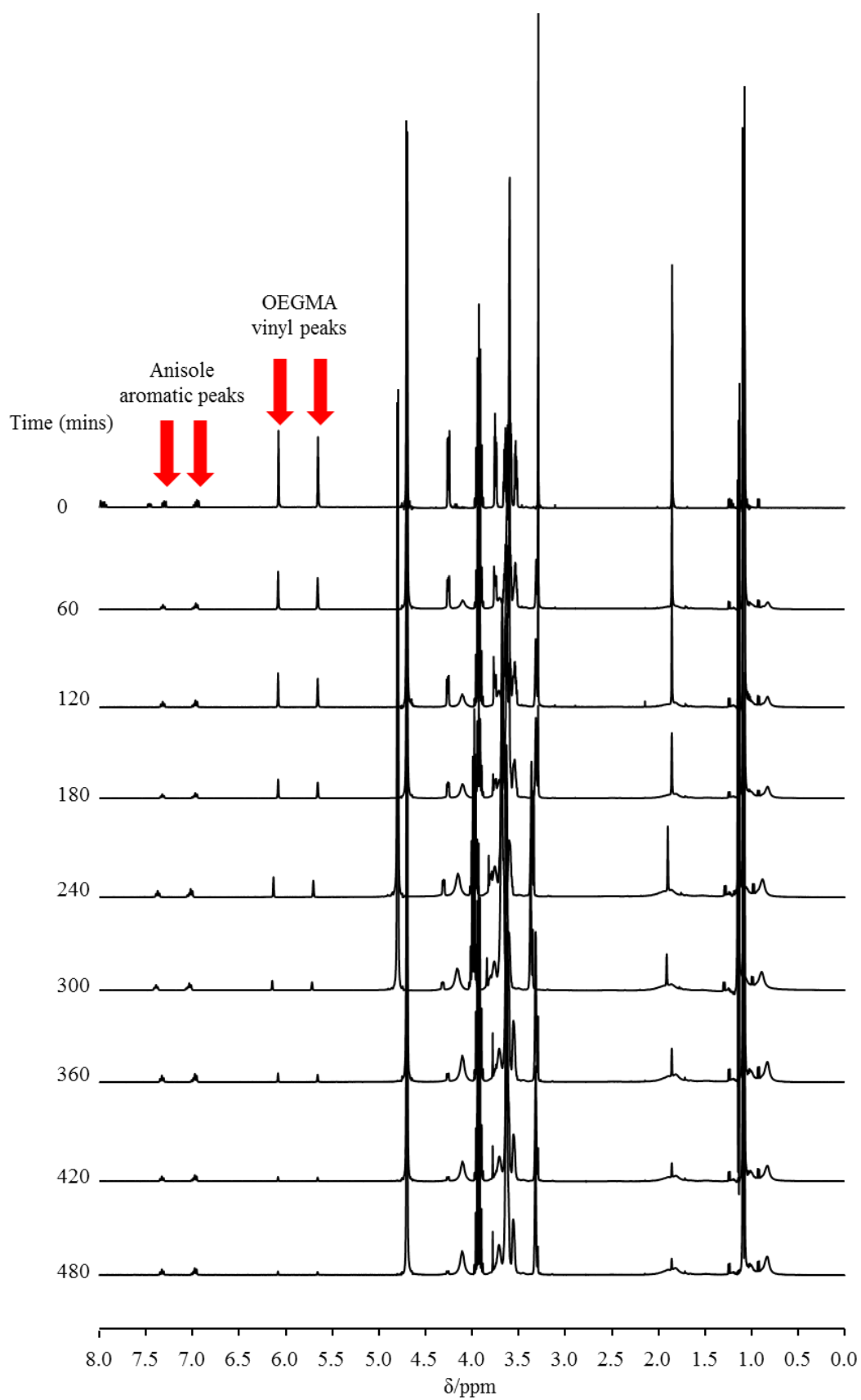
Figure 4.18 ^{1}H NMR (D$_2$O, 400 MHz) overlay of kinetic samples at hourly time points for p(OEGMA$_{30}$) synthesised using ATRP.

The kinetic plots for linear p(OEGMA) polymerisation, with different targeted DP_n values (Figure 4.19) show that each polymerisation reached a high conversion in less than 8 hours and followed first order kinetics. As would be expected, the targeting of shorter chains showed more rapid polymerisation.
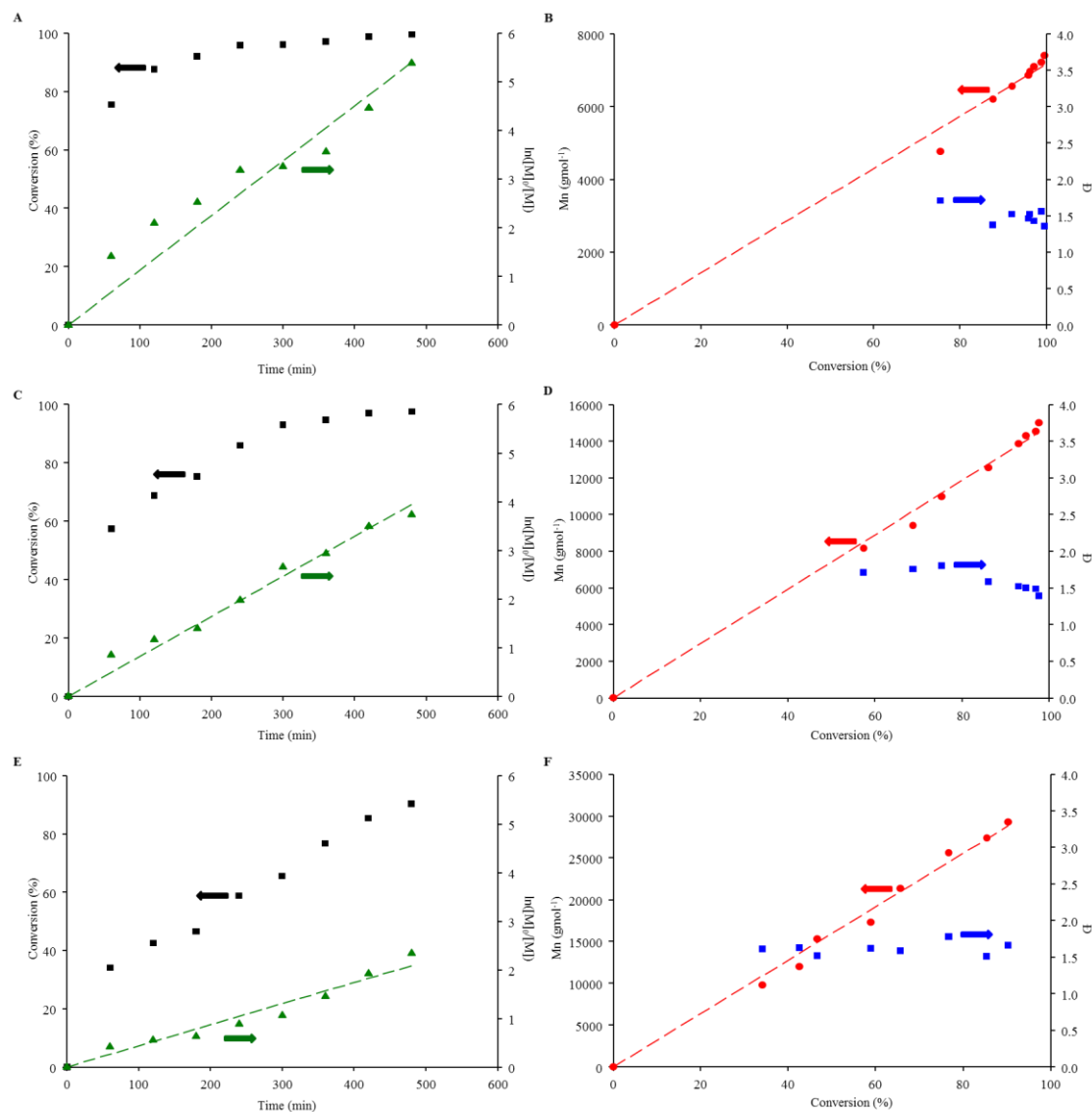
Figure 4.19 ATRP kinetic plots for linear p(OEGMA). A and B: p(OEGMA$_{15}$), C and D: p(OEGMA$_{30}$), E and F p(OEGMA$_{60}$). Conversion (■), ln([M]/[M]$_0$) (▲), M_n (●) and Đ (■).

The kinetics of OEGMA branched polymerisations using the divinyl PDMSDMA (M_n = 390 gmol^{-1}, n=1), with various targeted DP_n values for the primary chains (15, 30 and 60) were also investigated. First order kinetics were, again, observed as depicted in Figure 4.20 A, C and E. The plots of M_n and M_w are shown in Figure 4.20 B, D and F, initially both increase linearly, however, when conversion reaches

80-90 % the M_n and M_w rapidly increases due to formation of a branched structure when linear chains join together.
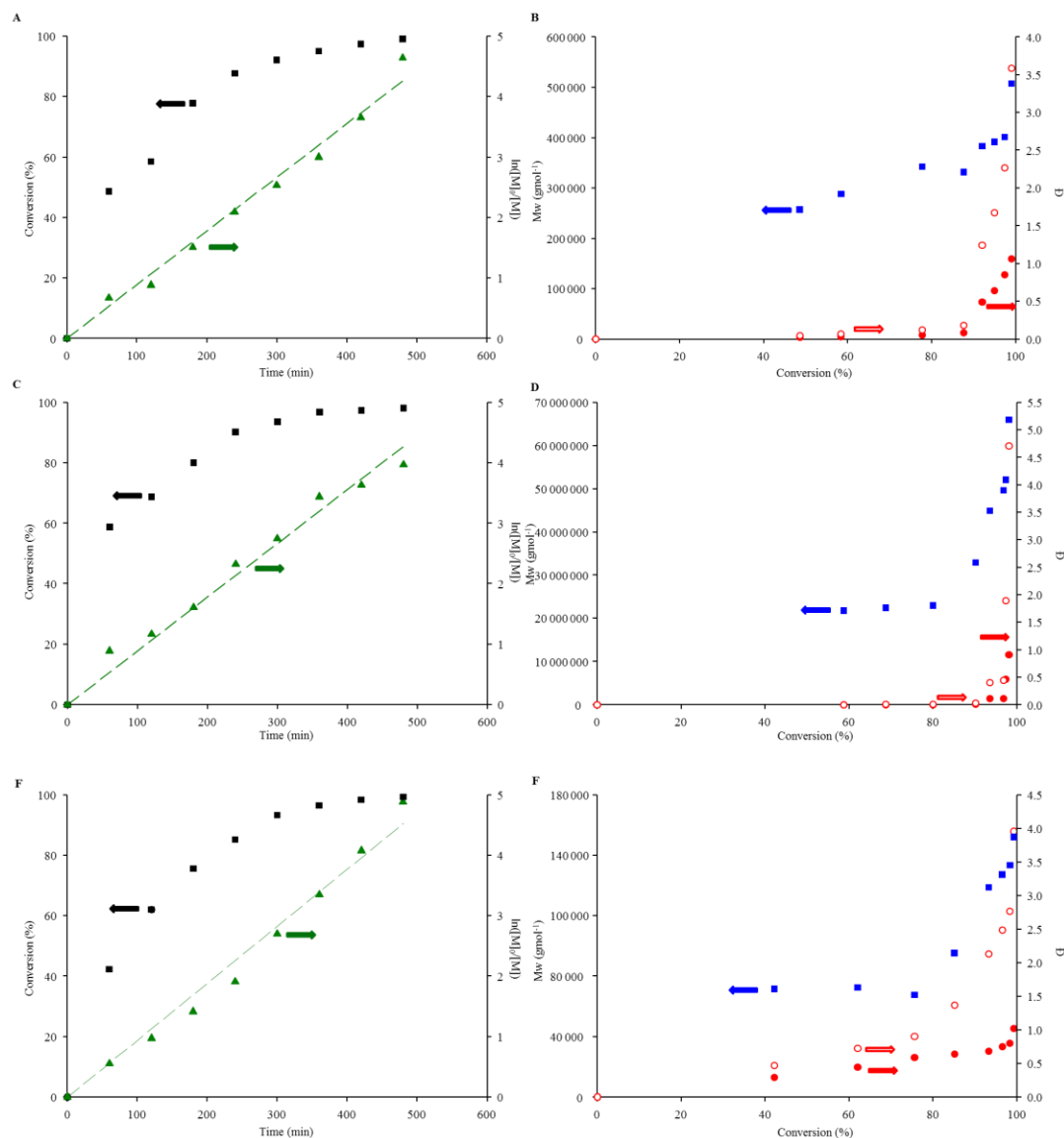
Figure 4.20 ATRP Kinetic plots for branched p(OEGMA) with PDMSDMA (M_n=390 gmol^{-1}, n=1). A and B: p(OEGMA$_{15}$), C and D: p(OEGMA$_{30}$), E and F p(OEGMA$_{60}$). Conversion (■), ln([M]/[M]$_0$) (▲), M_n (●), M_w (○) and Đ (■).

4.3.2 Synthesis of p(OEGMA)/PDMSDMA Branched Copolymers

After the kinetics of the branched ATRP copolymerisation of p(OEGMA) with PDMSDMA were determined to be controlled and first order, a range of materials were synthesised. Primary chains of p(OEGMA) with targeted DP$_n$ values of 15, 30 and 60 monomer units were synthesised in the presence of PDMSDMA of varying M_n 390 (m = 1), 1,275 (m =12), 4,460 (m = 55) and 21,250 (m = 282) gmol^{-1}. The

different materials with various combinations of p(OEGMA) and PDMSDMA are summarised in Scheme 4.8. These materials were analysed by ^{1}H NMR spectroscopy and GPC (DMF eluent at 60 °C) and their characteristics are presented in Table 4.4.

Table 4.4 ^{1}H NMR and GPC data for all branched p(OEGMA) synthesised.

Target Polymer Composition	Brancher	GPC[a]			^{1}H NMR[b]
		M_n (gmol^{-1})	M_w (gmol^{-1})	Đ	Conversion (%)
p(OEGMA$_{15}$)	PDMSDMA$_{0.95}$	28,050	483,200	17.23	99
p(OEGMA$_{30}$)	PDMSDMA$_{0.95}$	38,900	106,000	2.73	98
p(OEGMA$_{60}$)	PDMSDMA$_{0.95}$	185,900	479,000	2.58	82
p(OEGMA$_{15}$)	PDMSDMA$_{(12)0.95}$	210,100	1,577,000	7.51	83
p(OEGMA$_{30}$)	PDMSDMA$_{(12)0.95}$	215,700	1,436,000	6.66	88
p(OEGMA$_{60}$)	PDMSDMA$_{(12)0.95}$	43,950	385,500	8.77	99
p(OEGMA$_{15}$)	PDMSDMA$_{(55)0.95}$	14,200	20,400	1.44	98
p(OEGMA$_{30}$)	PDMSDMA$_{(55)0.95}$	18,300	27,400	1.50	99
p(OEGMA$_{60}$)	PDMSDMA$_{(55)0.95}$	32,250	48,250	1.50	94
p(OEGMA$_{15}$)	PDMSDMA$_{(282)0.95}$	11,000	15,200	1.38	98
p(OEGMA$_{30}$)	PDMSDMA$_{(282)0.95}$	19,700	28,800	1.46	99
p(OEGMA$_{60}$)	PDMSDMA$_{(282)0.95}$	33,300	45,250	1.36	99

[a] Determined by GPC (DMF eluent at 60 °C) [b] Determined by ^{1}H NMR in CDCl$_3$

It was observed the higher M_n PDMSDMA (4,460 and 21,250 gmol^{-1}) failed to produce high molecular weight branched materials seen when employing the shorter chain PDMSDMA (see Figure 4.21), and dispersity values < 1.5 were seen. The GPC chromatogram overlays of the different p(OEGMA) branched copolymers with the different PDMSDMA branchers are presented in Figure 4.21, and clearly show that the use of longer branchers failed to give highly branched materials.
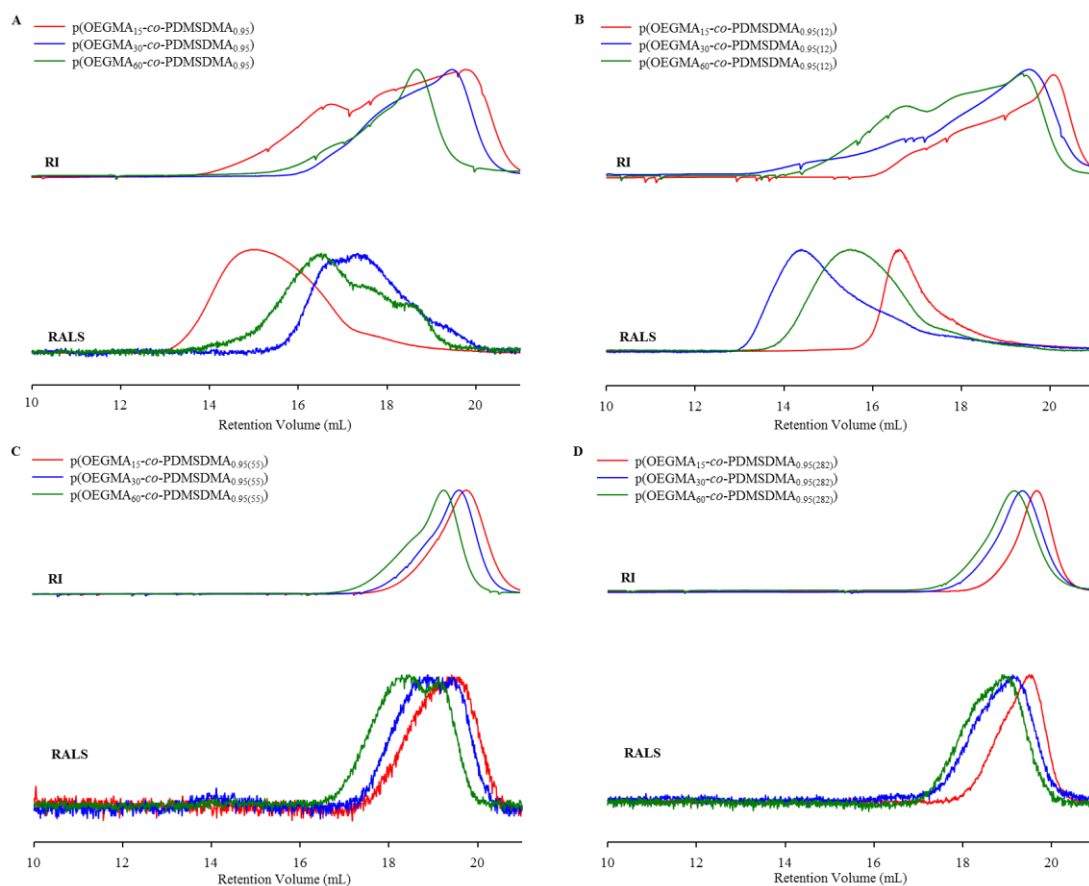
Figure 4.21 GPC chromatogram overlays of branched p(OEGMA) DP 15 (red), 30 (blue) and 60 (green). A: p(OEGMA) branched with PDMSDMA (M_n 390 gmol^{-1} m = 1). B: p(OEGMA) branched with PDMSDMA (M_n 1,275 gmol^{-1} m = 12). C: p(OEGMA) branched with PDMSDMA (M_n 4,460 gmol^{-1} m = 55). D: p(OEGMA) branched with PDMSDMA (M_n 21,250 gmol^{-1} m = 282).

Following the unsuccessful branched polymerisations with high molecular weight PDMSDMA, despite high conversion (<90 %) of the OEGMA monomer units, THF was added to the solvent system with the aim to remove any potential solubility issues of the longer PDMSDMA branchers that may inhibit the branching between chains. To ensure this new solvent system (IPA:H$_2$O:THF; 74.5:7.5:18) did not affect the ATRP polymerisation, kinetic studies of the p(OEGMA$_{30}$) branched ATRP copolymerisation, using the shortest PDMSDMA, were conducted and compared with the previous solvent system (see Figure 4.22). The addition of THF did not inhibit the polymerisation and first order kinetics were seen, suggesting a controlled polymerisation, however, the polymerisation was noticeably faster. Using this short brancher, branched architectures were obtained, as shown by the rapidly increase of M_n and M_w at high conversion.
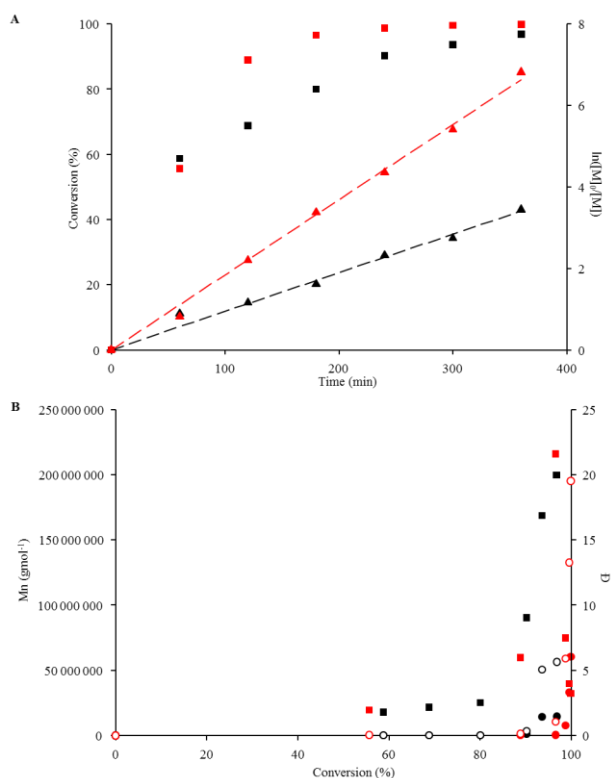
Figure 4.22 ATRP kinetic plots of p(OEGMA$_{30}$) branched with PDMSDMA (M$_n$ 390 gmol^{-1}) in IPA:H$_2$O (92.5:7.5) (black) and IPA:H$_2$O:THF (74.5:7.5:18) (red). A: Conversion (squares), ln([M]/[M]$_0$) (triangles). B: M$_n$ (filled circles), M$_w$ (unfilled circles) and Đ (squares).

As the kinetics confirmed that a controlled first order polymerisation was taking place with the addition of THF, ATRP reactions of the previously failed branched copolymerisations (primary p(OEGMA) DP$_n$ = 15, 30 and 60) with PDMSDMA branchers of M$_n$ = 4,460 and 21,250 gmol^{-1} were repeated. Table 4.5 summarises the characterisation of the resulting materials as analysed by ^{1}H NMR spectroscopy and GPC (DMF eluent at 60 °C).

Despite the addition of THF, the formation of high molecular weight, branched copolymers was not seen, as evidenced by the absence of high molecular weight materials and despite high conversions being obtained.

Table 4.5 ^{1}H NMR and GPC data for all branched p(OEGMA) synthesised using IPA:H$_2$O:THF (74.5:7.5:18) solvent system.

Target Polymer Composition	Brancher	GPC[a]			^{1}H NMR[b]
		M$_n$ (gmol^{-1})	M$_w$ (gmol^{-1})	Đ	Conversion (%)
p(OEGMA$_{15}$)	PDMSDMA$_{(55)0.95}$	6,700	11,300	1.68	94
p(OEGMA$_{30}$)	PDMSDMA$_{(55)0.95(55)}$	13,700	19,800	1.45	97
p(OEGMA$_{60}$)	PDMSDMA$_{(55)0.95(55)}$	25,000	45,100	1.80	99
p(OEGMA$_{15}$)	PDMSDMA$_{(282)0.95}$	8,300	11,000	1.32	99
p(OEGMA$_{30}$)	PDMSDMA$_{(282)0.95}$	13,800	17,400	1.26	99
p(OEGMA$_{60}$)	PDMSDMA$_{(282)0.95}$	6,500	11,100	1.71	99

[a] Determined by GPC (DMF eluent at 60 °C) [b] Determined by ^{1}H NMR in CDCl$_3$

4.3.3 Solubility Study of p(OEGMA-*co*-PDMSDMA) in SiO

Despite the lack of success with long PDMSDMA branchers, the solubility of the different p(OEGMA-*co*-PDMSDMA) branched architectures in SiO$_{1000}$ was investigated. Initially, a solubility study was carried out with linear homopolymers of p(OEGMA$_{15}$) which revealed that p(OEGMA) and SiO$_{1000}$ were practically immiscible. Blends of the amphiphilic copolymer of OEGMA (DP$_n$ = 15) branched with both PDMSDMA M$_n$ 390 and 1,275 gmol^{-1} (n =1 and 12 respectively) at 0.1, 1, 5 and 10 % (v/v) in SiO$_{1000}$ were prepared and stirred at ambient temperature for 2 days without any observable change. The samples were then placed at 37 °C for 2 days and stirred at ambient temperature for a further 3 days without appreciable dissolution of the branched polymers. To overcome the initial interfacial interactions which must happen for solids to solubilise in solvents the polymers were solubilised with SiO in THF by stirring overnight. The blends were then stirred and left open for 7 days at ambient temperature to allow the THF to evaporate. This process resulted in the formation of a homogeneous 0.1 % (v/v) blend of the p(OEGMA$_{15}$-*co*-PDMSDMA$_{0.95(12)}$) in SiO$_{1000}$, however, no other combinations were successful. Due to the observed immiscibility of the branched amphiphilic structures in SiO, a series of alternative polymer structures were considered.

4.4 ATRP COPOLYMERISATION OF OEGMA AND PDMSMA

To increase the solubility of the targeted amphiphilic polymer architectures within SiO, a higher ratio of the hydrophobic/lipophilic component was considered to be required when compared to the hydrophilic p(OEGMA). The divinyl monomer PDMSDMA, used as a brancher previously, was clearly not sufficient to induce solubility within these structures, therefore, the statistical linear copolymerisation of OEGMA with monomethacryloxypropyl PDMS (PDMSMA, Figure 4.23) was chosen for study .
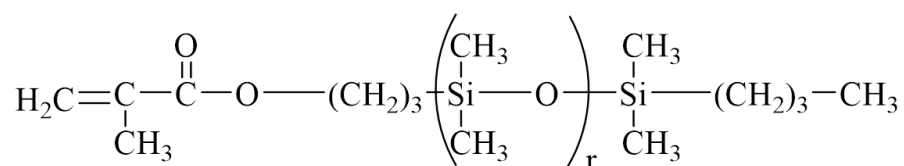
Figure 4.23 Chemical structure of monomethacryloxypropyl PDMS (PDMSMA).

Two different molecular weights of PDMSMA were selected (985 and 4,600 gmol^{-1}, r = 9 and 57 respectively), and the synthesis of a variety of copolymers was investigated. The target within this section was to statistically copolymerise OEGMA and PDMSMA with an overall targeted DP$_{60}$ monomer units and OEGMA/PDMSMA ratios of 80/20 and 50/50, Scheme 4.9.
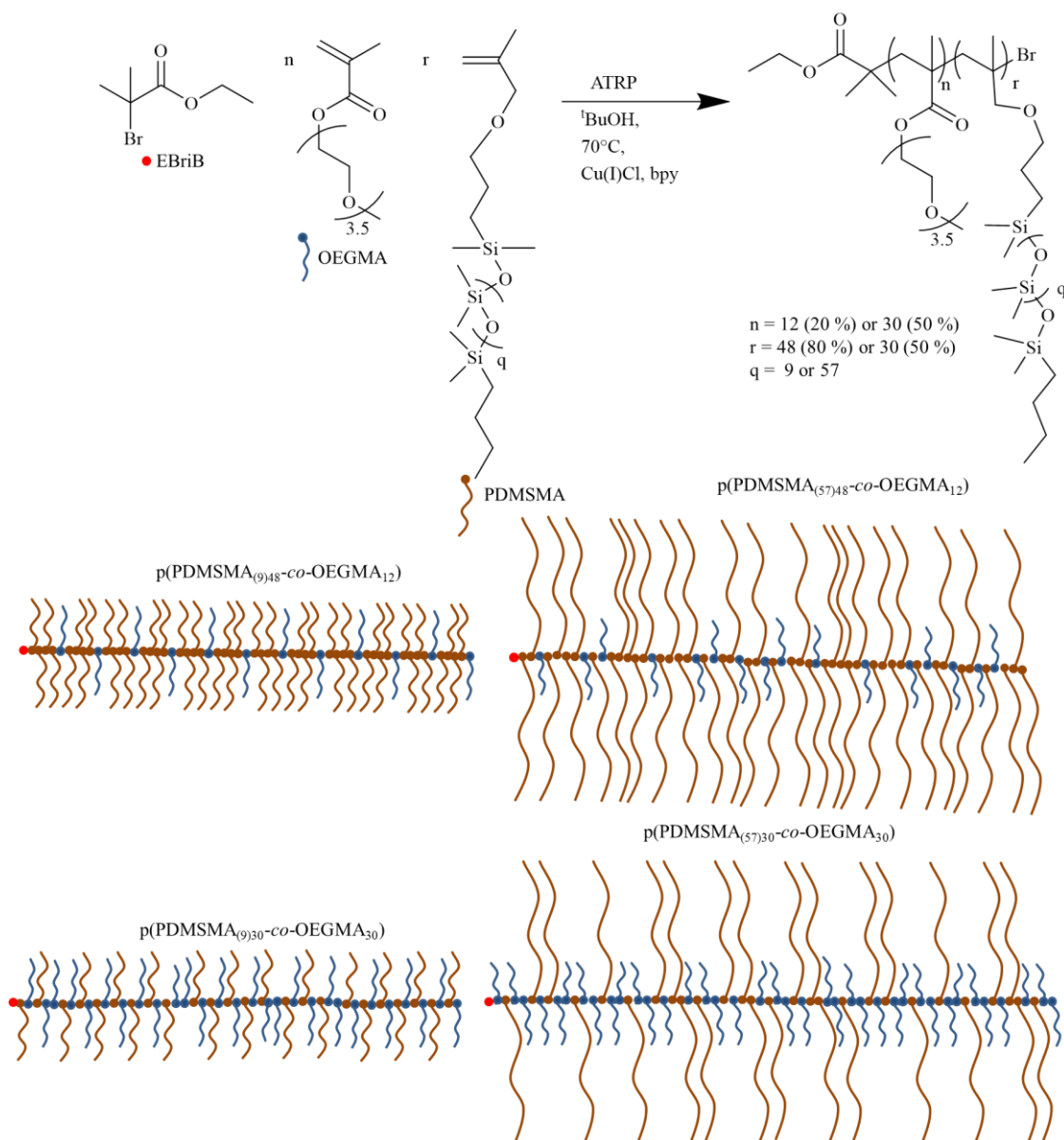
Scheme 4.9 Synthesis of statistical p(PDMSMA-*co*-OEGMA) *via* ATRP and schematic representations of the targeted amphiphilic polymeric materials.

4.4.1 ATRP Copolymerisation of OEGMA and PDMSMA

The polymerisation of PDMSMA in tertiary butanol (^{t}BuOH) using a PEO macroinitiator has been reported in the literature *via* ATRP at 30 % v/v and 90 °C.[59] The PEO macroinitiator would have similar hydrophilic properties to the OEGMA monomer, therefore, comparable conditions to those reported in the literature were employed, namely 90 °C in ^{t}BuOH at a concentration of 30 % w/v (monomer:solvent) with CuCl:bpy as the catalytic system and EBriB as the initiator. Initially the linear polymers p(PDMSMA$_{(9)60}$), p(OEGMA$_{60}$) and the 80/20 and 50/50

ratio copolymers were synthesised and analysed by ^{1}H NMR spectroscopy and GPC (THF eluent at 35 °C), Table 4.6.

Table 4.6 ^{1}H NMR spectroscopy and GPC data of homopolymers and copolymers of OEGMA and PDMSMA synthesised *via* ATRP in ^{t}BuOH.

Target Polymer Composition	GPC[a]			^{1}H NMR[b]		
					Conversion (%)	
	M_n (gmol^{-1})	M_w (gmol^{-1})	Đ	Polymer Composition	PDMS	OEGMA
p(OEGMA$_{60}$)	17,050	494,500	2.90	p(OEGMA$_{57}$)	n/a	92
p(PDMS$_{(9)60}$)	58,800	73,500	1.25	p(PDMSMA$_{(9)60}$)	99	n/a
p(PDMSMA$_{(9)48}$-*co*-OEGMA$_{12}$)	39,100	65,900	1.68	p(PDMSMA$_{(9)46}$-*co*-OEGMA$_{11}$)	95	94
p(PDMSMA$_{(9)30}$-*co*-OEGMA$_{30}$)	60,800	123,150	2.03	p(PDMSMA$_{(9)25}$-*co*-OEGMA$_{28}$)	83	92

[a] Determined by GPC (THF eluent at 35 °C) [b] Determined by ^{1}H NMR in CDCl$_3$

Copolymers prepared by the ATRP of PDMSMA and OEGMA gave materials with a large dispersity which indicates a lack of control when using ATRP under these conditions. The catalytic system was also seen to precipitate once the complex had been formed (Figure 4.24) and, therefore, was not efficient in controlling the reaction leading to premature termination of chains.
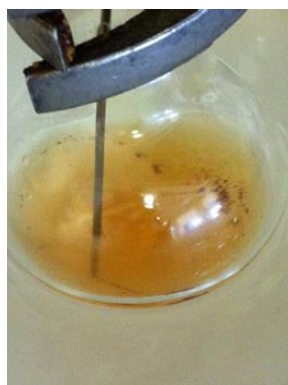
Figure 4.24 Picture of precipitate formation within the ATRP polymerisation of OEGMA and PDMSMA $_{(9)}$ DP$_{60}$ 50/50 ratio in ^{t}BuOH.

4.4.2 RAFT Polymerisation of OEGMA and PDMSMA

Due to the insolubility of the catalytic system within the ATRP solvent, an alternative polymerisation method was employed; the non-catalytic controlled radical polymerisation technique RAFT. Matching the exact conditions of an ATRP with RAFT polymerisation is not possible, as discussed in Section 4.1.3, as this method of polymerisation requires a chain transfer agent (CTA). 2-cyano-2-propyl benzodithioate (CPBD) was selected as the RAFT CTA due to the excellent

compatibility with methacrylate monomers. 2,2'-azobis(2-methylpropionitrile) (AIBN) was also selected as the free radical initiator due to excellent solubility within ^{t}BuOH. and copolymerisations were conducted at 30 wt.% monomer with respect to solvent and at 70 °C, Figure 4.25.
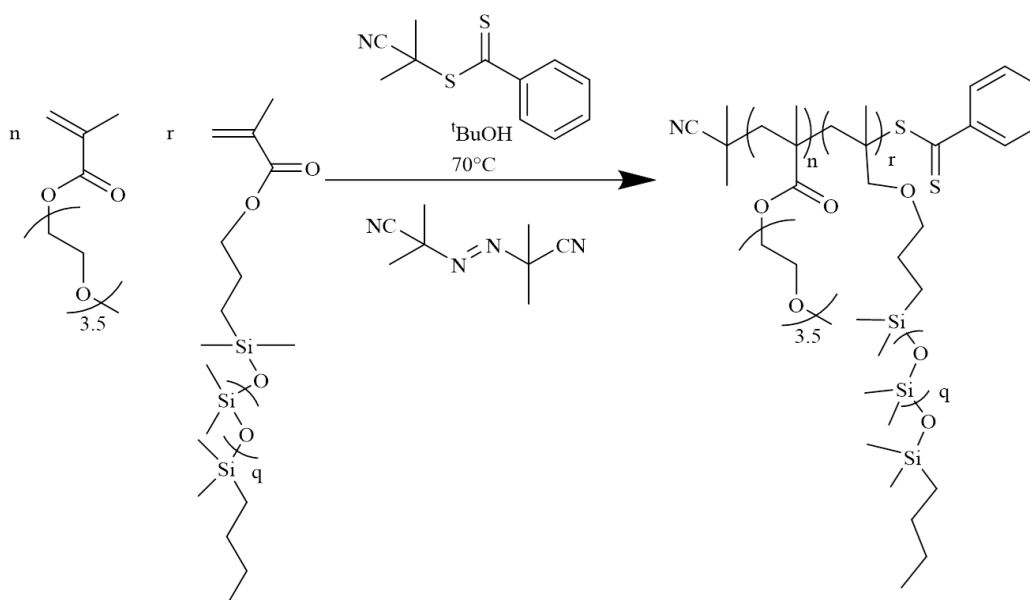
Figure 4.25 Controlled radical polymerisation of OEGMA and PDMSMA conducted in ^{t}BuOH at 70 °C *via* RAFT with 4,4′-azobis(4-cyanopentanoic acid) and 2-cyano-2-propyl benzodithioate.

4.4.2.1 Linear Amphiphilic Copolymers of OEGMA and PDMSMA *via* RAFT

Homopolymerisations of OEGMA and the two different chain length PDMSMA monomers, targeting $DP_n = 60$ monomer units, and copolymers of PDMSMA and OEGMA with identical targeted degrees of polymerisation at 80/20 and 50/50 ratios were synthesised. As previously, the resulting materials were analysed by ^{1}H NMR spectroscopy and GPC (THF eluent at 35 °C), Table 4.7.

Table 4.7 ^{1}H NMR and GPC data of all polymers synthesised *via* RAFT in ^{t}BuOH.

Target Polymer Composition	GPC (THF)[a]			^{1}H NMR[b]		
	Mn (gmol^{-1})	Mw (gmol^{-1})	Đ	Polymer Composition	Conversion (%)	
					PDMS	OEGMA
p(OEGMA${}_{60}$)	24,800	30,400	1.23	p(OEGMA${}_{55}$)	-	92
p(PDMSMA${}_{(9)60}$)	51,200	59,400	1.16	p(PDMSMA ${}_{(9)58}$)	96	-
p(PDMSMA${}_{(57)60}$)	376,000	439,900	1.17	p(PDMSMA ${}_{(57)23}$)	38	-
p(PDMSMA ${}_{(9)48}$-*co*-OEGMA${}_{12}$)	47,650	52,700	1.11	p(PDMSMA ${}_{(9)47}$-*co*-OEGMA${}_{12}$)	94	98
p(PDMSMA ${}_{(9)30}$-*co*-OEGMA${}_{30}$)	33,300	36,800	1.11	p(PDMSMA ${}_{(9)24}$-*co*-OEGMA${}_{29}$)	80	96
p(PDMSMA ${}_{(57)48}$-*co*-OEGMA${}_{12}$)	350,600	380,200	1.08	p(PDMSMA ${}_{(57)25}$-*co*-OEGMA${}_{11}$)	45	77
p(PDMSMA ${}_{(57)30}$-*co*-OEGMA${}_{30}$)	220,250	266,850	1.21	p(PDMSMA ${}_{(57)17}$-*co*-OEGMA${}_{23}$)	47	65

[a] Determined by GPC (THF eluent at 35 °C) [b] Determined by ^{1}H NMR in CDCl${}_3$

All materials synthesised have low dispersities (<1.25) indicating control within the polymerisation, and the difference between ATRP and RAFT was readily obvious when comparing the RI traces of p(OEGMA) and p(PDMSMA) (M_n 985 gmol^{-1}, r = 9) homopolymers, prepared by each technique (Figure 4.26). High conversions could not be reached with the longer chain PDMSMA monomers (45-47 % after 7 days), probably due to steric hindrance as RAFT requires a close proximity of two separate propagating polymer chain ends to undergo CTA exchange; however, these materials were still suitable for study after purification.
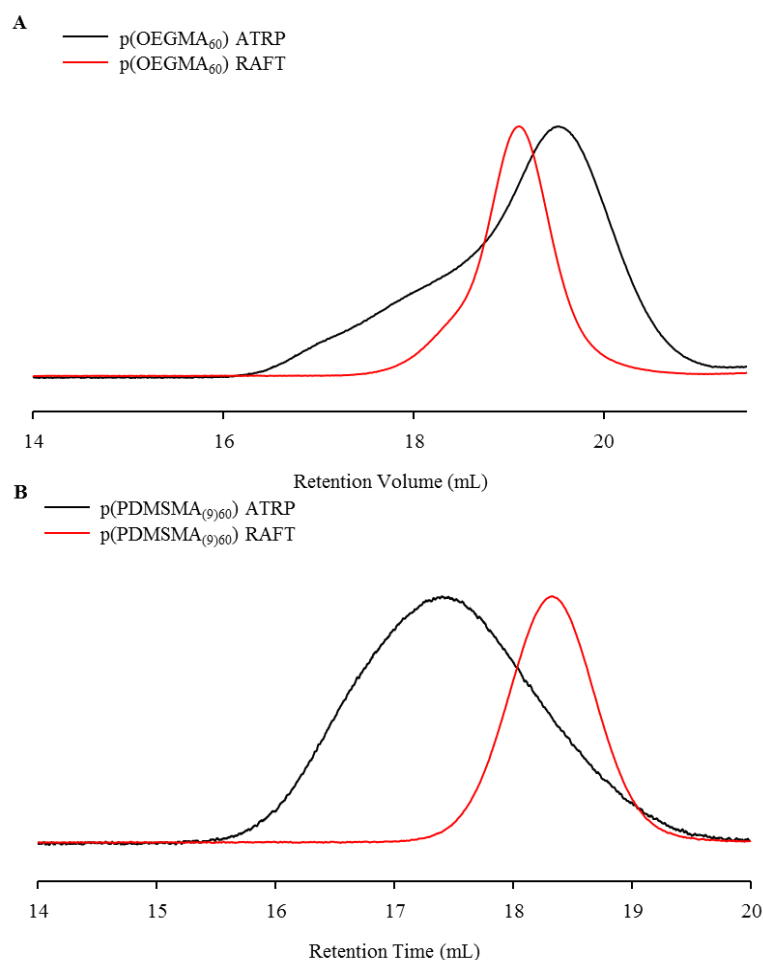
Figure 4.26 GPC RI chromatogram overlays of A) p(OEGMA$_{60}$) and B) p(PDMSMA$_{(9)60}$) synthesised by ATRP (black) and the RAFT synthesised equivalents (red).

4.4.2.2 Branched Amphiphilic Terpolymers of OEGMA, PDMSMA and PDMSDMA *via* RAFT

Due to the successful synthesis of the linear homopolymers and copolymers *via* RAFT, the introduction of the divinyl PDMS branchers (M_n = 1,275 and 4,460 gmol^{-1}; m = 12 and 55 respectively) to form branched terpolymers was reconsidered.

The brancher to CTA ratio was kept at 0.95: 1 for each attempt to ensure gelation did not occur.

$p(OEGMA_{15})$ was successfully branched with $PDMSDMA_{(55)}$, which was not possible when previously attempted by ATRP. The attainment of a branched architecture is clearly evidenced by the GPC (THF eluent at 35 °C) analysis of the copolymer (see Figure 4.27). This successful copolymerisation led to the synthesis of branched p(PDMSMA-*co*-OEGMA-*co*-PDMSDMA) terpolymer architectures with varying compositions, Table 4.8.
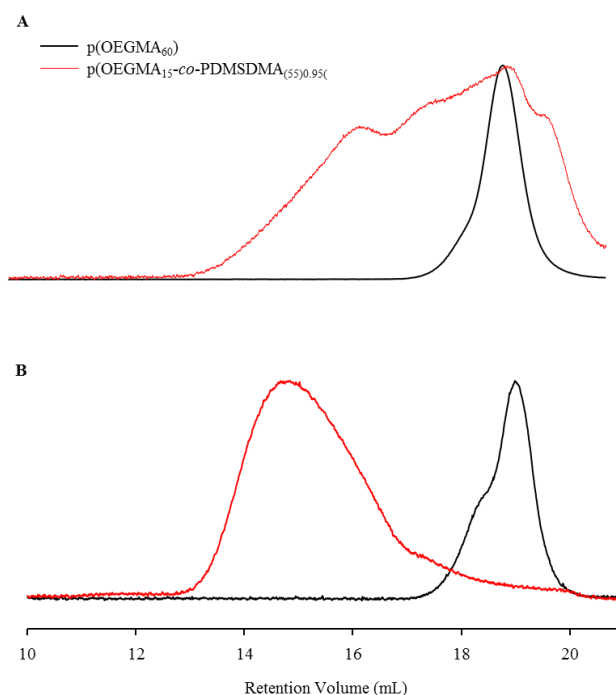
Figure 4.27 GPC chromatogram overlays of A) RI chromatograms and B) RALS chromatograms for linear $p(OEGMA_{60})$ (black) and branched $p(OEGMA_{15}-co-PDMSDMA_{(55)0.95})$ (red).

Table 4.8 ^{1}H NMR and GPC data of all branched polymers synthesised *via* RAFT.

Target Polymer Composition	Brancher	GPC			^{1}H NMR[b]		
		Mn (gmol^{-1})	Mw (gmol^{-1})	Đ	Polymer Composition	Conversion (%)	
						PDMS	OEGMA
p(OEGMA$_{15}$)	PDMSDMA$_{(55)}$	44,000	470,300	10.69	-	-	81
p(PDMSMA$_{(9)48}$-*co*-OEGMA$_{12}$)	PDMSDMA$_{(12)}$	56,200	74,200	1.32	-	94	98
p(PDMSMA$_{(9)30}$-*co*-OEGMA$_{30}$)	PDMSDMA$_{(12)}$	50,700	75,600	1.49	-	91	97
p(PDMSMA$_{(9)48}$-*co*-OEGMA$_{12}$)	PDMSDMA$_{(55)}$	423,900	3,590,000	8.47	-	91	98
p(PDMSMA$_{(9)30}$-*co*-OEGMA$_{30}$)	PDMSDMA$_{(55)}$	142,100	5,220,000	36.73	-	90	97
p(PDMSMA$_{(57)20}$-*co*-OEGMA$_5$)	PDMSDMA$_{(55)}$	95,400	108,600	1.14	-	71	91
p(PDMSMA$_{(57)20}$-*co*-OEGMA$_{20}$)	PDMSDMA$_{(55)}$	149,700	199,300	1.33	-	82	97
p(PDMSMA$_{(9)15}$-*co*-PDMSMA$_{(57)15}$-*co*-OEGMA$_{30}$)	-	95,400	108,600	1.14	p(PDMSMA$_{(9,57)23}$-*co*-OEGMA$_{29}$)	77	95
p(PDMSMA$_{(9)24}$-*co*-PDMSMA$_{(57)24}$-*co*-OEGMA$_{12}$)	-	149,700	199,300	1.33	p(PDMSMA$_{(9,57)37}$-*co*-OEGMA$_{11}$)	78	92
p(PDMSMA$_{(9)15}$-*co*-PDMSMA$_{(57)15}$-*co*-OEGMA$_{30}$)	PDMSDMA$_{(55)}$	235,600	323,200	1.37	-	79	91
p(PDMSMA$_{(9)24}$-*co*-PDMSMA$_{(57)24}$-*co*-OEGMA$_{12}$)	PDMSDMA$_{(55)}$	174,100	389,900	2.24	-	92	89

^{a} Determined by GPC (THF eluent at 35 °C) ^{b} Determined by ^{1}H NMR in CDCl$_3$

When branched terpolymer architectures were targeted using PDMSDMA$_{(12)}$ (only PDMSMA$_{(9)}$ was used in this case due to obvious steric constraints), low dispersities were achieved, and no high molecular weight materials were obtained, suggesting that the branching had, again, been unsuccessful. The use of the PDMS monofunctional monomer and bifunctional brancher of similar sizes (r = 9 and m = 12) may be expected to lead to steric constraints that prevent branching. When using the longer brancher, PDMSDMA$_{(55)}$, high molecular weight branched materials were obtained when the smaller monomer (PDMSMA$_{(9)}$) was used, which appears to confirm this assumption. Similar problems were evident when branched architectures of p(PDMSMA$_{(57)}$-*co*-OEGMA) were targeted, even with the longer PDMSDMA$_{(55)}$ branchers. Again, having PDMS monomer and brancher of similar sizes (r = 57 and m = 55) appears to lead to steric hindrance.

The GPC chromatograms of the different architectures synthesised using RAFT are presented in Figure 4.28. It can clearly be seen that only the combination of a small PDMS monomer (r = 9) and a long PDMS brancher (m = 55) leads to successful branching. The only architectures which display branching consist of p(PDMSMA$_{(9)48}$-*co*-OEGMA$_{12}$-*co*-PDMSDMA$_{(55)0.95}$) and p(PDMSMA$_{(9)30}$-*co*-OEGMA$_{30}$-*co*-PDMSDMA$_{(55)0.95}$) as evidenced by the very high molecular weights and Đ values obtained.

In an attempt to obtain branched polymers using the long chain (PDMSMA$_{(57)}$) monomer, the longer (PDMSDMA$_{(55)}$) brancher was used. Unfortunately, after leaving this reaction for 30 days, a high enough conversion was not reached in order to obtain highly branched materials (see Figure 4.29).
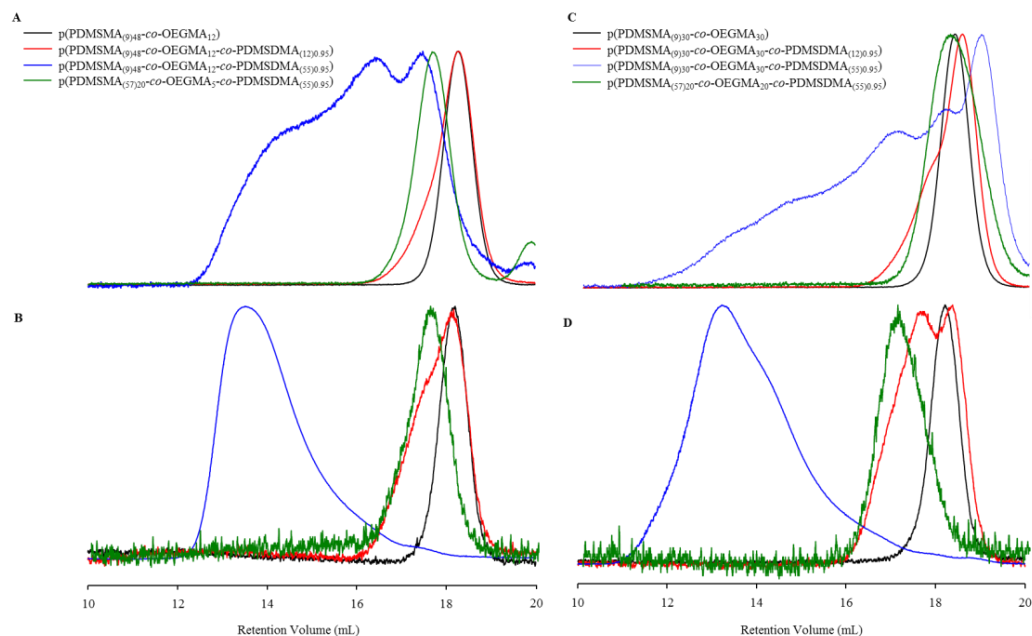
Figure 4.28 GPC chromatogram overlays of A) RI and B) RALS signals for linear p(PDMSMA$_{(9)47}$-co-OEGMA$_{12}$) (black) and branched equivalents with either PDMSDMA$_{(12)0.95}$ (red) or PDMSDMA$_{(55)0.95}$ (blue) and p(PDMSMA$_{(57)20}$-co-OEGMA$_5$-co-PDMSDMA$_{(55)0.95}$) (green). GPC analysis C) RI and D) RALS for linear p(PDMSMA$_{(9)30}$-co-OEGMA$_{30}$) (black) and branched equivalents with either PDMSDMA$_{(12)0.95}$ (red) or PDMSDMA$_{(55)0.95}$ (blue) and p(PDMSMA$_{(57)20}$-co-OEGMA$_{20}$-co-PDMSDMA$_{(55)0.95}$) (green).
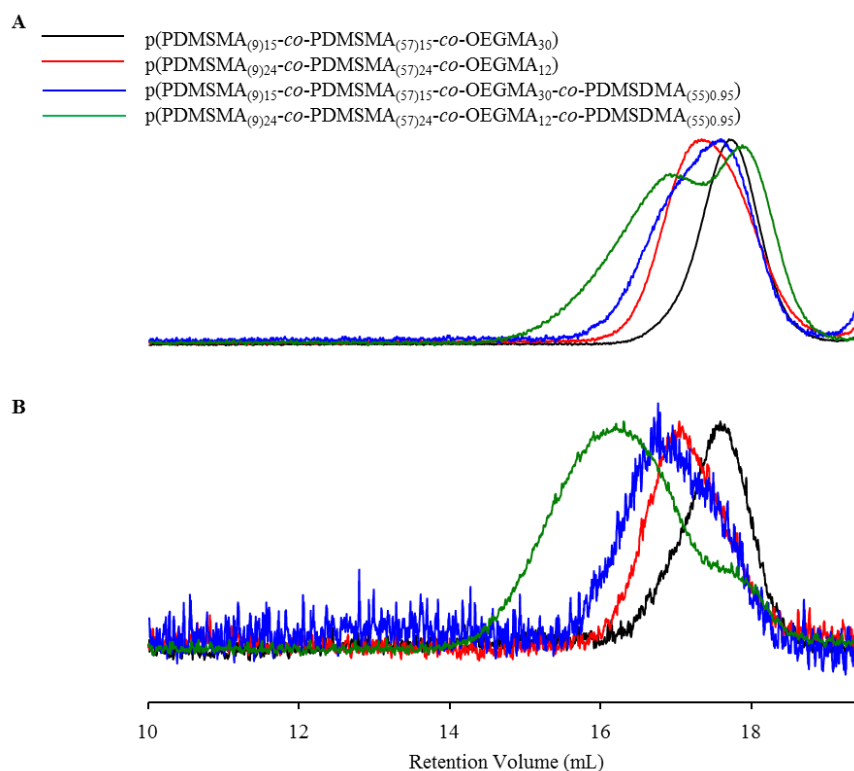
Figure 4.29 GPC chromatogram overlays of A) RI and B) RALS signals for linear p(PDMSMA$_{(9)15}$-co-PDMSMA$_{(57)15}$-co-OEGMA$_{30}$) (black) and p(PDMSMA$_{(9)24}$-co-PDMSMA$_{(57)24}$-co-OEGMA$_{12}$) (red) with their branched equivalents with PDMSDMA$_{(55)0.95}$ (blue and green respectively).

4.4.2.3 Solubility of Amphiphilic Copolymers and Terpolymers in SiO

As the aim of these studies was to investigate the ability to solubilise a hydrophilic polymer within SiO and evaluate drug release from the resulting mixture, it was essential to investigate the solubility of the amphiphilic co- and terpolymers, both linear and branched, in SiO. Table 4.9 summarises the materials tested for solubility in SiO and the results obtained.

Table 4.9 Solubility of the synthesised polymers in SiO (% v/v).

Primary Chain	Brancher	Solubility in SiO % (v/v)
p(OEGMA$_{15}$)	PDMSDMA$_{55}$	<1
p(PDMSMA$_{(9)60}$)		50
p(PDMSMA$_{(57)60}$)		50
p(PDMSMA$_{(9)48}$-*co*-OEGMA$_{12}$)		50
p(PDMSMA$_{(9)30}$-*co*-OEGMA$_{30}$)		5
p(PDMSMA$_{(57)48}$-*co*-OEGMA$_{12}$)		50
p(PDMSMA$_{(57)30}$-*co*-OEGMA$_{30}$)		50
p(PDMSMA$_{(9)48}$-*co*-OEGMA$_{12}$)	PDMSDMA$_{(55)}$	40
p(PDMSMA$_{(9)30}$-*co*-OEGMA$_{30}$)	PDMSDMA$_{(55)}$	40
p(PDMSMA$_{(57)20}$-*co*-OEGMA$_{5}$)	PDMSDMA$_{(55)}$	50
p(PDMSMA$_{(57)20}$-*co*-OEGMA$_{20}$)	PDMSDMA$_{(55)}$	50
p(PDMSMA$_{(9)15}$-*co*-PDMSMA$_{(57)15}$-*co*-OEGMA$_{30}$)		50
p(PDMSMA$_{(9)24}$-*co*-PDMSMA$_{(57)24}$-*co*-OEGMA$_{12}$)		50
p(PDMSMA$_{(9)15}$-*co*-PDMSMA$_{(57)15}$-*co*-OEGMA$_{30}$)	PDMSDMA$_{(55)}$	50
p(PDMSMA$_{(9)24}$-*co*-PDMSMA$_{(57)24}$-*co*-OEGMA$_{12}$)	PDMSDMA$_{(55)}$	50

The branched p(OEGMA$_{15}$-*co*-PDMSDMA$_{(55)0.95}$) had minimal SiO solubility (< 1 % v/v) and, as this contained the largest hydrophobic component possible through branching alone, co- and terpolymers of OEGMA with PDMSMA were clearly needed to increase solubility.

All other polymers were soluble at 40-50 % (v/v) apart from when a 50/50 ratio of OEGMA:PDMSMA$_{(9)}$ was copolymerised which represents the smallest content of hydrophobic monomer. This success represents a major increase in solubility compared to less than 1 % (v/v) that had been seen without the incorporation of PDMSMA.

4.4.2.4 Removal of CTA from Amphiphilic Co- and Terpolymers synthesised *via* RAFT

As the amphiphilic copolymers were soluble in SiO at high levels, the removal of the RAFT chain end was required as the CTA-end group is known to be highly coloured and the solutions were a bright pink colour (Scheme 4.10A). In some cases, gelation was also observed when the amphiphilic copolymers and linear homopolymers of

PDMSMA were stored, suggesting the presence of difunctionalised monomer impurities within the commercial PDMSMA. The removal and recovery of CPBD following RAFT polymerisations of PMMA has been reported by Perrier *et al.*[60] Excess AIBN was added to a solution of the purified polymer and subsequent AIBN thermal decomposition yields cyanoisopropyl radicals which react with the C=S bond of the thiocarbonyl-thio group. This results in an intermediate radical which can either fragment back to the previous state or free the thiocarbonyl-thio moiety from the polymer chain-end. The excess cyano-isopropyl radicals drive the equilibrium towards a radical chain end which is capped by additional cyano-isopropyl groups. It has been reported that too little AIBN under these conditions can lead to disproportionation and subsequent reactions between polymer chains.[61] The temperature and length of the reaction are important for the complete removal of the thiocarbonyl-thio end group and should follow the half-life time of the radical initiator used (in this case AIBN).

Similar conditions to those previously reported were employed for the removal of CPBD from p(PDMSMA$_{(9)48}$-*co*-OEGMA$_{12}$). The purified polymer was dissolved in toluene and a 20 molar excess of AIBN added to the solution which was degassed and heated to 80 °C for 150 minutes (the half-life time of AIBN in these conditions is 80 minutes). The polymer was isolated by precipitation into cold MeOH which afforded a white solution (Scheme 4.10 B).
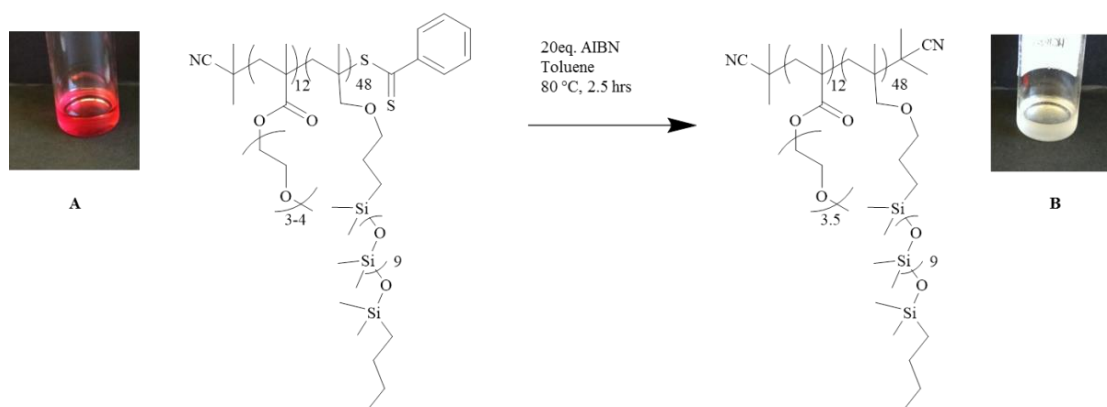
Scheme 4.10 Scheme of CPBD removal and pictures of p(PDMSMA$_{(9)48}$-*co*-OEGMA$_{12}$) synthesised *via* RAFT polymerisation A: before and B: after reaction with AIBN.

The colour change indicated removal of the CPBD and the recovered polymer was analysed by ^{1}H NMR spectroscopy (Figure 4.30) which confirmed the CTA removal

as the peaks at 7.30, 7.38, and 7.93 ppm, characteristic of the dithiobenzoate moiety, were no longer present.
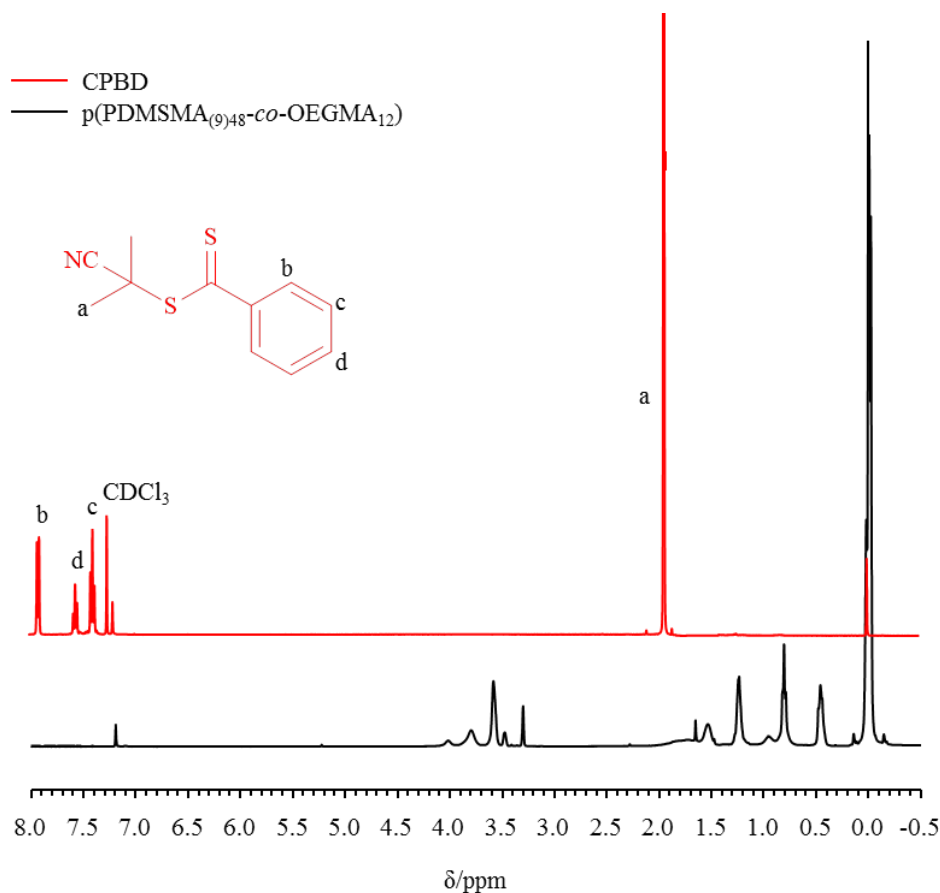
Figure 4.30 ^{1}H NMR spectra (CDCl$_3$, 400 MHz) of CPBD (red) and p(PDMSMA$_{(9)48}$-*co*-OEGMA$_{12}$) after CTA removal drug (black).

4.5 CONCLUSION

The initial strategy investigated within this Chapter involved the synthesis of copolymers of OEGMA and HEMA with branching *via* PDMSDMA. These terpolymers were to act as scaffolds for conjugation of atRA or Ibu *via* the HEMA component either to the monomer or after polymerisation. The synthesis of the amphiphilic branched terpolymer p(OEGMA-*co*-HEMA-*co*-PDMSDMA$_{(9)}$) was successfully achieved and the copolymer was soluble in SiO at 20 % (v/v). HEMA monomer was successfully functionalised with atRA and Ibu *via* Steglich esterifications; however, the ATRP of atRA-functionalised monomers failed due to retardation of the polymerisation by the antioxidant nature of atRA. A copolymer of p(IbuEMA-*co*-OEGMA) was successfully synthesised, however, when a branched structure was targeted, no appropriate solvent system could be found to solubilise all

the different components of the ATRP reaction and provide a controlled polymerisation. Post-functionalisation of p(HEMA) was then attempted but was unsuccessful in the case of atRA and only yielded 14 % product in the case of Ibu after 4 days.

Following the unsuccessful attempts to generate SiO-soluble polymer prodrugs, a focus on blends of SiO and amphiphilic polymers, as shown with the SiO blends containing PDMS-drug additives, was targeted. Branched architectures of p(OEGMA-co-PDMSDMA) were attempted via ATRP, but only the low molecular weight PDMSDMA branchers (M_n 395 and 1,275 gmol^{-1}) successfully led to branched architectures. This was initially considered to be a solubility issue when using of the longer PDMSDMA branchers, however, upon addition of THF to the ATRP polymerisation no improvement was observed. The solubility of the branched polymer architectures that had been successfully synthesised was investigated, but only low solubility within SiO was achieved (0.1 % v/v) even with p(OEGMA$_{15}$-co-PDMSDMA$_{(12)0.95}$) which contains the largest lipophilic component. To improve the content of PDMS within these target polymers, a new series of co- and terpolymer architectures were developed which incorporated the monofunctional PDMSMA within the OEGMA chains. Due to solubility issues of the catalytic system needed for ATRP, RAFT was employed and both linear and branched amphiphilic architectures were successfully synthesised which were highly soluble within SiO (40-50 % v/v). Unfortunately due to time constraints the solubility and release of atRA and Ibu in these amphiphilic polymer/SiO blends were not conducted.

4.6 REFERENCES

1. K. Matyjaszewski, S. Gaynor and J.-S. Wang, *Macromolecules*, 1995, **28**, 2093-2095.

2. C. J. Hawker, *Journal of the American Chemical Society*, 1994, **116**, 11185-11186.

3. J. Chiefari, Y. Chong, F. Ercole, J. Krstina, J. Jeffery, T. P. Le, R. T. Mayadunne, G. F. Meijs, C. L. Moad and G. Moad, *Macromolecules*, 1998, **31**, 5559-5562.

4. G. Moad, E. Rizzardo and S. H. Thang, *Accounts of Chemical Research*, 2008, **41**, 1133-1142.

5. A. Tardy, V. Delplace, D. Siri, C. Lefay, S. Harrisson, B. de Fatima Albergaria Pereira, L. Charles, D. Gigmes, J. Nicolas and Y. Guillaneuf, *Polymer Chemistry*, 2013, **4**, 4776-4787.

6. K. Matyjaszewski and J. Xia, *Chemical Reviews*, 2001, **101**, 2921-2990.

7. S. Perrier and P. Takolpuckdee, *Journal of Polymer Science Part A: Polymer Chemistry*, 2005, **43**, 5347-5393.

8. K. Matyjaszewski, J.-L. Wang, T. Grimaud and D. A. Shipp, *Macromolecules*, 1998, **31**, 1527-1534.

9. Y. Kotani, M. Kamigaito and M. Sawamoto, *Macromolecules*, 2000, **33**, 3543-3549.

10. N. K. Singha, B. de Ruiter and U. S. Schubert, *Macromolecules*, 2005, **38**, 3596-3600.

11. V. Percec, C. Grigoras and H.-J. Kim, *Journal of Polymer Science Part A: Polymer Chemistry*, 2004, **42**, 505-513.

12. H. Fischer, *Macromolecules*, 1997, **30**, 5666-5672.

13. M. Kato, M. Kamigaito, M. Sawamoto and T. Higashimura, *Macromolecules*, 1995, **28**, 1721-1723.

14. V. Percec, A. D. Asandei, F. Asgarzadeh, B. Barboiu, M. N. Holerca and C. Grigoras, *Journal of Polymer Science Part A: Polymer Chemistry*, 2000, **38**, 4353-4361.

15. K. Matyjaszewski, K. Davis, T. E. Patten and M. Wei, *Tetrahedron*, 1997, **53**, 15321-15329.

16. M. Long, D. W. Thornthwaite, S. H. Rogers, F. R. Livens and S. P. Rannard, *Polymer Chemistry*, 2012, **3**, 154-161.

17. K. Matyjaszewski, H.-J. Paik, P. Zhou and S. J. Diamanti, *Macromolecules*, 2001, **34**, 5125-5131.

18. J. Queffelec, S. G. Gaynor and K. Matyjaszewski, *Macromolecules*, 2000, **33**, 8629-8639.

19. T. E. Patten and K. Matyjaszewski, *Accounts of Chemical Research*, 1999, **32**, 895-903.

20. K. A. Davis, H.-j. Paik and K. Matyjaszewski, *Macromolecules*, 1999, **32**, 1767-1776.

21. J.-L. Wang, T. Grimaud and K. Matyjaszewski, *Macromolecules*, 1997, **30**, 6507-6512.

22. V. Percec, B. Barboiu and H. J. Kim, *Journal of the American Chemical Society*, 1998, **120**, 305-316.

23. A. Kajiwara, K. Matyjaszewski and M. Kamachi, *Macromolecules*, 1998, **31**, 5695-5701.

24. N. O'Brien, A. McKee, D. C. Sherrington, A. T. Slark and A. Titterton, *Polymer*, 2000, **41**, 6027-6031.

25. Y. Li and S. P. Armes, *Macromolecules*, 2005, **38**, 8155-8162.

26. P. A. Costello, I. K. Martin, A. T. Slark, D. C. Sherrington and A. Titterton, *Polymer*, 2002, **43**, 245-254.

27. F. Isaure, P. A. G. Cormack and D. C. Sherrington, *Journal of Materials Chemistry*, 2003, **13**, 2701-2710.

28. A. T. Slark, D. C. Sherrington, A. Titterton and I. K. Martin, *Journal of Materials Chemistry*, 2003, **13**, 2711-2720.

29. I. Bannister, N. C. Billingham, S. P. Armes, S. P. Rannard and P. Findlay, *Macromolecules*, 2006, **39**, 7483-7492.

30. A. R. Wang and S. Zhu, *Polymer Engineering & Science*, 2005, **45**, 720-727.

31. A. R. Wang and S. Zhu, *Journal of Polymer Science Part A: Polymer Chemistry*, 2005, **43**, 5710-5714.

32. N. M. B. Smeets, *European Polymer Journal*, 2013, **49**, 2528-2544.

33. D. J. Keddie, G. Moad, E. Rizzardo and S. H. Thang, *Macromolecules*, 2012, **45**, 5321-5342.

34. J. Skey and R. K. O'Reilly, *Chemical Communications*, 2008, 4183-4185.

35. J. Skey and R. K. O'Reilly, *Chemical Communications*, 2008, **35**, 4183-4185.

36. D. J. Keddie, *Chemical Society Reviews*, 2014, **43**, 496-505.

37. J. Chiefari, Y. K. Chong, F. Ercole, J. Krstina, J. Jeffery, T. P. T. Le, R. T. A. Mayadunne, G. F. Meijs, C. L. Moad, G. Moad, E. Rizzardo and S. H. Thang, *Macromolecules*, 1998, **31**, 5559-5562.

38. R. T. A. Mayadunne, E. Rizzardo, J. Chiefari, Y. K. Chong, G. Moad and S. H. Thang, *Macromolecules*, 1999, **32**, 6977-6980.

39. M. Destarac, D. Charmot, X. Franck and S. Z. Zard, *Macromolecular Rapid Communications*, 2000, **21**, 1035-1039.

40. R. Francis and A. Ajayaghosh, *Macromolecules*, 2000, **33**, 4699-4704.

41.   B. Klumperman, E. T. A. van den Dungen, J. P. A. Heuts and M. J. Monteiro, *Macromolecular Rapid Communications*, 2010, **31**, 1846-1862.

42.   G. Moad, E. Rizzardo and S. H. Thang, *Australian Journal of Chemistry*, 2005, **58**, 379-410.

43.   J. J. Vosloo, M. P. Tonge, C. M. Fellows, F. D'Agosto, R. D. Sanderson and R. G. Gilbert, *Macromolecules*, 2004, **37**, 2371-2382.

44.   J. F. Quinn, R. P. Chaplin and T. P. Davis, *Journal of Polymer Science Part A: Polymer Chemistry*, 2002, **40**, 2956-2966.

45.   Y.-z. You, C.-y. Hong, W.-p. Wang, P.-h. Wang, W.-q. Lu and C.-y. Pan, *Macromolecules*, 2004, **37**, 7140-7145.

46.   B. Liu, A. Kazlauciunas, J. T. Guthrie and S. Perrier, *Macromolecules*, 2005, **38**, 2131-2136.

47.   B. Liu, A. Kazlauciunas, J. T. Guthrie and S. Perrier, *Polymer*, 2005, **46**, 6293-6299.

48.   X. S. Wang, S. F. Lascelles, R. A. Jackson and S. P. Armes, *Chemical Communications*, 1999, **18**, 1817-1818.

49.   S. Perrier, S. P. Armes, X. S. Wang, F. Malet and D. M. Haddleton, *Journal of Polymer Science Part A: Polymer Chemistry*, 2001, **39**, 1696-1707.

50.   X. S. Wang, R. A. Jackson and S. P. Armes, *Macromolecules*, 2000, **33**, 255-257.

51.   T. He, D. J. Adams, M. F. Butler, A. I. Cooper and S. P. Rannard, *Journal of the American Chemical Society*, 2009, **131**, 1495-1501.

52.   K. L. Robinson, M. A. Khan, M. V. de Paz Báñez, X. S. Wang and S. P. Armes, *Macromolecules*, 2001, **34**, 3155-3158.

53.   K. Matyjaszewski, *Macromolecules*, 2012, **45**, 4015-4039.

54.   M. A. D. Gonçalves, V. D. Pinto, R. C. S. Dias and M. R. P. F. N. Costa, *Macromolecular Symposia*, 2010, **296**, 210-228.

55.   I. Bannister, N. C. Billingham and S. P. Armes, *Soft Matter*, 2009, **5**, 3495-3504.

56.   B. Reining, H. Keul and H. Höcker, *Polymer*, 1999, **40**, 3555-3563.

57.   J. Xia, S. G. Gaynor and K. Matyjaszewski, *Macromolecules*, 1998, **31**, 5958-5959.

58. K. Davis and K. Matyjaszewski, in *Advances in Polymer Science:Statistical, Gradient, Block and Graft Copolymers by Controlled/Living Radical Polymerisations*, Springer-Verlag, Heidelberg Germany, 2007, pp. 79-103.

59. A. Halim, T. D. Reid, J. M. Ren, Q. Fu, P. A. Gurr, A. Blencowe, S. E. Kentish and G. G. Qiao, *Journal of Polymer Science Part A: Polymer Chemistry*, 2014, **52**, 1251-1262.

60. S. Perrier, P. Takolpuckdee and C. A. Mars, *Macromolecules*, 2005, **38**, 2033-2036.

61. G. Moad and D. H. Solomon, *The Chemistry of Radical Polymerization*, Elsevier, Oxford, 2005.

CHAPTER 5

Conclusions and Future Work

5.1 CONCLUSIONS

The aim of this research was to investigate different methodologies to develop a sustained and controlled DDS to treat PVR *via* the use of a SiO tamponade acting as a drug reservoir. This was investigated by modifying the chemistries of both the drug and the SiO. The drugs chosen to be investigated throughout were atRA and Ibu.

The cytotoxic limits of both drugs were determined *via* MTT, resazurin, phalloidin and BrdU assays on ARPE-19 cells. The cytotoxic threshold was observed to be dependent on level of confluence and time of exposure. When both pre- and post-confluent cells were exposed to the drugs for 1 day the cytotoxic limit for atRA was determined to be 10^{-5} M, whilst the Ibu cytotoxic limit was higher and toxicity was observed at concentrations above 10^{-4} M. Upon 7 days exposure, cytotoxicity in the case of post-confluent cells was observed at the same concentrations; however, for pre-confluent cells the toxic limit decreased by a factor of ten for both atRA and Ibu to concentrations above 10^{-6} M and 10^{-5} M respectively. Subsequently, the cytotoxic limits determined were used to decide concentrations of drug used for loading and release studies.

To achieve a prolonged release of approximately 6 weeks, the desired clinical treatment period for PVR, prodrugs were investigated and solubilised in SiO with the aim that cleavage of the ester linkages, which bonded the drugs to the pro-moiety, would control the release. Initially a hydrophilic promoiety, PEO, was investigated and a number of prodrugs were successfully synthesised with various molecular weights and substitution number. The cytotoxicity of these prodrugs was investigated and it was found that PEO did not affect the cytotoxicity limits previously established. The cleavage of the drug from PEO was successfully completed without degradation of the drug; however, these studies were carried out in harsh conditions not representative of *in vivo* conditions. Due to SiO being a lipophilic environment, prodrug solubility was known to be a considerable challenge, however, the attachment of a lipophilic drug the PEO chain-ends was expected to modify solubility. Unfortunately this was not the case, and it was observed that the

drug concentrations that could be successfully achieved within SiO were not sufficient for a DDS to treat PVR.

A change of pro-moiety to PDMS was investigated in an attempt to improve solubility to provide post-cleavage side products that were chemically very similar to the surrounding SiO tamponade. The synthesis of PDMS prodrugs with both drugs was successful; however, drug cleavage *via* degradation of the ester bond was not readily achieved. It was hypothesised that this was due to a hydrophilicity/hydrophobicity issue of the prodrugs within the cleavage conditions and the synthesis of a tripartite PDMS prodrug with a PEO spacer between drug and PDMS supported this view.

Due to the unsuccessful cleavage of the PDMS prodrugs, they were then studied as additives to SiO to attempt to modify drug solubility and release. Biological evaluation of the PDMS prodrugs blended at 10 % (v/v) into SiO indicated no cytotoxicity at this concentration. Different methodologies were tested to investigate drug solubility in SiO; a protocol from the literature was followed which involved extraction of drug from the oil followed by UV-Vis spectroscopy analysis. While the solubility reported for atRA in SiO in the literature is 20 μg/mL, higher concentrations, in the order of 28 μg/mL, were measured when the same protocol was used. It was observed that the calibration curve used for UV-Vis spectroscopic analysis was in the range of 0.5×10^{-4} M to 1×10^{-6} M, with the reported 20 μg/mL saturation concentration of atRA (0.6×10^{-4} M) being on the cusp of the maximum value; therefore, higher concentrations need extrapolation from the curve, leading to potential errors. There were also issues with insufficient extraction of Ibu from SiO which was confirmed by ^{1}H NMR spectroscopy of the SiO, however ^{1}H NMR spectroscopy also has sensitivity limits at such low concentrations. The use of tritiated drugs allowed accurate solubility concentrations to be determined *via* liquid scintillation and a saturation concentration of atRA in SiO was established to be 20 times higher than that reported in the literature. Overall an accurate method to measure solubility of atRA and Ibu in SiO has been established using radiolabelling techniques and a fundamental inaccuracy in the published literature has been identified.

The presence of PDMS-atRA in SiO had a positive effect on atRA solubility, possibly due to the affinity of attached drug to free drug in the blend. PDMS-atRA also had a very positive effect on release, with the release period being independent of atRA starting concentration but dependant on the PDMS-atRA concentration in the blend. Excitingly, a prolonged release of atRA from a SiO blend with PDMS-atRA was observed for over 7 weeks. Unfortunately, the presence of PDMS-Ibu in a SiO blend did not have any significant effect on Ibu solubility, nor did it affect the release rates of Ibu from SiO.

Another strategy to develop a DDS for PVR that was investigated involved the synthesis of amphiphilic branched copolymers of OEGMA and HEMA with PDMSDMA. These polymers were to act as scaffolds for conjugation of atRA or Ibu *via* the HEMA component, by either pre-functionalisation of the monomer or post-functionalisation of the polymer. HEMA monomer was successfully functionalised with atRA and Ibu, however, the ATRP of atRA-functionalised monomers failed due to retardation of the polymerisation by the antioxidant nature of atRA. A linear copolymer containing IbuEMA and OEGMA was successfully synthesised, however no appropriate solvent system could be found to solubilise all the different components of the ATRP reaction and provide a controlled polymerisation when a divinyl monomer, PDMSDMA, was added. Post-functionalisation of p(HEMA) was then attempted but was inefficient for both drugs.

Amphiphilic branched copolymers were studied as additives to SiO with the aim to investigate the improvement of drug solubility using the hydrophilic and hydrogen-bonding environment (in this case OEGMA) within SiO. Branched architectures of p(OEGMA-*co*-PDMSDMA) were attempted *via* ATRP, but only the low molecular weight PDMSDMA branchers (M_n 395 and 1,275 gmol^{-1}) successfully led to branched architectures. The solubility of these branched polymer architectures was investigated, but only low solubility within SiO was achieved (0.1 % v/v) even with p(OEGMA$_{15}$-*co*-PDMSDMA$_{(12)0.95}$) which contains the largest lipophilic component. To improve the content of PDMS within these target polymers, a new series of co- and ter-polymer architectures were developed which incorporated the monofunctional PDMSMA within the OEGMA chains. Due to solubility issues of the catalytic system needed for ATRP, RAFT was employed and both linear and

branched amphiphilic architectures were successfully synthesised which were highly soluble within SiO (40-50 % v/v). Unfortunately, due to time constraints, studies of the solubility and release of atRA and Ibu in these amphiphilic polymer/SiO blends were not conducted.

5.2 FUTURE WORK

Further study into the cytotoxicity limits of the drugs could be carried out on ARPE-19 cells to determine a more precise toxicity limit with smaller increments than the ones studied within this project. The cell line chosen to evaluate the cytotoxic drug effects was ARPE-19, which is somewhat representative of RPE cells *in vivo,* however, there are many other cell types that the drug would come into contact with if the tamponade releasing DDS were to be used clinically. In the future it would be vital to carry out cytotoxicity studies on other cell types present within the eye, particularly those in the retina and involved in PVR such as retinal glial cells, but also others that would contact the DDS such as corneal endothelium cells. The use of primary cells, which may, in certain aspects, behave more like those *in vivo*, should also be used to confirm the important findings. *In vivo* studies using animal models would be the next step in moving the DDS towards the clinic.

Alternate linkers to ester bonds between drug and the pro-moiety of the pro-drug could be used. Anhydride bonds may be a good alternative, as they are more sensitive to hydrolysis and cleavage would be expected to occur more readily. Investigations on cleavage could be carried out for all linkages in more biologically-relevant conditions.

An exciting prospect of distinguishing a starting concentration of atRA within a 10% PDMS-atRA in SiO (v/v) which may lead to the burst release being below the toxic range but also allow the sustained release to be above the therapeutic level for an antiproliferative effect, was determined to be possible. Therefore, investigations into this starting concentration of atRA are required.

Whilst the synthesis of the modified HEMA monomer, IbuEMA, was successful, it was the lack of a suitable solvent system, capable of solubilising the different components of the ATRP reaction, which restricted this strategy. Later in the project

an alternate polymerisation method, RAFT, was utilised. Polymerisation of branched architectures of IbuEMA may be possible *via* the RAFT mechanism.

Finally, investigations into the synthesised amphiphilic branched copolymers which were successfully solubilised at a high concentrations (40-50 % v/v) within SiO could be conducted. An analogous approach to that described in PDMS-drug blends with respect to drug solubility and release may lead to options for further study. Biological evaluation of these polymers would also be crucial if they were to be used within a DDS for PVR.

CHAPTER 6

Experimental

6.1 CHARACTERISATION

6.1.1 NMR Spectroscopy

NMR spectra were recorded using a Bruker DPX-400 spectrometer operating at 400 MHz for ^{1}H NMR and 100 MHz for ^{13}C NMR in CDCl$_3$, D$_2$O, EtOH-*d6*, DMSO-*d6*, 1,4-Dioxane-*d8* and Acetone-*d6*.

6.1.2 Mass Spectrometry

Chemical ionisation (CI) and electrospray (ES) mass spectrometry data was recorded in the Mass Spectrometry Laboratory at the University of Liverpool. The CI-MS was obtained on an Agilent GCQTOF 7200 using methane CI gas. ES-MS was analysed using a MicroMass LCT mass spectrometer using electron ionisation and direct infusion syringe pump sampling.

6.1.3 Melting Point

Melting points were measured on an Optimelt Automatic Melting Point System (Stanford Research Systems) with 90 mm × 1 mm sample tubes.

6.1.4 High-Performance Liquid Chromatography (HPLC)

All solvents were analytical grade and purchased from Fisher. HPLC was run on a Dionex HPLC using an ODS 2 C18 column (100 mm x 4.6 mm i.d., 5 μm), sample size: 5 μL. The mobile phase consisted of 95 % ACN, 5 % MeOH and 0.6 % acetic acid. Elution peaks were monitored with a UV-Vis detector at 364 nm and subsequently analysed using Chromeleon v.6.8.software.

6.1.5 UV-Vis Spectroscopy

UV-Vis spectra were collected using a Thermo Fisher NanoDrop 2000c spectrophotometer, either with a quartz cuvette or directly with the nanodrop functionality of the equipment depending on the solvent used. Data was analysed using the NanoDrop2000 software.

6.1.6 Rheometry

All rheological measurements were carried out using a TA Instruments Rheolyst AR 1000 N controlled-stress rheometer (TA Instruments, Elstree, United Kingdom). A 40 mm diameter, 2° acrylic cone geometry was used. Temperature control of the rheometer is achieved *via* a plate that utilises the Peltier effect to control the temperature of the sample within ±0.1 °C. Shear viscosity was calculated from the gradient of the plot of shear stress against shear rate.

6.1.7 Scintillation Counter

ProSafe+ scintillation cocktail (Meidian Biotechnologies Ltd.) was used as received. All radiation measurements were carried out using a liquid scintillation counter (Packard Tri-carb 3100TR; Isotech).

Liquid scintillation counting relies upon the use of a scintillation cocktail which contain scintillators (materials which exhibit luminescence when excited by ionising radiation). The solvent molecules absorb energy emitted from beta particles (see Chapter 3 Section 3.4.1) and transfer this energy until it is transferred to a scintillant. The scintillant then emits photons following the energy absorption which are detectable by the scintillation counter.

6.1.8 Gel Permeation Chromatography (GPC)

Triple detection GPC was performed to measure molecular weights and molecular weight distributions using Malvern Viscotek instruments. One instrument was equipped with a GPCmax VE2001auto-sampler, two Viscotek D6000 columns (and a guard column) and a triple detector array TDA305 (refractive index, light scattering and viscometer) with a mobile phase of DMF containing 0.01 M lithium bromide at 60 °C and a flow-rate of 1 mL min^{-1}.

The second instrument was equipped with a GPCmax VE2001 autosampler, two Viscotek T6000 columns (and a guard column), a refractive index (RI) detector VE3580 and a 270 Dual Detector (light scattering and viscometer) with a mobile

phase of THF containing 2 v/v % of trimethylamine at 35 °C with a flow rate of 1 mL min^{-1}.

GPC determines molecular weight and molecular weight distributions by separating different polymeric chain length within a molecular weight distribution. This is performed by the use of columns which contain porous beads with different pore sizes. Larger polymeric materials cannot pass through the pores which results in a shorter path-length through the column and elute at earlier retention volumes. Whereas smaller polymeric materials pass through the porous beads so have a longer path-length through the column which results in later retention volumes. The triple detection system then uses RI, differential viscometry and light scattering detectors to calculate the absolute molecular weight of the polymer.

6.2 MATERIALS USED THROUGHOUT THE THESIS

atRA was purchased from Xian Bosheng Biological Technology Co., Ltd. and used as received. Ibu was purchased from Tokyo Chemical Industry UK Ltd. and used as received. SiO (technical grade, SiO$_{1000}$ and SiO$_{5000}$) was donated to the project by Fluron GmbH and used as received. All deuterated solvents were purchased from Aldrich apart from DMSO-d_6 which was purchased from Goss Scientific. All deuterated solvents were used as received except CDCl$_3$ where 0.1 % TMS was added. All solvents used were analytical grade and purchased from Fisher. Resazurin and (3-(4,5-dimethylthiazol-2-yl)-2,5-diphenyl tetrazolium bromide) (MTT) were purchased from Sigma and used as received. Alexa Fluor® 488 Phalloidin (Phalloidin) was purchased from Invitrogen and used as received.

6.3 CELL CULTURE

All cell culture was carried out under strict aseptic conditions in a class II laminar flow biological safety cabinet. All the cells cultured were incubated at 37 °C with a 5 % CO$_2$ atmosphere unless stated otherwise.

6.3.1 Cell Source

ARPE-19 cells are an established human cell line from a healthy 19 year old male donor which show many functional and characteristic properties of RPE cells *in vivo*. These cells were previously bought from American Type Culture Collection, Manassas, VA, USA, catalogue number CRL 2302, but were obtained from frozen stocks stored in-house for these experiments.

6.3.2 Media Preparation

The solutions used for media preparation throughout cell culture for this project are summarised in Table 6.1.

Table 6.1 Solutions used to prepare culture media for ARPE-19 cells.

Name	Abbreviation	Company	Catalogue Number
Dulbecco's Modified Eagle Medium/Ham's Nutrient Mixture F-12 Formulation	DMEM/F12	Sigma-Aldrich	D6421
Penicillin Strptomycin 10 mg/mL strptomycin in 0.9 % NaCl	Pen-Strep	Sigma-Aldrich	P0781
L-Glutamine 200mM	L-Glut	Sigma-Aldrich	G7513
Foetal Calf Serum	FCS	BioSera	S1900

Cells were cultured in a 1:1 (vol/vol) mixture of DMEM/F12 containing 1 % L-Glut , 1 % Pen-Strep, 1 % Fungizone and supplemented with 10 % FCS.

6.3.3 Cell Retrieval

ARPE-19 cells were stored in cryovials under liquid nitrogen in complete media with 10 % DMSO. To retrieve the cells, a cryovial was placed in a water bath at 37 °C then emptied into a universal tube containing pre-warmed media (15 mL), therefore, diluting the amount of DMSO. This was split evenly into 3x T75 flasks each containing an additional 7 mL of fresh media.

6.3.4 Cell Culture Maintenance/Seeding

Cells were fed twice weekly by replacing approximately 7 mL old media with 8 mL fresh medium, ensuring to examine cells using light microscopy to check for any abnormalities or preliminary infections. For these studies, cells were used between passages 8 and 24.

Cell subculture was carried out at around 80 % confluence, which usually occurred after 1 week. Culture medium, sterile Dulbecco's calcium and magnesium free phosphate buffered saline catalogue number P1447 from Sigma-Aldrich (PBS) and Trypsin-EDTA containing 5 g porcine trypsin and 2 g ethylenediaminetetraacetic acid from Sigma-Aldrich catalogue number T4174 (Tryspin) were all pre-warmed to 37 °C in a water bath. All media was removed from the flask then rinsed briefly with PBS (5 mL) to remove any serum which would inhibit trypsin activity. Trypsin-EDTA (5 mL) was added, and incubated at 37 °C for approximately 3 minutes until all the cells had lifted off the flask. Cells that were rounded but still attached were removed by gently agitating the flask. Media (5 mL) was added to inactivate and neutralise the trypsin reaction. For subculture 2.5 mL of this cell suspension was placed in a fresh flask with 9 mL fresh culture media. To seed samples for experiments, the cell suspension was pipetted into a centrifuge tube and spun at 1200 rpm/ 259 g for 5 minutes. The supernatant was removed and the cell pellet resuspended in media (1 mL). A haemocytometer was prepared by cleaning all surfaces with 70% ethanol and dried before the coverslip was centred. 20 μL of cell suspension was pipetted onto the top edge of the coverslip to allow the cells to enter the counting chamber. After cells were counted calculations were made to determine the volumes needed to obtain the desired seeding density for experimental procedures.

6.3.5 Cell Storage

The surplus ARPE-19 cells were frozen and stored in liquid nitrogen until needed. A cell pellet was obtained by following the procedure described in Section 6.2.4 then suspended in a solution of media with 10% DMSO. The cell suspension was transferred into a cryovial and placed in a Nagene freezing container at -80 °C

overnight then transferred into liquid nitrogen dewars where they were stored until required.

6.4 CHAPTER 2

6.4.1 Extraction of atRA from Media

0.3 mL of 1 M sodium acetate buffer (pH 4.0) was added to a culture medium and atRA solution (2 mL); samples were immediately vortex-mixed. Acetonitrile (3.6 mL) was added and samples centrifuged (5 minutes at 3,000 g and 4 °C); 100 μL of the clear supernatant was transferred to an auto-sampler vial and HPLC mobile phase (900 μL) added.

6.4.2 Cellular Assays

Multiple assays were carried out on ARPE-19 cells to study toxicity and antiproliferative effects of different drug concentrations. 8,000 cells/well were seeded in a 96 well tissue culture plate and left for 1 or 7 days to adhere to the plate and generate a cell monolayer. The 7 day samples were fed once within the week by replacing 150 μL old medium with 180 μL fresh culture medium. After the predetermined time period, the media was aspirated from all wells and replaced with spiked media (either 10^{-3} M to 10^{-10} M atRA, 10^{-3} M to 10^{-10} M Ibu or 1 – 20 % DMSO) then incubated for 1 to 7 days. Following this cell set-up the following assays could be performed.

6.4.2.1 MTT Assay

MTT was dissolved in PBS at 5 mg/mL, sterilised by filtration and stored at -20 °C. Stock MTT solution (10 μL per 100 μL medium) was added to wells of the assay apart from control wells of media alone and cells with media, plates were incubated at 37 °C for 4 hours. Acidified isopropanol (100 μl of 0.04 M HCl in isopropanol) was added to all wells and mixed thoroughly to dissolve the formazan crystals. After 15 minutes of further incubation cells plates were read on a μQuant spectrophotometer ($\lambda_{Measured}$ = 570 nm; $\lambda_{Reference}$ = 690 nm). The amount of absorbance is proportional to the mitochondrial activity of the cells; therefore,

toxicity can be deduced. All values were normalised to control wells on each plate which contained cells and culture medium.

6.4.2.2 Resazurin Assay

Resazurin was dissolved in PBS at 0.1 mg/mL and filtered to sterilize, stored at 4 °C in the dark. Stock resazurin solution (10 μL per 100 μL medium) was added to wells of the assay apart from control wells, plates were incubated at 37 °C for 4 hours. Media was removed and put in black 96-well plastic plates; resorufin fluorescence was read using a Biotek FLx800 spetrofluorometer ($\lambda_{Excitation}$ = 530 nm; $\lambda_{Emission}$ = 590 nm). All values were normalised to control wells on each plate which contained culture medium from cells.

6.4.2.3 Detecting Cell Morphology

In a 24 well tissue culture plate, cells were seeded at 25,000 cells/well then the same protocol as in Section 6.4.2 was followed. After incubation the media was discarded and the cells washed with PBS (500 μL) then fixed for 10 minutes in 10 % neutral buffered formalin (NBF; 10 % formalin, approximately 4 % formaldehyde). NBF was discarded and the cells washed again with PBS. A phalloidin solution was used to stain the F-actin of the cytoskeleton of the cell. A phalloidin solution was produced at 1 mg powder in 1.5 mL MeOH according to manufacturer's instruction. The solution was then diluted 1 in 100 (in fresh PBS) and 75 μL was placed in each well followed by 30 minutes of incubation at 4 °C. Phalloidin solution was removed and the cells washed with PBS.

4′,6-Diamidino-2-phenylindole dihydrochloride (DAPI, purchased from Invitrogen) was used to stain the nuclei of the cell. A stock solution of DAPI was made at 1:1,000 with PBS, then further diluted to a working solution of 1:10 PBS, 75 μL was placed in each well and incubated for 10 minutes at 4 °C. Cells were washed with PBS and placed under 500 μL PBS.

6.4.2.4 Cell Proliferation/Cell Counting

Table 6.2 Solutions required for BrdU incorporation.

Name	Abbreviation	Company	Catalogue Number	Working Solution
Dulbecco's calcium and magnesium free phosphate buffered saline	PBS	Sigma-Aldrich	P1447	1 tablet/100 mL distilled water
Bromodeoxyuridine solution	BrdU	Sigma-Aldrich	B9285	100 μM in PBS
Neutral buffered formalin	NBF	Sigma-Aldrich	HT501128	10 % Formalin ($\approx$ 4 % formaldehyde)
Triton X-100	Triton X	Sigma-Aldrich	X100	0.5 % Triton X in PBS
Hydrochloric acid	HCl	Sigma-Aldrich	SAJ1683	2 M
Goat serum	-	Sigma-Aldrich	G9023	1 % in PBS
Bovine serum albumin	BSA	Sigma-Aldrich	A2153	1 % in PBS
Mouse raised anti-BrdU	Primary anti-body solution	Abcam	ab8039	1:1,000 in 1 % BSA
Goat raised anti-mouse AlexFluor conjugated 594	Secondary anti-body solution	Invitrogen	A-11001	1:500 in 1 % BSA
Hoechst 33342	Hoechst	Invitrogen	H3570	2:10,000 in distilled water

Approximately 25,000 cells/well were seeded in a 24 well tissue culture plate and then the same protocol as Section 6.4.2 was followed. After incubation the media was removed and cells washed (3xPBS, 200 μL; 2 minutes/wash). This wash step was repeated after each incubation unless otherwise stated. BrdU (200 μL) was placed on cells and incubated at 37 °C for 4 hours. Cells were fixed for 10 minutes in 10% NBF then Triton-X (200μL) was added to cells followed by 15 minutes incubation at 4 °C. HCl (500 μL) was added to the cells and incubated for 30 minutes at 37 °C then washed 5xPBS (200 μL). The following steps were carried out on an orbital shaker in the dark at ambient temperature; again wash steps were carried out after each incubation period unless otherwise stated. Goat serum (200 μL) was added and incubated for 30 minutes, removed without washing, primary anti-body solution (200 μL) added and left for 2 hours. This was removed and the secondary

antibody solution (200 µL) added and incubated for 1 hour. Finally Hoechst (200 µL) was added and incubated for 30 minutes followed by a final wash. These samples were then stored under PBS (500 µL) in the dark at 4 °C for up to 7 days.

6.5 CHAPTER 3

6.5.1 Materials

Sodium sulphate (Na_2SO_4), sodium chloride (NaCl), sodium hydrogen sulphate ($NaHSO_4$), magnesium sulphate ($MgSO_4$), sodium hydrogen carbonate ($NaHCO_3$), potassium hydroxide (1 M) (KOH), sodium hydroxide (1 M) (NaOH) and hydrochloric acid (1 M) (HCl) were purchased from Fischer and used as received. Benzoic Acid (99.5 %), 1,1-carbonyl diimidazole ($\geq$97 %) (CDI), 4-(dimethylamino) pyridine (>99 %) (DMAP), N,N' – dicyclohexylcarbodiimide (>99 %) (DCC), poly(ethylene glycol) methyl ether (average M_n 750, 2,000 and 5,000 gmol^{-1}) (Me-PEO), poly(ethylene glycol) (average M_n 600, 1,000 and 2,000 gmol^{-1}), bis(hydroxyalkyl) terminated poly(dimethylsiloxane) (average M_n 4,700 gmol^{-1}), bis(3-aminopropyl) terminated poly(dimethyl siloxane) (average M_n 3,000 gmol^{-1}) and succinic anhydride (97%) were purchased from Sigma Aldrich and used as received. All solvents used were of analytical standard, obtained from Fischer and used as received.

6.5.2 PEO Prodrug Synthesis

6.5.2.1 General CDI Synthesis of Esters

Dry toluene (50 mL) was added to a 100 mL round-bottom flask containing a magnetic stirrer bar and fitted with a reflux condenser and N_2 inlet. CDI (1.459 g, 9 mmol) and either benzoic acid or atRA (10 mmol) were added and the mixture heated to 60 °C, purged with N_2 and stirred for 30 minutes. Alcohol either butanol or PEO (18 mmol) was added and the reaction mixture was stirred for a further 3 hours. The reaction mixture was then concentrated *in vacuo* and the remaining oil dissolved in DCM (5 mL) and washed three times with water (3x10 mL) and once with brine (10 mL). The solution was dried over Na_2SO_4, filtered and concentrated *in vacuo* to give the final product.

6.5.2.2 CDI Synthesis of PEO-atRA with Catalyst

Dry Toluene (7.5 mL) was added to a 100 mL round-bottom flask containing a magnetic stirrer bar and fitted with a reflux condenser and N_2 inlet. CDI (0.486 g, 3 mmol) and atRA (1 g, 3.33 mmol) were added and the mixture heated to 60 °C, purged with N_2 and stirred for 30 minutes. PEO (M_n 750 gmol^{-1}, 0.75 g, 1 mmol) and p-toluenesulfonic acid (0.19 g, 1 mmol) were added and the reaction mixture was stirred for a further 3 hours. The reaction was followed by TLC. The reaction mixture was concentrated *in vacuo* and the remaining oil dissolved in DCM (5 mL) and washed three times with water (3x10 mL) and once with brine (10 mL). The final solution was dried over Na_2SO_4, filtered and concentrated *in vacuo*.

6.5.2.3 Synthesis of PEO Prodrugs *via* a Steglich Esterification

PEO* (10 mmol OH) and DCM (20 mL) were added to a 50 mL round-bottom flask containing a magnetic stirrer bar and fitted with a N_2 inlet. 12 mmol of either atRA (0.33 g) or Ibu (0.247 g), along with DMAP (0.2 g, 1.67 mmol) were dissolved in degassed DCM (10 mL), then added to the mixture. DCC (2.75 g, 13 mmol) was dissolved in DCM (5 mL) then added dropwise to start the reaction under N_2. The mixture was stirred at ambient temperature for 22 hours for Ibu and up to 4 days for atRA in the dark. The DCU precipitate was removed by filtration and the solution was concentrated *in vacuo*. The resulting ester was isolated by precipitation from the minimum amount of THF into cold petroleum ether; yields above 50 % and above 90 % were observed for atRA and Ibu respectively.

PEO*: Me-PEO M_n 750, 2,500 and 5,000 gmol^{-1} and PEO M_n 600, 1,000, 2,000 gmol^{-1}.

PEO prodrugs were analysed by ^{1}H NMR. ^{1}H NMR (400 MHz, CDCl$_3$):

PEO-atRA: δ 7.01 (dod, 1H, CH-C$\underline{H}$=CH), 6.31 (m, 1H×2, C-C$\underline{H}$=CH and C=C$\underline{H}$-C(CH$_3$)), 6.15 (m, 1H×2, C=C$\underline{H}$-C(CH3)=C$\underline{H}$-CH, 5.80 (s, 1H, C(CH3)=C$\underline{H}$-C(O)O), 4.27 (m, 2H, O-CH$_2$-C$\underline{H}_2$-OCO), 3.73 (q, 2H, O-C$\underline{H}_2$-CH$_2$), 3.64 (t, 2H×3, C$\underline{H}_2$-O-C$\underline{H}_2$-C$\underline{H}_2$-O), 3.56 (t, 2H, CH$_2$-C$\underline{H}_2$-O), 3.38 (s, 3H O-C$\underline{H}_3$), 2.35 (s, 2H, CH-C(C$\underline{H}_3$)=CH) 2.02 (m, 1Hx2, CH-C$\underline{H}$-C(CH$_3$)=C), 1.72 (s, 3H, CH-C(C$\underline{H}_3$)=C), 1.62 (dod, 2H, CH$_2$-C$\underline{H}_2$-CH$_2$), 1.47 (d, 2H, CH$_2$-C$\underline{H}_2$-C(CH$_3$)$_2$), 1.03 (s, 3H×2, CH$_2$-C(C$\underline{H}_3$)$_2$-C).

PEO-Ibu: δ 7.21/7.10 (d, 2H×2, C$\underline{H}$ from aromatic ring), 4.21 (m, 2H×2, O-CH$_2$-C$\underline{H}_2$-OCO), 3.82 (q, 1H×2, OC(O)-C$\underline{H}$(CH$_3$)-C), 3.64 (t, 2H×3, O-C$\underline{H}_2$-CH$_2$-OCO), 3.38 (s,3H O-CH$_3$), 2.44 (d, 2H×2, C-C$\underline{H}_2$-CH(CH$_3$)$_2$), 1.84 (m, 1H×2, C-CH$_2$-C$\underline{H}$(CH$_3$)$_2$), 1.49 (d, 3H×2, OC(O)-CH(C$\underline{H}_3$)-C), 0.89 (d, 6H×2, C-CH$_2$-CH(C$\underline{H}_3)_2$).

atRA-PEO-atRA: δ 7.01 (dod, 1Hx2, CH-C$\underline{H}$=CH), 6.31 (m, 1H×4, C-C$\underline{H}$=CH and C=C$\underline{H}$-C(CH$_3$)), 6.15 (m, 1H×4, C=C$\underline{H}$-C(CH3)=C$\underline{H}$-CH, 5.80 (s, 1Hx2, C(CH3)=C$\underline{H}$-C(O)O), 4.27 (m, 2H, O-CH$_2$-C$\underline{H}_2$-OCO), 3.73 (q, 2H, O-C$\underline{H}_2$-CH$_2$), 3.64 (t, 2H×3, C$\underline{H}_2$-O-C$\underline{H}_2$-CH$_2$-O), 3.56 (t, 2H, CH$_2$-C$\underline{H}_2$-O), 2.35 (s, 2Hx2, CH-C(C$\underline{H}_3$)=CH) 2.02 (m, 1Hx4, CH-C$\underline{H}$-C(CH$_3$)=C), 1.72 (s, 3Hx2, CH-C(C$\underline{H}_3$)=C), 1.62 (dod, 2Hx2, CH$_2$-C$\underline{H}_2$-CH$_2$), 1.47 (d, 2Hx2, CH$_2$-C$\underline{H}_2$-C(CH$_3$)$_2$), 1.03 (s, 3H×4, CH$_2$-C(C$\underline{H}_3)_2$-C).

Ibu-PEO-Ibu: δ 7.21/7.10 (d, 2H×2, C$\underline{H}$ from aromatic ring), 4.21 (m, 2H×2, O-CH$_2$-C$\underline{H}_2$-OCO), 3.82 (q, 1H×2, OC(O)-C$\underline{H}$(CH$_3$)-C), 3.64 (t, 2H×3, O-C$\underline{H}_2$-CH$_2$-OCO), 2.44 (d, 2H×2, C-C$\underline{H}_2$-CH(CH$_3$)$_2$), 1.84 (m, 1H×2, C-CH$_2$-C$\underline{H}$(CH$_3$)$_2$), 1.49 (d, 3H×2, OC(O)-CH(C$\underline{H}_3$)-C), 0.89 (d, 6H×2, C-CH$_2$-CH(C$\underline{H}_3)_2$).

6.5.2.4 Analysis of PEO Esterification by External NMR Reference

^{1}H NMR samples of atRA and Ibu were prepared at a concentration of 10 mg/mL in a 2 mg/mL solution of DMSO-*d6* and anisole. Integrals were calibrated against anisole (7.23-7.35 ppm; aromatic C$\underline{H}$ next to C-O). Upon integration of the retinoates signal at 0.9-1.1 ppm (s, 3H×4, CH$_2$-C(C$\underline{H}_3)_2$-C) and the Ibu ester signal at 0.89 ppm (d, 3H×2, C-CH$_2$-CH(C$\underline{H}_3)_2$), the concentration of drug in ester was calculated. Concentration of drug in ester = (Integral of CH$_3$ ester x concentration of free drug NMR) / Integral of CH$_3$ in free drug.

6.5.3 Cleavage of PEO Prodrugs

In an NMR tube, 1 mL sample of PEO prodrug (0.20 mmol) in either D$_2$O, dioxane-*d8* or acetone-*d6* was prepared. NaOD or DCl was added at 0.01 to 0.2 equivalents per ester function. The mixture was incubated at 37 °C for up 7 days. ^{1}H NMR spectroscopy was used to follow cleavage progress.

6.5.4 Solubility of Drugs in SiO

6.5.4.1 atRA

A saturated solution of atRA (10-12 mg) in SiO (30 mL) was prepared and stirred gently in the dark, in a sealed flask, for approximately 2 weeks. Samples were taken at different time points over the 2 week period, filtered using a syringe pump (4 mL/h) and 0.45 μm PTFE filters. The drug was extracted from the SiO three times with acetone (1/2 v/v). The acetone layers were combined, the solvent was evaporated and the remaining solid was dried at ambient temperature. 2 mL of DMSO/H_2O (8/2) were used to solubilise the remaining solid. The samples were then analysed by UV-Vis. A standard curve previously determined for atRA (see Figure 6.1) was used to determine concentration values.

$y = 27431x + 0.0047$

$R^2 = 0.9987$
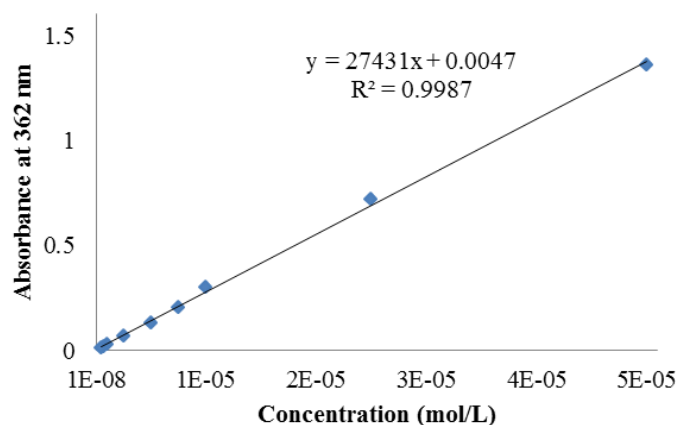
Figure 6.1 Calibration curve of atRA in DMSO/H_2O 8:2 from 5 x 10^{-5} – 5 x 10^{-7} M.

6.5.4.2 Ibu

A saturated solution of Ibu (60 mg) in SiO (30 mL) was prepared and stirred gently in a sealed flask for approximately 3 – 4 days. Samples were filtered using a syringe pump (4 mL/h) and 0.45 μm PTFE filters. The drug was extracted from the SiO three times with acetone (1/2 v/v). The acetone layers were combined, the solvent was evaporated and the remaining solid was dried at ambient temperature.

UV-Vis: 2 mL of PBS were used to solubilise the remaining solid. A standard curve previously determined for Ibu (see Figure 6.2) was used to determine concentration values.
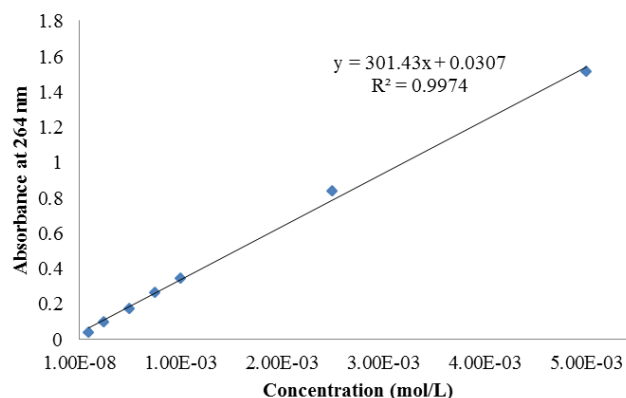
Figure 6.2 Calibration curve of Ibu in from $5 \times 10^{-3} - 1 \times 10^{-4}$ M.

^{1}H NMR: 0.2 mL of filtered oil was solubilised in 0.7 mL of CDCl$_3$ containing anisole (2 mg/mL), in a sample vial, then vortexed for 20 seconds. The mixture was then left to stand for approximately 30 minutes before being pipetted into a NMR tube.

6.5.5 Release of PEO-Ibu Prodrugs into Media

1 mL samples of oil saturated with Ibu ester (PEO-Ibu or Ibu-PEO-Ibu) was placed in several wells in a 24 well plate over 0.5 mL media. 0.2 mL of oil were taken daily from different wells using a 1mL syringe and analysed by ^{1}H NMR spectroscopy in CDCl$_3$ following the same protocol as in Section 6.5.2.4. Media was either left throughout the experiment or changed daily using a 1 mL syringe and 26 gauge needle as this was narrow enough not to take up any oil.

6.5.6 PDMS Prodrug Synthesis

6.5.6.1 atRA-PDMS-atRA

Bis(hydroxyalkyl) terminated poly(dimethylsiloxane), ($M_n = 4,700$ gmol^{-1}, 4 g, 1.7 mmol OH) was dissolved in degased DCM (10 mL), followed by the addition of a degased solution of atRA (0.6 g, 2 mmol) and DMAP (64 mg, 0.5 mmol) in DCM (30 mL). Finally 10 mL of a degased solution of DCC (0.41 g, 2 mmol) in DCM was added. This mixture was stirred at room temperature, under argon (Ar), in the dark, for 4 days. After filtration of the residual DCU, the solvent was eliminated under reduced pressure. The residual yellow oil was washed three times with cold methanol

then dried *in vacuo*. The purified yellow oil was filtered through a 0.45 μm PTFE filter, then stored under Ar in dark conditions at ambient temperature. atRA-PDMS-atRA was analyzed by ^{1}H NMR and FTIR. ^{1}H NMR (400 MHz, CDCl$_3$): δ 7.00 (q, 1H×2, =CH-C$\underline{\text{H}}$=CH), 6.29-6.11 (4H×2, =C$\underline{\text{H}}$-C-CH$_3$, -C$\underline{\text{H}}$=C-CH$_3$ and C-C$\underline{\text{H}}$=CH-C-CH$_3$), 5.82/5.69 (s, 1H×2, -OCOC$\underline{\text{H}}$=C), 4.26 (t, 2H×2, O-CH$_2$-C$\underline{\text{H}}_2$-OCO), 3.66 (t, 2H×2, O-C$\underline{\text{H}}_2$-CH$_2$-OCO), 3.44 (t, 2H×2, Si-CH$_2$-CH$_2$-C$\underline{\text{H}}_2$-O), 2.35 (s, 3H×2, C(C$\underline{\text{H}}_3$)=CH-C(O)O), 2.02 (t, 2H×2, C$\underline{\text{H}}_2$-C(CH$_3$)=C), 2.00 (s, 3H×2, C(C$\underline{\text{H}}_3$)=CH-CH=CH), 1.71 (s, 3H×2, CH$_2$-C(C$\underline{\text{H}}_3$)=C), 1.61 (m, 2H×2, 2H×2, Si-CH$_2$-C$\underline{\text{H}}_2$-CH$_2$-O, CH$_2$-C$\underline{\text{H}}_2$-CH$_2$-C(CH$_3$)=C), 1.47 (m, 2H×2, C$\underline{\text{H}}_2$-CH$_2$-CH$_2$-C(CH$_3$)=C), 1.02 (s, 6H×2, CH$_2$-C(C$\underline{\text{H}}_3$)$_2$-C), 0.54 (qt, 2H×2, Si-C$\underline{\text{H}}_2$-CH$_2$-CH$_2$-O), 0.07 (s, 6H×n, Si(C$\underline{\text{H}}_3$)$_2$-O). IR: 1,738 cm^{-1} $\upsilon_{(C=O)}$ in ester.

6.5.6.2 Ibu-PDMS-Ibu

Bis(hydroxyalkyl) terminated Poly(dimethylsiloxane)(M$_n$ = 4,700 gmol^{-1}, 4 g, 1.7 mmol OH), ibuprofen (0.4 g, 1.9 mmol) and DMAP (30 mg, 0.24 mmol) were dissolved in DCM (15 mL), followed by addition of a 10 mL DCC (0.4 g, 1.9 mmol) solution in DCM. This mixture was stirred at room temperature for 24 hours. After filtration of the residual DCU, the solvent was eliminated under reduced pressure. The residual colourless oil was washed two times with room temperature methanol then dried *in vacuo*. The purified oil was filtered through a 0.45 μm PTFE filter. Ibu-PDMS-Ibu was analyzed by ^{1}H NMR and FTIR. ^{1}H NMR (400 MHz, CDCl$_3$): δ 7.21/7.08 (d, 4H×2, C$\underline{\text{H}}$ from aromatic ring), 4.21 (m, 2H×2, O-CH$_2$-C$\underline{\text{H}}_2$-OCO), 3.73 (q, 1H×2, OC(O)-C$\underline{\text{H}}$(CH$_3$)-C), 3.57 (t, 2H×2, O-C$\underline{\text{H}}_2$-CH$_2$-OCO), 3.35 (t, 2H×2, Si-CH$_2$-CH$_2$-C$\underline{\text{H}}_2$-O), 2.43 (d, 2H×2, C-C$\underline{\text{H}}_2$-CH(CH$_3$)$_2$), 1.83 (m, 1H×2, C-CH$_2$-C$\underline{\text{H}}$(CH$_3$)$_2$), 1.57 (m, 2H×2, Si-CH$_2$-C$\underline{\text{H}}_2$-CH$_2$-O), 1.49 (d, 3H×2, OC(O)-CH(C$\underline{\text{H}}_3$)-C), 0.89 (d, 6H×2, C-CH$_2$-CH(C$\underline{\text{H}}_3$)$_2$), 0.50 (t, 2H×2, Si-C$\underline{\text{H}}_2$-CH$_2$-CH$_2$-O), 0.07 (s, 6H×n, Si(C$\underline{\text{H}}_3$)$_2$-O). IR: 1,738 cm^{-1} $\upsilon_{(C=O)}$ in ester.

6.5.6.3 Anhydride Route

6.5.6.3.1 Preparation of atRA Anhydride

atRA (2 g, 66 mmol) and DCC (1 g, 34 mmol) were dissolved in DCM (20 mL) and the reaction mixture was gently stirred at ambient temperature in the dark for 2 days.

After filtration of the mixture and removal of the DCM *in vacuo*, the final product was isolated with a 67 % yield and analysed by ^{1}H and ^{13}C NMR spectroscopy. ^{1}H NMR (400 MHz, CDCl$_3$): δ 7.00 (q, 1H×2, =CH-C$\underline{H}$=CH), 6.29-6.11 (4H×2, =C$\underline{H}$-C-CH$_3$, -C$\underline{H}$=C-CH$_3$ and C-C$\underline{H}$=C$\underline{H}$-C-CH$_3$), 5.82/5.69 (s, 1H×2, -OCOC$\underline{H}$=C), 2.35 (s, 3H×2, C(C$\underline{H}_3$)=CH-C(O)O), 2.02 (t, 2H×2, C$\underline{H}_2$-C(CH$_3$)=C), 2.00 (s, 3H×2, C(C$\underline{H}_3$)=CH-CH=CH), 1.71 (s, 3H×2, CH$_2$-C(C$\underline{H}_3$)=C), 1.61 (m, 2H×2, 2H×2, CH$_2$-C$\underline{H}_2$-CH$_2$-O, CH$_2$-C$\underline{H}_2$-CH$_2$-C(CH$_3$)=C), 1.47 (m, 2H×2, C$\underline{H}_2$-CH$_2$-CH$_2$-C(CH$_3$)=C), 1.02 (s, 6H×2, CH$_2$-C(C$\underline{H}_3$)$_2$-C). ^{13}C NMR (100 MHz, CDCl$_3$): δ 163 ($\underline{C}$=O), 156 ($\underline{C}$H$_2$-C(CH$_3$)=C), 141 (-C-$\underline{C}$(CH)=C-), 138 (C=$\underline{C}$(H)-C-), 137 (CH-$\underline{C}$(CH$_3$)=C-), 135 (CH=$\underline{C}$(H)-C-), 132 (C-$\underline{C}$(CH$_3$)=C-), 130 (C=$\underline{C}$H-C-, C), 118 (C=$\underline{C}$H-C(O)), 40 (C-$\underline{C}$H$_2$-C), 35 (C-$\underline{C}$(CH$_3$)$_2$), 34 (C-$\underline{C}$H$_2$-C=C), 29 (2 x CH$_3$ off ring), 22 (CH$_3$ off ring), 20 (CH$_2$-$\underline{C}$H$_2$-CH$_2$), 14 ($\underline{C}$H$_3$ chain), 13 ($\underline{C}$H$_3$ chain near C=O).

6.5.6.3.2 Preparation of atRA-PDMS-atRA

Poly(dimethylsiloxane) bis(hydroxyalkyl) terminated (M$_n$ = 4,700 gmol^{-1}, 3 g, 1.2 mmol OH) was dissolved in degased DCM (10 mL), followed by the addition of a degased solution of atRA anhydride synthesised in the previous step (1.06 g, 1.8 mmol) and DMAP (37 mg, 0.25 mmol) in DCM:Pyridine (30 mL 1:1 v/v). This mixture was stirred at room temperature, under Ar and in the dark for 4 days. After this time approximately 2 mL of water was added to quench the excess anhydride and the mixture was stirred for a further 2 hours. The product was purified by diluting the mixture with DCM (150 mL) and washing it with 1 M NaHSO$_4$ (3 x 150 mL), 1 M NaHCO$_3$ then brine (2 x 150 mL). The organic layer was dried over MgSO$_4$ and the solvent was removed *in vacuo*. The remaining oil was washed with MeOH (5 x 30 mL) to remove unattached atRA then dried *in vacuo*. The purified yellow oil was filtered through a 0.45 μm PTFE filter, then stored under Ar in dark conditions. atRA-PDMS-atRA was analyzed by ^{1}H NMR. ^{1}H NMR (400 MHz, CDCl$_3$): δ 7.00 (q, 1H×2, =CH-C$\underline{H}$=CH), 6.29-6.11 (4H×2, =C$\underline{H}$-C-CH$_3$, -C$\underline{H}$=C-CH$_3$ and C-C$\underline{H}$=C$\underline{H}$-C-CH$_3$), 5.82/5.69 (s, 1H×2, -OCOC$\underline{H}$=C), 4.26 (t, 2H×2, O-CH$_2$-C$\underline{H}_2$-OCO), 3.66 (t, 2H×2, O-C$\underline{H}_2$-CH$_2$-OCO), 3.44 (t, 2H×2, Si-CH$_2$-CH$_2$-C$\underline{H}_2$-O), 2.35 (s, 3H×2, C(C$\underline{H}_3$)=CH-C(O)O), 2.02 (t, 2H×2, C$\underline{H}_2$-C(CH$_3$)=C), 2.00 (s, 3H×2, C(C$\underline{H}_3$)=CH-CH=CH), 1.71 (s, 3H×2, CH$_2$-C(C$\underline{H}_3$)=C), 1.61 (m, 2H×2, 2H×2, Si-CH$_2$-C$\underline{H}_2$-CH$_2$-O, CH$_2$-C$\underline{H}_2$-CH$_2$-C(CH$_3$)=C), 1.47 (m, 2H×2, C$\underline{H}_2$-CH$_2$-

CH$_2$-C(CH$_3$)=C), 1.02 (s, 6H×2, CH$_2$-C(C$\underline{H}_3$)$_2$-C), 0.54 (qt, 2H×2, Si-C$\underline{H}_2$-CH$_2$-CH$_2$-O), 0.07 (s, 6H×n, Si(C$\underline{H}_3$)$_2$-O).

6.5.7 Cleavage of PDMS Prodrugs

6.5.7.1 Basic Conditions

PDMS-drug (70 mg) was dissolved in THF (2.3 mL). 0.2 mL of an aqueous solution of either KOH, NaOH or DMAP, containing either 2 or 5 equivalents per ester function was added. The solution was stirred at 40°C for up to 13 days. Then the reaction was stopped, DCM was added and the solution was washed with distilled water until neutral pH was obtained. The organic phase was recovered, dried over Na$_2$SO$_4$ and filtered. The solvent was eliminated under reduced pressure, and the recovered product was dried for few hours in a vacuum oven (40ºC), then analysed by ^{1}H NMR spectroscopy using CDCl$_3$.

6.5.7.2 Acidic Conditions

PDMS-drug (70 mg) was dissolved in either THF or dioxane (2.5 mL). The appropriate volume of a 1M HCl solution was added (5 to 10 equivalents per ester function). The solution was stirred at either 40°C or 60ºC in an oil bath, for up to 24 hours. Then the reaction was stopped, DCM was added and the solution was washed with distilled water until neutral pH was obtained. The organic phase was recovered, dried over Na$_2$SO$_4$ and filtered. The solvent was eliminated under reduced pressure, and the recovered product was dried for few hours in a vacuum oven (40ºC), then analyzed by ^{1}H NMR spectroscopy using CDCl$_3$.

6.5.8 Synthesis of PDMS-PEO Prodrug

HOOC-PDMS-COOH. Poly(dimethylsiloxane) bis(3-aminopropyl) terminated (H$_2$N-PDMS-NH$_2$) (3,000 gmol^{-1}, 1 g, 0.33 mmol) and succinic anhydride (84.5 mg, 0.84 mmol, 1.2 eq. per NH$_2$ function) were solubilized in DCM (10 mL). The reaction mixture was stirred at room temperature for 2 hours. HOOC-PDMS-COOH was obtained with 100% conversion as confirmed by ^{1}H NMR analysis (CDCl$_3$) of

the crude product. The crude solution was used straightaway without any treatment in the next step.

HO-PEO-PDMS-PEO-OH. DCC (137.5 mg, 0.66 mmol) was added to the HOOC-PDMS-COOH solution before it was added dropwise to a solution of PEO (600 gmol^{-1}, 8 g, 13.2 mmol, 20 eq. per COOH function) and DMAP (10 mg, 0.082 mmol, 1/8 eq) in DCM (20 mL). Once the slow addition was completed, the reaction was left to stir at room temperature. After 2 days, the DCU by-product was removed by filtration, the solvent was removed under vacuum and a white oil was recovered. The excess PEO was removed by extraction using diethyl ether and water. The extraction was repeated 3 times, then the organic phase was dried with Na_2SO_4, filtered, the solvent was then evaporated and the recovered product was dried under vacuum at 40°C for few hours. ^{1}H NMR (CDCl$_3$) confirmed the obtaining of the HO-PEO-PDMS-PEO-OH with 75% conversion and 18% yield.

Ibu-PEG-PDMS-PEG-Ibu. HO-PEO-PDMS-PEO-OH (5,350 gmol^{-1} and 1.5 OH function per chain, determined from ^{1}H NMR analysis) (0.12 g, 0.018 mmol) was solubilised in DCM (2 mL). Both Ibu (9 mg, 0.043 mmol, 1.2 eq per OH function) and DMAP (2 mg, 0.016 mmol) were added to the solution that was then stirred at room temperature. A solution of DCC (9 mg, 0.043 mmol) in DCM (1 mL) was added dropwise, and the reaction mixture was left to stir at room temperature. After 20 hours, the DCU by-product was removed by filtration, the solvent was removed under vacuum and a white solid was recovered. The obtained product was purified by extraction using DCM and water. The extraction was repeated 3 times, then the organic phase was dried with Na_2SO_4, filtered, the solvent was then evaporated and the recovered product was dried under vacuum at 40°C for few hours. ^{1}H NMR (CDCl$_3$) confirmed the obtaining of the Ibu-PEO-PDMS-PEO-Ibu final product with 100% conversion and 40% yield.

6.5.9 Cleavage of PDMS-PEO Prodrug

PDMS-PEG-Ibu (50 mg) was dissolved in dioxane-*d8* (1 mL). 0.2 mL of concentrated HCl were added to the solution which was then left to stir at 80 °C for 16 hours. ^{1}H NMR of the crude solution in dioxane-d8 confirmed the complete

cleavage of both ester functions (between PDMS and PEO, and between PEO and Ibu). DCM was added and the solution was washed with distilled water until neutral pH was obtained. The organic phase was recovered, dried over Na_2SO_4 and filtered. The solvent was eliminated under reduced pressure, and the recovered product dried for a few hours in a vacuum oven (40 °C), then analysed by ^1H NMR using $CDCl_3$, which evidenced the complete disappearance of PEO upon washings.

6.5.10 PDMS-atRA/PDMS-Ibu SiO Blends

Blends of PDMS-atRA or PDMS-Ibu and SiO_{1000} at 0.1, 1, 5 and 10% vol content of PDMS-drug were prepared and mixed in a sealed container (in the dark for PDMS-atRA blends) for approximately 4 days. Saturated solutions of either atRA or Ibu in their respective blends, i.e. PDMS-atRA/SiO_{1000} and PDMS-Ibu/SiO_{1000}, were then prepared as described below, using radiolabeled atRA and Ibu.

6.5.11 Radiolabeled Drugs

6.5.11.1 atRA Solubility in SiO

Saturated solutions of atRA in SiO were prepared by mixing atRA (11.6 mg) with tritiated atRA (10 µCi) in EtOH (2 mL); after evaporation of the solvent at ambient temperature, SiO_{1000} (5 mL) was added to the residual solid and the solution was stirred for 2 weeks. The sample was filtered using a syringe pump (4 mL/h) and 0.45 µm PTFE filters. Samples of the filtered oils (20 µL) were then solubilised in diethyl ether (8 mL) before scintillation cocktail (10 mL) was added. Radiation was then measured on the scintillation counter and saturation concentrations were determined.

Amounts of atRA added to the samples were altered depending on targeted final concentrations . Solutions of 100 µg/mL: atRA (0.5 mg) and tritiated atRA (3 µCi) were mixed in EtOH (2 mL) and the same protocol was followed. Solutions of 20 µg/mL: atRA (0.1 mg) and tritiated atRA (2 µCi) were mixed in EtOH (2 mL) and the same procedure was carried out.

6.5.11.2 Ibu Solubility in SiO

Saturated solutions of Ibu in SiO were prepared by mixing Ibu (32 mg) with tritiated Ibu (10 μCi) in EtOH (2 mL); after evaporation of the solvent at ambient temperature, SiO_{1000} (5 mL) was added to the residual solid and the solution was stirred for 1 week. The sample was filtered using a syringe pump (4 mL/h) and 0.45 μm PTFE filters. Samples of the filtered oils (20 μL) were then solubilised in diethyl ether (8 mL) before scintillation cocktail (10 mL) was added. Radiation was then measured on the scintillation counter and saturation concentrations were determined.

Solutions of 100 μg/mL: Ibu (0.5 mg) and tritiated Ibu (3 μCi) were mixed in EtOH (2 mL) and the same protocol was followed. Solutions of 20 μg/mL: Ibu (0.1 mg) and tritiated Ibu (2 μCi) were mixed in EtOH (2 mL) and the same procedure was carried out.

6.5.11.3 atRA/Ibu Solubility in PDMS-atRA/PDMS-Ibu SiO Blends

The same protocol as in the previous sections (6.5.11.1 and 6.5.11.2) was followed for the preparation of both atRA and Ibu solutions in their respective blends, i.e. PDMS-atRA/SiO_{1000} and PDMS-Ibu/SiO_{1000} (0.1, 1, 5 and 10% vol content of PDMS-drug). Saturated solutions were prepared as well as solutions with alternate concentrations.

6.5.11.4 Release of Drug from SiO and SiO Blends into Media

1 mL of SiO or blend with determined concentration of drug was placed in a 24 well plate over 0.5 mL media. Samples of media (0.5 mL) were taken and replaced daily using a 1 mL syringe and 26 gauge needle. Media (250 μL) was mixed with scintillation cocktail (10 mL) and analysed by liquid scintillation counting.

6.6 CHAPTER 4

6.6.1 Materials

Poly (ethylene glycol) methyl ether methacrylate (average M_n 300 gmol^{-1}) (98%) (OEGMA), (hydroxyethyl) methacrylate (98%) (HEMA), α-bromoisobutyryl

bromide (98%) (EBrIB), 2,2'-bipyridyl (>99%) (bpy), Copper (I) Chloride (Cu(I)Cl) (97%), 2-cyano-2-propyl benzodithioate (97%) (CPBD) and 2,2'-azobis(2-methylpropionitrile) (98%) (AIBN) were purchased from Sigma Aldrich and used as received. Mono methacryloxypropyl polydimethylsiloxane methacrylate (molecular weight 985 and 4,600 gmol^{-1}) (PDMSMA) and methacryloxypropyl polydimethylsiloxane dimethacrylate (molecular weight 390, 4,460 and 21,250 gmol^{-1}) (PDMSDMA) were purchased from Gelest and used as received. Activated aluminum oxide (neutral) was also purchased from Sigma Aldrich and used as received.

6.6.2 ATRP

All ATRP polymerisations were conducted at a constant ratio to initiator bromine atoms of [Br]:[Cu(I)Cl]:[Bpy] = 1:1:2.

6.6.2.1 Linear Polymerisation: p(OEGMA)

In a typical synthesis, targeting DP_n = 30 monomer units, OEGMA (5 g, 17 mmol), EBrIB (0.11 g, 0.55 mmol) and bpy (0.17 g, 1.09 mmol) were added to a 25 mL round-bottomed flask equipped with a magnetic stirrer bar. IPA/H$_2$O (92.5/7.5, 5.1 mL, 55 wt.% with respect to monomer; deoxygenated *via* Ar purge) was added and the resulting solution was purged with Ar for 15 minutes. Cu(I)Cl (54.99 mg, 0.55 mmol) was rapidly added to the flask whilst maintaining a positive Ar flow, instantly forming a brown mixture. The reactor was submerged into an oil bath pre-heated to 30 °C, and left to stir. The polymerisation was stopped by cooling the flask to ambient temperature, exposing its contents to air and diluting the reaction medium with THF forming a blue mixture. The polymer solution was passed through a neutral alumina column to remove the catalyst using THF as the mobile phase. The solution was concentrated by rotary evaporation and precipitated into cold petroleum-ether (40-60) to give a white solid. The sample was dried under vacuum at 40 °C for 24 hours and analysed by ^{1}H NMR in D$_2$O and GPC with a mobile phase of DMF.

6.6.2.2 Linear Copolymerisation: p(OEGMA-*co*-HEMA)

In a typical synthesis, targeting DP_n = 30 monomer units (50/50 OEGMA/HEMA), OEGMA (2.5 g, 8.33 mmol), HEMA (1.09 g, 8.33 mmol), EBrIB (0.11 g, 0.55 mmol) and bpy (0.17 g, 1.09 mmol) were added to a 25 mL round-bottomed flask equipped with a magnetic stirrer bar. IPA/H_2O (92.5/7.5, 3.6 mL, 55 wt % wrt. monomer; deoxygenated *via* Ar purge) was added and the resulting solution was purged with Ar for 15 minutes. Cu(I)Cl (54.99 mg, 0.55 mmol) was rapidly added to the flask whilst maintaining a positive Ar flow, instantly forming a brown mixture. The reactor was submerged into an oil bath pre-heated to 30 °C, and left to stir. The polymerisation was stopped by cooling the flask to ambient temperature, exposing its contents to air and diluting the reaction medium with MeOH forming a blue mixture. The polymer solution was passed through a neutral alumina column to remove the catalyst using MeOH as the mobile phase. The solution was concentrated by rotary evaporation and precipitated into cold petroleum-ether (40-60) to give a white solid. The sample was dried under vacuum at 40 °C for 24 hours and analysed by ^{1}H NMR in MeOH-*d3* and GPC with a mobile phase of DMF.

6.6.2.3 Branched Polymerisation: p(OEGMA-*co*-HEMA-*co*-PDMSDMA)

In a typical synthesis, targeting DP_n = 30 monomer units (50/50 OEGMA/HEMA), OEGMA (2.5 g, 8.33 mmol), HEMA (1.09 g, 8.33 mmol), PDMSDMA (M_n 390 gmol^{-1}, 0.21 g, 0.53 mmol; 0.95 equiv. relative to initiator), EBrIB (0.11 g, 0.55 mmol) and bpy (0.17 g, 1.09 mmol) were added to a 25 mL round-bottomed flask equipped with a magnetic stirrer bar. IPA/H_2O (92.5/7.5, 3.6 mL, 55 wt % wrt. monomer; deoxygenated *via* Ar purge) was added and the resulting solution was purged with Ar for 15 minutes. Cu(I)Cl (54.99 mg, 0.55 mmol) was rapidly added to the flask whilst maintaining a positive Ar flow, instantly forming a brown mixture. The reactor was submerged into an oil bath pre-heated to 30 °C, and left to stir. The polymerisation was stopped by cooling the flask to ambient temperature, exposing its contents to air and diluting the reaction medium with $CHCl_3$ forming a blue mixture. The polymer solution was passed through a neutral alumina column to remove the catalyst using $CHCl_3$ as the mobile phase. The solution was concentrated by rotary evaporation and precipitated into cold petroleum-ether (40-60) to give a white solid. The sample was dried under vacuum at 40 °C for 24 hours and analysed by ^{1}H NMR spectroscopy in $CDCl_3$ and GPC with a mobile phase of THF.

6.6.2.4 Kinetic Studies

Kinetic studies (i.e. plots $\ln([M]_0/[M]) = f$ (conversion)) were performed by taking samples from the reaction medium under positive pressure of Ar and analysing them by ^{1}H NMR spectroscopy (with anisole as an internal reference) and GPC. The monomer conversion was determined by ^{1}H NMR; the vinyl protons of the residual monomer located at 6.08 and 5.65 ppm were integrated and compared to the integrated values of the anisole aromatic peaks (6.97 and 7.32 ppm). This allowed the conversion to be estimated using the following equation:

$$\text{Conversion} = [1 - (2*I_1/I_2)]*100$$

where I_1 and I_2 are the integrals of the NMR signals at 5.6 (or 6.08 ppm) and 6.97 ppm. The catalytic system was removed from the kinetic samples prior to GPC analysis by passing them through a neutral alumina column.

6.6.3 Monomer Functionalisation

DCM (20 mL) and HEMA (5 g, 38.42 mmol) were added to a 50 mL round-bottom flask containing a magnetic stirrer bar and fitted with a N_2 inlet. atRA or Ibu (42.26 mmol) and DMAP (0.94 g, 7.68 mmol) were dissolved in DCM (10 mL) and added to the mixture. DCC (8.72 g, 42.26 mmol) was dissolved in DCM (5 mL) and added to start the reaction. The mixture was stirred at ambient temperature for 48 hours, in the dark for atRA. The precipitated DCU by-product was removed by filtration. The product was isolated by diluting the mixture with DCM and washing it twice with water to remove the unreacted HEMA and twice with 1 M $NaHSO_4$ to remove the DMAP catalyst. The organic layer was dried over $MgSO_4$ and evaporated to dryness. A purified product was then obtained following column chromatography (silica gel, eluting hexane increasing to hexane/ethyl acetate 50/50) and analysed by ^{1}H NMR (400 MHz, CDCl$_3$ atRAEMA and MeOD IbuEMA).
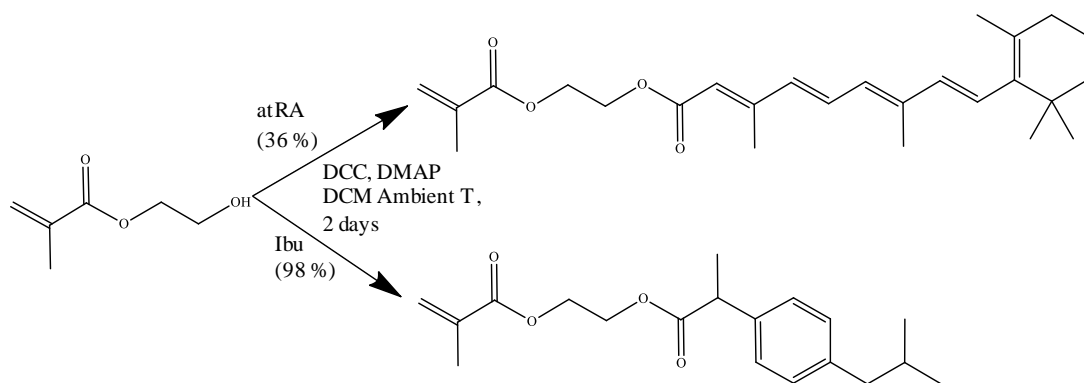
Scheme 6.1 Steglich esterification of both atRA and Ibu with HEMA monomer.

atRAEMA: δ 7.01 (dod, 1H, CH-C$\underline{H}$=CH), 6.29 (m, 1H×2, C-C$\underline{H}$=CH and C=C$\underline{H}$-C(CH$_3$)), 6.14 (m, 1H×2, C=C$\underline{H}$-C(CH3)=C$\underline{H}$-CH and 1H, C$\underline{H}_2$=C(CH$_3$) 5.79 (s, 1H, C(CH3)=C$\underline{H}$-C(O)O), 5.59 (s, 1H C$\underline{H}_2$=C(CH$_3$)), 4.37 (m, 2Hx2, O-CH$_2$-C$\underline{H}_2$-OCO), 2.35 (s, 3H, CH-C(C$\underline{H}_3$)=CH) 2.02 (m, 1Hx2, CH-C$\underline{H}$-C(CH$_3$)=C), 1.95 (s, 3H, CH$_2$=C(C$\underline{H}_3$)) 1.72 (s, 3H, CH-C(C$\underline{H}_3$)=C), 1.62 (dod, 2H, CH$_2$-C$\underline{H}_2$-CH$_2$), 1.47 (d, 2H, CH$_2$-C$\underline{H}_2$-C(CH$_3$)$_2$), 1.03 (s, 3H×2, CH$_2$-C(C$\underline{H}_3$)$_2$-C).

IbuEMA: δ 7.08/6.97 (d, 2H×2, C$\underline{H}$ from aromatic ring), 5.88/5.46 (s, 1Hx2, C$\underline{H}_2$=C(CH$_3$)), 4.74 (m, 2Hx2, O-CH$_2$-C$\underline{H}_2$-OCO), 3.63 (q, 1H, OC(O)-C$\underline{H}$(CH$_3$)-C), 2.32 (d, 2H, C-C$\underline{H}_2$-CH(CH$_3$)$_2$), 1.74 (m, 1H, C-CH$_2$-C$\underline{H}$(CH$_3$)$_2$) and 3H, CH$_2$=C(C$\underline{H}_3$)), 1.34 (d, 3H×2, OC(O)-CH(C$\underline{H}_3$)-C), 0.79 (d, 6H, C-CH$_2$-CH(C$\underline{H}_3$)$_2$).

6.6.4 Postfunctionalisation of p(HEMA)

Toluene (20 mL) and p(HEMA) (0.5 g, 0.13 mmol) were added to a 50 mL round-bottom flask containing a magnetic stirrer bar, fitted with a N_2 inlet and heated to 40 °C. atRA or Ibu (4.55 mmol) and DMAP (0.159 g, 1.3 mmol) were dissolved in degased toluene (10 mL) and added to the mixture. DCC (0.939 g, 4.55 mmol) was dissolved in degased toluene (5 mL) and added dropwise to start the reaction. The mixture was stirred at ambient temperature for 4 days, in the dark for atRA. The precipitated DCU by-product was removed by filtration. The liquid was concentrated *in vacuo* and the resulting ester was isolated by precipitation from the minimum amount of MeOH into ethyl acetate and analysed by ^{1}H NMR (400 MHz, CDCl$_3$).

6.6.5 RAFT

All RAFT polymerisations were conducted at a constant ratio of chain transfer agent to initiator [CPBD]:[AIBN] = 1:0.2.

6.6.5.1 Linear Polymerisation: p(OEGMA)

In a typical synthesis, targeting DP_n = 60 monomer units, AIBN (2.7 mg, 0.016 mmol), CPBD (18.4 mg, 0.083 mmol) and OEGMA (1.5 g, 5 mmol) were added to a 25 mL Schlenk tube equipped with a magnetic stirrer bar. ^{t}BuOH (4.5 mL, 30 wt % wrt. monomer, deoxygenated *via* N_2 purge) was added and the resulting solution degassed by five cycles of freeze/pump/thaw. After the final thaw cycle, the flask was backfilled with N_2. The reaction flask was placed into a pre-heated oil bath (70 °C) and stirred for 8 hours, after which the reaction medium was observed to be slightly turbid. The polymerization was stopped by cooling the flask to ambient temperature, exposing its contents to air and diluting the reaction medium with ^{t}BuOH. The solution was concentrated by rotary evaporation and precipitated into cold petroleum-ether (40-60) to give a pink solid. The sample was dried under vacuum at 40 °C for 24 hours and analysed by ^{1}H NMR in D_2O and GPC with a mobile phase of DMF.

6.6.5.2 Linear Polymerisation p(OEGMA-*co*-PDMSMA)

In a typical synthesis, targeting DP_n = 60 monomer units (OEGMA/PDMSMA 50/50), AIBN (2.7 mg, 0.016 mmol), CPBD (18.4 mg, 0.083 mmol), OEGMA (0.148 g, 0.492 mmol) and PDMSMA (M_n 985 gmol^{-1}, 1.5 g, 1.524 mmol) were added to a 25 mL Schlenk tube equipped with a magnetic stirrer bar. ^{t}BuOH (4.96 mL, 30 wt % wrt. monomer, deoxygenated *via* N_2 purge) was added and the resulting solution degassed by five cycles of freeze/pump/thaw. After the final thaw cycle, the flask was backfilled with N_2. The reaction flask was placed into a pre-heated oil bath (70 °C) and stirred for 24 hours, after which the reaction medium was observed to be slightly turbid. The polymerisation was stopped by cooling the flask to ambient temperature, exposing its contents to air and diluting the reaction medium with ^{t}BuOH. The solution was concentrated by rotary evaporation and precipitated into

cold MeOH to give a pink liquid. The sample was dried under vacuum at 40 °C for 24 hours and analysed by ^{1}H NMR in CDCl$_3$ and GPC with a mobile phase of THF.

6.6.5.3 Branched Polymerisation: p(OEGMA-*co*-PDMSMA-*co*-PDMSDMA)

In a typical synthesis, targeting DP$_n$ = 60 monomer units (OEGMA/PDMSMA 50/50), AIBN (5.6 mg, 0.034 mmol), CPBD (37.5 mg, 0.169 mmol), OEGMA (1.524 g, 5 mmol), PDMSMA (M$_n$ 985 gmol^{-1}, 5 g, 5 mmol) and PDMSDMA (M$_n$ 1,275 gmol^{-1}, 0.205g, 0.158 mmol) were added to a 100 mL Schlenk tube equipped with a magnetic stirrer bar. ^{t}BuOH (20.3 mL, 30 wt % wrt. monomer, deoxygenated *via* N$_2$ purge) was added and the resulting solution degassed by five cycles of freeze/pump/thaw. After the final thaw cycle, the flask was backfilled with N$_2$. The reaction flask was placed into a pre-heated oil bath (70 °C) and stirred for 24 hours, after which the reaction medium was observed to be slightly turbid. The polymerization was stopped by cooling the flask to ambient temperature, exposing its contents to air and diluting the reaction medium with ^{t}BuOH. The solution was concentrated by rotary evaporation and precipitated into MeOH) to give a pink liquid. The sample was dried under vacuum at 40 °C for 24 hours and analysed by ^{1}H NMR spectroscopy in CDCl$_3$ and GPC with a mobile phase of THF.

6.6.5.4 CTA Removal from p(PDMS$_{(9)48}$-*co*-OEGMA$_{12}$)

A ratio of polymer:AIBN = 1:20 was used. p(PDMS$_{(9)48}$-*co*-OEGMA$_{12}$) (5.3811 g, 0.112 mmol) was dissolved in toluene (73 mL, deoxygenated *via* Ar purge) in a 100 mL schlenk flask equipped with a stirrer bar. AIBN (369 mg, 2.24 mmol) was added to the reaction flask and purged with Ar. The temperature was raised to 80 °C for 2.5 hours. After the reaction with AIBN, the polymer was precipitated in cold MeOH and a white liquid was isolated by decanting the MeOH. The product was dried in *vacuo* then analysed by ^{1}H NMR spectroscopy in CDCl$_3$.

6.6.6 Solubility of Polymers in SiO

6.6.6.1 p(OEGMA-*co*-HEMA) Linear and Branched

In a typical solubilisation experiment, p(OEGMA-*co*-HEMA) copolymer (1 mL) and SiO_{1000} (1 mL) were syringed into a glass vial to create a 50 v/v % mixture and placed on a roller for 3 days. The solutions were diluted systematically by adding SiO_{1000} to decrease the amount of polymer by 10 v/v%, rolled for 3 days each time, until a soluble concentration was reached (i.e. 40, 30, 20, 10 and also 5 and 1 v/v% were tested).

6.6.6.2 p(OEGMA-*co*-PDMSDMA) Branched

Blends of the amphiphilic $p(OEGMA_{15})$ branched with both PDMSDMA M_n 390 and 1,275 $gmol^{-1}$ (m = 1 and 12 respectively) at 0.1, 1, 5 and 10 % (v/v) in SiO_{1000} were made. The blends were stirred at ambient temperature for 2 days without any change, then placed at 37 °C for 2 days and stirred at ambient temperature for a further 3 days. No change occurred, no solubility was observed. THF (5 mL) was added to solubilise the mixtures which were then left covered overnight. THF was allowed to evaporate over 7 days by stirring the blends in a fume cupboard at ambient temperature.

6.6.6.3 p(OEGMA-*co*-PDMSMA) Linear and Branched

Same methodology as 6.6.4.1 was used.

APPENDIX
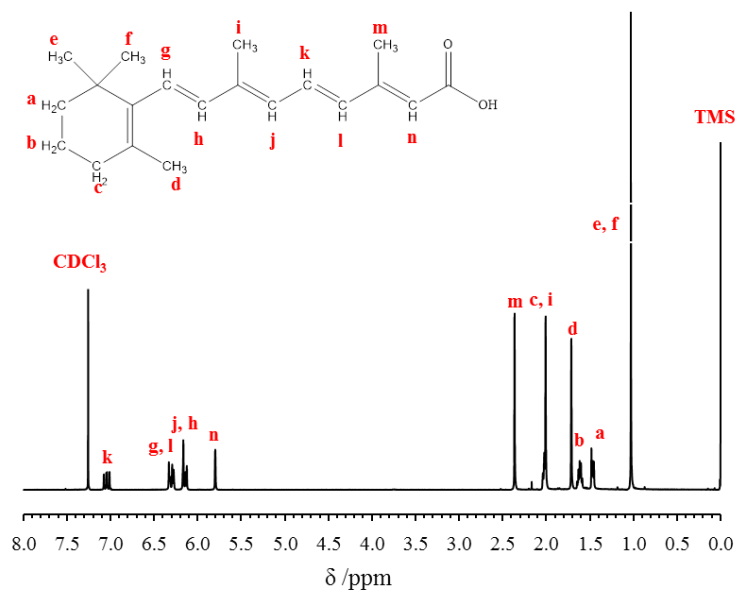
Figure A1 ^{1}H NMR (CDCl$_3$, 400 MHz) of atRA. 3.5 years after receipt.
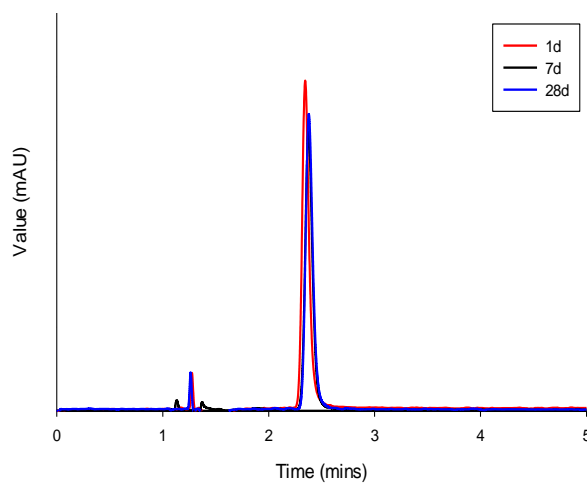
Figure A2 HPLC of atRA stored at -20 °C in the dark under Argon.
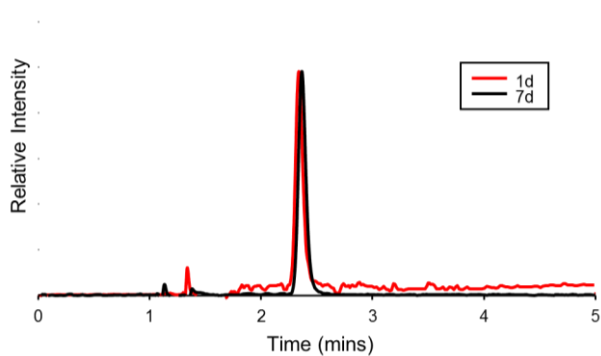
Figure A3 HPLC of atRA stored at ambient temperature in light under Argon after 1 and 7 days.
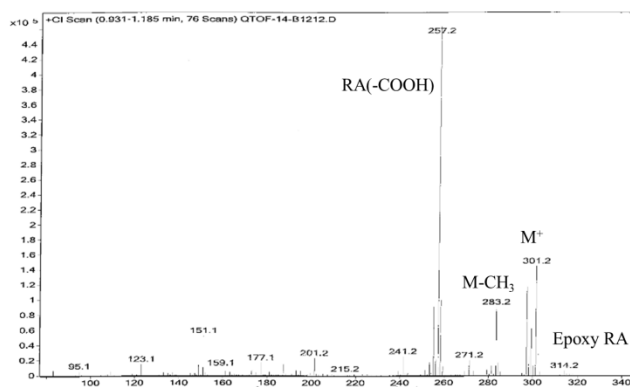
Figure A4 CI-MS of atRA stored at ambient temperature in light under Argon after 7 days.
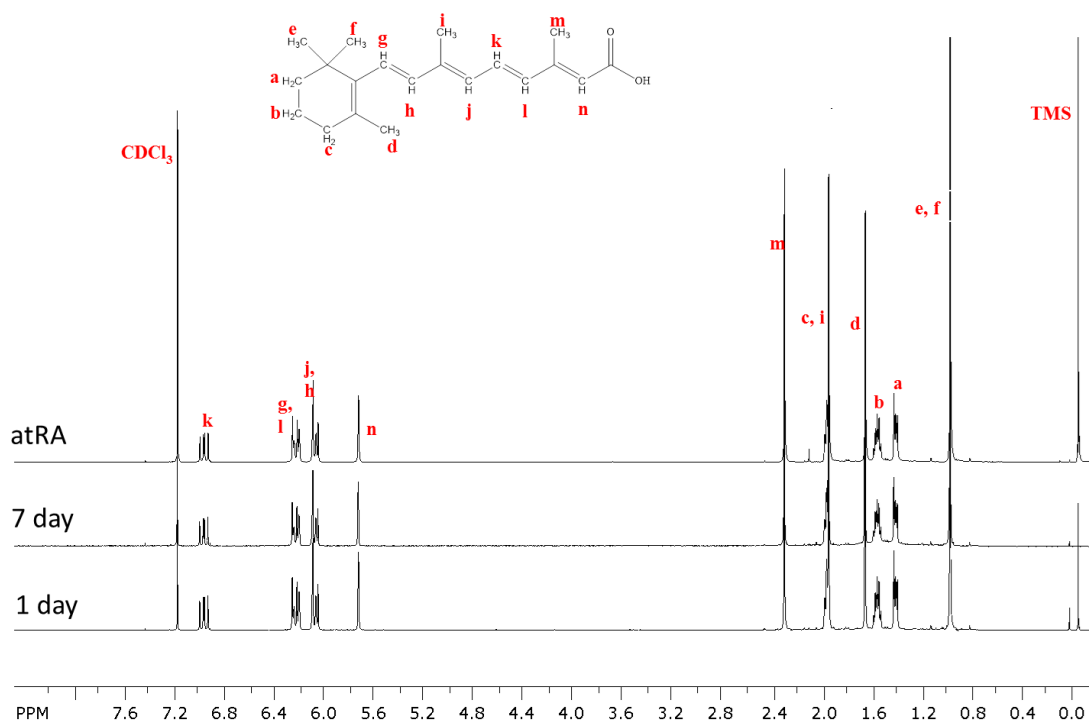
Figure A5 ^{1}H NMR (CDCl$_3$, 400 MHz) of atRA stored at ambient temperature in light under Argon after 1 and 7 days with atRA reference spectra.
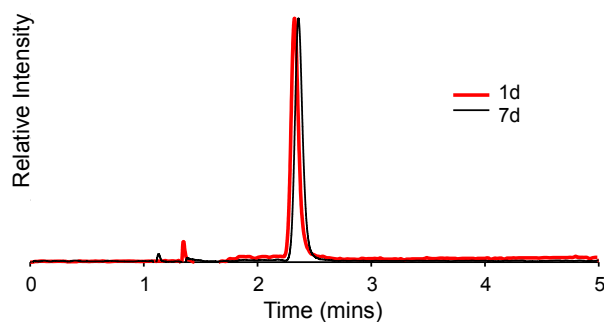
Figure A6 HPLC of atRA stored at ambient temperature in light and air after 1 and 7 days.
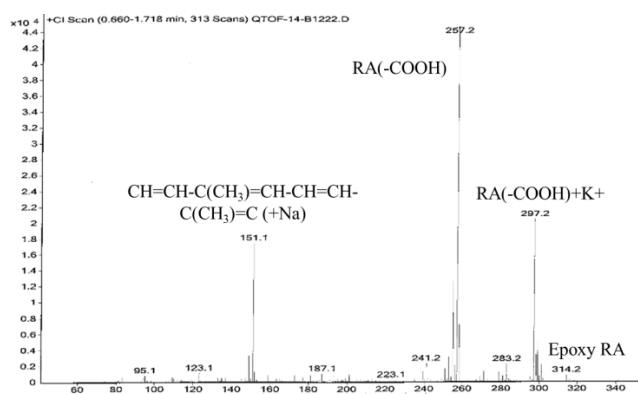
Figure A7 CI-MS of atRA stored at ambient temperature in light in air after 7 days.
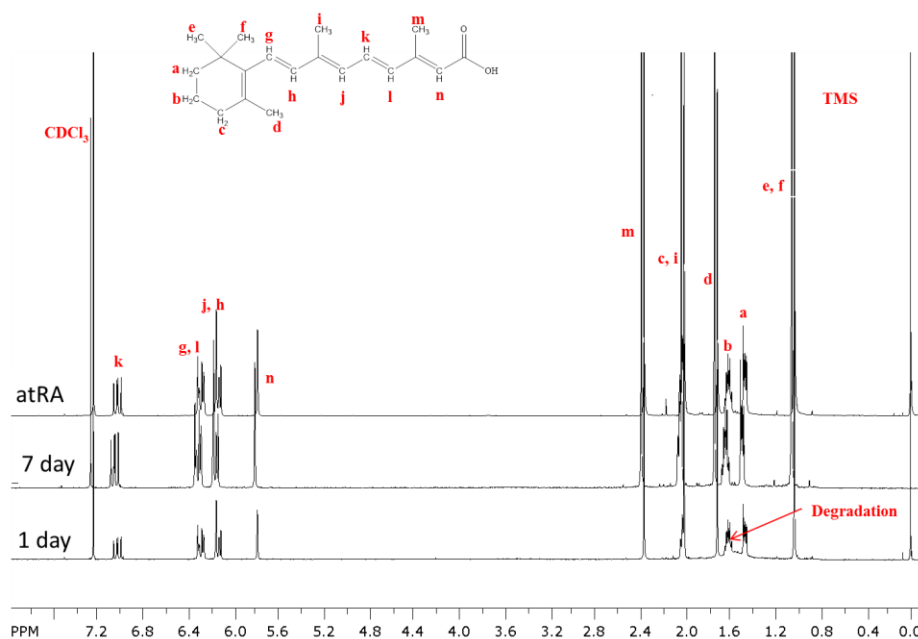
Figure A8 ^{1}H NMR (CDCl$_3$, 400 MHz) of atRA stored at ambient temperature in air after 1 and 7 days with atRA reference spectra.
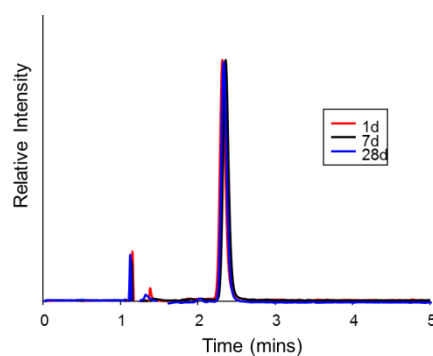
Figure A9 HPLC of atRA stored in EtOH at -20 °C in the dark under Argon after 1, 7 and 28 days.
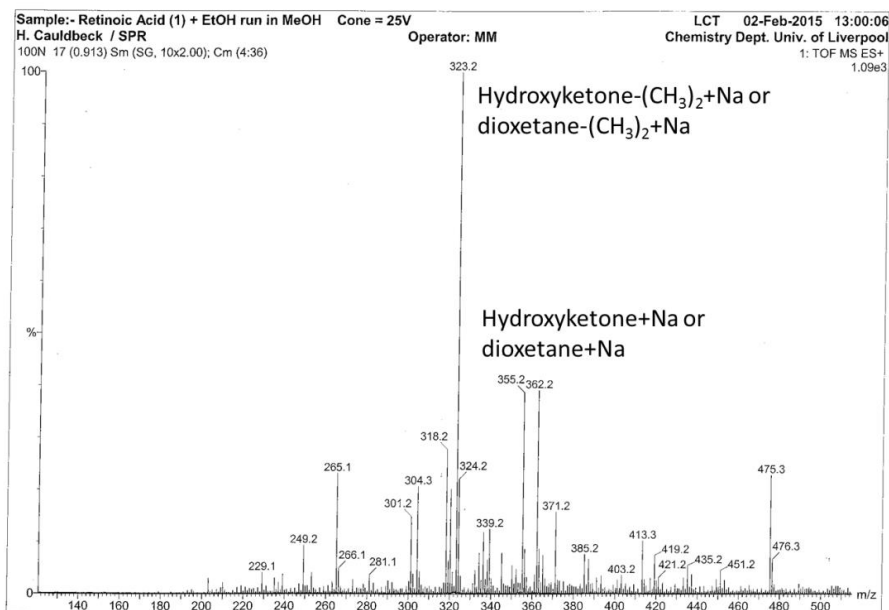
Figure A10 ES-MS of atRA stored in EtOH at -20 °C in the dark under Argon after 28 days.
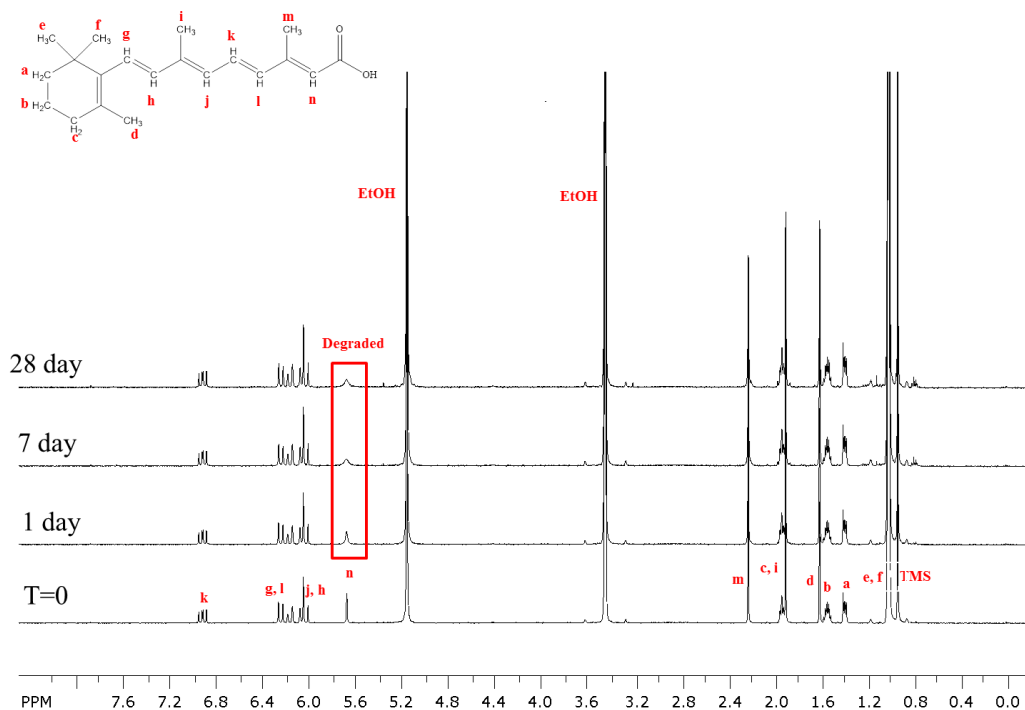
Figure A11 ^{1}H NMR (EtOH-*d6*, 400 MHz) of atRA stored in EtOH at -20 °C in the dark under Argon at t=0 and after 1, 7 and 28 days.
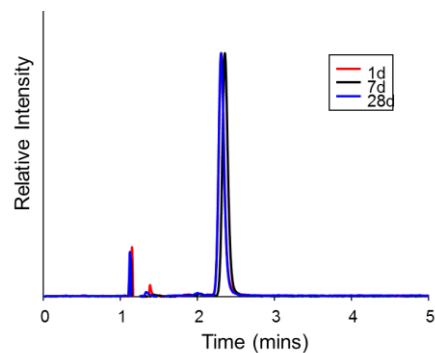
Figure A12 HPLC of atRA stored in EtOH at -20 °C in the dark in air after 1, 7 and 28 days.
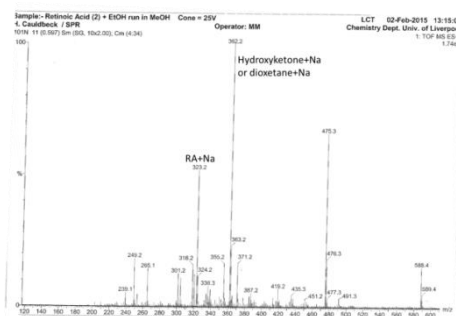
Figure A13 ES-MS of atRA stored in EtOH at -20 °C in the dark in air after 28 days.
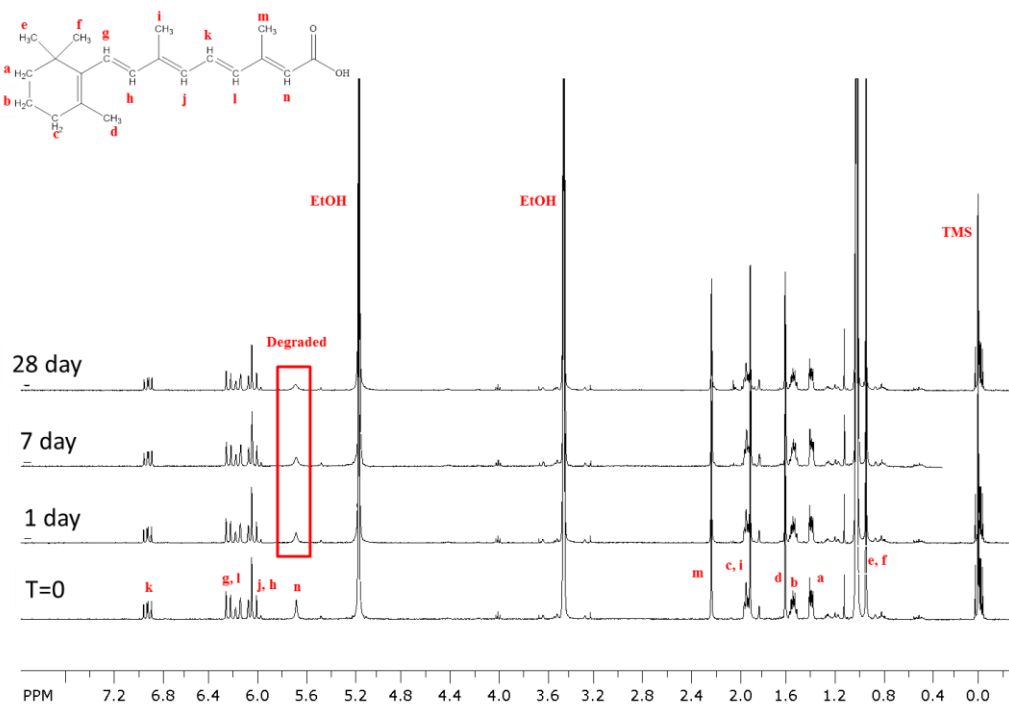
Figure A14 ¹H NMR (EtOH-*d6*, 400 MHz) of atRA stored in EtOH at -20 °C in the dark in air at t=0 and after 1, 7 and 28 days.
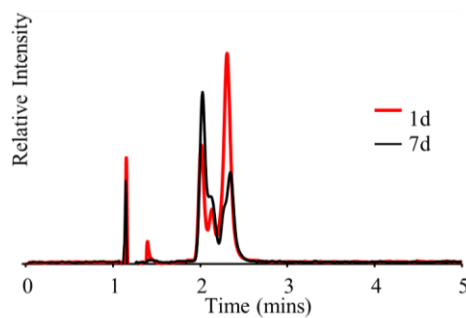
Figure A15 HPLC of atRA stored in EtOH at ambient temperature in the light in air after 1 and 7 days.
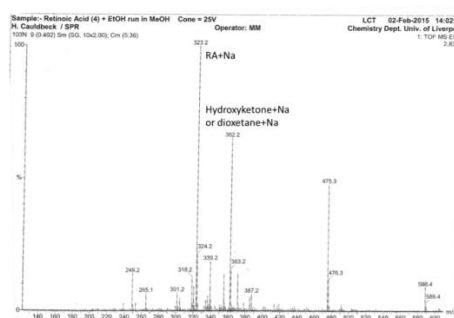
Figure A16 ES-MS of atRA stored in EtOH at ambient temperature in the light in air after 7 days.
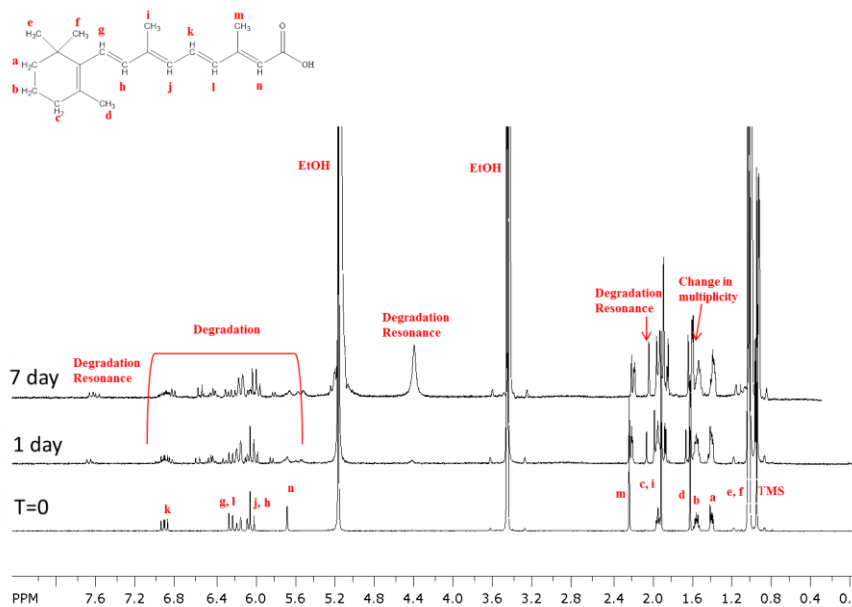
Figure A17 ^{1}H NMR (EtOH-d_6, 400 MHz) of atRA stored in EtOH at ambient temperature in the light in air at t=0 and after 1 and 7 days.
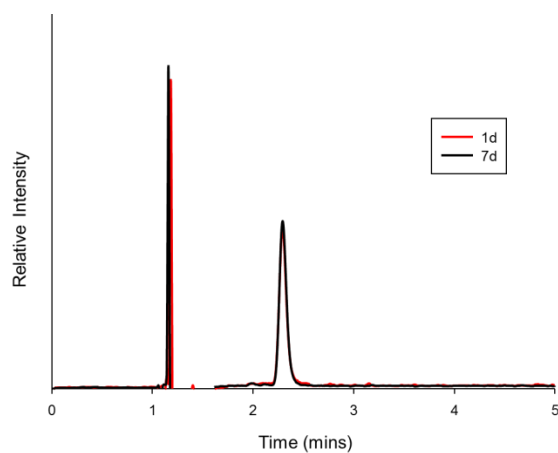
Figure A18 HPLC of atRA stored in DMSO at -20 °C in the dark in air after 1 and 7 days.
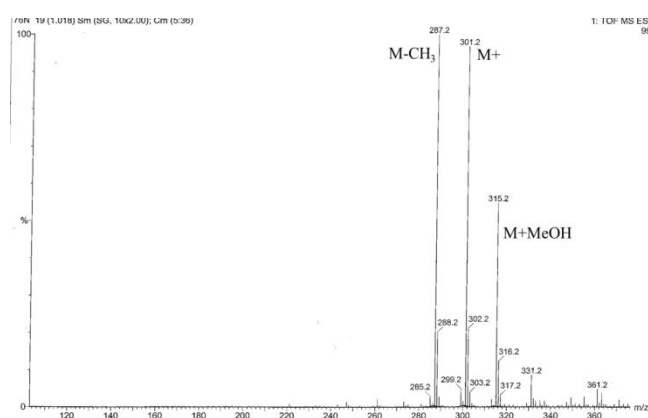
Figure A19 ES-MS of atRA stored in DMSO at -20 °C in the dark in air after 7 days.
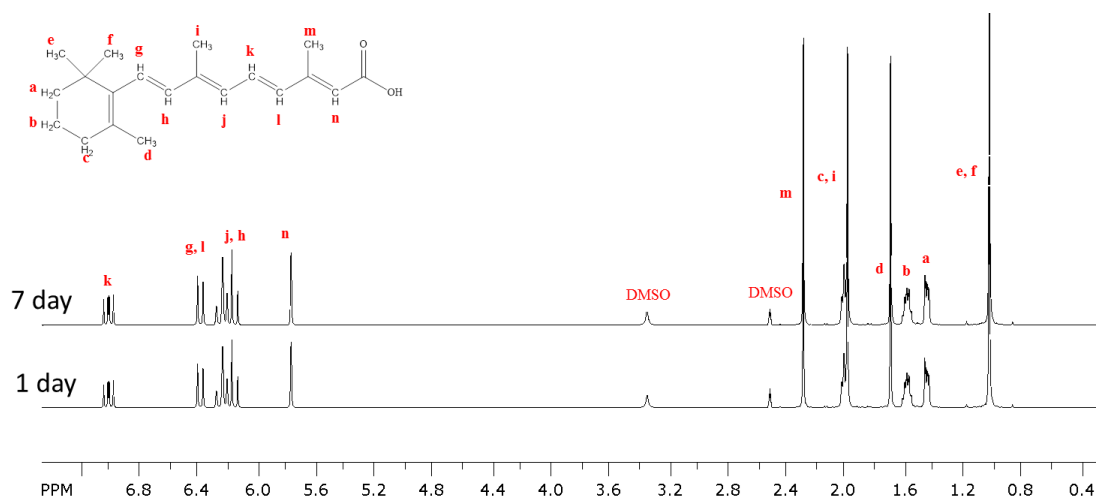
Figure A20 ^{1}H NMR (DMSO-d_6, 400 MHz) of atRA stored in DMSO at -20 °C in the dark in air after 1 and 7 days.
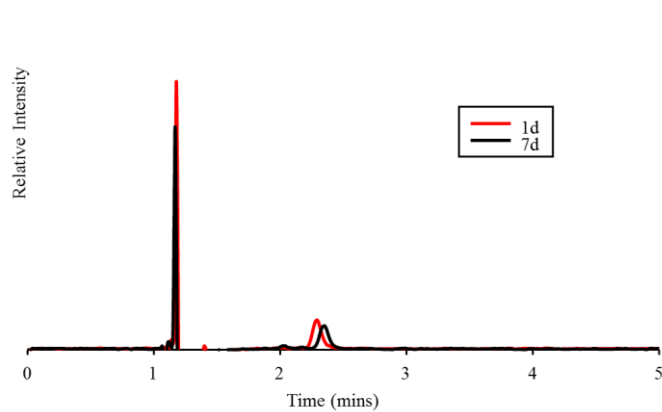
Figure A21 HPLC of atRA stored in DMSO at 37 °C in light, in air after 1 and 7 days.
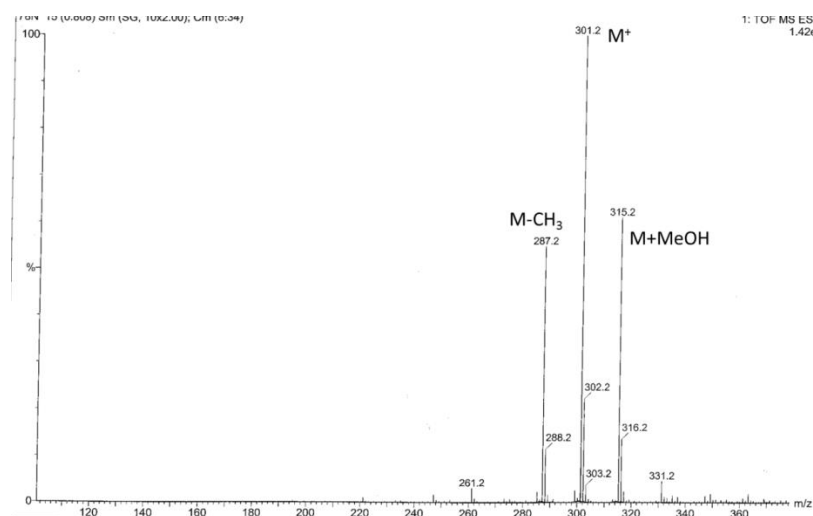
Figure A22 ES-MS of atRA stored in DMSO at 37 °C in light, in air after 7 days.
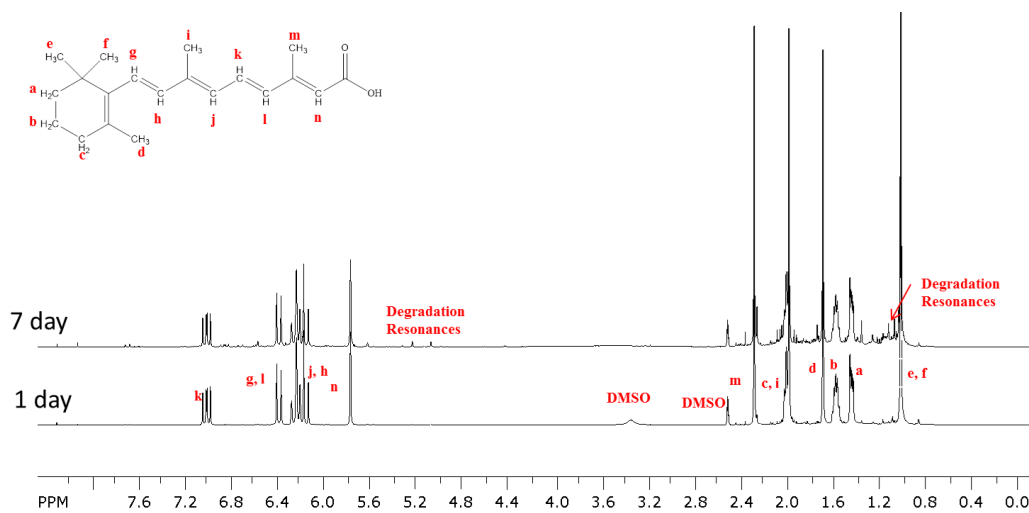
Figure A23 ^{1}H NMR (DMSO-d_6, 400 MHz) of atRA stored in DMSO at 37 °C in light, in air after 1 and 7 days.
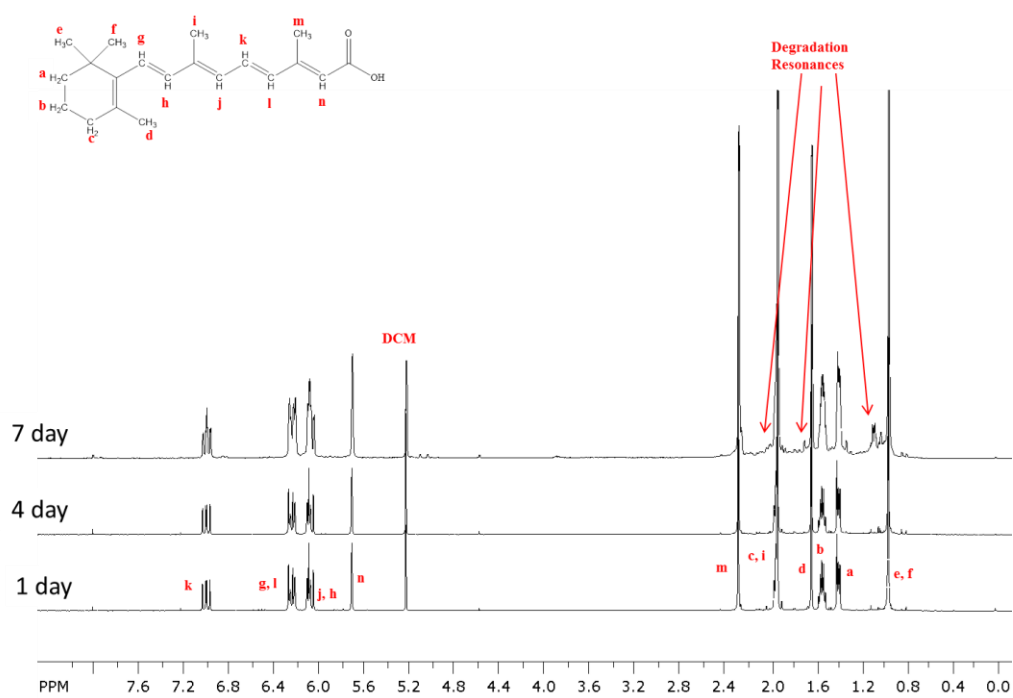
Figure A24 ^{1}H NMR (DCM-d_2, 400 MHz) of atRA stored in DCM at ambient temperature in the dark, under argon after 1, 4 and 7 days.
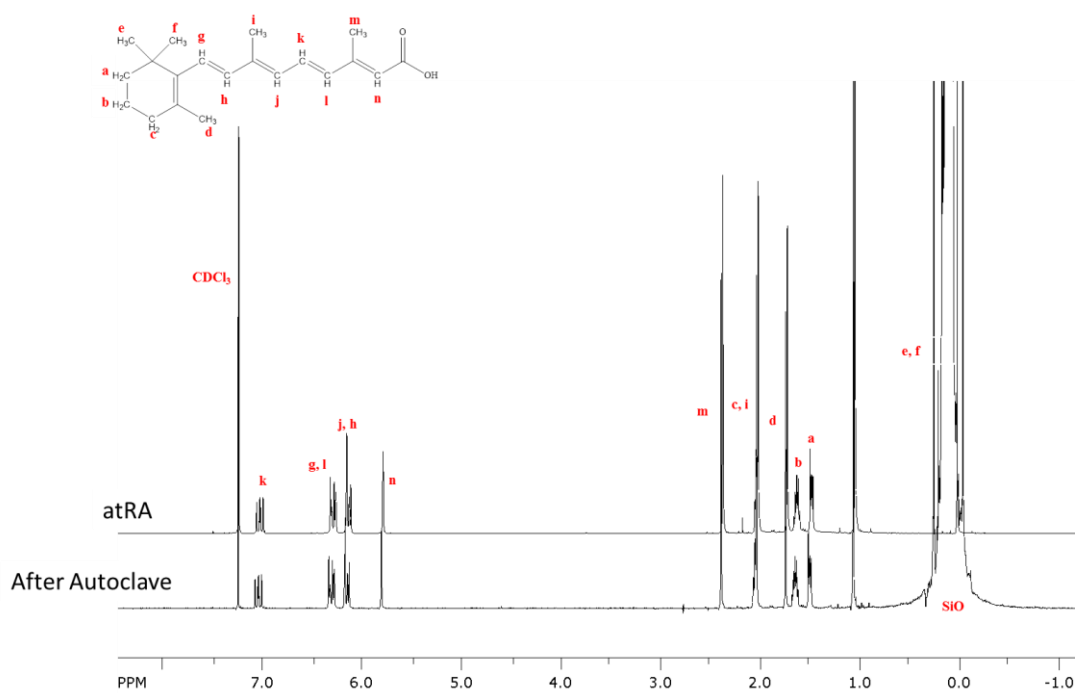
Figure A25 ^{1}H NMR (CDCl$_3$, 400 MHz) of atRA and atRA in SiO after autoclave.
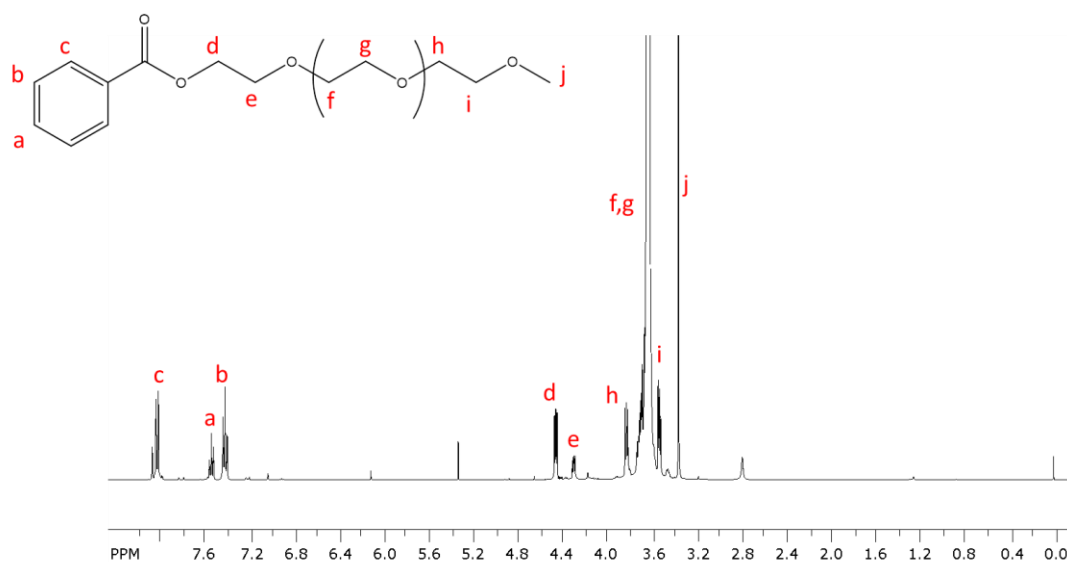
Figure A26 ^{1}H NMR (CDCl$_3$, 400 MHz)of Me-PEO Benzoate.
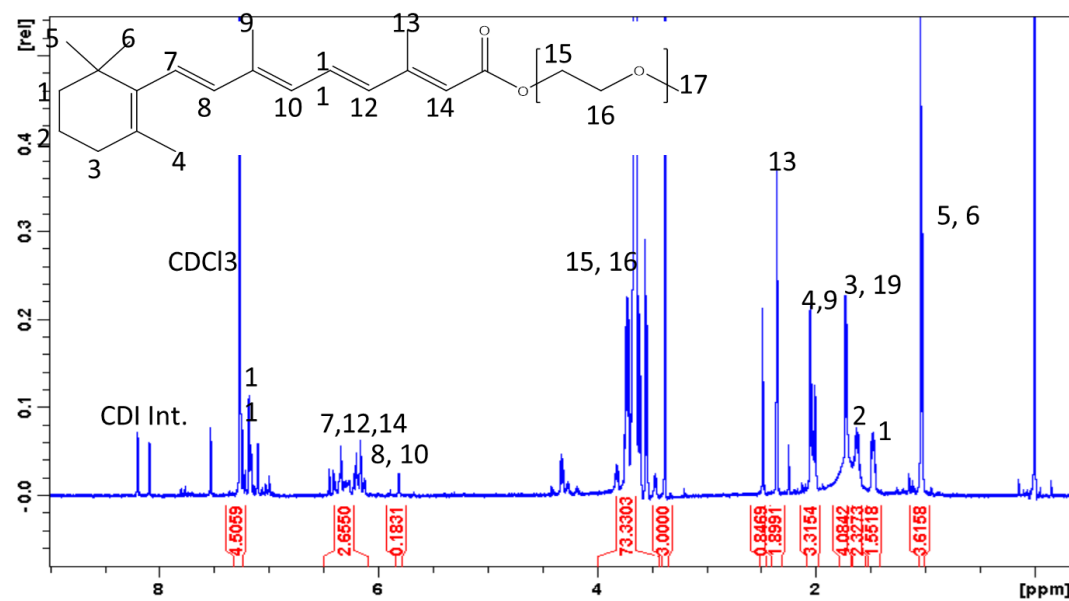
Figure A 27 ^{1}H NMR (CDCl$_3$, 400 MHz)of Me-PEO Retinoate with CDI intermediate.
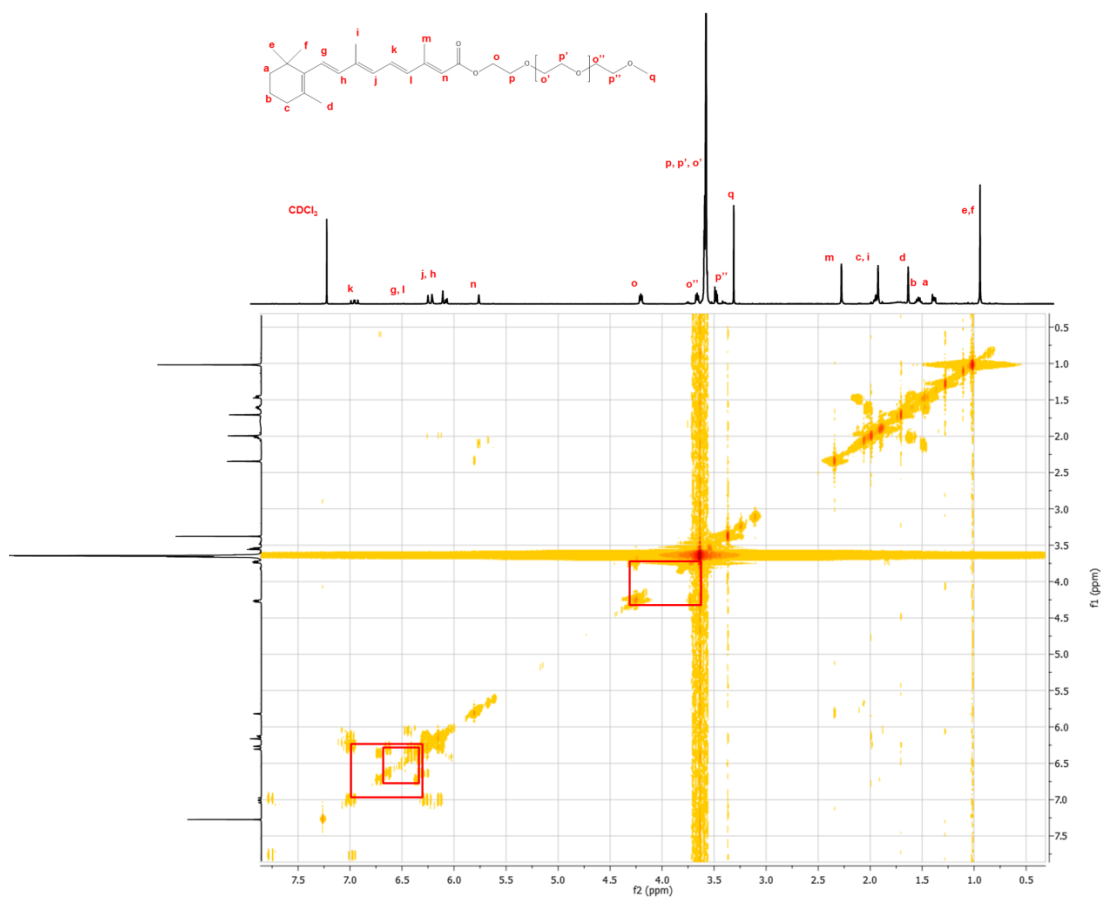
Figure A28 ^{1}H-^{1}H NMR (CDCl$_3$, 400 MHz) of Me-PEO Retinoate
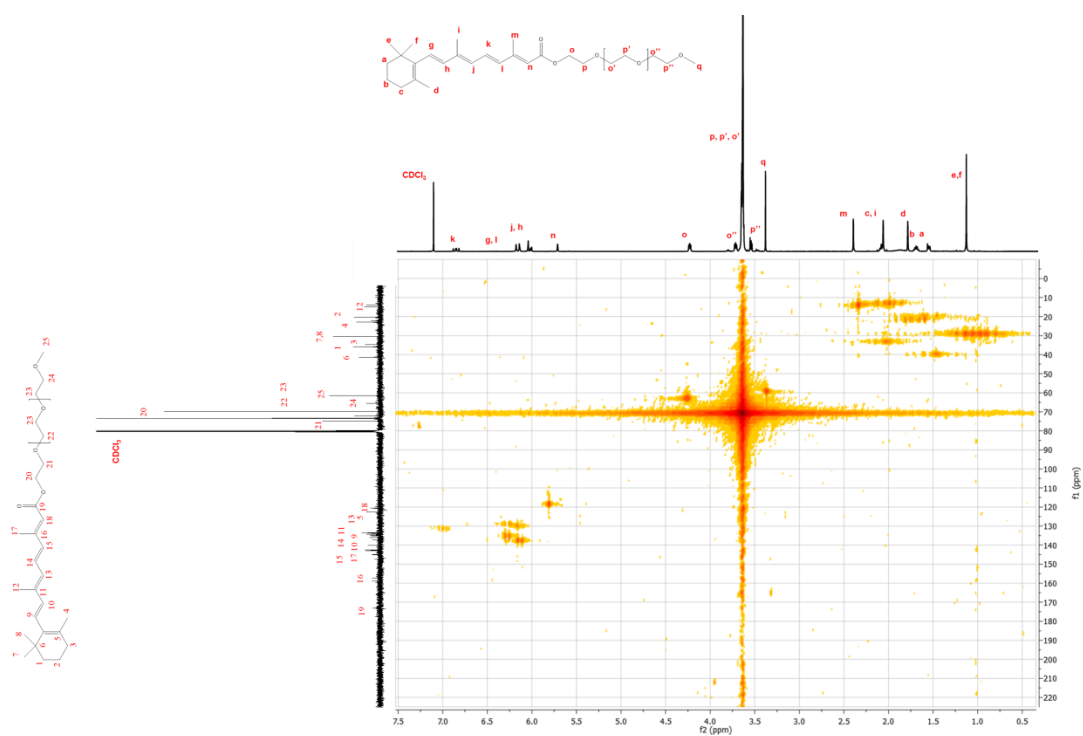
Figure A29 ^{1}H-^{13}C NMR (CDCl$_3$, 400 MHz) of Me-PEO Retinoate.
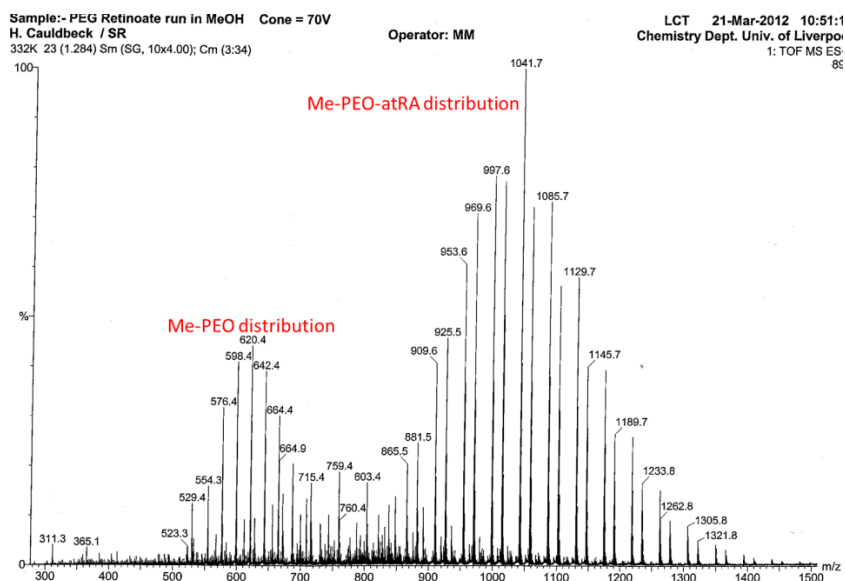
Figure A30 CI-MS of Me-PEO-atRA.
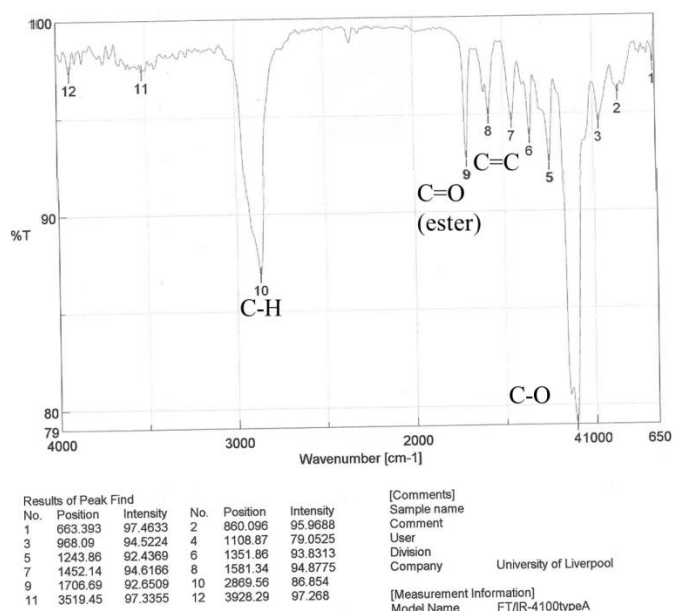
Figure A31 IR spectroscopy of Me-PEO-atRA.
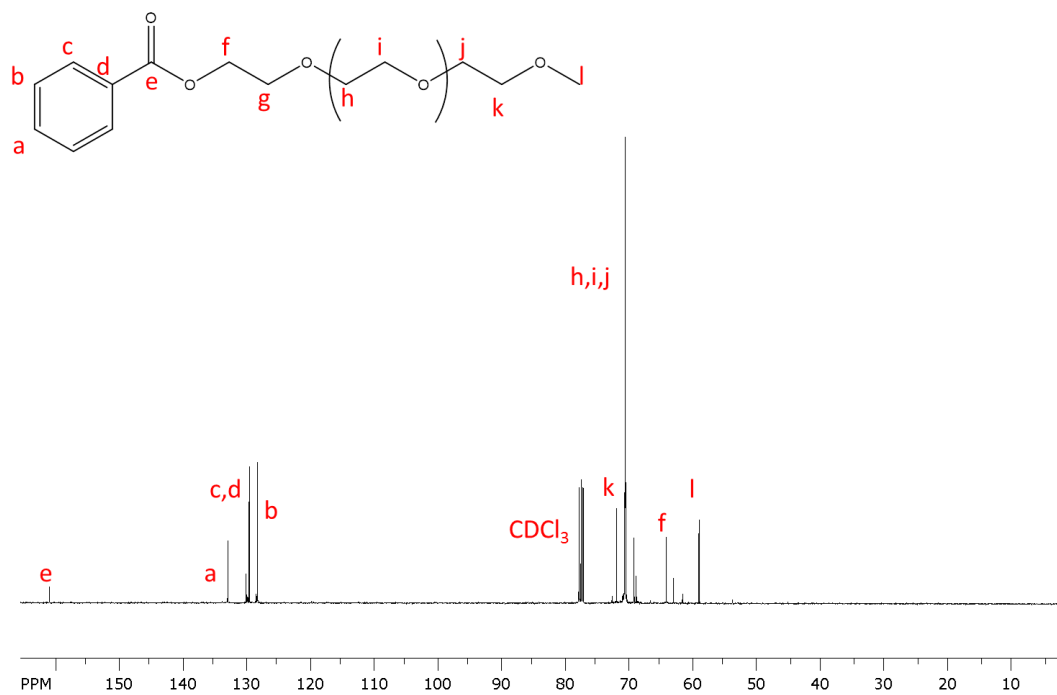
Figure A32 ^{13}C NMR (CDCl$_3$, 100 MHz), of Me-PEO Benzoate.
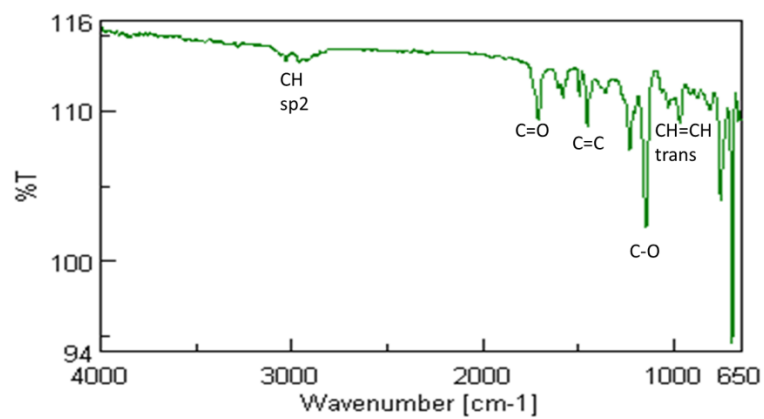
Figure A33 IR Spectroscopy of Me-PEO Benzoate.
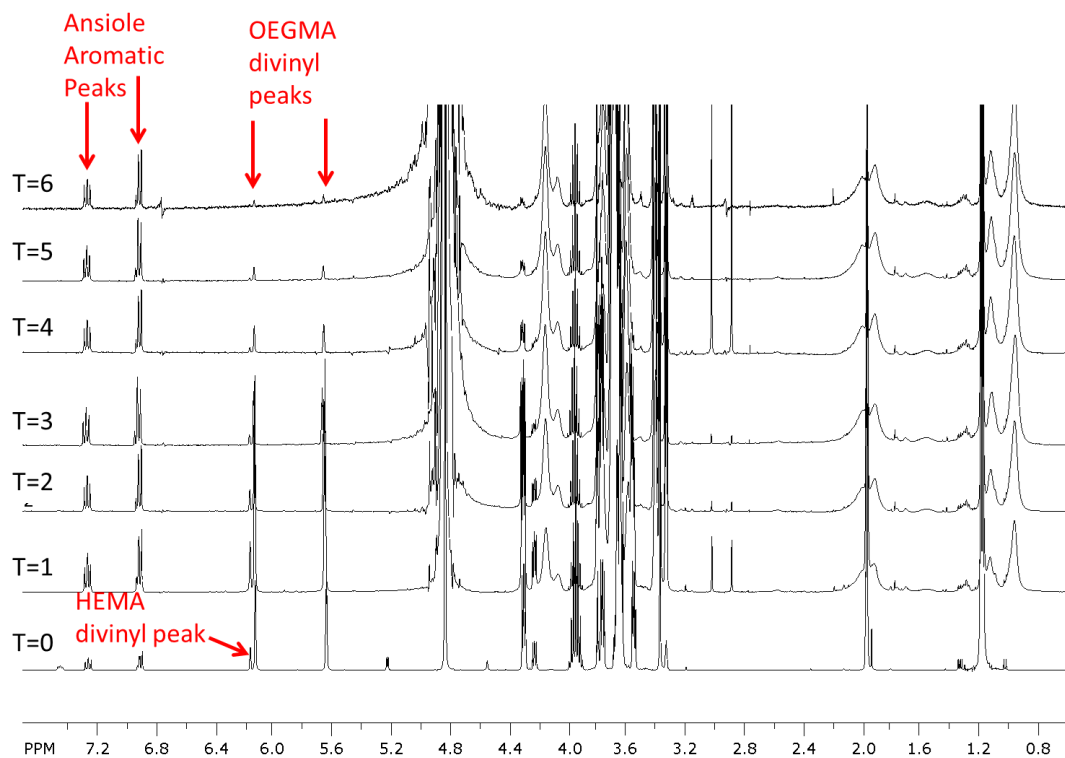
Figure A34 ^{1}H NMR (CDCl$_3$, 400 MHz) p(OEGMA$_{24}$-*co*-HEMA$_6$) at hourly time points throughout polymerisation.
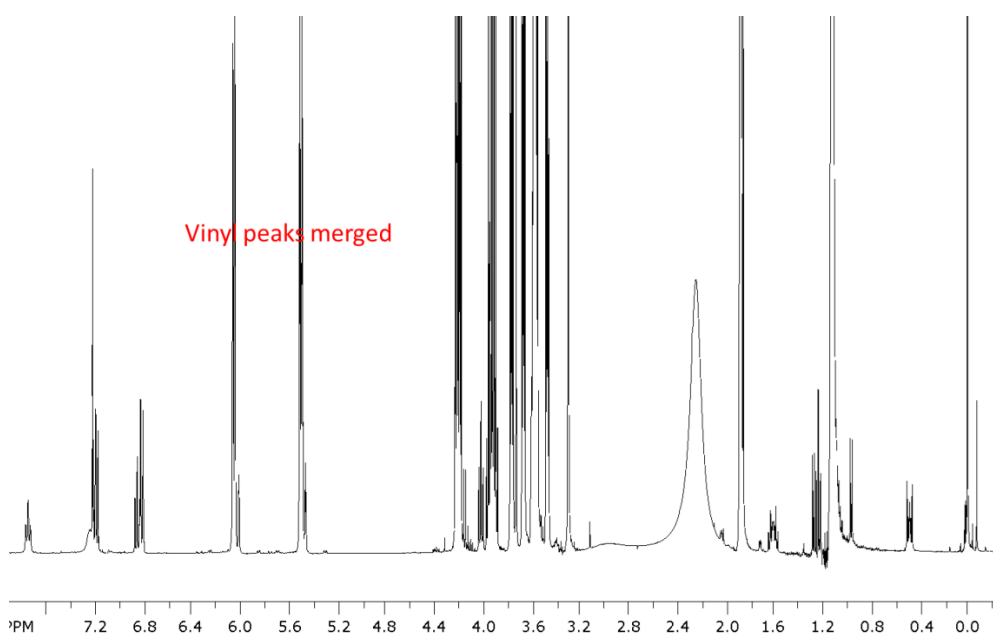
Figure A35 ^{1}H NMR (CDCl$_3$, 400 MHz) Polymerisation of p(OEGMA$_{24}$-*co*-HEMA$_6$-*co*-PDMSDMA$_{0.95}$) at T=0.
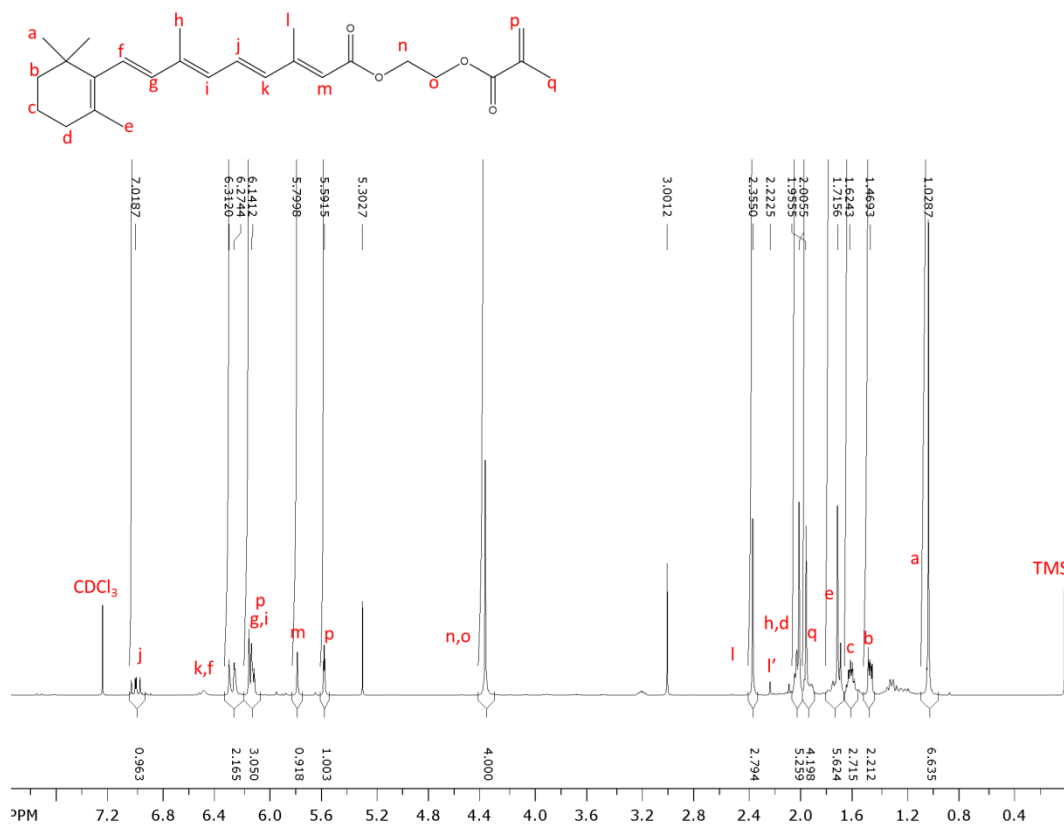
Figure A36 ^{1}H NMR (CDCl$_3$, 400 MHz) atRAEMA with integrations.
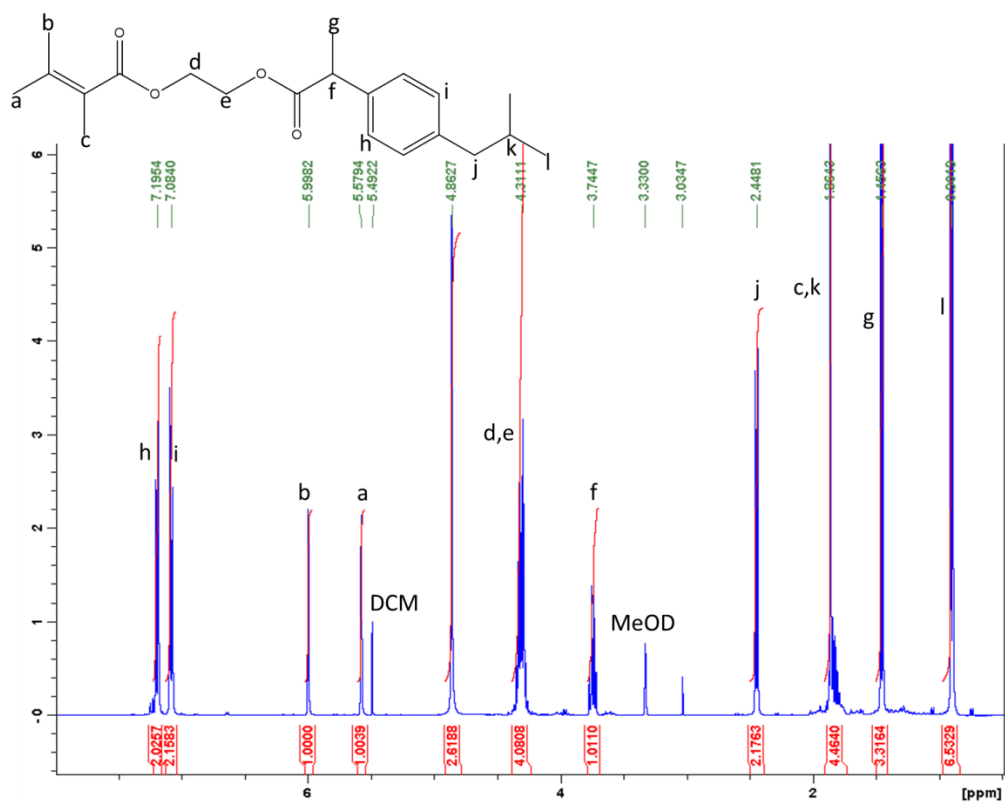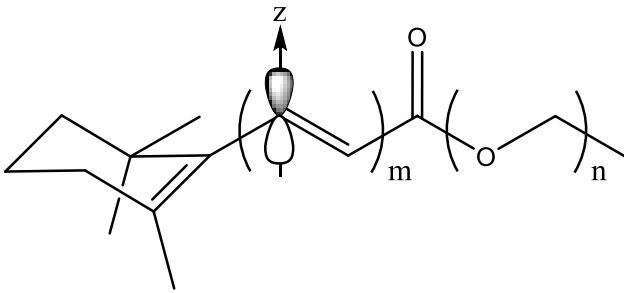
Figure A37 ^{1}H NMR (MeOD, 400 MHz) IbuEMA with integrations.

Computational modelling was performed by E. Eden (University of Liverpool) using the following: ground state geometries of conjugated esters were optimised at the HF/6-31G(d) level of theory using the Spartan '10 v1.1.0 software package. Calculations were conducted *in vacuo* using default parameters in Spartan '10. Orbital energies and coefficients were calculated at the same level of theory. Coefficients, associated with the contribution of the p_z orbital at the carbonyl carbon to the HOMO, were used to estimate reactivity of the carbonyl moiety.

Double Bonds Present (m)	Ethylene Glycol units (n)	E_{LUMO} (eV)	E_{HOMO} (eV)	P(z)
1	4	3.07	-8.95	1.00
2	4	1.67	-8.67	0.86
3	4	1.98	-7.95	0.73
4	4	1.78	-7.55	0.67

A38 Computational Modelling Parameters
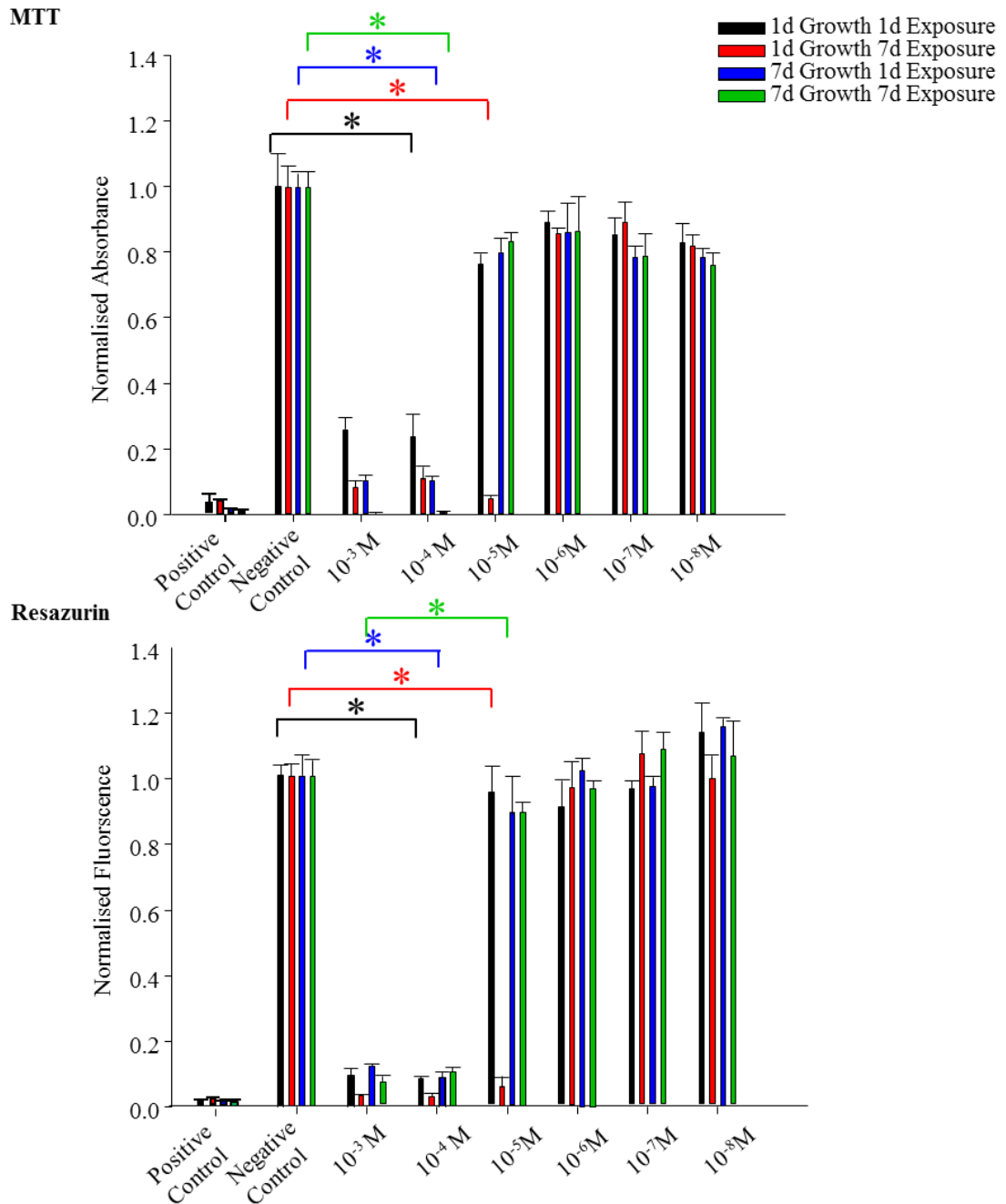
Figure A39 MTT and resazurin assay to determine the cytotoxicity of Me-PEO$_{48}$-atRA at different concentrations from 10^{-3} – 10^{-8} M, and control cells without exposure and with 20 % DMSO. ARPE-19 cells were grown and treated for different time scales. Pre-confluent cells (grown for 1 d) were exposed to Me-PEO$_{48}$-atRA for 1 d (black) and 7 d (red). Post-confluent cells (grown for 7 d) were also exposed to Me-PEO$_{48}$-atRA for 1 d (blue) and 7 d (green). (mean, error bars represent $\pm$ 1 standard deviation); n=3. *, Significance by ANOVA and Dunnett's T3 post- hoc evaluation (p$\leq$0.05).
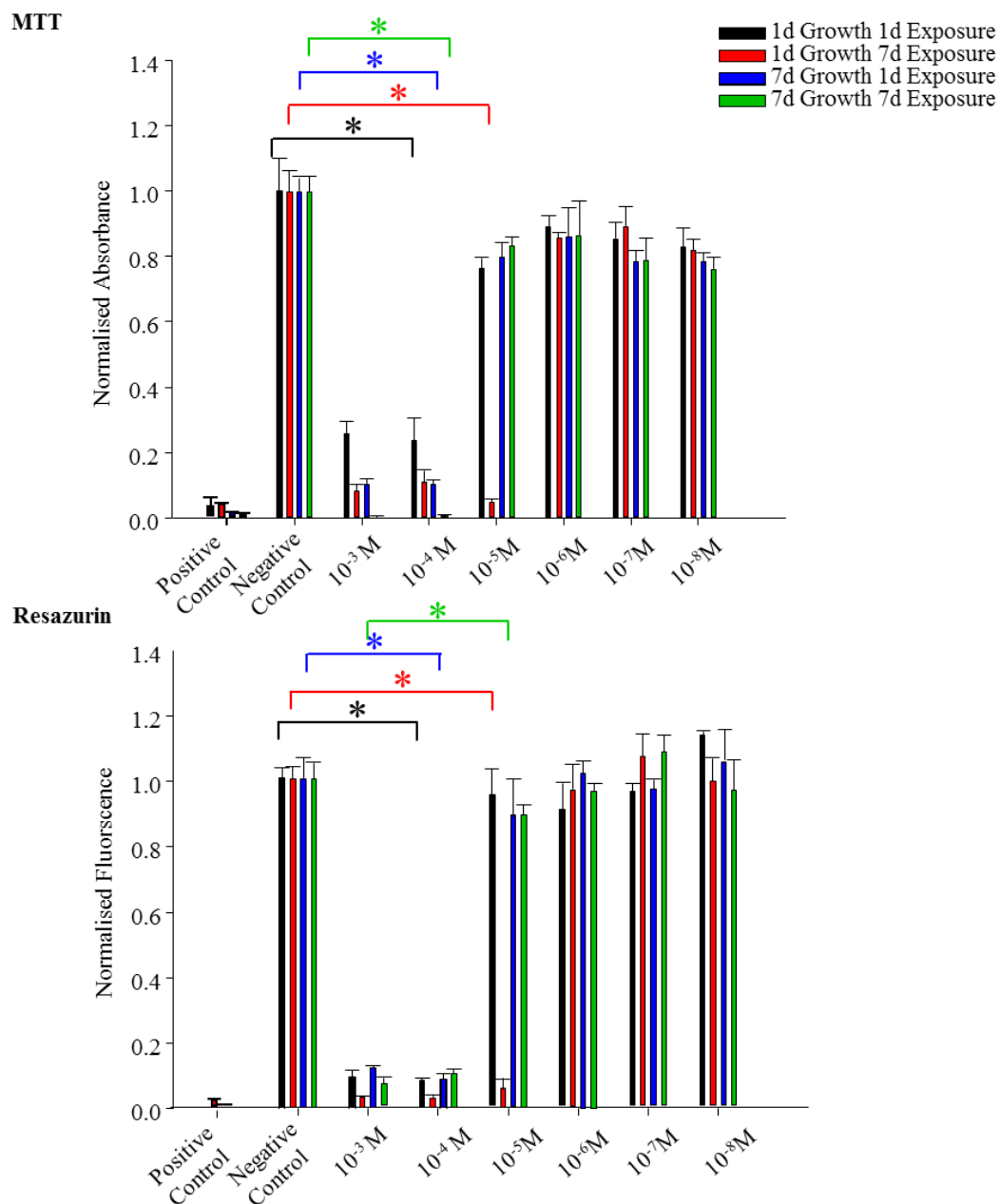
Figure A40 MTT and resazurin assay to determine the cytotoxicity of Me-PEO$_{48}$-Ibu at different concentrations from 10^{-3} – 10^{-8} M, and control cells without exposure and with 20 % DMSO. ARPE-19 cells were grown and treated for different time scales. Pre-confluent cells (grown for 1 d) were exposed to Me-PEO$_{48}$-Ibu for 1 d (black) and 7 d (red). Post-confluent cells (grown for 7 d) were also exposed to Me-PEO$_{48}$-Ibu for 1 d (blue) and 7 d (green). (mean, error bars represent ± 1 standard deviation); n=3. *, Significance by ANOVA and Dunnett's T3 post-hoc evaluation (p≤0.05).
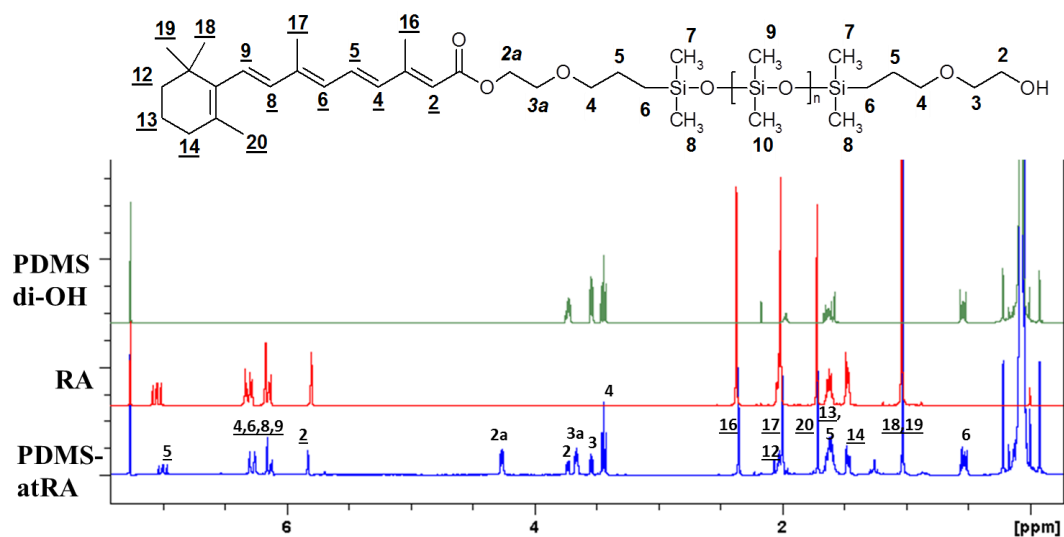
Figure A41 ^{1}H NMR (CDCl$_3$, 400 MHz) atRA-PDMS.
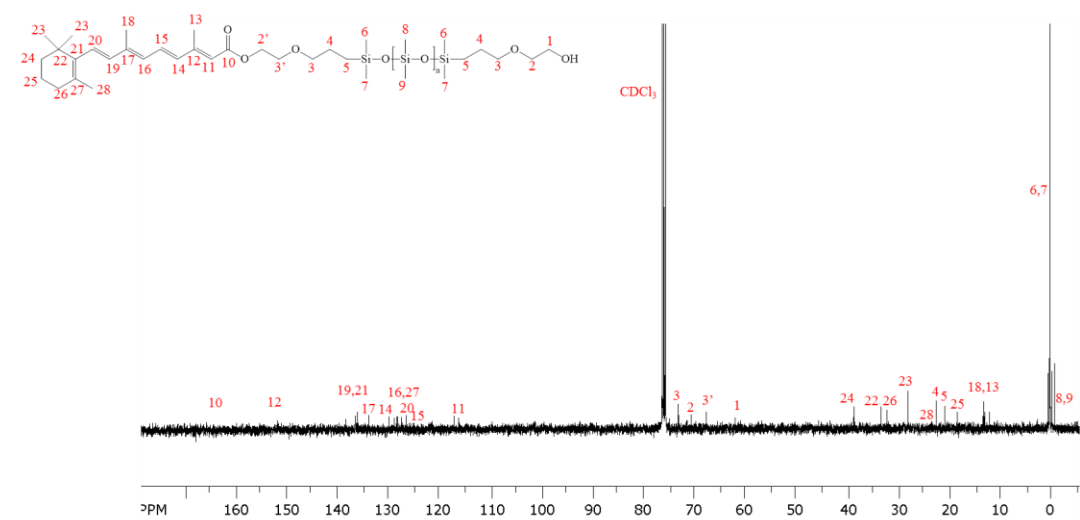
Figure A42 ^{13}C NMR (CDCl$_3$, 100 MHz) atRA-PDMS.
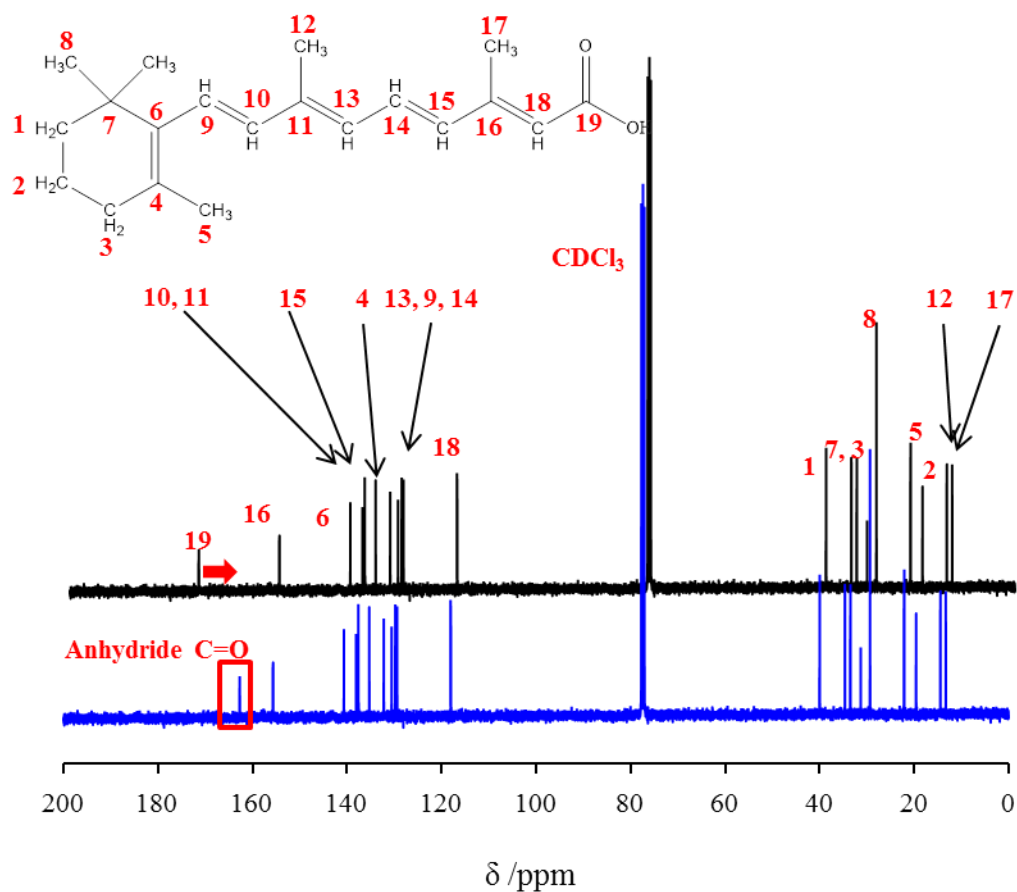
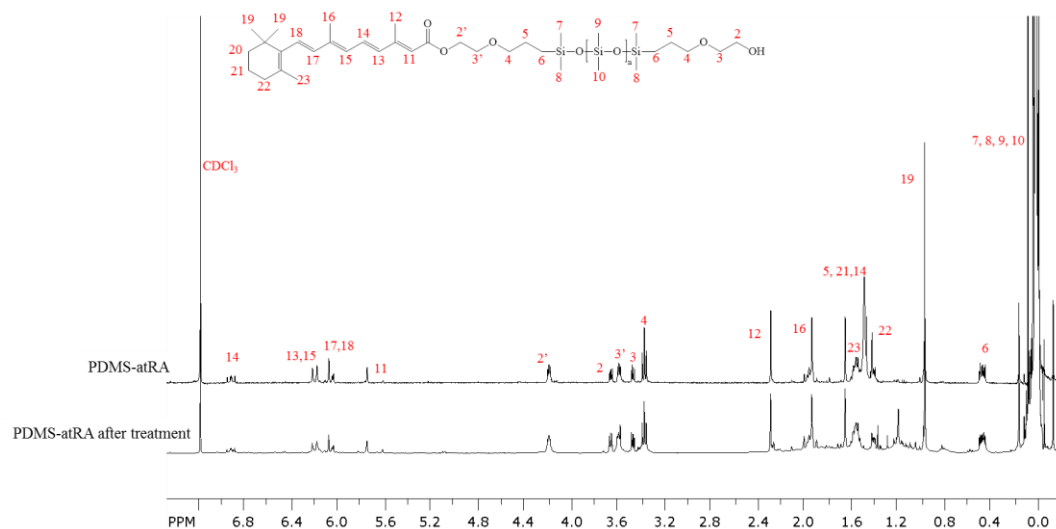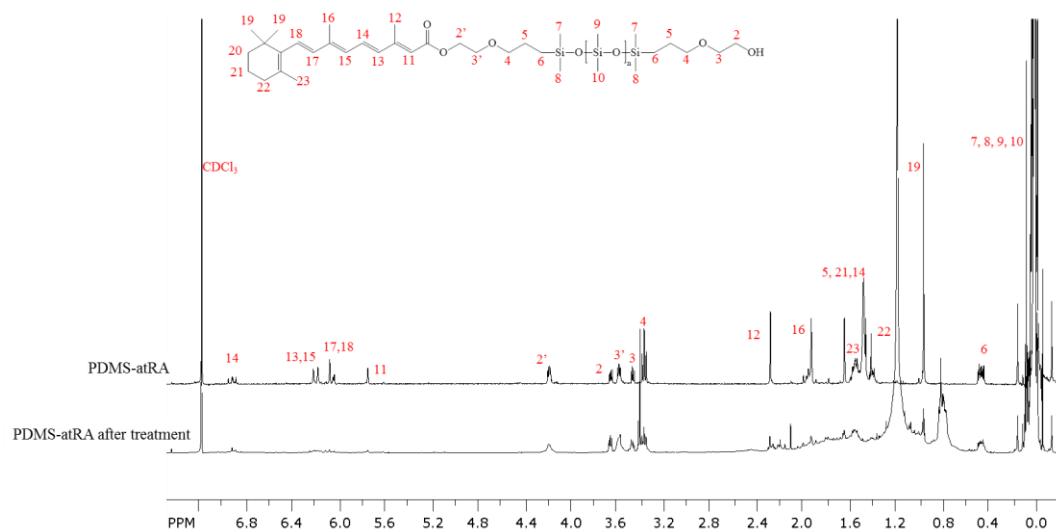**Figure A43** ^{13}C NMR (CDCl$_3$, 100 MHz) atRA (black) and atRA anhydride (blue).
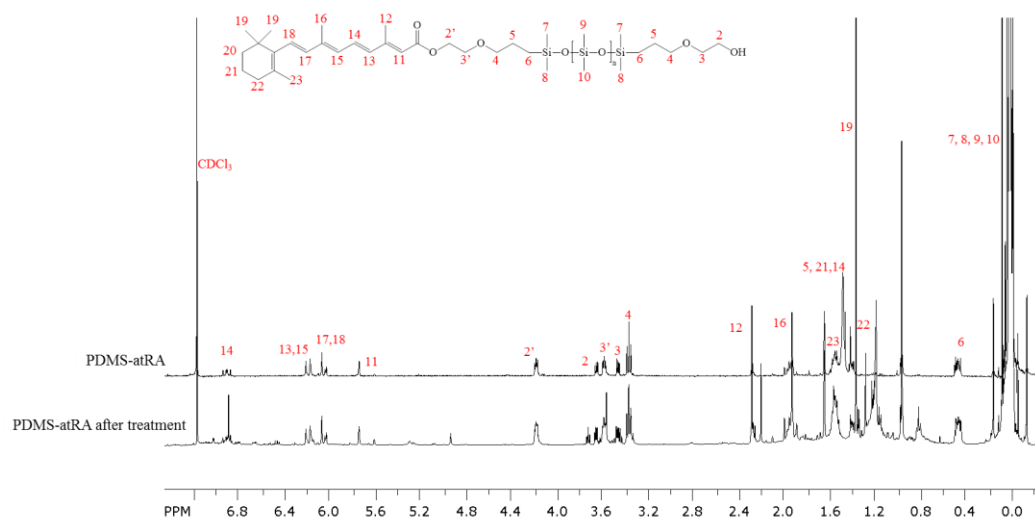
Figure A44 ^{1}H NMR (CDCl$_3$, 400 MHz) PDMS-atRA before (black) and after treatment with 10 equivalents HCl in THF at 40 °C (blue).
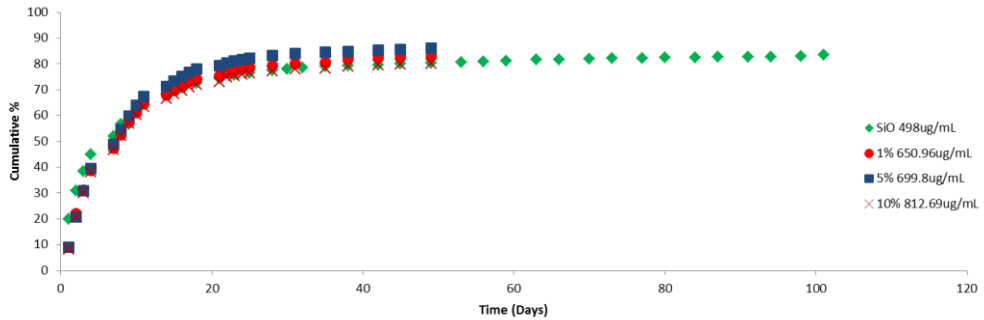
Figure A45 ^{1}H NMR (CDCl$_3$, 400 MHz) PDMS-atRA before (black) and after treatment with 10 equivalents HCl in dioxane at 40 °C (blue).
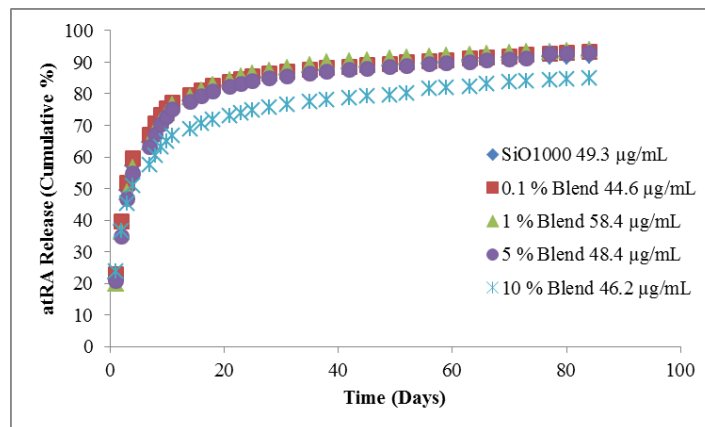

Figure A46 ^{1}H NMR (CDCl$_3$, 400 MHz) PDMS-atRA before (black) and after treatment with 10 equivalents HCl in dioxane at 60 °C (blue).
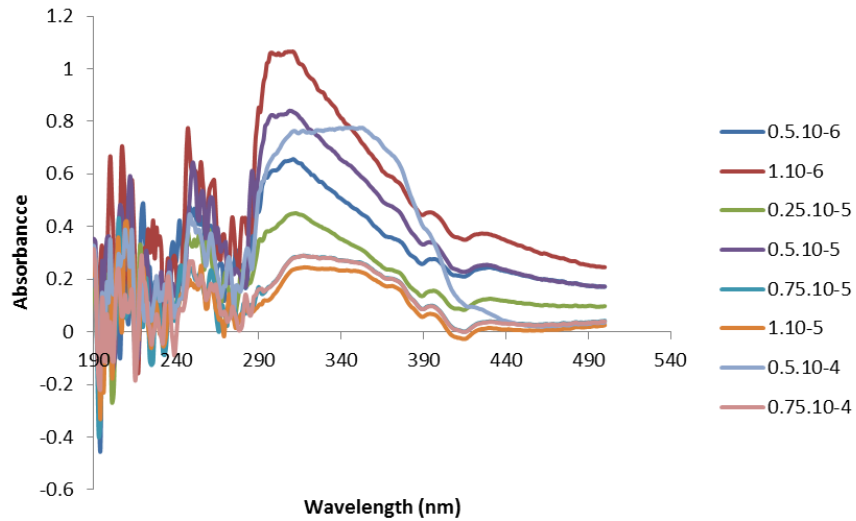
Figure A47 UV-Vis Spectra of atRA in media at various concentrations, showing overlap of FCS peak with atRA at 364 nm.

Figure A48 Cumulative percentage release of atRA from SiO and blends from saturation concentration.

Figure A49 Cumulative percentage release of atRA from SiO and blends from a starting concentration of approximately 50 μg/mL.
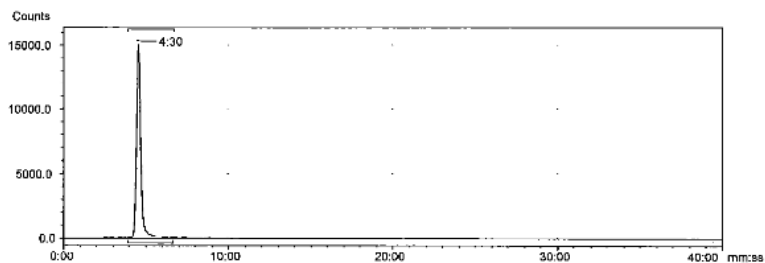
American Radiolabeled Chemicals, Inc.

101 ARC Drive
Saint Louis, MO 63146 USA
Phone: 314-991-4545 or 800-331-6661
Fax: 314-991-4692 or 800-999-9925
Web: http://www.arc-inc.com
Email: arcinc@arc-inc.com

ART 633A
all trans **Retinoic acid [11,12-³H(N)]**
Lot# 140612

Scan after removal of Tocopherol

Name	Start (mm:ss)	End (mm:ss)	Retention (mm:ss)	Area (Counts)	%ROI (%)
Region 1	3:57	6:42	4:30	264799.0	100.00

Figure A 50 Technical data sheet supplied by ARC with ³H atRA of HPLC using Zorbex ODS column and the mobile phase: ACN 1 % triethylammonium acetate PH 4, (70:30).